VOLUME 93 NO. EM5
OCTOBER, 1967

JOURNAL of the

Engineering Mechanics Division

PROCEEDINGS OF THE
AMERICAN SOCIETY
OF CIVIL ENGINEERS

REQUIREMENTS FOR MANUSCRIPTS

This Journal is published by the Society to deliver information to the engineering profession as speedily as practicable. To this end the material herein has been selected and required less than more formal publications.

Preprints and discussions of current papers should be submitted to the Technical Publications Department. This final date on which a discussion will be received is given in the Table of Contents with each paper. Those who are interested in the review and publication procedure should comply with the following basic requirements:

The author should supply a brief abstract, not exceeding 50 characters and spaces.

A brief abstract or summary should accompany the paper.

The manuscript (a ribbon copy and two copies) should be double spaced on one side of 8½-in. by 11-in. paper. Papers that were originally prepared for oral presentation must be carefully edited by the author before being submitted.

The author's full name, Society membership grade, and footnote reference to present employment should appear on the first page of the paper.

Illustrations are reproduced directly from the copy that is submitted. It is necessary that all lettering be drawn, in black ink, 3/16-in. high for capital letters, with proportionate lower case characters in the proportions dictated by standard drafting practice. It is important that no line of mathematics be longer than 6½ in. Typewritten copies of typewriter quality may be used but they will be proportionately reduced.

Tables should be typed (double spaced copies) on one side of 8½-in. by 11-in. paper. Small tables should be grouped. Table titles should be descriptive and explanation should be made in the text.

Illustrations should be drawn in black ink on one side of 8½-in. by 11-in. paper. Figures that are to be reduced to 6½ in. by 10½ in. the maximum size that can be printed within the frame. Because illustrations will be reduced in the publication process, the lettering should be 3/16-in. high. Photographs should be submitted as glossy prints that are not more than 6½ in. by 10½ in. Explanations and descriptions should be made within the text for each illustration.

Papers should not exceed about 12,000 words in length and should be no shorter than 2,000 words. For approximation, each full page of typed text, including figures, is the equivalent of 300 words.

Information concerning the preparation of technical papers is contained in the "Technical Publications Handbook" which can be obtained from

---

Publication of this Journal may be made on condition that the full title of the paper, name of author, reference (or paper number), and date of publication by the Society are given. The Society is not responsible for any statement made or opinion expressed in its publications.

Journal of the Engineering Mechanics Division is published quarterly by the American Society of Civil Engineers, Publication Office, 2500 South State Street, Ann Arbor, Michigan. Editorial and General Offices, 33 West 39 Street, New York 18, New York.

Subscriptions are accepted only as annual subscription to this Journal. Second-class postage paid at Ann Arbor, Michigan.

EM 5/61

Journal of the
ENGINEERING MECHANICS DIVISION
Proceedings of the American Society of Civil Engineers

CONTENTS

October, 1957

Papers

Paper 1389 October, 1957 EM 4

Journal of the
ENGINEERING MECHANICS DIVISION
Proceedings of the American Society of Civil Engineers

ON THE DYNAMIC STRENGTH OF RIGID-PLASTIC BEAMS UNDER BLAST LOADS[a]

Mario G. Salvadori,[1] M. ASCE and Paul Weidlinger,[2] M. ASCE
(Proc. Paper 1389)

SYNOPSIS

Upper bounds to the dynamic strength of simply-supported beams acted upon by a uniformly distributed blast pressure are obtained under the assumption of rigid-plastic behavior in bending and/or in shear (development of "plastic hinges" and/or "plastic slides").

The time variation of the blast pressure is approximated by a negative exponential time function with peak value at t = o. Maximum allowable values of the peak pressure are obtained for beams of rectangular and I section. The results of the present analysis are valid for other types of impulsive forces.

INTRODUCTION

The dynamic strength of an elasto-plastic system under an impulsive load producing fairly large plastic deformations may be evaluated in a sufficiently accurate, but very simple manner by assuming that the system is made of an ideal rigid-plastic material.(3) The solution thus obtained neglects the elastic part of the deformation and assumes that the work done by the loads is all expended in plastic flow. The response predicted by this type of solution is accurate only if plastic deformations are large compared to elastic

Note: Discussion open until March 1, 1958. Paper 1389 is part of the copyrighted Journal of the Engineering Mechanics Division of the American Society of Civil Engineers, Vol. 83, No. EM 4, October, 1957.

a. Presented at a meeting of the American Society of Civil Engineers in Pittsburgh, Pa., October, 1956.

1. Prof. of Civ. Eng., Columbia Univ., New York, N. Y. and Associate, Paul Weidlinger, Cons. Eng., New York, N. Y.
2. Cons. Engr., New York, N.Y.

deformations.[4] But, the rigid, plastic approach may be used to determine upper bounds of allowable blast loads, even if the elastic deformations are not negligible, by introducing a criterion of strength based on allowable plastic strains, provided the time of maximum plastic displacement be large in comparison with the fundamental periods of the beam in bending and shear.

The mathematical solution of blast problems is also greatly simplified by approximating the positive phase of the blast pressure between zero and infinity by a single function, rather than by two or more functions requiring successive integrations of the differential equations. This can be done by assuming that the uniform pressure p acting on the beam has a negative-exponential time history:

$$p(\tau) = p_o e^{-\beta\tau}, \tag{1}$$

where τ is the time, p_o the peak value of the pressure, and β the so-called decay constant.

In order to compare pressures with different peak values and decay constants, the pressures of Eq. (1) will be assumed to have the same total impulse k:

$$\int_o^\infty p_o e^{-\beta\tau} \, d\tau = p_o/\beta = k . \tag{2}$$

Whenever the pressure decay is rapid, the beam response is known to depend essentially on the impulse but not on the time variation of the pressure. Hence, the results of the present analysis, and in particular the graphs for the evaluation of maximum deflections and of maximum allowable pressures, may be used in connection with other pulse forms having the same total impulse.

The beams considered are assumed to undergo plastic deformations: a) in bending, by developing "plastic hinges" at mid-span; b) in shear, by developing "plastic slides" at the supports; c) in bending and shear, by developing both plastic hinges and plastic slides. The beams are supposed to be braced laterally so that no lateral or local buckling may occur.

The Development of Plastic Hinges

A simply supported beam of length L, depth h. width b, and cross-section area A (Fig. 1) is loaded at time $\tau = 0$ with the uniform pressure of Eq. (1). We indicate by s_o the uniaxial dynamic yield stress of its material (Fig. 2) and by $S_p = k_1 A h$ its plastic section modulus. The plastic form factor k_1 varies between 1/4 (for a rectangular cross-section) and 1/2 (for an ideal I section). Under the assumption of rigid-plastic behavior in bending, the beam will not move unless the moment at mid-span, which takes its maximum value:

$$M_o = \frac{1}{8} p_o b L^2 \tag{2}$$

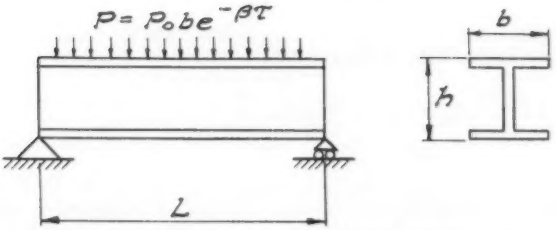

Simply supported beam under impulsive load.

FIG. 1

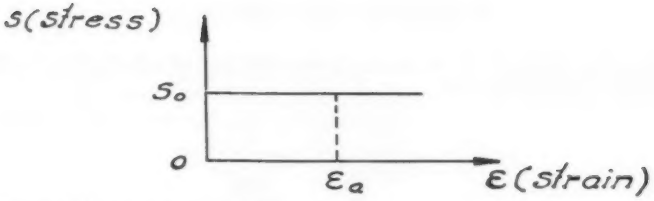

Rigid-plastic stress-strain diagram.

FIG. 2

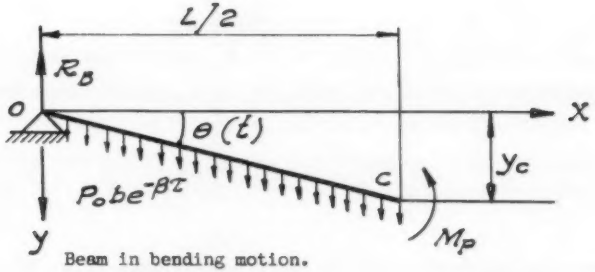

Beam in bending motion.

FIG. 3

at $\tau = 0$, is greater than the capacity plastic moment:

$$M_p = s_o k_1 A h . \tag{3}$$

Hence, motion will only start if p_o is larger than:

$$p_{oB,min.} = s_o \frac{8k_1 A}{bL} \left(\frac{h}{L}\right) . \tag{4}$$

If M_o is slightly greater than M_p, the middle section of the beam is entirely plastic and the two halves of the beam rotate as rigid bodies about the supports, while the middle section moment has the constant value M_p. In other words, a plastic hinge develops at the middle section and the beam becomes a mechanism.

For values of M_o much greater than M_p an entire central portion of the beam may become plastic. This second possibility is considered in Sec. 5.

Single-Hinge Displacements

Referring the left half of the beam to coordinate axes as in Fig. 3, its angular acceleration $\ddot{\theta}$ is given by:

$$\ddot{\theta} = 3 \frac{p_o b}{mL} e^{-t} - 24 \frac{M_p}{mL^3} \tag{5}$$

where m is the mass of the beam per unit of length and

$$t = \beta\tau \tag{6}$$

is the non-dimensional time. Integrating Eq. (5) with rest conditions, $\theta(0) = \dot{\theta}(0) = 0$, and letting:

$$r = M_p/M_o \ (< 1) , \tag{7}$$

the center deflection of the beam, $y_C = \frac{L}{2}\theta$, is given non-dimensionally by:

$$\frac{2}{3}\frac{m\beta^2}{p_o b} y_C = (e^{-t} + t - 1) - \frac{r}{2} t^2 , \tag{8}$$

y_C becomes maximum, and the beam motion stops ($\dot{y}_C = 0$), at a time t_B defined by the equation:

$$1 - e^{-t_B} - r\, t_B = 0. \tag{9}$$

Fig. 4 gives t_B as a function of r:

$$t_B = f(r). \tag{10}$$

By Eqs. (8) and (9) the maximum value, δ_B of y_C becomes:

$$\frac{2}{3}\frac{m\beta^2}{p_o b}\,\delta_B = t_B\left[1 - r\left(1 + \frac{t_B}{2}\right)\right] . \tag{11}$$

By Eq. (10), the right-hand member of this equation is a function of r only and may be written as:

$$\frac{2}{3}\frac{m\beta^2}{p_o b}\,\delta_B = \phi(r) , \tag{12}$$

where $\phi(r)$ is the function plotted in Fig. 5.

Single-Hinge Moments and Shears

Taking into account the inertia forces, $-m\,x\,\ddot{\theta}$, and the applied load, pb, per unit of length, the dynamic reaction R_B, shears V_B and bending moments M_B during motion are given non-dimensionally by:

$$\frac{R_B L}{M_p} = 3 + \frac{1}{r}e^{-t} \tag{13}$$

$$v_B(z) = \frac{V_B L}{M_p} = 3(1 - z^2) + \left(\frac{1}{r}e^{-t}\right)(1 - z)(1 - 3z) \tag{14}$$

$$m_B(z) = \frac{M_B}{M_p} = \frac{1}{2}z(3 - z^2) + \left(\frac{1}{r}e^{-t}\right)\frac{1}{2}z(1 - z)^2 , \tag{15}$$

where:

$$z = 2x/L \tag{16}$$

Figs. 6 and 7 give v_B and m_B versus z for $\frac{1}{r}e^{-t}$ varying between 1 and 10. These curves may be interpreted either as shear and bending moment diagrams at t = O for r varying between $\frac{1}{10}$ and 1, or as diagrams of a given beam, i.e., for a given value of r, as t grows from zero on. The diagrams corresponding to $\frac{1}{r}e^{-t} = 1$ are the static diagrams (straight line shear and parabolic moment).

The Spreading of the Central Hinge

An investigation of the first and second derivatives of m_B with respect to z shows that m_B is maximum at mid-span provided $r \geq 1/3$. Hence a single plastic hinge will be present at mid-span all through the motion for all

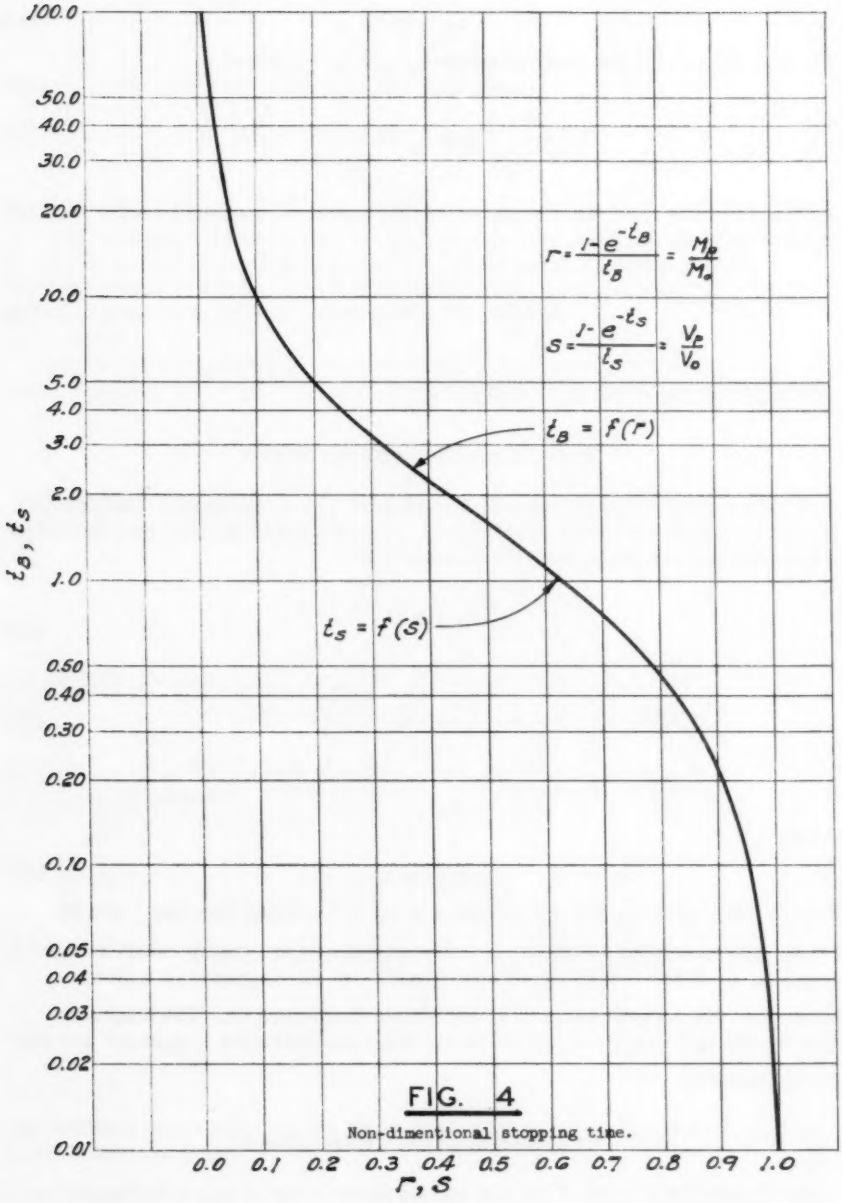

FIG. 4

Non-dimentional stopping time.

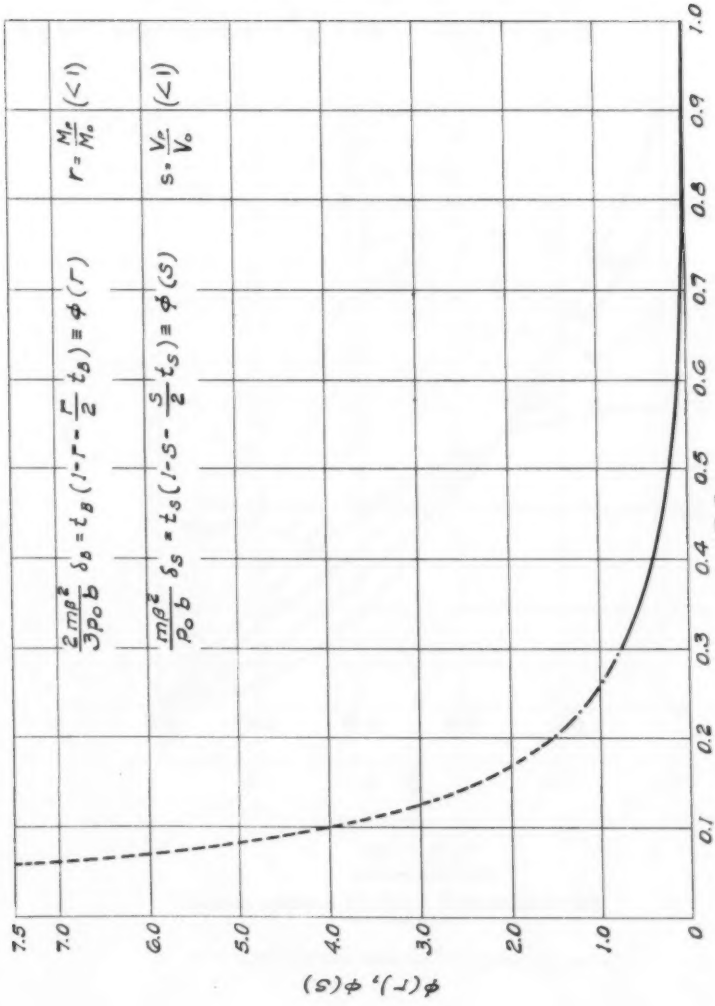

FIG. 5

Non-dimensional maximum displacements.

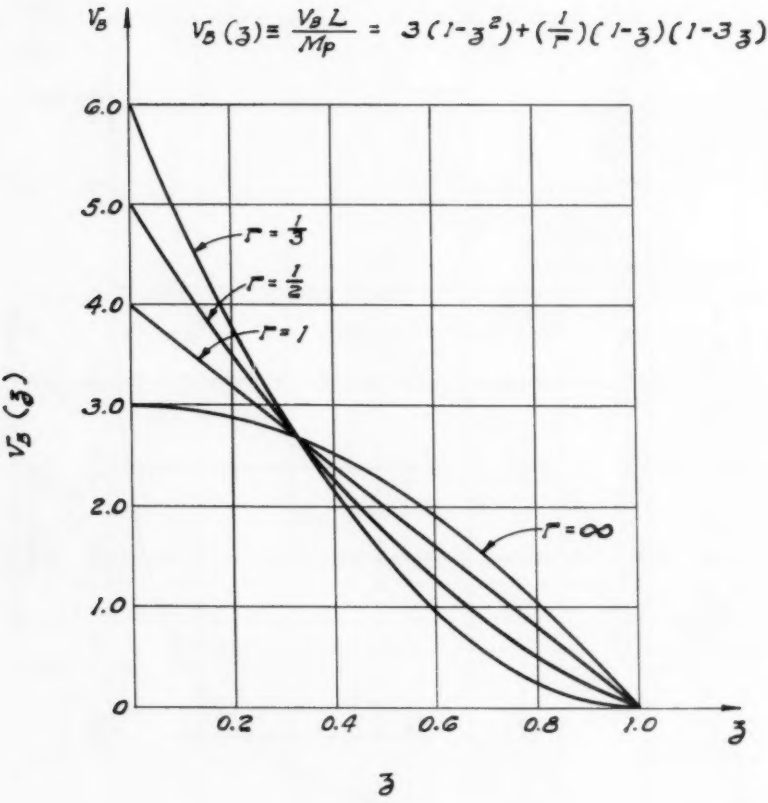

FIG. 6

Non-dimensional shear in bending motion.

$$m_B(\zeta)\Big]_{t=0} \equiv \frac{M_B}{M_P} = \frac{1}{2}\zeta(3-\zeta^2) + \left(\frac{1}{r}\right)\frac{1}{2}\zeta(1-\zeta)^2$$

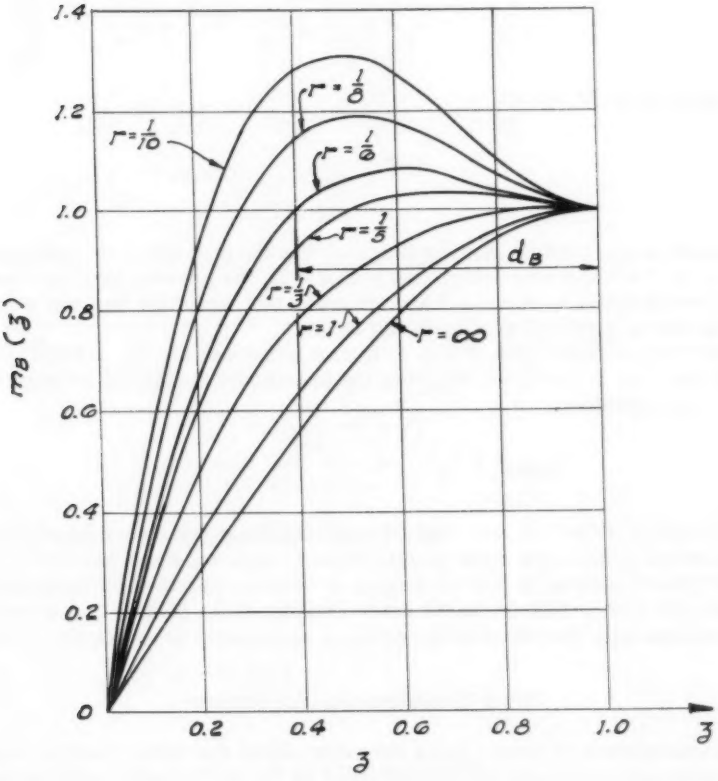

FIG. 7

Non-dimensional moments in bending motion.

beams for which:

$$\frac{8k_1A}{bL}\left(\frac{h}{L}\right) \leq \frac{p_o}{s_o} \leq \frac{24k_1A}{bL}\left(\frac{h}{L}\right) \tag{17}$$

For $r < 1/3$, m_B is equal to 1 and minimum at mid-span, maximum at:

$$z_1 = \frac{1}{3}\frac{\frac{1}{r}e^{-t} + 3}{\frac{1}{r}e^{-t} - 1} \tag{18}$$

and again equal to one at:

$$z_2 = \frac{2}{\frac{1}{r}e^{-t} - 1}\,. \tag{19}$$

Inasmuch as the bending moment diagram was derived under the assumption that $m_B \leq 1$ at all points (single hinge at $z = 1$), the present analysis breaks down theoretically when $r < 1/3$ and indicates that when this happens plasticity will spread to a central portion of the beam.

However, an inspection of Fig. 8, (giving graphs of m_B for $1/6<r<1/3$), shows that, for $1/5<r<1/3$, m_B remains practically horizontal between $z = 1$ and $z = z_2$, and that:

$$m_{B,max.} = m_B(z_1) < 1.04 \quad \text{for} \quad r > 1/5\,. \tag{20}$$

Hence, when $1/5<r<1/3$, the single-hinge analysis gives a good approximation of the actual motion of a rigid-plastic beam of constant mass per unit length, whose central section is only 4% weaker in bending than the adjoining sections. In view of the uncertainties in the determination of the plastic flow stress s_o, this analysis may therefore be accepted as sufficiently accurate for $1/5<r<1$.

Final Displacements and Strains

The assumption of rigid-plastic behavior allows the determination of displacements and rotations, and in particular of the final plastic angle at the central hinge (Fig. 9):

$$\theta_f = \frac{2\,\delta_B}{L}\,. \tag{21}$$

In order to evaluate strains it becomes necessary to take again into consideration the elastic behavior of the material.

If the time of maximum deflection is large in comparison with the period of the fundamental bending mode of the beam, the influence of the strain rate on the magnitude of the final strains may be ignored and the final strains may be evaluated as if the dynamic bending moment diagram were applied statically to an elasto-plastic beam. This also implies that s_o may be chosen equal to the static flow stress.

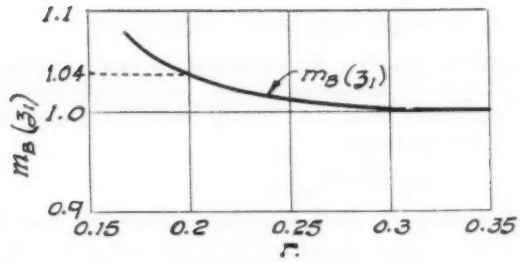

Moment at mid-span.

FIG. 8

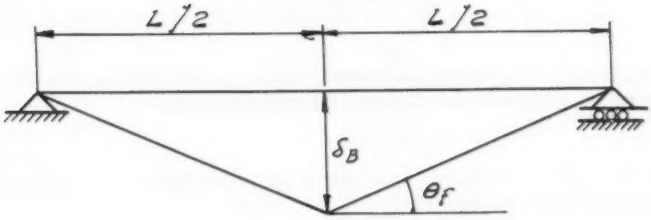

Plastic angle.

FIG. 9

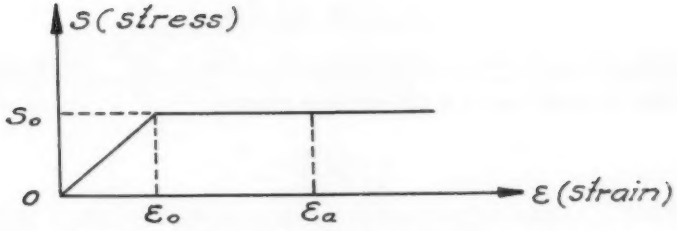

Elasto-plastic stress-strain diagram.

FIG. 10

The stress-strain diagram for an elasto-plastic material is given in Fig. 10, where ε_o indicates the maximum elastic strain and s_o the corresponding maximum elastic stress or flow stress.

Indicating by M_e the capacity elastic moment of the beam:

$$M_e = s_o S_e \tag{22}$$

where S_e is the elastic section modulus, the stress at the extreme fibers of all the sections for which $M_B \geq M_e$ will be equal to s_o. Hence the extreme fiber stress will be s_o in a plastic zone from z = 1 (beam center) to $z = z_3$, where z_3 is the only real root of the equation:

$$m_B(z) = M_e/M_p \tag{23}$$

The ratio $M_e/M_p = S_e/S_p$ equals 2/3 for rectangular sections and one for ideal I sections.

At the time t_B of maximum displacement, the abscissa z_3 limiting the plastic zone is defined by the equation:

$$\frac{1}{2} z(3-z^2) + \frac{1}{r} e^{-t_B} \qquad \frac{1}{2} z(1-z)^2 = M_e/M_p \ . \tag{24}$$

Since z_3 decreases with r and increases with time, as seen by the curves of Fig. 7, the largest non-dimensional width of the plastic zone:

$$d_B = 1 - z_3 \tag{25}$$

is obtained for r = 1/5 at t = O, and may either be taken from the graphs of Fig. 8, or computed from the equation:

$$\frac{1}{2} z(3 - z^2) + (5) \frac{1}{2} z(1 - z)^2 = M_e/M_p \tag{26}$$

d_B is given in Fig. 11 as a function of M_e/M_p for r = 1/5.

When r > 1/3 and motion occurs with a single hinge, the extreme fibers of the central section are displaced by an amount (Fig. 12):

$$u_o = \frac{h}{2} \theta_f = \frac{h}{L} \delta_B \tag{27}$$

Assuming that u_o is evenly distributed over a length $\frac{d_B/L}{2}$ we obtain a lower bound for the final strain at the extreme fibers:

$$\varepsilon_f = \frac{2u_o}{L d_B} \ . \tag{28}$$

When r < 1/3 the beam (Fig. 13) presents a kink at C and also a plastic curvature over the plasticized portion of the beam from C to D. But while the kink angle θ_c varies substantially with the value of r and can only be determined by a complete solution of the rigid-plastic problem, the final angle θ_f between the rigid portions of the beam and the horizontal is insensitive to the values of r, particularly if the motion is of the impulsive type.[3, 4] This means that while the displacement u_o is theoretically concentrated at the mid-span section in the single-hinge analysis, it is distributed over a length ℓ if r < 1/3 and a plastic zone is developed. Hence an estimate of ε_f may still

be obtained by Eq. (28) for $r < 1/3$, and this estimate will be a bound lower than for $r > 1/3$, since u_o is smaller for a single-hinge than for a partially plastic beam.

A Criterion for Allowable Peak Pressure in Bending

A beam will be assumed to have reached its maximum allowable load when the final strain ε_f of Eq. (28) equals an allowable strain ε_a:

$$\frac{2u_o}{Ld_B} = \varepsilon_a . \tag{29}$$

The value of p_o defined by Eq. (29) is an upper bound of p_o since ε_f is a lower bound for the strain.

Substituting in Eq. (29), u_o from Eq. (27), δ_B from Eq. (12), and $\beta = p_o/k$ from Eq. (2), we obtain a transcendental equation for the maximum allowable peak pressure p_{oB} in the form:

$$\frac{B_1}{p_{oB}/s_o} \; \phi\left(\frac{B_1}{p_{oB}/s_o}\right) = B_2 \tag{30}$$

where:

$$B_1 = \frac{8k_1 Ah}{bL^2}, \quad B_2 = \frac{8}{3} d_B \varepsilon_a k_1 \frac{A}{b^2} \frac{ms_o}{k^2} \tag{31}$$

and ϕ is the function graphed in Fig. 5. The constants B_1 and B_2 are typical of the beam since the impulse k is assumed constant. Once a beam is chosen, i.e., B_1 and B_2 are given, Eq. (30) is easily solved by means of the graph of Fig. 14, giving $X\phi(X)$, where $X = B_1/(p_{oB}/s_o)$.

The Development of Plastic Slides

The beam of the previous sections develops a maximum static shear at the ends given by

$$V_o = \frac{1}{2} p_o b L \tag{32}$$

Indicating by τ_o the dynamic yield stress in shear of the material, which by the von Mises criterion equals:

$$\tau_o = s_o/\sqrt{3} , \tag{33}$$

the plastic capacity shear of the beam is:

$$V_p = \tau_o A. \tag{34}$$

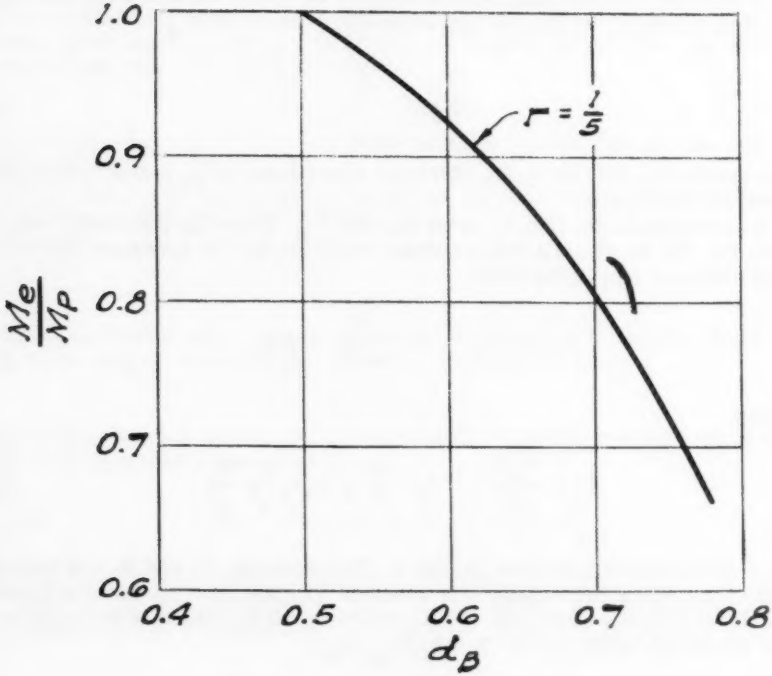

Width of plasticized zone.

FIG. 11

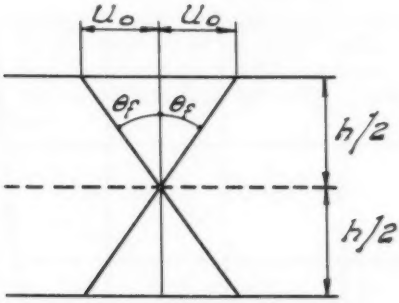

Plastic longitudinal displacement at mid-span.

FIG. 12

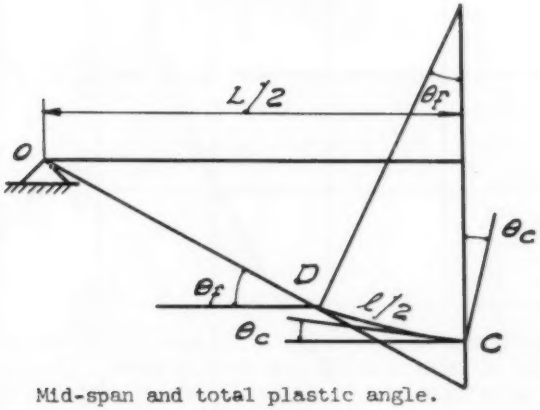

Mid-span and total plastic angle.

FIG. 13

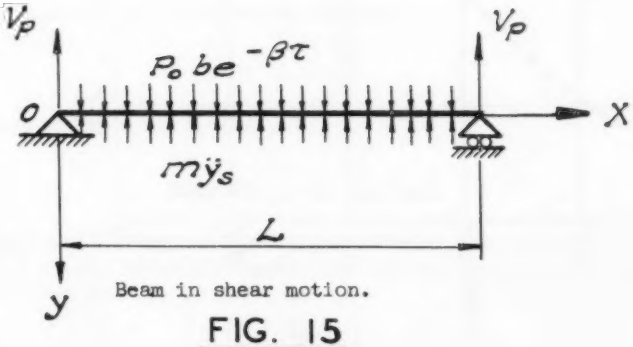

Beam in shear motion.

FIG. 15

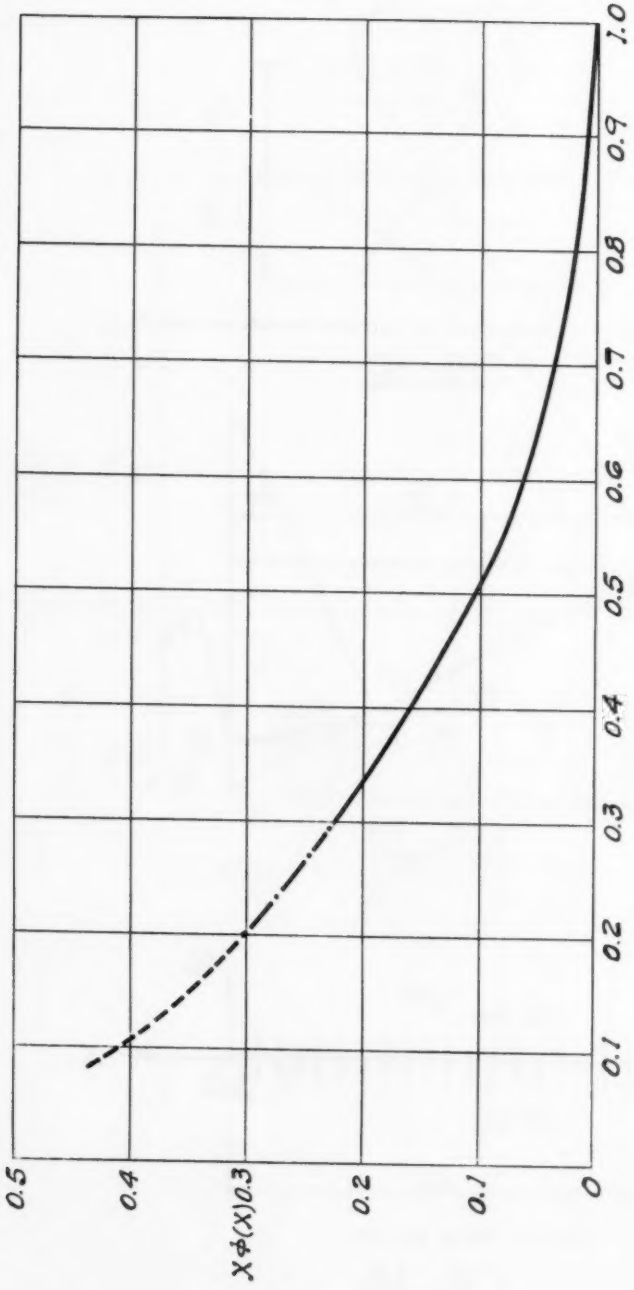

Function for evaluation of allowable peak pressure in bending motion.

FIG. 14

Whenever the beam dimensions make it stronger in bending than in shear and V_o is larger than V_p, the end sections of the beam become entirely plastic in shear and the beam moves downward as a rigid body along two "plastic shear slides", while the end shears maintain the value V_p. Plastic slides will thus occur if p_o is larger than:

$$p_{oS,\,min.} = \tau_o \frac{2A}{bL} . \tag{35}$$

Slide Displacements

Referring the beam motion to the axes of Fig. 15, the beam acceleration is given by:

$$\ddot{y}_s = \frac{p_o b}{m} e^{-t} - \frac{2V_p}{mL} , \tag{36}$$

from which by double integration with rest conditions:

$$\frac{m\beta^2}{p_o b} y_s = (e^{-t} + t - 1) - \frac{s}{2} t^2 , \tag{37}$$

where:

$$s = V_p/V_o \ (< 1). \tag{38}$$

A comparison of Eq. (37) with Eq. (8) shows that the law of motion of the center section of the beam in bending is identical with the law of motion in shear provided m be substituted for $\frac{2}{3}$ m and r be equal to s. Hence the maximum deflection in shear δ_S is given by:

$$\frac{m\beta^2}{p_o b} \delta_S = \phi(s) \tag{39}$$

and occurs at a time t_S defined by the equation:

$$1 - e^{-t_S} - s\, t_S = 0 . \tag{40}$$

$\phi(s)$ appears in Fig. 5 and t_S in Fig. 4.

Slide Shears and Moments

The shear and bending moment diagrams during slide motion are the static diagrams of a beam uniformly loaded, with end reactions equal to V_p. They are given in non-dimensional form by:

$$v_S = \frac{V_S}{V_p} = 1 - z \tag{41}$$

$$m_S = \frac{M_S}{V_p L} = \frac{1}{2} z(1 - \frac{1}{2} z) \tag{42}$$

Final Shear Strains

When the time of maximum shear displacement is larger than the fundamental shear period of the beam, shear strains may be approximated by assuming that the beam behaves elasto-plastically in shear, as shown in Fig. 16, where γ_o is the maximum elastic shear strain and τ_o the corresponding flow stress.

The portion of the beam ends in which the neutral plane fibers reach the strain γ_o is determined non-dimensionally from the shear diagram of Eq. (41) by letting:

$$v_S = 1 - z = V_e/V_p \,, \tag{43}$$

where V_e is the maximum elastic shear. Since $V_e/V_p = 2/3$ for rectangular sections and is more than 2/3 for I sections, the non-dimensional width d_S of the plastic shear zones varies between 1/3 and zero.

For deep beams the elastic shear distribution across the depth of the beam differs from the distribution in shallow beams, and the maximum elastic strain does not occur at the neutral axis, as assumed above. But since the value of V_e does not vary substantially with the depth of the beam, if $h < L/4$, the evaluation of d_S may still be obtained from Eq. (43).

The value of the final strain γ_f is then obtained by means of δ_S and d_S (Fig. 17):

$$\gamma_f = \frac{2\delta_S}{d_S L} \,. \tag{44}$$

A Criterion for Allowable Peak Pressure in Shear

A beam will be assumed to have reached its maximum allowable load when its final shear strain γ_f of Eq. (44) equals an allowable shear strain γ_a:

$$\frac{2\delta_S}{d_S L} = \gamma_a \,. \tag{45}$$

Substituting in Eq. (45) δ_S from Eq. (39), and β from Eq. (2), we obtain the transcendental equation for the maximum allowable peak stress in shear in the form:

$$\frac{S_1}{p_{oS}/\tau_o}\, \phi\left(\frac{S_1}{p_{oS}/\tau_o}\right) = S_2 \tag{46}$$

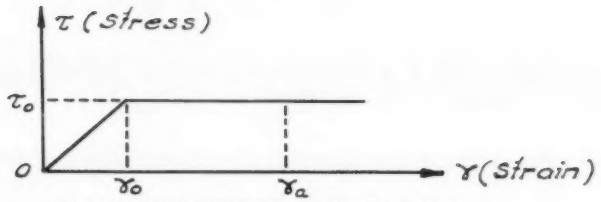

Elasto-plastic shear stress-strain diagram.

FIG. 16

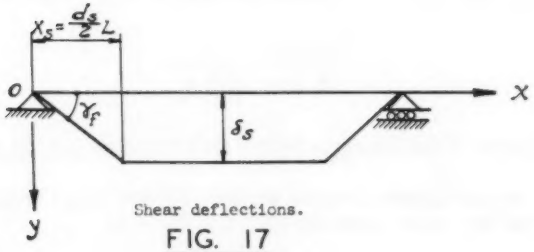

Shear deflections.

FIG. 17

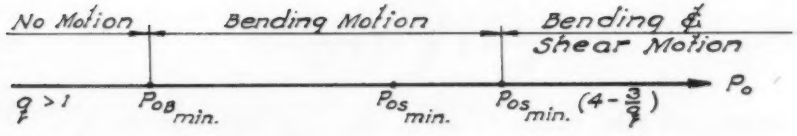

$$q = \frac{1}{4\sqrt{3}k_1}\frac{L}{h} = \frac{s}{r}$$

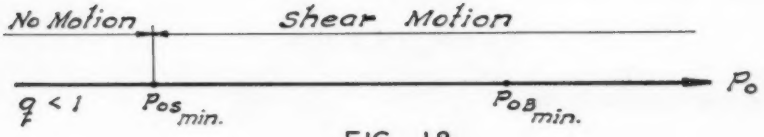

FIG. 18

Bending, shear and bending and shear motion possibilities.

where:

$$S_1 = \frac{2A}{bL} \quad ; \quad S_2 = \gamma_a d_S \frac{A}{b^2} \frac{m \tau_o}{k^2} \tag{47}$$

The constants S_1 and S_2 are typical of the beam. Equation (46) is easily solved by the graph of Fig. 14, where $x = s_1/(p_{oS}/\tau_o)$.

The Possibility of Simultaneous Shear and Bending Displacements

It was proved in Secs. 2 and 8 that bending motion can only start at a value of the pressure given by Eq. (4), and shear motion at a value of the pressure given by Eq. (35), but it is easy to see that, if the parameter:

$$q = \frac{p_{oS,min}}{p_{oB,min}} = \frac{1}{4\sqrt{3}\, k_1} \frac{L}{h} = \frac{s}{r}, \tag{48}$$

which is typical if the beam, is less than 1, bending motion can never take place.

In fact, the maximum dynamic moment during shear motion is independent of p_o and has the value, given by Eq. (42) at $z = 1$:

$$M_{S,max.} = \frac{1}{4} V_p L$$

and this moment cannot be larger than M_p if $q < 1$, since:

$$\frac{M_{S,max}}{M_p} = \frac{1}{4} \frac{V_p L}{M_p} = \frac{1}{4} \frac{\tau_o AL}{k_1 s_o Ah} = q \tag{49}$$

On the other hand, when $q > 1$ and $p_o > p_{oB,min}$ (and hence also $p_o > p_{oS,min} = p_{oB,min}/q$), shear and bending motions may occur simultaneously provided the maximum dynamic bending reaction R_B at $\tau = 0$ be larger than the shear capacity V_p, i.e., by Eq. (13) if:

$$R_B L = 3M_p + M_o > V_p L .$$

Solving this equation for M_o:

$$M_o = \frac{1}{8} p_o b L^2 > V_p L - 3M_p = \tau_o AL - s_o k_1 Ah,$$

and, substituting τ_o from Eq. (35) and s_o from Eq. (4), the value of p_o capable of inducing bending and shear motion is:

$$p_o > 4p_{oS,min} - 3p_{oB,min} = p_{oS,min}\,(4 - 3/q) . \tag{50}$$

Hence when $q > 1$, bending motion occurs for $p_{oB,min} < p_o > p_{oS,min}\,(4 - 3/q)$, and simultaneous bending and shear motion develops for $p_o > p_{oS,min}$

(4-3/q). Fig. 18 shows the various types of possible motion in a bending and shear beam.

Simultaneous Slide and Hinge Displacements ($q > 1$)

Indicating by $\ddot{y}_A$ the acceleration of the left end of the beam and by α its angular acceleration, Fig. 19, the equations of motion in bending and shear become:

$$- V_p + \frac{p_o bL}{2} e^{-t} = \frac{1}{2} mL \ddot{y}_A + \frac{1}{8} mL^2 \alpha$$

$$- M_p + \frac{p_o bL^2}{8} e^{-t} = \frac{1}{8} mL^2 \ddot{y}_A + \frac{1}{24} mL^3 \alpha \qquad (51)$$

from which:

$$\ddot{y}_A = \frac{p_o b}{m} e^{-t} + \frac{24M_p}{mL^2} - \frac{8V_p}{mL} \qquad (52)$$

$$\alpha = \frac{24V_p}{mL^2} - \frac{96M_p}{mL^3} \qquad (53)$$

The acceleration of the center of the beam is $\ddot{y}_C = \ddot{y}_A + \frac{L}{2} \alpha$ or:

$$\ddot{y}_C = \frac{p_o b}{m} e^{-t} - \frac{24M_p}{mL^2} + \frac{4V_p}{mL} \quad . \qquad (54)$$

Integrating Eqs. (53) and (54) with rest conditions and letting:

$$s_A = (4 - 3/q)s \; ; \qquad r_C = (3 - 2q)r \qquad (55)$$

we obtain:

$$\frac{m\beta^2}{p_o b} y_A = e^{-t} - 1 + t - \frac{s_A}{2} t^2 \; , \qquad (56)$$

$$\frac{m\beta}{p_o b} \dot{y}_A = 1 - e^{-t} - s_A t \; , \qquad (57)$$

$$\frac{m\beta^2}{p_o b} y_C = e^{-t} - 1 + t - \frac{r_C}{2} t^2 \; , \qquad (58)$$

$$\frac{m\beta}{p_o b} \dot{y}_C = 1 - e^{-t} - r_C t \; , \qquad (59)$$

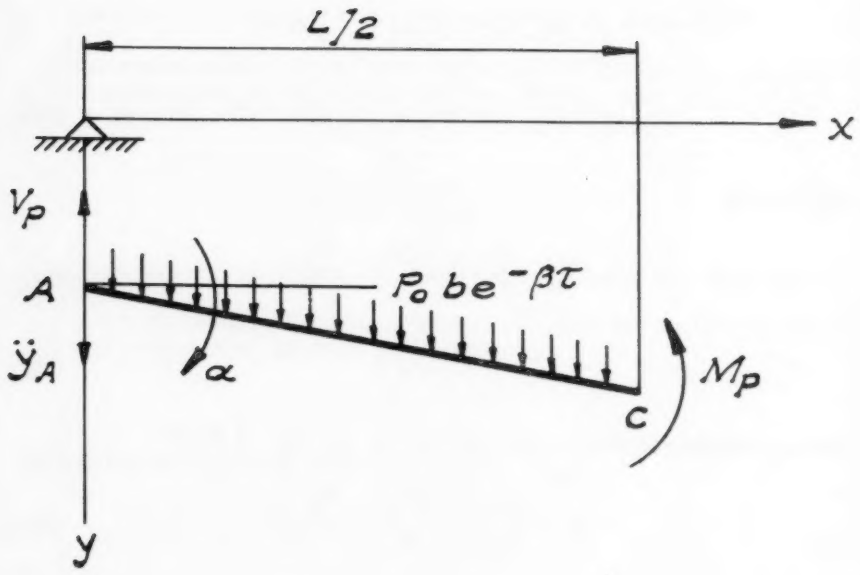

FIG. 19

Beam in bending and shear motion.

and the relative displacement and speed of C with respect to A:

$$\frac{m\beta^2}{p_o b}\,(y_C - y_A) = 3r\,(q-1)\,t^2\ , \tag{60}$$

$$\frac{m\beta}{p_o b}\,(\dot{y}_C - \dot{y}_A) = 6r\,(q-1)\,t\ . \tag{61}$$

The motion of A ends when $\dot{y}_A = 0$, i.e., at a time t_A defined by the equation:

$$1 - e^{-t_A} - s_A t_A = 0\ , \tag{62}$$

and obtainable directly from Fig. 4 with $s = s_A$.

The absolute motion of C ends when $\dot{y}_C = 0$, i.e., at a time t_C defined by the equation:

$$1 - e^{-t_C} - r_C t_C = 0 \qquad (r_C > 0) \tag{63}$$

and obtainable directly from Fig. 4 with $r = r_C$.

Since by Eq. (55) with $q > 1$:

$$s_A = 4 - 3/q > 3 - 2q = r_C\ , \tag{64}$$

and $t = f(r)$ is a decreasing function of r:

$$t_A < t_C \tag{65}$$

and A stops before C.*

The maximum displacement δ_A of A is given by Eq. (39) with $s = s_A$:

$$\frac{m\beta^2}{p_o b}\,\delta_A = \phi\,(s_A)\ . \tag{66}$$

The displacement δ'_C and velocity v_C of C at $t = t_A$ by Eqs. (60) and (61) are:

$$\frac{2}{3}\,\frac{m\beta^2}{p_o b}\,\delta'_C = 2r\,(q-1)\,t_A^2\ , \tag{67}$$

$$\frac{2}{3}\,\frac{m\beta}{p_o b}\,v_C = 4r\,(q-1)\,t_A\ . \tag{68}$$

*Since the translational motion stops before the rotational motion, there is no jump in momentum at $t = t_A$.

Since at $t = t_A$ the motion of the beam ends stops, the additional motion of C for $t > t_A$ is single-hinge motion with initial conditions:

$$y_C]_{t-t_A=0} = \delta \qquad \dot{y}_C]_{t-t_A=0} = v_C \,. \tag{69}$$

Under the assumption of small displacements, y_C is added to δ'_C to obtain the total displacement for C for $t > t_A$.

Letting:

$$t' = t - t_A \tag{70}$$

integration of Eq. (5), where $\ddot{\theta} = 2\ddot{y}_C/L$ with the initial conditions of Eqs. (69) gives:

$$\frac{2}{3}\frac{m\beta^2}{p_o b} y_C = e^{-t_A}(e^{-t'} - 1 + t') - \frac{r}{2}t'^2 + 4r(q-1)t_A.t' \,, \tag{71}$$

$$\frac{2}{3}\frac{m\beta}{p_o b}\dot{y}_C = e^{-t_A}(1-e^{-t'}) - r\,t' + 4r(q-1)t_A \,, \tag{72}$$

The motion of C stops when $\dot{y}_C = 0$, i.e., at a time t'_C defined by the equation:

$$e^{-t_A}(1 - e^{-t'_C}) - r\,t'_C = -4r(q-1)t_A. \tag{73}$$

Since t_A is a function of r and q, t'_C is also a function of these variables:

$$t'_C = f_C(r,q) \,; \tag{74}$$

f_C is plotted in Fig. 20 versus r with q as a parameter.

Substitution of t'_C from Eq. (74) in Eq. (71) gives the maximum value δ''_C of y_C:

$$\frac{2}{3}\frac{m\beta^2}{p_o b}\delta''_C = t'_C\left[e^{-t_A} - r\left(1 + \frac{t'_C}{2} - 4(q-1)t_A\right)\right] + 4r(q-1)t_A \,,$$

or:

$$\frac{2}{3}\frac{m\beta^2}{p_o b}\delta''_C = \phi_C(r,q) \,, \tag{75}$$

where $\phi(r, q)$ is the function plotted in Fig. 21 versus r with q as a parameter.

The maximum <u>relative</u> displacement δ_C of C with respect to A is the sum of δ'_C and δ''_C:

$$\frac{2}{3}\frac{m\beta^2}{p_o b}\delta_C = \psi(r,q), \tag{76}$$

where:

$$\psi(r,q) = 2r(q-1)[f(s_A)]^2 + \phi_C(r,q) \tag{77}$$

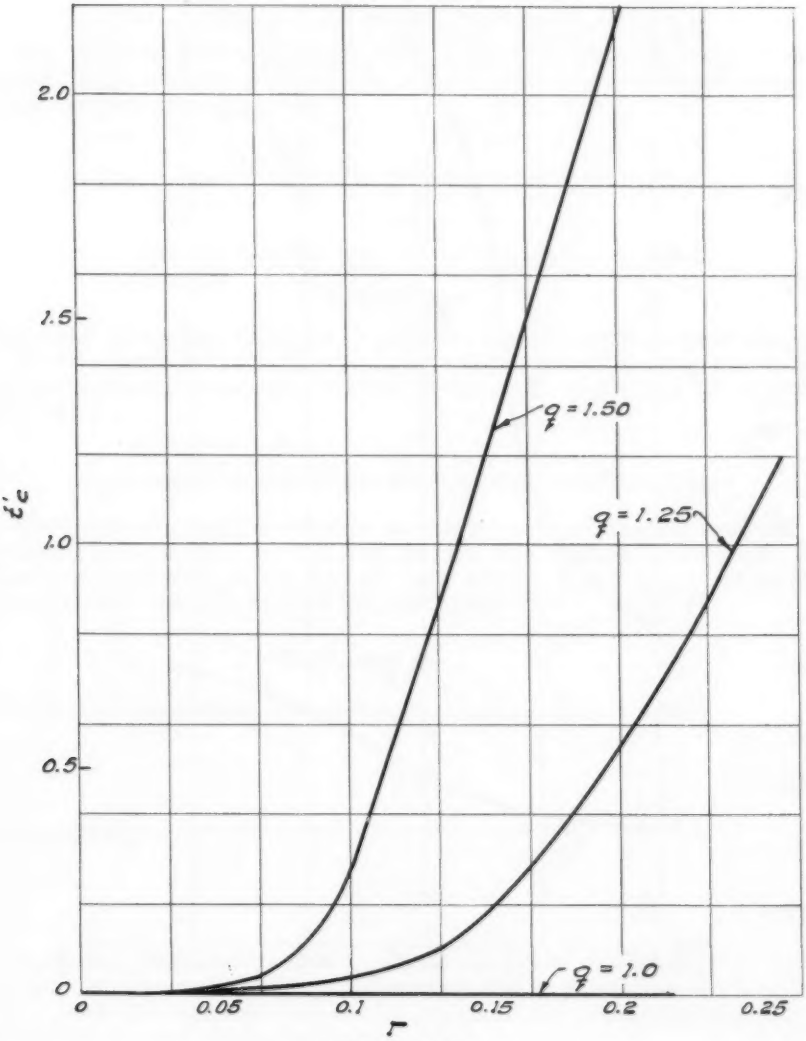

FIG. 20

Stopping time of mid-span in bending and shear motion.

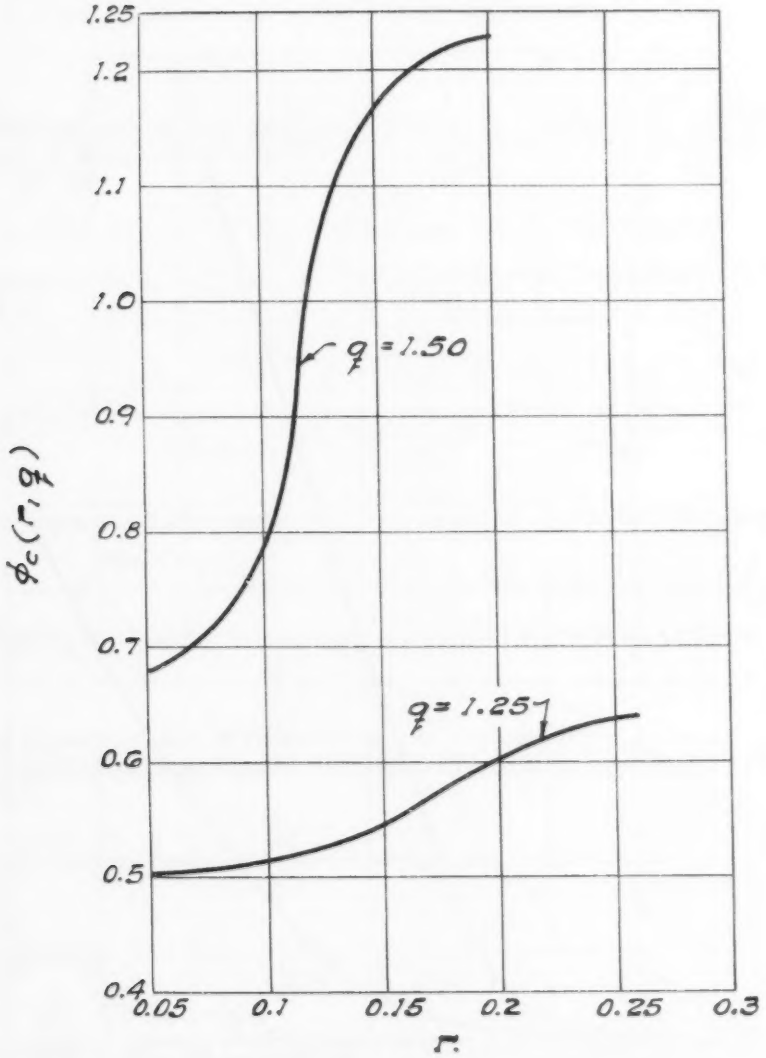

FIG. 21

Maximum bending displacement in bending and shear motion.

is given in Fig. 22 versus r with q as a parameter.

Slide-and-Hinge Shears and Moments

The expressions for the accelerations of Eqs. (52), (53), and (54) allow the evaluation of the inertia forces during the slide-and-hinge motion and hence of the shears and the moments:

$$v_{BS}(z) \equiv \frac{V_{BS}L}{M_p} = 4q\,(3z-1)(z-1) - 12\,z(z-1)\,, \tag{78}$$

$$m_{BS}(z) \equiv \frac{M_{BS}}{M_p} = 2q\,z(1-z)^2 + z^2\,(3-2z)\,. \tag{79}$$

The shear and moment diagrams are given in Figs. 23 and 24, respectively.

After the slide motion ends at $t = t_A$, the shears and moments are given by the bending motion equations, i.e., Eqs. (14) and (15), in which $t_A + t'$ is substituted for t.

Spreading of the Central Hinge in Slide-and-Hinge Motion

The single hinge analysis fails as soon as the moment diagram becomes minimum at $z = 1$; from Eq. (86) it is seen that this happens when $q = 3/2$. Since slide-and-hinge motion can only occur if $q > 1$, this phase of motion only takes place for beams satisfying the limitations:

$$1 < q < 3/2\,. \tag{80}$$

When $q > 3/2$ the moment is maximum at:

$$z_1' = \frac{1}{3}\,\frac{q}{q-1} \tag{81}$$

and equals M_p at:

$$z_2' = \frac{2q-3}{2q-2}\,. \tag{82}$$

The graph of Fig. 25 shows that if $q \leq 2$ the moment is at most equal to 1.04 M_p and that, hence, the single-hinge analysis may be considered practically valid, since it is rigorously correct for beams having a center section only 4% weaker than the neighboring sections.

After the slide motion stops, at $t = t_A$, the single-hinge analysis theoretically fails for:

$$r < \frac{1}{3}\,e^{t_A} \tag{83}$$

As shown in Sec. 5, the analysis is still practically acceptable (within 4% accuracy in the maximum moment) provided $r < \frac{1}{5}\,e^{t_A}$.

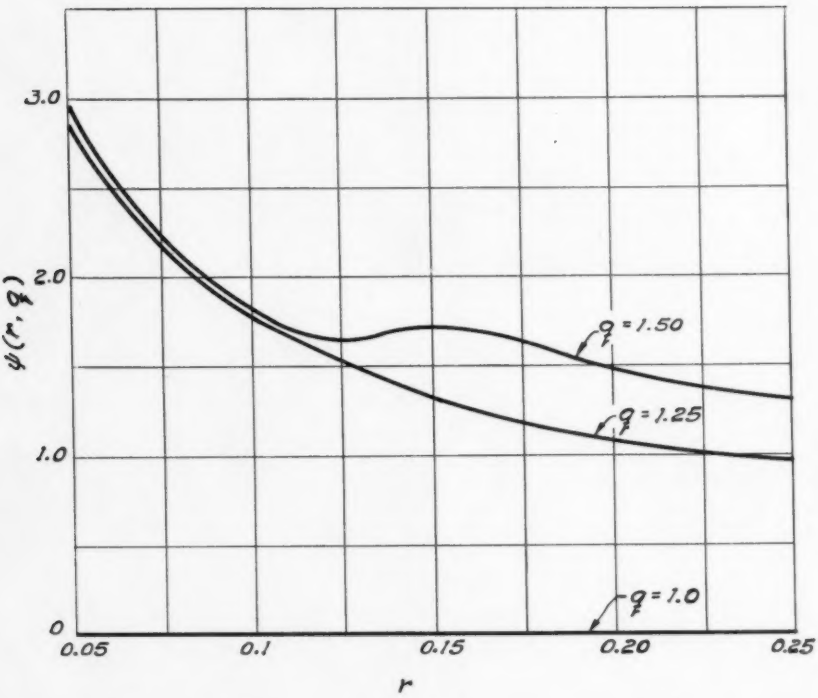

Maximum displacement of mid-span relative to beam ends in bending and shear motion.

FIG. 22

$$V_{BS}(\zeta) = \frac{V_{BS}\,L}{M_p} = 4q_f(3\zeta-1)(\zeta-1) - 12\zeta(\zeta-1)$$

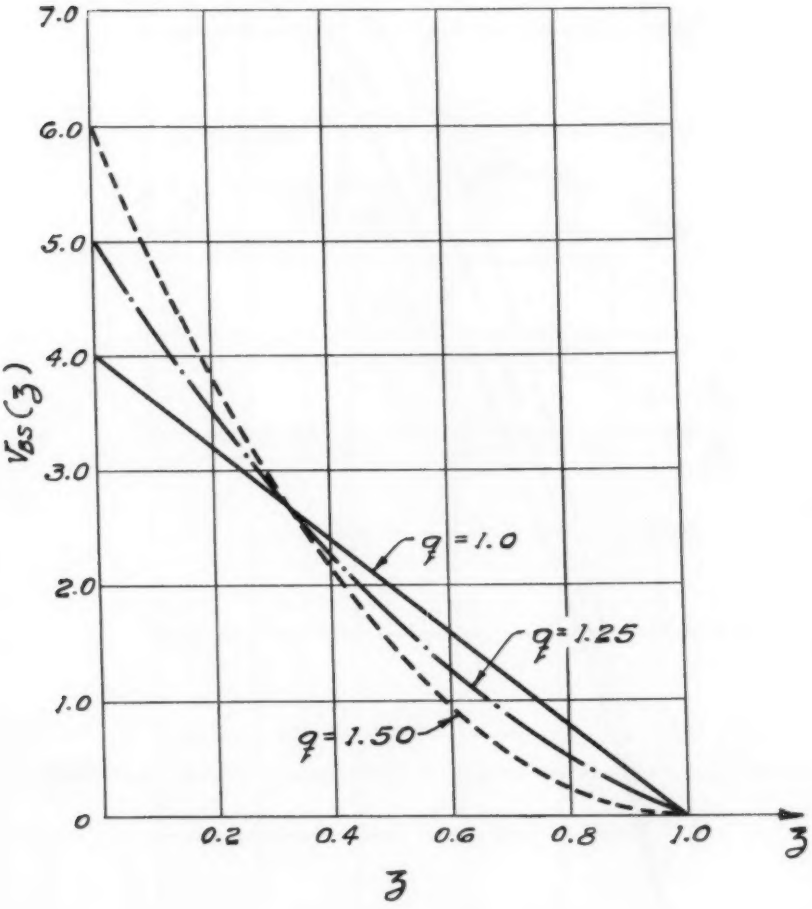

FIG. 23

Non-dimensional shear in shear and bending motion.

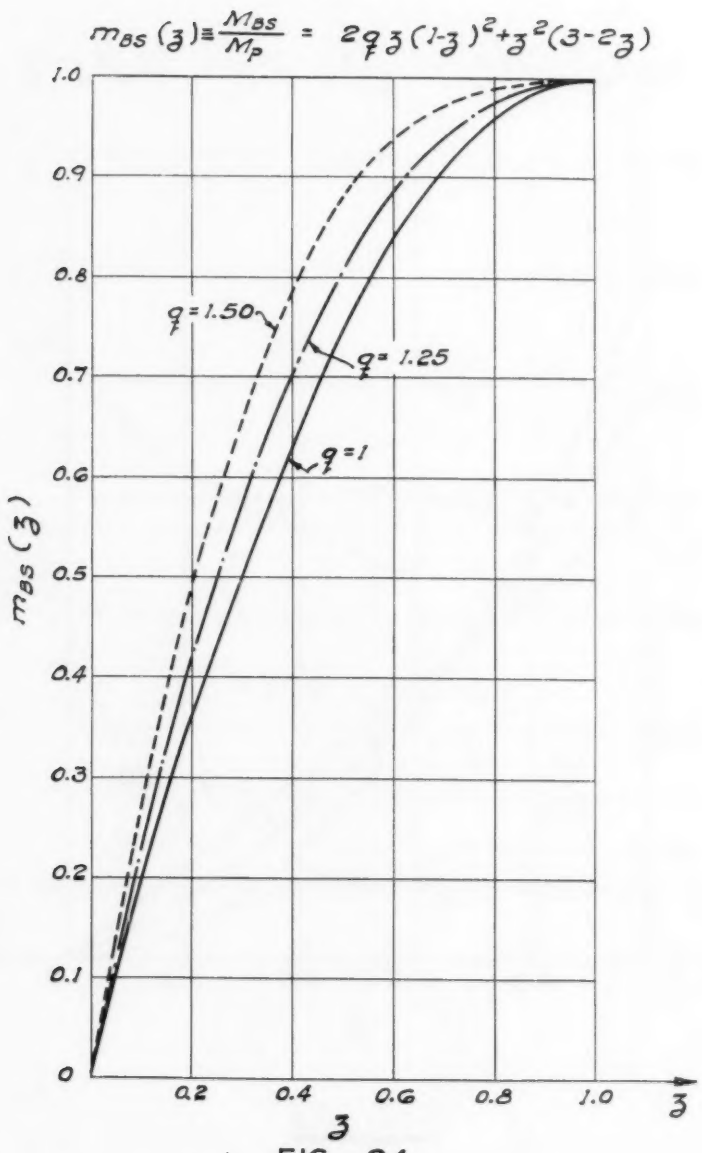

FIG. 24

Non-dimensional moment in shear and bending motion.

$$z_1' = \frac{1}{3}\left(\frac{q}{q_f} - 1\right)$$

$$m_{BS}(z_1') = 2\frac{q}{q_f} z_1'(1 - z_1')^2 + (z_1')^2(3 - 2z_1')$$

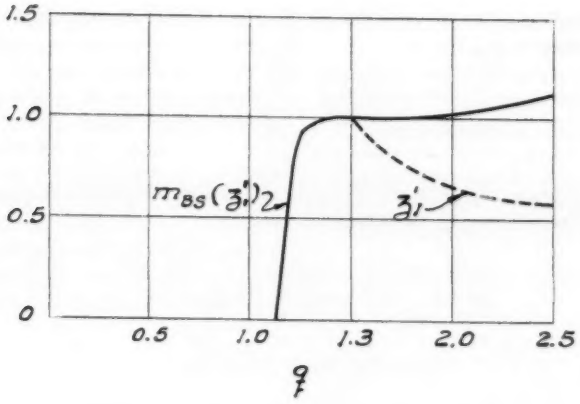

FIG. 25

Non-dimensional maximum bending moment diagram in bending and shear motion.

It can be shown that additional slides cannot develop and the end slides cannot spread during bending-and-shear motion of beams with constant bending strength under uniform pressure, although additional slides may appear (starting at the quarter points) in beams with weakened center sections which prevent the spreading of the central hinge.

Criteria for Allowable Peak Pressures in Slide-and-Hinge Motion

In the case of slide-and-hinge motion the peak allowable pressure may be determined either by shear or by bending.

When shear governs, the non-dimensional width of the plastic zone, d'_S, is evaluated from the equation:

$$v_{BS} = V_e L/M_p \tag{84}$$

or from the graph of Fig. 23, and the final shear strain is equated to the allowable shear strain γ_a:

$$\gamma'_f = \frac{2\delta_A}{d'_S L} = \gamma_a . \tag{85}$$

Substituting δ_A from Eq. (66) and β from (2), the transcendental equation defining the peak pressure p'_{oS} in shear becomes:

$$\frac{S'_1}{p'_{oS}/\tau_o}\ \phi\left(\frac{S'_1}{p'_{oS}/\tau_o}\right) = S'_2 , \tag{86}$$

where:

$$S'_1 = (4-3/q)\frac{2A}{bL} \quad ; \quad S'_2 = (4-3/q)\gamma_A d'_S \frac{A}{b^2}\frac{m\tau_o}{k^2} . \tag{87}$$

Equation (86) is easily solved by the graph of Fig. 14, where $X = S'_1/(p'_{oS}/\tau_o)$.

When bending governs, the non-dimensional width of the plastic zone d'_B is determined from the equation:

$$m_{BS} = M_e/M_p \tag{88}$$

or from Fig. 24, and the final strain ε'_f is equated to the allowable strain ε_a:

$$\varepsilon'_f = \frac{2u_o}{Ld'_B} = \varepsilon_a . \tag{89}$$

Substituting:

$$u_o = \frac{h}{L}\delta_C , \tag{90}$$

where δ_c is given by Eq. (76) and β from Eq. (2), the transcendental equation for the peak pressure p'_{oB} in bending becomes:

$$\frac{B_1}{p'_{oB}/s_o}\,\psi\left(\frac{B_1}{p'_{oB}/s_o}\,;\,q\right) = B'_2 \qquad (91)$$

where B'_2 is obtained from Eqs. (31) by substituting d'_B for d_B. Equation (91) is easily solved by the graphs of Fig. 26, where $X\,\psi(X,q)$ is plotted versus X with q as a parameter.

The lower of the two pressures p'_{oS} and p'_{oB} will be the allowable peak pressure in shear and bending motion.

CONCLUSIONS

The results of the present analysis allow the determination of upper bounds for allowable peak pressures of rigid-plastic beams under blast loads. Inasmuch as the total blast energy is assumed absorbed in plastic flow and strains are supposed to be evenly distributed, within the limits for which this analysis is valid, actual elasto-plastic beams will not take higher pressures for the given allowable strains.

The range of pressures, for which this simple analysis is valid, is limited because of the assumption of single-hinge development.

The typical behavior of beams with respect to shear and bending motion is clearly brought out by this treatment.

The analysis can be obviously extended to other types of beam supports and other types of impulsive loads.

ACKNOWLEDGEMENTS

The research leading to the results given above was sponsored by The RAND Corporation, Santa Monica, California.

BIBLIOGRAPHY

1. Lee, E. H., and Symonds, P. S., "Large Plastic Deformations of Beams under Transverse Impact", Transactions, ASME, Vol. 74, 1952, p. 308.
2. Salvadori, M. G. and DiMaggio, F., "On the Development of Plastic Hinges in Rigid-Plastic Beams", Quart. Appl. Math. Vol. XI, No. 2, July 1953.
3. Bleich, H. H. and Salvadori, M. G., "Impulsive Motion of Elasto-Plastic Beams," Transactions, ASCE, Vol. 120, 1955, p. 499.
4. Cotter, B. A. and Symonds, P. S., "Plastic Deformations of a Beam Under Impulsive Loading," Proc. ASCE, Vol. 81, April 1955, Sep. No. 675.

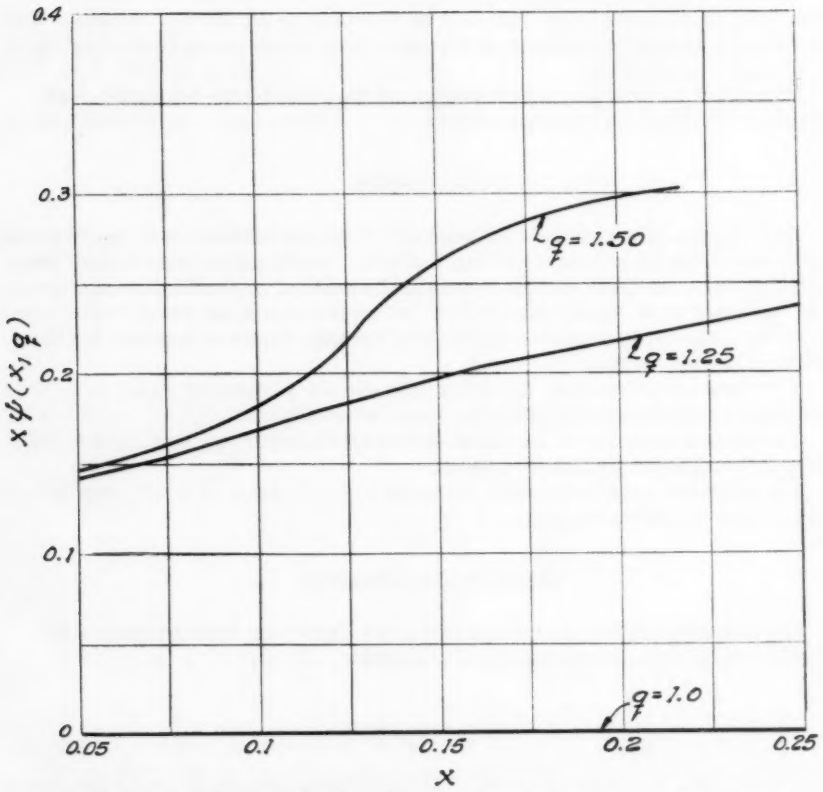

Function for the evaluation of allowable peak pressure in bending and shear motion.

FIG. 26

Paper 1390 October, 1957 EM 4

Journal of the
ENGINEERING MECHANICS DIVISION
Proceedings of the American Society of Civil Engineers

DEMONSTRATIONS OF PLASTIC BEHAVIOUR OF STEEL FRAMES[a]

H. M. Nelson,* D. T. Wright,** J.M. ASCE,
and J. W. Dolphin***
(Proc. Paper 1390)

SYNOPSIS

This paper presents the results of full scale tests which were made to illustrate the behaviour under load of structures designed by the plastic theory. The tests were made on beams, small scale frames, and a full scale pitched portal frame, all fabricated from standard rolled sections. Plastic analysis of moment redistribution was verified, and shear, instability and flange buckling effects were checked.

INTRODUCTION

The analytical basis for the Plastic Design of Steel Structures has been well established, and a large amount of testing has been carried out in connection with research.(1,2) Because of the unusual nature of Plastic Design, there appears to be some need for full-scale demonstration tests on practical structures and structural elements. However, the number of such tests which have been completed is still rather limited. The tests to be described were performed to supplement a course of lectures on Plastic Design of Steel Structures given at the Royal Military College and Queen's University in Kingston, Ontario, in May of 1956.(3) The tests were intended to demonstrate the characteristic behaviour under load of steel-framed structures and their elements - to show the accuracy of plastic methods of analysis and design, and to show the actual physical appearance of practical structures when loaded up to collapse.

Note: Discussion open until March 1, 1958. Paper 1390 is part of the copyrighted Journal of the Engineering Mechanics Division of the American Society of Civil Engineers, Vol. 83, No. EM 4, October, 1957.

a. Presented at a meeting of the American Society of Civil Engineers in Pittsburgh, Pa., October, 1956.

*Now lecturer in Civ. Eng., The University of Glasgow, Scotland.
**Asst. Prof. of Civ. Eng., Queen's University, Canada.
***Prof. and Head of Dept. of Civ. Eng., Royal Military College, Canada.

The tests are arranged to show:

i) the moment-curvature relationship characteristic of structural steel members,
ii) the fundamental idea of moment redistribution - the key to the plastic design of continuous structures,
iii) the correspondence of predicted and observed collapse form and loads,
iv) the effects of shear and instability,
v) the behaviour of a practical rigid frame when loaded up to and past the working range, and on to failure.

Testing Arrangements

Most of the tests were performed on a test-bed made up of a pair of heavy rolled steel beams. Loads were applied by hydraulic jacks, and measured by pressure gauges located on the oil line near the pumps. The gauges were calibrated by jacking against the weighing system of a conventional testing machine, and the rate of testing was slow enough for the arrangement to be sufficiently accurate for the intended purposes. Some other tests were performed in conventional testing machines. Dynamometers with electric resistance strain gauges as sensing elements were used to weigh reactions and measure loads in a few cases.

Slow rate coupon tests were made on each shape used and the results tabulated in Table 1 under the heading "Average Yield Stress." These coupons were cut from

a) a flange, extreme edge
b) same flange, adjacent to the web, on the side of the web away from (a).

The values of M_y, M_p and ultimate loads were calculated using the average of of the tensile yield stresses so found.

Deflections and deformations were measured by means of fixed telescopes trained on scales fastened to the element undergoing test. No measurements of strain whatsoever were made on any of the test pieces. It may be noted that except for special matters such as fatigue, the actual stresses in a structure are of no consequence providing the structure can support the required load without excessive deformation. It is an indication of the rational nature of plastic design that it is concerned with load-capacity and deformation of entire structures, rather than with stresses and strains.

Moment Curvature Relationship

The development of the plastic strength of steel frame structures depends on the formation of more or less fully plastic sections in the members. Deformation is concentrated at these sections, which behave as "stiff" hinges, and collapse occurs only when sufficient hinges have formed to transform the structure into a mechanism. In the theory the material is assumed to be ideally elasto-plastic, (i.e. perfectly elastic up to the yield stress and then able to strain indefinitely at constant stress), and it follows that the plastification of a standard structural shape will be as shown in Fig. 1. When the maximum fibre stress reaches the yield value it remains constant and, with

TABLE 1

Section	Area sq. in.	Depth in	Flange Width in	Flange Thick in	Web Thick in	Axis X - X I_{in^4}	Axis X - X S_{in^3}	Axis X - X Z_{in^3}	Axis X - X f	Av. Yield Stress p.s.i.
10 WF 25										
Handbook	7.35	10.08"	5.762	0.430	0.252	133.2	26.4	29.5	1.12	41,800
Measured	7.11	10.15	5.773	0.415	0.249	130.4	25.7	28.7	1.12	
% Variation	-3.4	+0.7	+0.3	-3.5	-1.2	-2.1	-2.6	-2.7	0	
8 B 13										
Handbook	3.83	8.00	4.000	0.254	0.230	39.5	9.88	11.35	1.15	45,000
Measured	3.71	8.03	3.937	0.236	0.245	37.1	9.25	10.75	1.16	
% Variation	-3.2	+0.4	-1.6	-7.1	+6.5	-6.5	-6.4	-5.3	+0.9	
4 B 13										
Handbook	3.82	4.00	3.937	--	0.250	10.4	5.2	6.11	1.17	47,300 (five frames)
Measured	3.62	3.98	3.867	0.360	0.255	10.0	5.0	5.82	1.16	38,000 (one frame)
% Variation	-5.2	-0.5	-1.8	--	+2.0	-3.9	-3.8	-4.7	-0.9	
6 WF 15.5										
Handbook	4.62	6.00	6.000	0.269	0.240	30.3	10.1	11.29	1.12	49,300
Measured	4.56	5.96	6.020	0.274	0.232	29.7	10.0	11.09	1.11	
% Variation	-1.3	-0.7	+0.3	+1.9	-3.3	-2.0	-1.0	-1.8	-0.9	
8 WF 17										
Handbook	5.00	8.00	5.250	0.308	0.230	56.4	14.1	15.8	1.12	47,250
Measured	5.07	8.02	5.275	0.309	0.245	56.8	14.2	16.1	1.14	
% Variation	+1.4	+0.3	+0.5	+0.3	+6.5	+0.4	+0.7	+1.9	+1.8	
6 B 12										
Handbook	3.53	6.00	4.000	0.279	0.230	21.7	7.24	8.25	1.14	45,300
Measured	3.56	5.99	3.975	0.283	0.242	21.6	7.21	8.20	1.14	
% Variation	+0.9	-0.2	-0.6	+1.4	+5.2	-0.7	-0.4	-0.6	0	

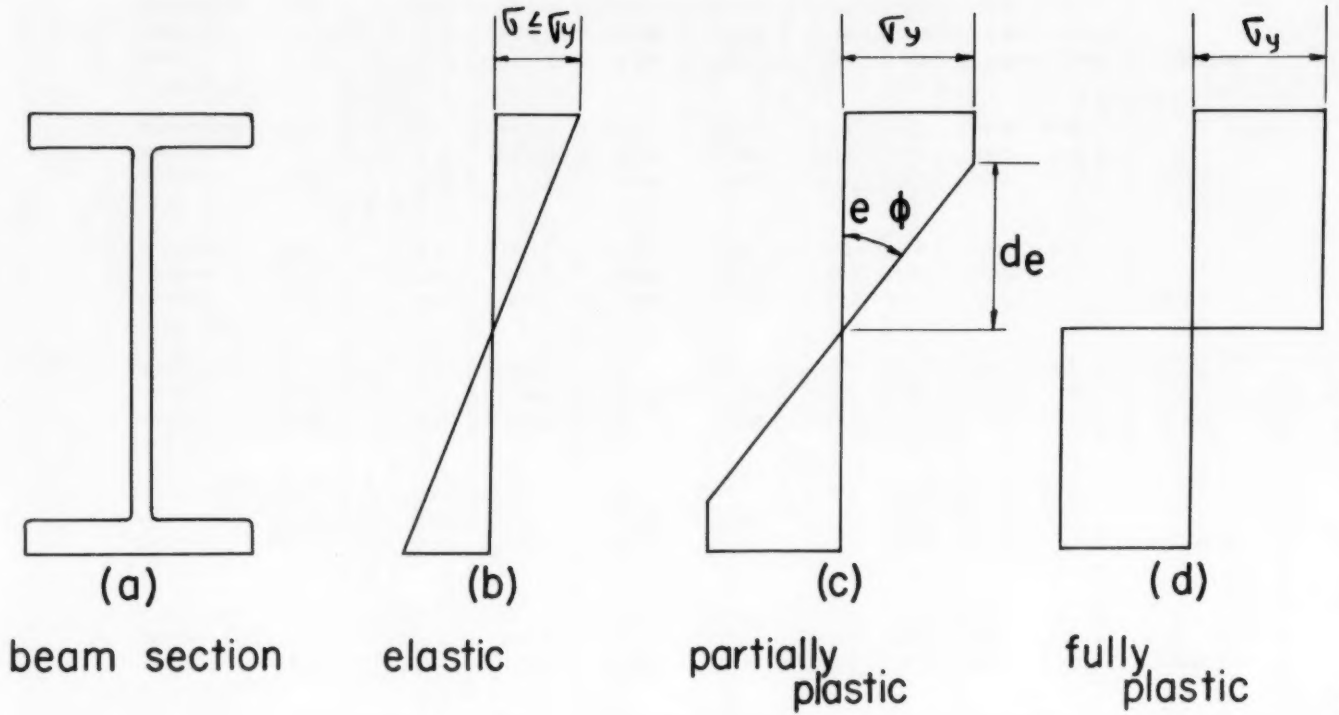

FIG. 1 STRESS DISTRIBUTIONS

increasing strain, yield penetrates the section until full plasticity is reached (Fig. 1d). Curvature can then increase indefinitely at a constant moment.

At any stage in the development of yielding the moment capacity can be found by taking moments of the stress blocks about the neutral axis. The curvature is easily obtained since, at the edge of the elastic core, the strain is just sufficient to cause yield, i.e., in Fig. 1c.

$$\varphi = \frac{\sigma_Y/E}{d_e}$$

At full plasticity the fully plastic moment

$$M_p = \sigma_y Z$$

where Z = Plastic Section modulus

$\cong$ 1.14 x Elastic modulus for WF and I sections

Figure 2 shows the results of a test on a 10WF 25 beam loaded at its third points. Curvature was measured by recording the change in distance between plates welded to the top and bottom flanges a distance of 10 inches apart as shown in Fig. 3. Section properties are given in Table 1.

The early divergence of the experimental curve in Fig. 2 from the predicted curve is due to local yielding caused by residual stresses in the beam. This was shown, during the test, by some flaking of mill scale at relatively low loads. In spite of this, the fully plastic moment capacity was realized, and the characteristic flat top of the M - ϕ curve demonstrates the ability of structural steel members to deform plastically. The extent of yielding is shown clearly in Fig. 3 by yield lines extending almost to the centre of the web. At the conclusion of the test the maximum strain in the extreme fibres was still below the work hardening level. Additional deformation would have finally caused strain hardening and a slight increase in moment capacity.

It should be noted that this simple test also reveals some of the inconsistency of conventional design methods. At the load at which maximum fibre stresses are presumed to just reach 20 ksi, yielding has already occurred due to residual stresses. Thus, if the load capacity of such a member was in fact limited to the load at which maximum stresses actually reached 20 ksi, (as implied in the usual specifications), steel design would be seriously and unnecessarily restricted. On the other hand, the ultimate load as predicted by plastic theory is attained in spite of such factors as residual stresses and imperfections.

For practical purposes it is most convenient to describe the moment-curvature relationship as shown in Fig. 4, using just the two tangent lines, and disregarding the curved transition between them. Although this approximation is obviously satisfactory in defining moment capacity at full plasticity (large curveture), it is less accurate for determining deformations at intermediate stages of partial plasticity.

Bending Moment Re-distribution

For the realization of the fully plastic load capacity of an indeterminate structure, it is necessary that once the most highly stressed section reaches

FIG. 2 MOMENT-CURVATURE RELATION

FIG 3 BEAM TESTED UNDER PURE BENDING, SHOWING EXTENT OF YIELDING AT CONCLUSION OF TEST

FIG.4 IDEALIZED MOMENT-CURVATURE RELATION

full plasticity deformation must occur there (without loss of strength) thereby allowing other parts of the structure to take an increasing share of the load. The simplest demonstration of this behaviour is given by the propped cantilever, which is only once indeterminate.

A 12 ft. span, 8 B 13 beam was rigidly fixed at one end and simply supported at the other, and loaded at a point 40 inches from the fixed end. Lateral supports were provided at the load point and at a point 48 inches from the propped end. The reaction at the prop was measured by a resistance strain gauge dynamometer. The results of the test, curves of bending moment and deflections, are given in Fig. 5. At a load of 28 kips, the support section reached full plasticity but continued to deform until, at a load of 31.5 kips., full plasticity was approached at the load point. The structure was then transformed into a mechanism, and the deflection at the load point increased under constant load.

The load at collapse can be readily calculated by plastic design methods. At collapse, fully yielded sections, i.e. plastic hinges, develop at A and B so that the bending moment diagram is defined,

$$\text{from Fig. 6b,} \quad M_p + \frac{b}{L} M_p = \frac{W.a.b}{L}$$

$$\text{and therefore} \quad W = M_p \frac{(L + b)}{ab}$$

For the section properties given in Table 1 and the dimensions given in Fig. 5 W = 29,300 lb. It is seen from Fig. 5 that not until this load is reached do the deflections become excessive. For purposes of this calculation the plastic hinge at the fixed end A was assumed at a point one half inch away from the face of the support. This results in the segments a and b becoming 39-1/2 inches and 103-1/2 inches respectively. Fig. 7 shows clearly the concentration of deformation in the two "hinge" locations indicated in Fig. 6c.

The combination of large shearing force and bending moment at the support section caused early yielding and a reduction in the fully plastic moment capacity at this section. Characteristic shear yield lines are shown in Fig. 8. On the other hand, and tending to compensate, the steep moment gradient at the clamped end leads to a very short yield zone there and large strains occur. The resulting strain hardening caused the moment at A to continue to increase as the moment at B approached a constant value.

In the test it was impossible to develop perfect fixity at the clamped end A. It may be noted that had A been perfectly fixed, M_A would have been equal to 1.88 times M_B in the elastic range. It may be seen from Fig. 5 that this difference was not realized. Nevertheless, the fully plastic strength of the structure was developed. In general, the rotation and settlement of supports while perhaps affecting the order of formation of plastic hinges, have no effect whatsoever in the ultimate plastic capacity so long as the required resistance at the support can be finally realized.

Simple Collapse Mechanisms

Rectangular portal frames, 8 ft in span and 4 ft high, fabricated throughout of 4B13 section, were tested to failure under three kinds of loading:

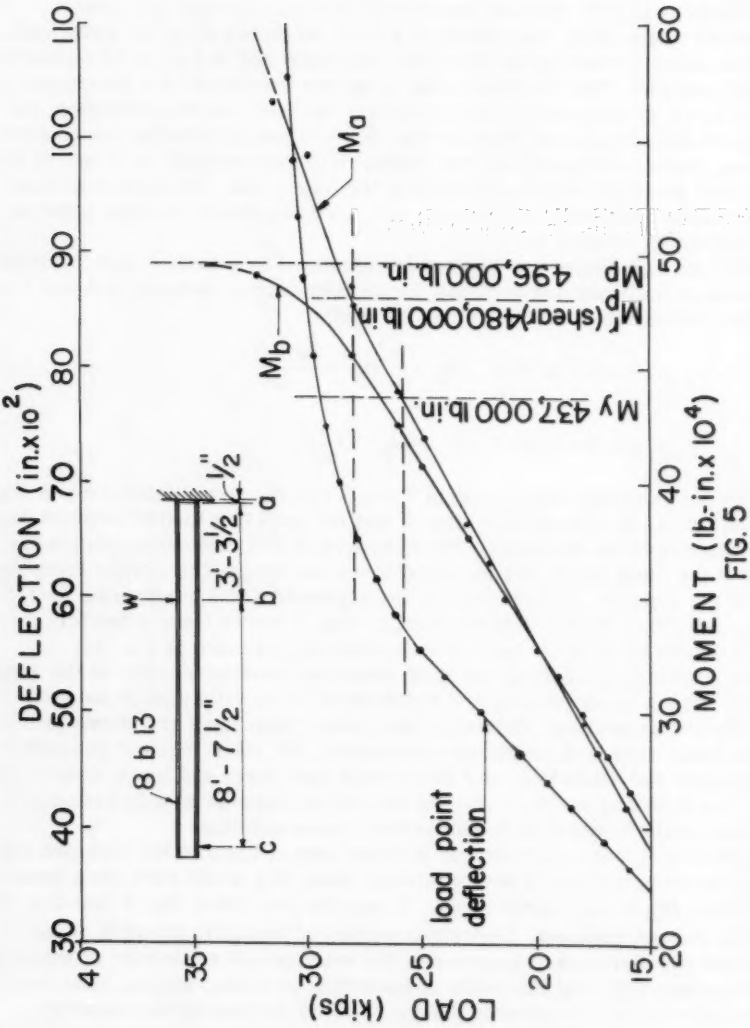
DEFLECTION (in.x10²)
LOAD (kips)
MOMENT (lb.-in.x 10⁴)
8 b 13
8'-7½"
3'-3½"
1½"
w
a
b
c
load point deflection
Mb
Ma
My 437,000 lb.in.
Mp (shear) 480,000 lb.in.
Mp 496,000 lb.in.

FIG. 5

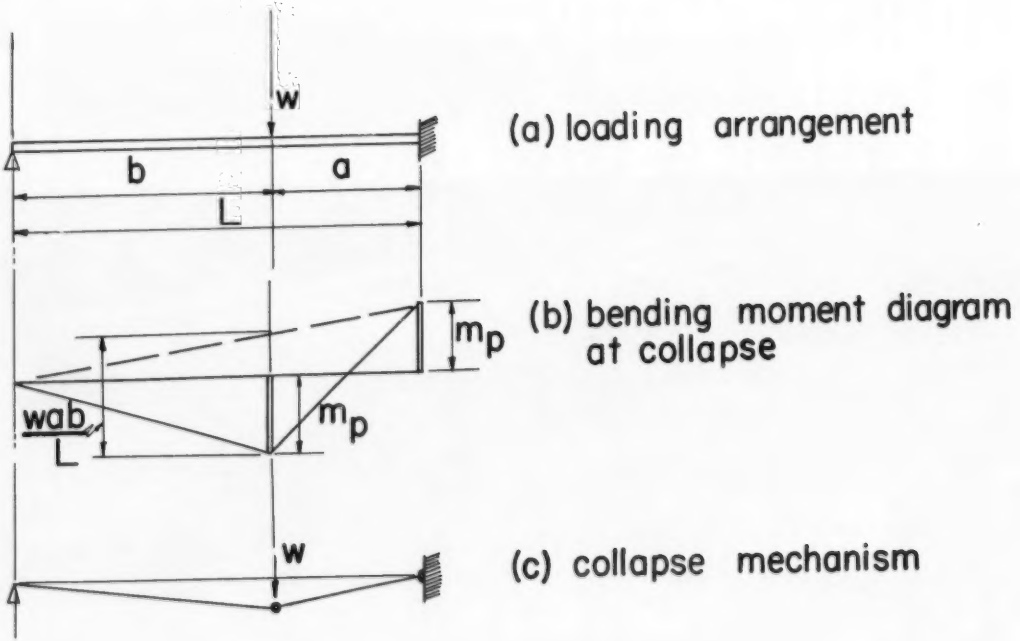

FIG.6 ANALYSIS OF PROPPED CANTILEVER

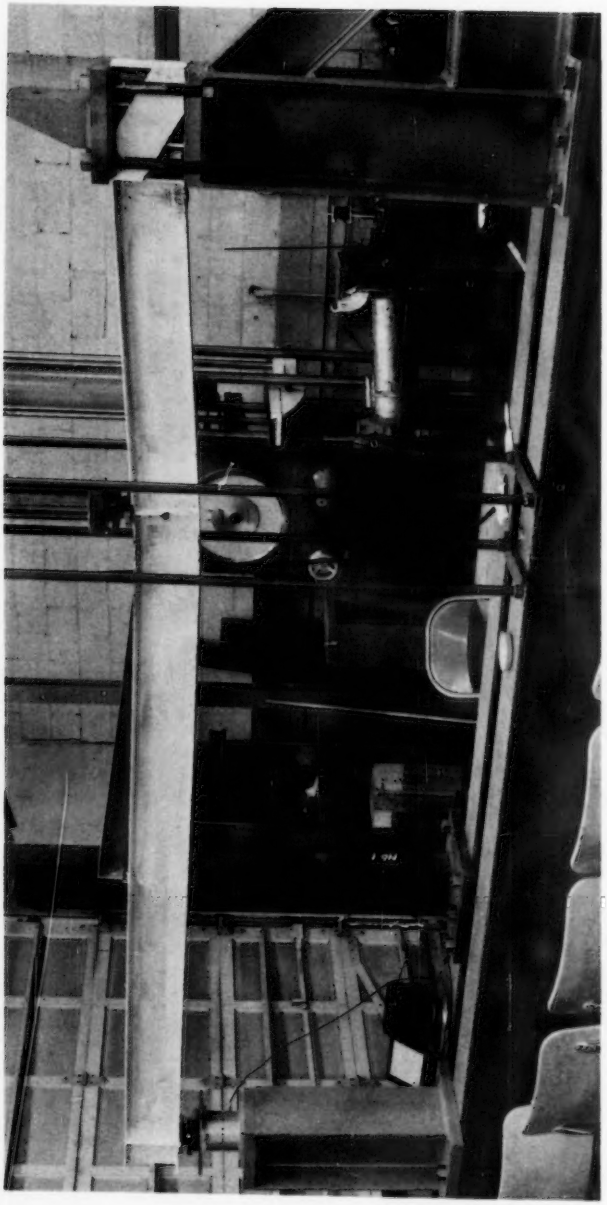

FIG 7 PROPPED CANTILEVER BEAM AFTER TEST, SHOWING DEFORMATION TO HAVE BEEN CONCENTRATED AT HINGE LOCATIONS

a) with a single vertical load, applied at midspan of the beam
b) with a single horizontal load applied at the top of the columns
c) with the vertical and horizontal loads combined.

According to the Plastic Theory, failure of a structure requires that the structure as a whole or in part must be able to deform a finite amount under constant load. A mechanism with one degree of freedom is thus the minimum requirement for structural collapse. If a structure, or part, has "n" statically indeterminate reactions, the occurrence of "n" plastic hinges forms a statically determinate system. The formation of one more plastic hinge provides the necessary single degree of freedom.

The plastic collapse modes associated with each of the three test loading conditions are shown in Fig. 9. The bending moment diagram associated with each collapse mode is characterised by a sufficient number of peaks of bending moment of alternating sign, each equal to the fully plastic moment of the member, to provide enough plastic hinges to form a mechanism. The bending moment diagrams are shown in Fig. 10 and in each case the collapse load can be calculated from conditions of simple static equilibrium as shown in the figure.

A pair of tests were carried out for each of the three loading arrangements, (6 tests in all), and the results are shown in Figs. 11, 12, and 13. A complete analysis of the combined loading case is set out in Appendix II; the same methods are also applicable to the simpler single load cases.

In each test the behaviour of the frame was essentially elastic until the yield stress was exceeded at the most highly stressed section. Because of imperfect fixing of the column bases, the elastic stiffness of the frames (as revealed by the load-deflection curves) was somewhat less than elastic theory predictions. In fact, perfect rigidity of column footings is almost never found in practice. As a result, stresses predicted from elastic theory are often grossly inaccurate in such cases. It cannot be too often emphasized that such things as imperfect fixity, support settlements and residual stresses have no effect on the plastic strength of a structure. Following the load-deflection curves, it is seen that there is a marked change in deflection rate as each hinge is formed, and that between the formation of the penultimate and final hinges the curves become asymptotic to the ordinate of the predicted plastic collapse load.

In the case of the frame carrying the single vertical load, the plastic hinges occurred in the tops of the columns, where axial and bending effects are combined, rather than at the ends of the beam. There was no reduction in moment capacity due to this axial load, however.

In the case of the test with the single horizontal load, hinges occurred at the bases of the columns and in the ends of the beam.

Fig. 14 shows the frame subjected to combined loading after completion of the test. The flaked whitewash shows clearly the hinge locations and the carpenters square clamped to the "windward" knee shows the corner to have remained undeformed. This figure also shows the lateral bracing used in the tests.

In each case, then, the methods of simple plastic design are seen to give an accurate accounting for behaviour and a realistic value for the collapse load. This must be contrasted with orthodox methods which do not indicate either ultimate strength or actual behaviour of a structure.

FIG 8 CLAMPED END OF PROPPED CANTILEVER AFTER TEST, SHOWING SHEAR YIELD LINES AND LOCAL BUCKLING OF FLANGE

COLLAPSE MECHANISM FOR PORTAL FRAME TEST FIG. 9

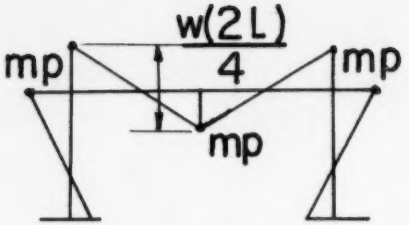

$$mp = \frac{wL}{4}$$

$$\text{or } w = \frac{4mp}{L}$$

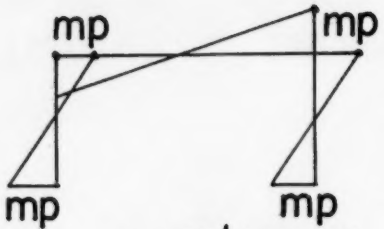

$$mp = \frac{wL}{4}(\text{Sway})$$

$$w = \frac{4mp}{L}$$

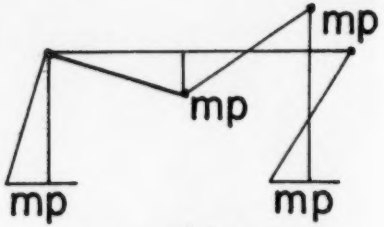

$$mp = \frac{wL}{3}(\text{Sway})$$

$$w = \frac{3mp}{L}$$

ANALYSIS OF PORTAL FRAMES FIG. 10

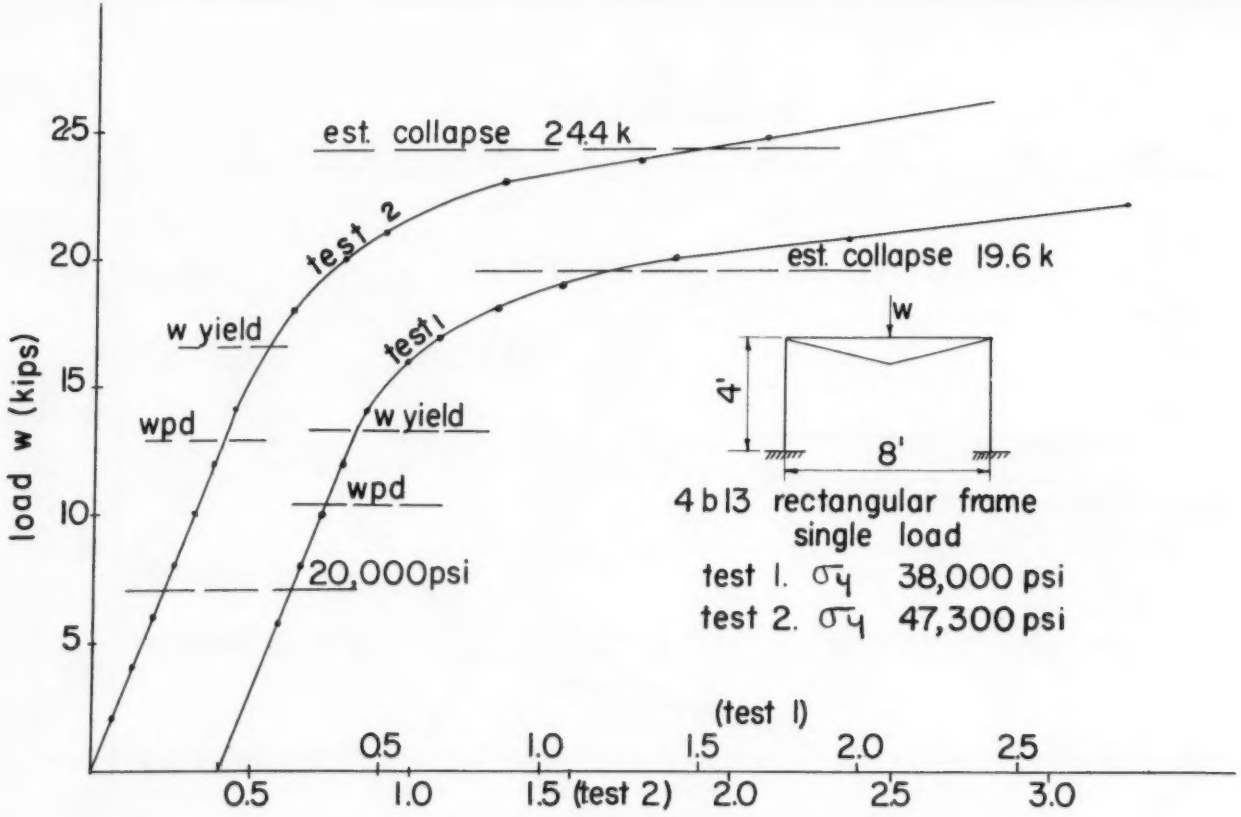

FIG. 11 LOAD POINT DEFLECTION (inches)

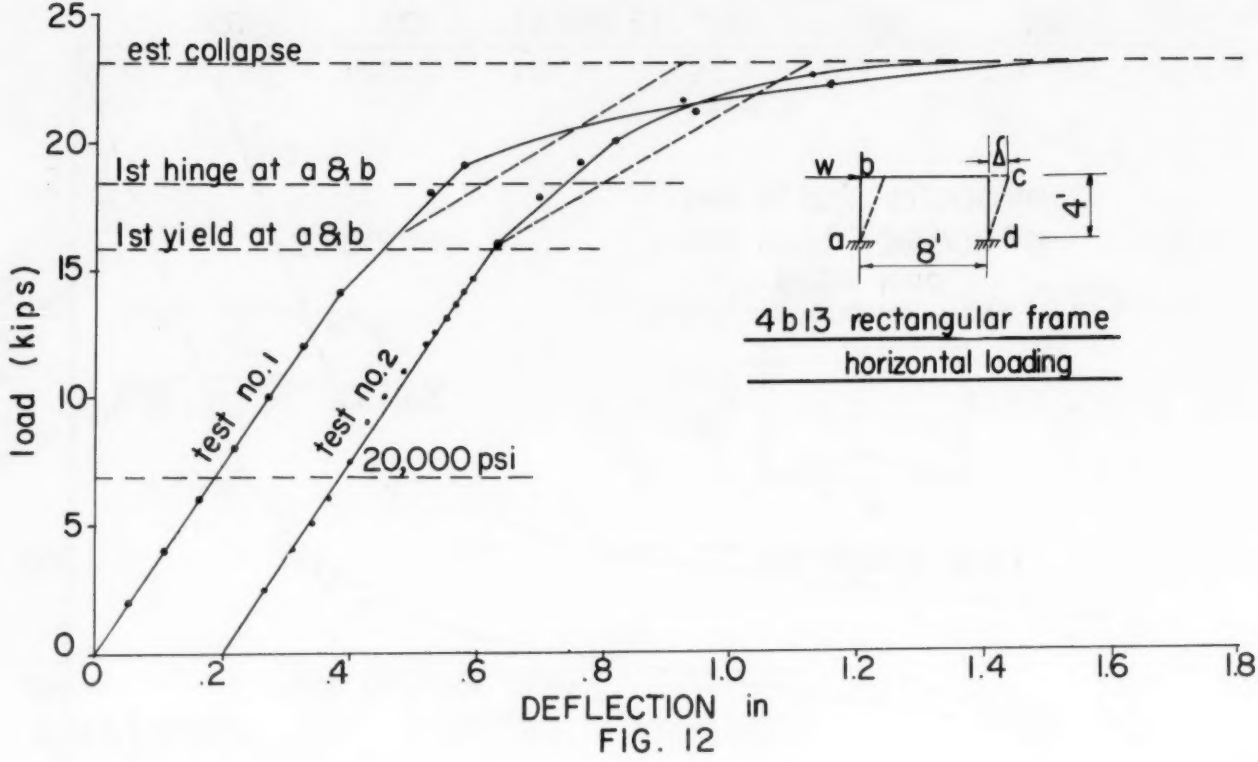
25
20
15
10
5
0
load (kips)
est collapse
1st hinge at a & b
1st yield at a & b
test no.1
test no.2
20,000 psi
0
.2
.4
.6
.8
1.0
1.2
1.4
1.6
1.8
DEFLECTION in
w
b
Δ
c
4'
a
8'
d
4 b 13 rectangular frame
horizontal loading

FIG. 12

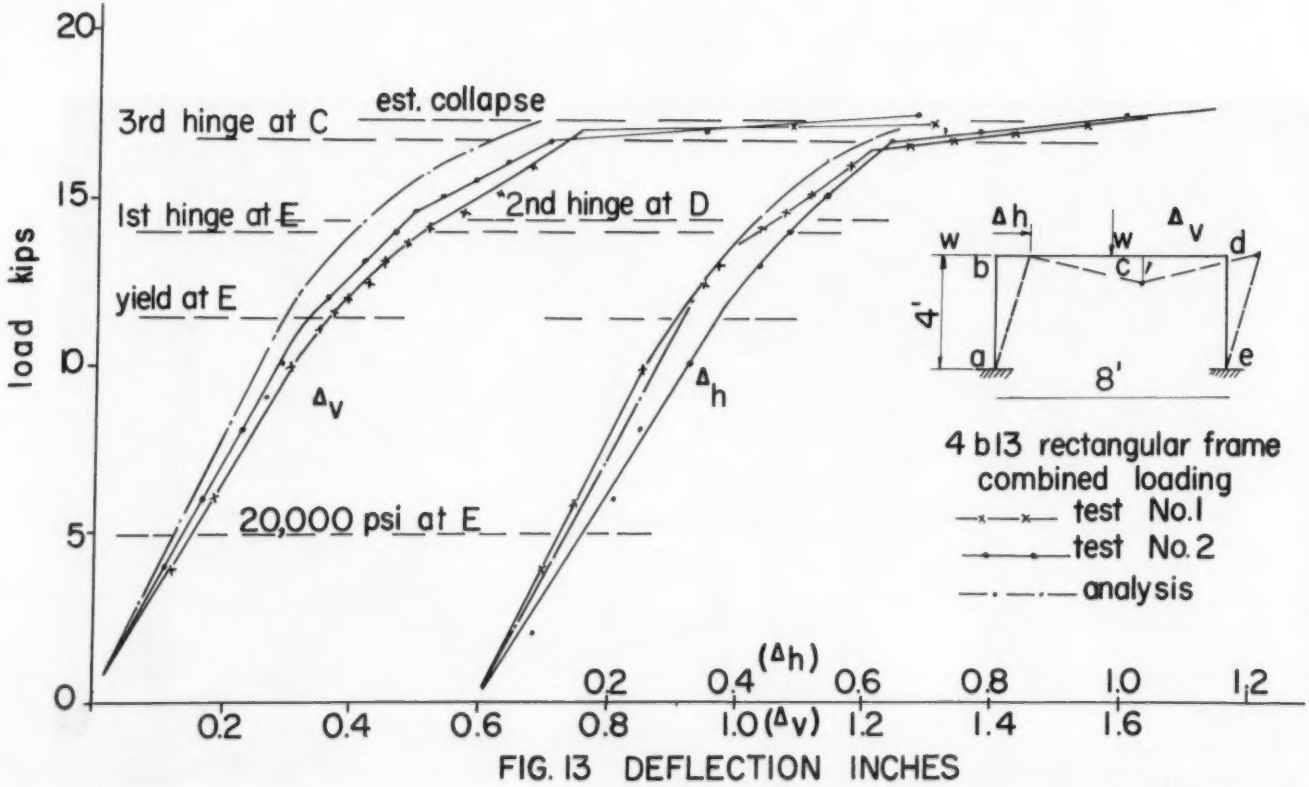

FIG. 13 DEFLECTION INCHES

FIG 14 SIMPLE PORTAL FRAME AFTER TEST, SHOWING LOCATION OF PLASTIC HINGES REVEALED BY FLAKING OF WHITEWASH

Effects of Shear, Local and Lateral Instability

(a) Shear

Although the simple plastic theory of structures is based upon the ideal elasto-plastic behaviour of a ductile member subjected to pure flexure (Figs. 2 and 4), members in actual structures are seldom found to be acting solely in flexure. The effect of shear on plastic behaviour is somewhat complex, but essentially the result is a reduction in plastic bending capacity due to yielding of the web under combined stresses. There is a marked divergence from linear elastic behaviour, and deflections increase rapidly as the flanges become fully plastic.

The reduction in bending capacity due to shear is small except in cases where shears are relatively large. Methods for estimating the reduction have been developed by both the Cambridge and Lehigh research teams,(4,5) and the respective results are quoted below:

(the symbols are defined in Appendix I).

$$\frac{M_p'}{M_p} = 1 - \frac{M_w}{M_p}\left[1 - \sqrt{1 - 3\left(\tau_w/\sigma_y\right)^2}\right] \tag{1}$$

$$\frac{M_p'}{M_p} = 3.53\,\frac{M_w}{M_p}\left(\frac{a}{d_w}\right)^2\left[-1 + \sqrt{1 + 0.566\left(\frac{d_w}{a}\right)^2\frac{M_p}{M_w}}\right] \tag{2}$$

or in the form of an approximate design rule (2) becomes

$$\frac{M_p'}{M_p} = 0.65 + 0.117\,\frac{a}{d} \tag{3}$$

Fig. 15 shows the result of a test on an 8 ft-span 10WF25 beam loaded equally at points 21 in. distant from the end reactions. Marked on the load deflection curve are the capacities predicted by the above formulas. It is seen that the actual reduction in flexural strength due to shear is somewhat less than predicted, being only about 5 percent. Fig. 15 also shows that the combination of shear and flexure does not inhibit the plastic hinge rotation capacity. As full plasticity is approached, large deformations occur with no reduction in flexural capacity. Fig. 16, showing an end panel of the beam tested, reveals a combination of shearing and flexural deformation.

It should be noted that as shear increases moment gradients increase proportionally. The steeper the moment gradient, the shorter must be the "length" of the plastic hinge and accordingly, the greater the curvature at the plastic hinge. It follows then that large shears are associated with sharp curvatures and a tendency to early strain-hardening. The result of this is that the reduction in capacity due to the shear is at least partly compensated for by the increased resistance due to strain-hardening. The theoretical results noted before do not take account of this phenomenon, and the result is as seen in Fig. 15 with the observed behaviour somewhat better than that predicted.

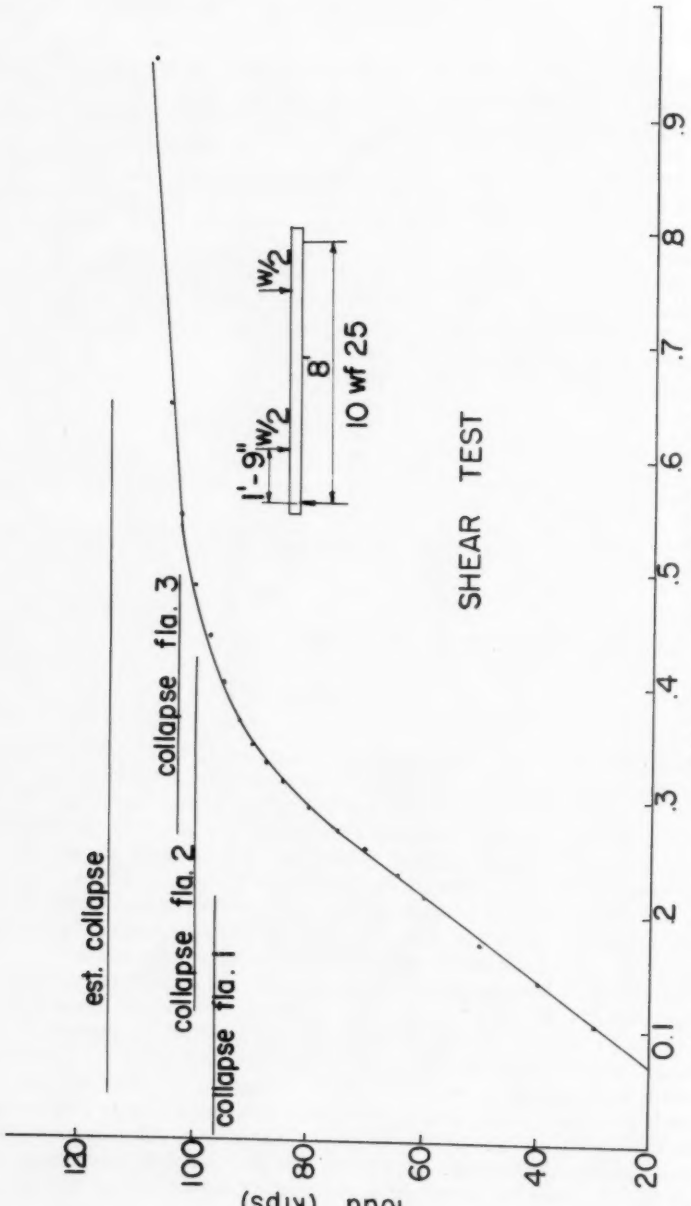
est. collapse
collapse fla. 2
collapse fla. 3
collapse fla. 1
load (kips)
120
100
80
60
40
20
0.1
.2
.3
.4
.5
.6
.7
.8
.9
1'-9"
w/2
w/2
8'
10 wf 25
SHEAR TEST
DEFLECTION inches

FIG. 15

(b) Lateral Instability

The problem of reduction of fully plastic moment capacity due to failure by lateral buckling has not yet been satisfactorily solved from the designers point of view. Work by both Horne[6] and the Lehigh Team[7] have produced values of the allowable unsupported length under a condition of pure bending. Plastic hinges usually occur at points where there is shear and a moment gradient, and the case of pure flexure seldom arises. The usual problem is thus that of a member mainly elastic but with localized fully plastic zones. A suitable solution for the lateral stability of such a member is not available.

In practice, points of maximum moment, i.e. possible hinge locations, are braced laterally. Between these points, lateral bracing is provided according to the rules used in conventional elastic design.

Fig. 17 shows the crippling lateral deformation of a 10 ft. span 10 WF 21 beam which was loaded equally at two points 28 inches from the supports. No lateral bracing was provided, and the deformation seen in the photograph had resulted when the load was only 65 percent of the estimated plastic collapse load.

(c) Local Instability

The essential requirement of a "plastic hinge" is that large rotation must be realized at a nearly constant load.

For a given total rotation, the required curvature (which is proportional to the maximum strain) depends on the length of the plastic hinge. With a steep moment gradient, a plastic hinge tends to be very short, and maximum strains may become quite large. Present knowledge indicates that if deformation up to strain-hardening can be tolerated, hinge rotations will be sufficient to permit full moment re-distribution and the realization of the fully plastic capacity of practical structures.

Beam sections commonly used - wide flange and I-shapes - sometimes tend to deform locally when strains become large. It is, of course, essential that the cross-section of a beam remains stable as a plastic hinge develops. To ensure a rotation capacity up to strain-hardening, it has been proposed[8] that sections be chosen such that

$$\frac{\text{flange breadth}}{\text{flange thickness}} \leq 17$$

Less rotational capacity is required of the web, and it has been proposed that for section stability up to the yield point

$$\frac{\text{web depth}}{\text{web thickness}} \leq 43.$$

A 6 WF 15.5 beam of 10 ft. span was loaded at its third points and the full plastic moment of resistance attained without any signs of flange buckling. In this case the ratio of flange breadth to thickness was over 22. In cases of more localized deformation, for example, at the point of support of the propped cantilever (seen in Figs. 7 and 8) ultimate failure was accompanied by local buckling, though there was no reduction in strength. In some other tests as well, local strains were large and local deformations occurred, but not before collapse mechanisms had formed so that there was no reduction in carrying capacity.

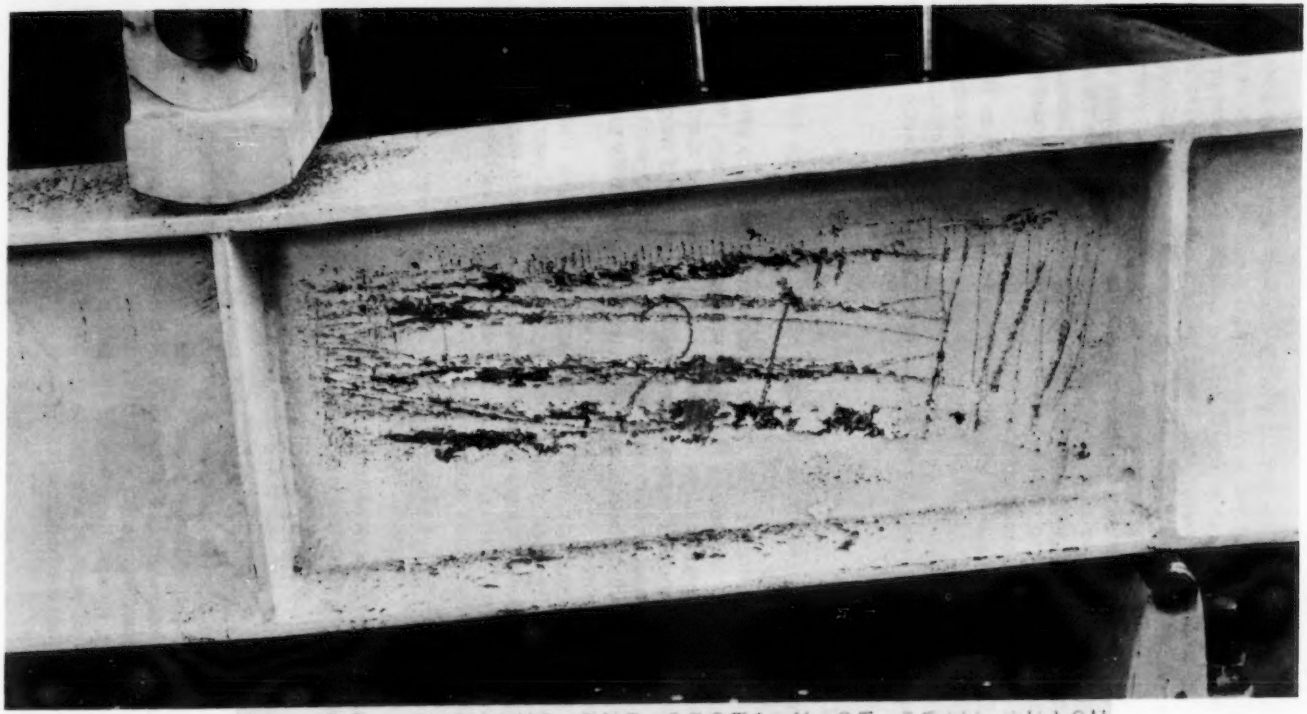

FIG 16 SHOWING END SECTION OF BEAM WHICH FAILED UNDER COMBINED ACTION OF SHEAR AND FLEXURE

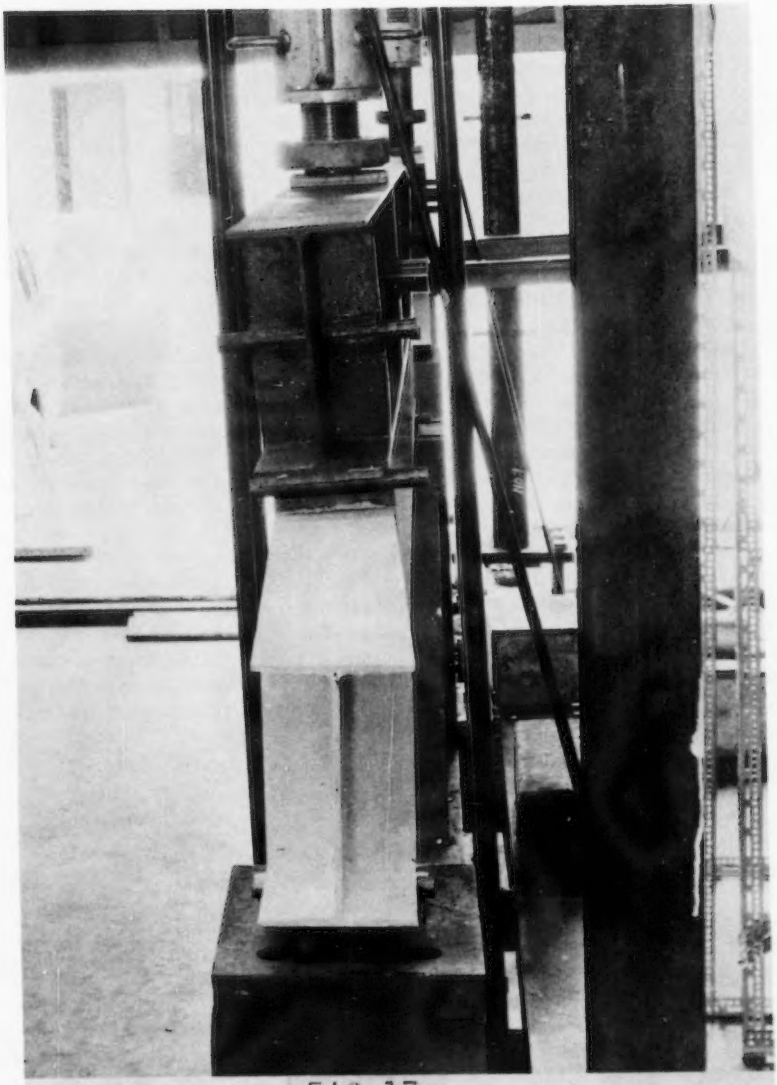

FIG 17

TEST OF BEAM WITHOUT LATERAL SUPPORT SHOWING FAILURE BY LATERAL INSTABILITY

Connections - Knee Joints

Connections in conventional steel-skeleton construction generally serve only to transfer shear, a function which can be adequately fulfilled with riveted or bolted joints. In plastic design, however, more or less complete continuity of the structural frame is essential, and most connections must be able to transfer both shear and moment. Welding provides the best practical means of making such connections. In designing connections for "plastic" structures not only must strength requirements be met, but hinge rotation capacity must be assured in order that plastic redistribution of moments can proceed. Brittle or unstable behaviour must be avoided at all costs. If there is danger from either of these sources, the best solution is often to so strengthen the brittle or unstable element that it will function elastically while plastic deformations occur nearby.

To date, the most common application of plastic design has been to single-storey sheds and frames. In these a rigid knee-joint is required. Although in some cases a built-up haunched knee may be suitable (in spite of its tendency to instability), the simple square knee-joint formed by welding directly together the leg and beam sections is most often used. Since the transfer of moment around the corner of the knee produces very large shearing stresses in the web, the web must be reinforced in most cases. Simple design rules have been proposed for this operation.(9,10)

Fig. 18 shows the proportions of two knee joints which were tested, together with the results of the tests. One knee joint, without web reinforcement, failed by shear in the web and the moment capacity realized was considerably less than that of the section used. The other was reinforced, and it is seen that its capacity was sensibly the same as that of the beam-section. It should also be noted that in both cases the load-deflection curves reveal satisfactory ductile behaviour, indicating that such connections are altogether suitable for use in structures designed on plastic theory.

Behaviour of a Practical Frame

Previous tests on full sized frames have been summarized by Beedle.(11) The following tests of two 20-foot span frames under side (wind) and vertical loading provide additional evidence of the applicability of Plastic Design methods.

The general details of the frames are shown in Fig. 19; one feature differentiating these frames from previous tests lies in the use of practical erection joints (using high tensile bolts) in the rafters near points of low bending moment. As can be seen in Fig. 20 the joints did not reduce the structural stiffness of the frames. Lateral support was provided at the knees and at the vertical load points.

The predicted collapse mechanism is that shown in Fig. 20b, with plastic hinges at B, C, E and F. The collapse load can be calculated by the principle of virtual work.

Fig. 20 shows the measured vertical deflection at the ridge and the horizontal deflections at the knee. Using the section properties in Table 1 the predicted collapse load is: P = 16,250 lb. This was slightly exceeded. The results also show a divergence from linear elastic behaviour slightly below the load calculated to produce first yield at the lee knee. This might be

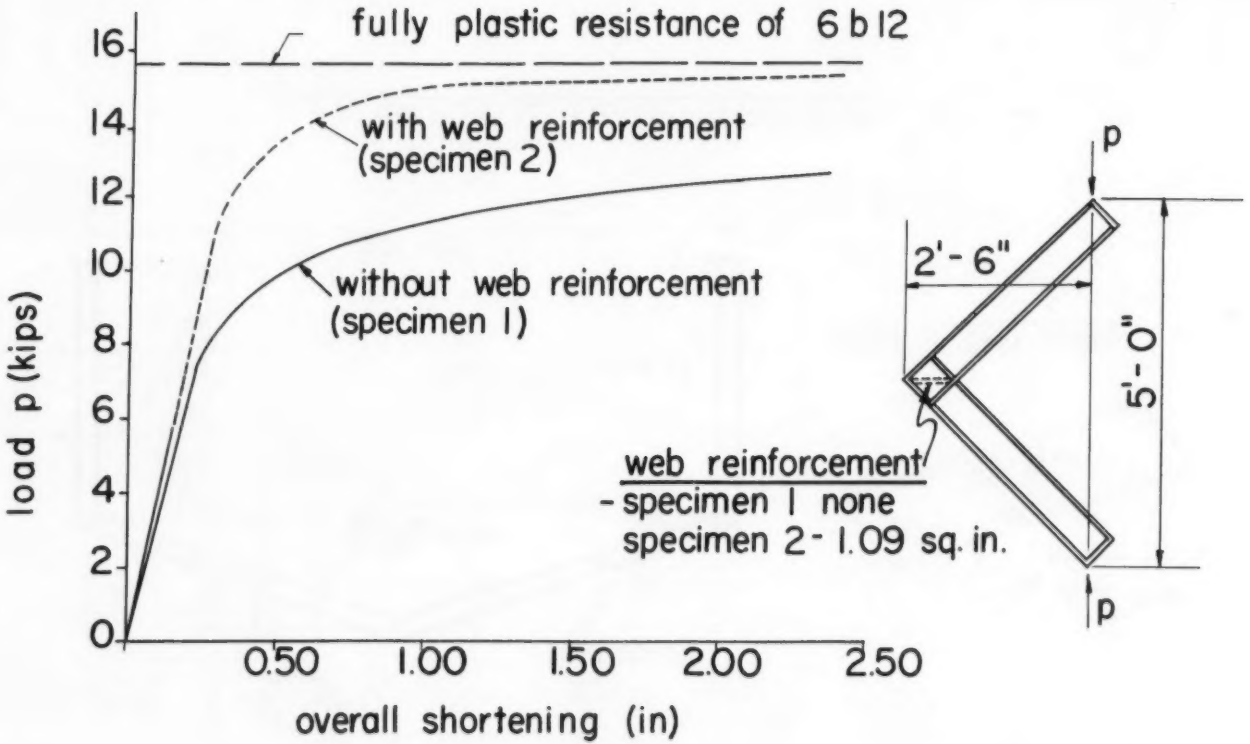

FIG. 18 KNEE-JOINT TEST

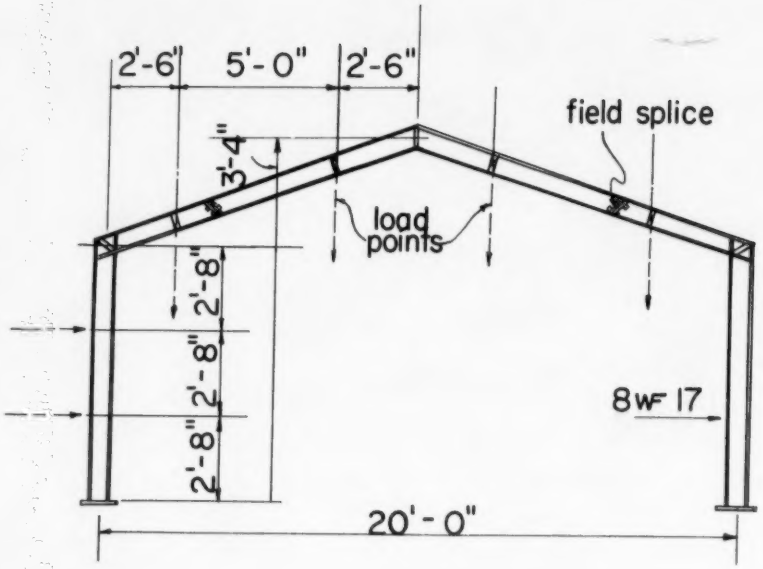

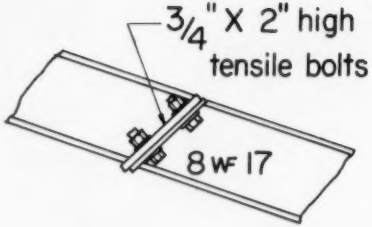

detail of field splice

FIG. 19 PORTAL FRAME SPECIMENS

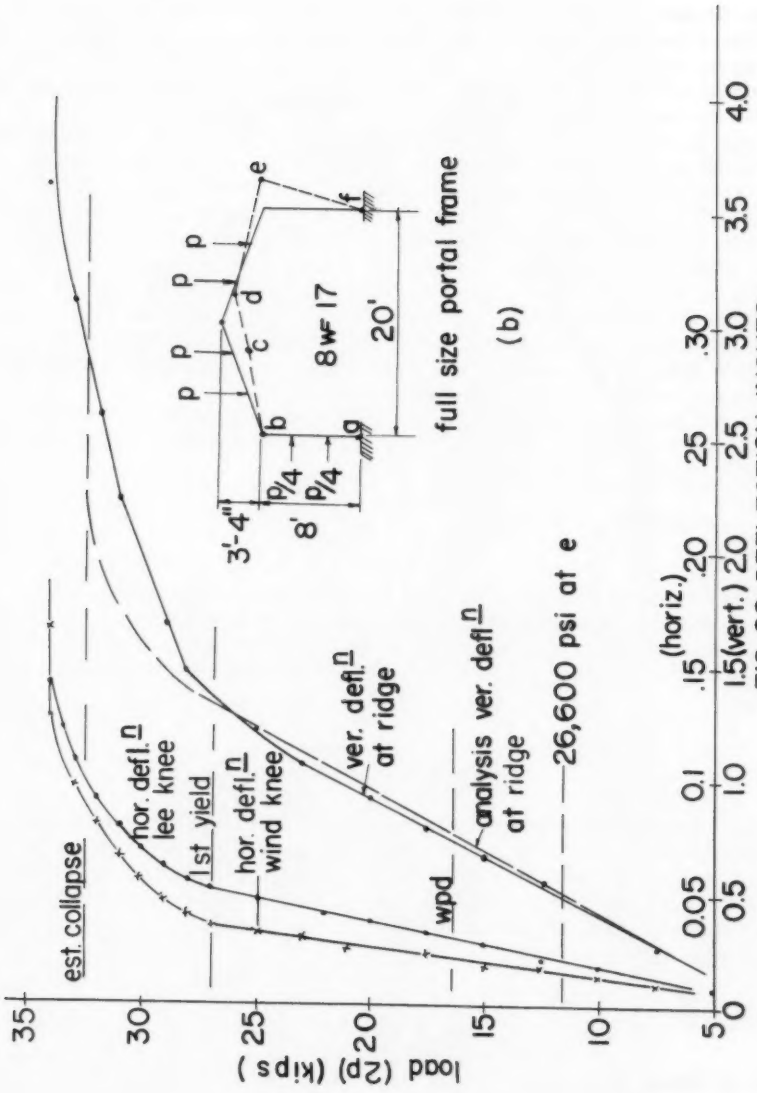

FIG. 20 DEFLECTION INCHES

expected due to the effect of residual stresses and elastic stress concentrations.

By the methods of Appendix II(b) an estimate can be made of the final deflection at the point of failure; this is seen to give a reasonable, though conservative, value. At the load in question, the frame is becoming seriously deformed and an accurate prediction of deflection is really not necessary.

For the sake of comparison, the load at which the maximum stress reaches 26,600 psi. - the orthodox design combined live load - is compared in Fig. 20 with the design load found from plastic design methods. In the later case, the yield stress has been taken at its nominal value of 33,000 psi. and, for the combined wind and live loading, a load factor of 1.41 has been applied. It is seen that plastic design provides a clear, and safe, increase in possible working load of 40 percent.

Fig. 21 shows the state of the frame at collapse, the flaking of the whitewash clearly showing the development of plastic hinges as predicted. After large deformation at the collapse load, final crippling occurred by local flange buckling at the knees as in Fig. 22 and by lateral distortion of the frames between points of lateral support.

The test results show clearly that plastic theory accurately predicts behaviour and load capacity. It is seen that plastic design methods are not only rational, but can lead to marked economy.

CONCLUSION

The tests which have been described present further evidence of the validity value of the plastic theory of structures. It is seen that the behaviour of practical structures - with the usual imperfections and residual effects - is accurately predicted by plastic theory up to and including the ultimate strength.

ACKNOWLEDGMENTS

The Authors wish to acknowledge the assistance of the Canadian Institute of Steel Construction that made possible the course during which these tests were made, and to thank Queen's University and the Royal Military College where the work was carried out. Mr. L. H. Stirling, senior technician of the Civil Engineering Department at the R.M.C., was in charge of the test arrangements and instrumentation.

REFERENCES

1. J. F. Baker, M. R. Horne and J. Heyman, The Steel Skeleton, Vol 2, Plastic Behaviour and Design, Cambridge University Press, 1956.
2. L. S. Beedle et al, Welded Continuous Frames and Their Components, Report Series, Lehigh University Department of Civil Engineering.
3. J. W. Dolphin, H. M. Nelson and D. T. Wright, Plastic Design of Steel Structures, Kingston, 1956.

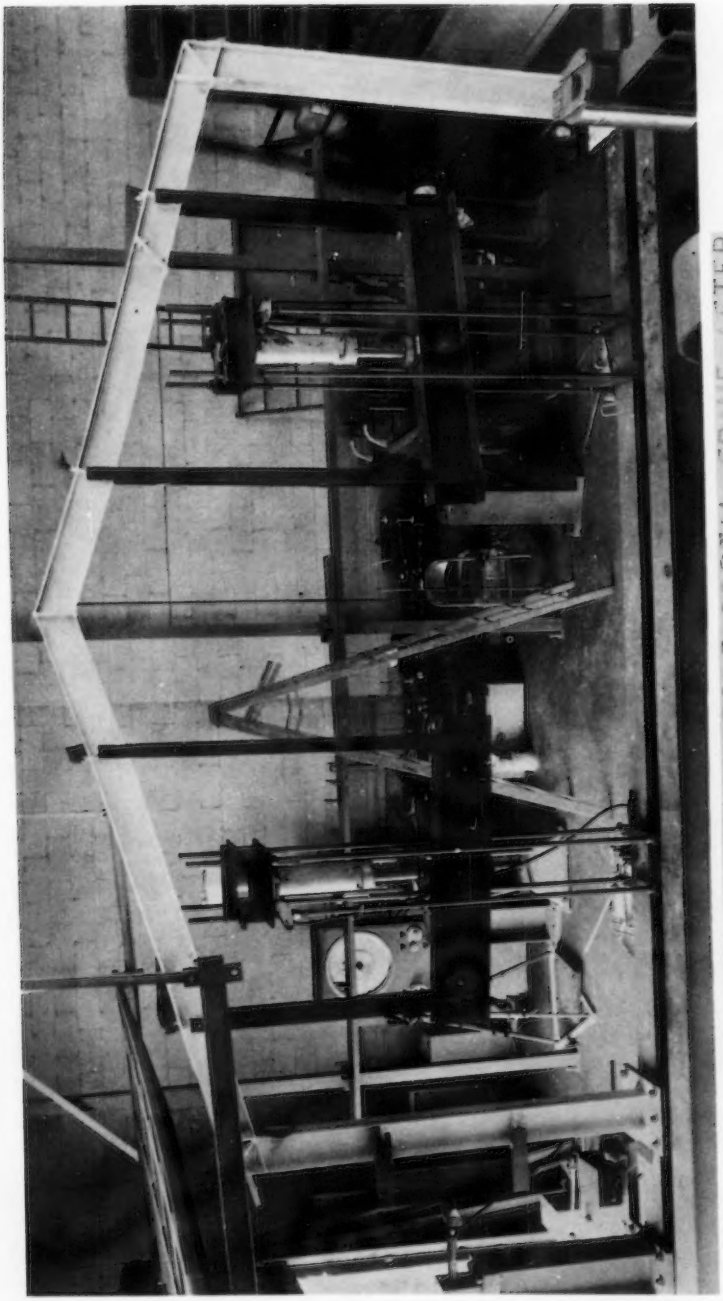

FIG 21 PITCHED ROOF PORTAL FRAME AFTER TEST, SHOWING DISPLACEMENT OF FRAME DUE TO HINGE ROTATIONS

FIG 22 KNEE JOINT FROM PITCHED ROOF PORTAL FRAME AFTER TEST, SHOWING EXTENT OF YIELDING AND TENDENCY TO LOCAL BUCKLING OF FLANGES

4. J. F. Baker, M. R. Horne and J. Heyman, op. cit. Chapter 11.

5. L. S. Beedle, B. Thurlimann, and R. L. Ketter, Plastic Design in Structural Steel, Lehigh University, 1955, (Chapter 9.2).

6. J. F. Baker, M. R. Horne and J. Heyman, op. cit. Chapter 12.

7. L. S. Beedle, B. Thurlimann and R. L. Ketter, op. cit. Chapter 9.4.

8. ibid. Chapter 9.3.

9. D. T. Wright, The Design of Knee Joints for Rigid Steel Frames, British Welding Research Association, Report No. FE 1/38, 1954.

10. A. A. Toprac, B. G. Johnston, and L. S. Beedle, Connections for Welded Continuous Portal Frames, Welding Journal v 30, n 7 and 8, and v 31 n 11, 1951 and 1952.

11. L. S. Beedle, Experimental Verification of Plastic Theory, Proc. Nat. Conf. Amer. Inst. of Steel Construction, p 36, 1956.

APPENDIX I

Notation

ϕ - Curvature

E - Young's Modulus

Z - Plastic Section Modulus

d_e - Half depth of Elastic Core

M_p - Full Plastic Moment

M^r_p - Full Plastic Moment, reduced due to shear.

M_w - Plastic Moment of Web

= (yield stress x clear web area x clear web depth) $\div$ 4.

τ - Av. Web Shear

σ_y - Tensile Yield Stress

a - Member Length, from point of max. moment to point of zero moment.

d_w - clear web depth.

d - overall depth of beam.

APPENDIX II

(a) Order of Hinge Formation

The order of formation of plastic hinges and the loads at which individual plastic hinges occur, are of no importance in design when only the actual collapse load need be considered. An idea of the order may however be obtained by assuming a shape factor of unity. Thus

Moment at Yield = Fully Plastic Moment, or

$$M_y = M_p$$

With this simplification, a complete analysis becomes fairly easy.

The analysis shown in Fig. 23 has been carried out for the simple portal frame subjected to combined loading. Fig. 23(a) shows the elastic moment distribution. For $M_y = M_p$, the first plastic hinge will occur at E (the point of maximum moment) when,

$$W = W_1 = \frac{80}{33} \frac{M_p}{L}$$

Increase of the loads by a factor "N_1" will increase the bending moment at D to M_p, but at the same time the moment at E will exceed M_p. This obviously cannot occur and the support moment must change by a value M^1 such that M_E remains equal to M_p. The bending moment is then as in Fig. 23 and

$$\text{at D: } \frac{31}{80} W_1 L (N_1) + M^1 = M_p$$

$$\text{at E: } \frac{33}{80} W_1 L (N_1) - M^1 = M_p$$

and since $M_p = \frac{33}{80} W_1 L$

$$N = 33/32$$

Increase of the loads (W_1) by a larger factor N_2 will produce M_p at C but M_E and M_D will both exceed M_p so that the reactions must change by M^1 and H^1 to maintain all moments less than or equal to M_p. The new bending moment diagram is shown in Fig. 23(c) and

$$\text{at C: } \frac{24}{80} W_1 L(N_2) - M^1 + H^1 L = M_p$$

$$\text{at D: } \frac{31}{80} W_1 L(N_2) + M^1 - H^1 L = M_p$$

$$\text{at E: } \frac{33}{80} W_1 L(N_2) - M^1 = M_p$$

Then $N_2 = 66/55$.

Finally, increase of the loads (W_1) by a factor N_3 will produce a plastic hinge at A and reaction changes M^1, H^1 and V^1 are necessary to maintain M_E, M_D and M_C equal to M_p. In a similar manner N = 99/80. That is to say, the first hinge occurs at E when

$$W_1 = \frac{80}{33} \frac{M_p}{L}$$

the second hinge occurs at D when

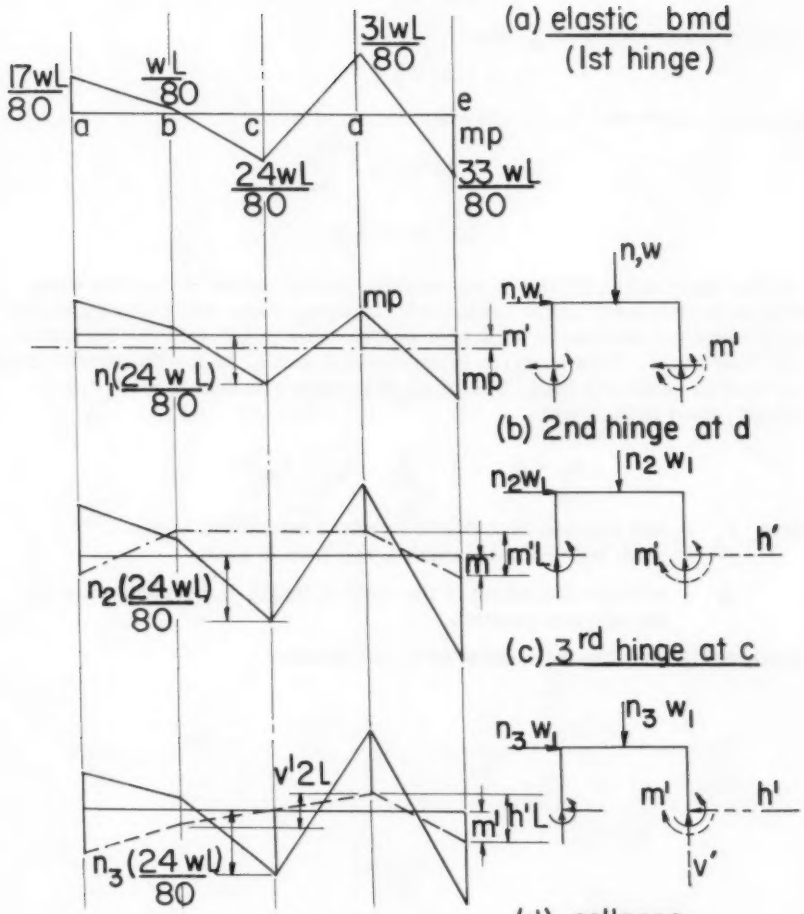

over de: $2mp + h'L = \frac{wL}{80}(64)$

over cd: $2mp + v'L = \frac{wL}{80}(54)$

ate: $mp + m' = \frac{wL}{80}(33)$

$$mp = \frac{wL}{3} \text{ or } w = \frac{3mp}{L}$$

FIG. 23

$$W_2 = 1.03\ W_1$$

the third hinge occurs at C when

$$W_3 = 1.20\ W_1$$

collapse occurs when the fourth hinge forms at A

$$W_4 = 1.24\ W_1 = 3\ \frac{M_p}{L}$$

(b) Deflection

It has been shown (4) that a reasonable estimate of the deflection when collapse is imminent can be obtained by applying slope-deflection equations to the statically determine structure which exists just before the formation of the last hinge. This analysis is carried out in Fig. 24 for the simple frame subjected to combined load. The slope deflection equation is most conveniently used in the form

$$\theta_A = \theta'_A + \frac{\Delta}{L} + \frac{L}{3EI}\ (M_{AB} - M_{BA}/2)$$

where θ'_A = end rotation of A due to lateral loads in the length L when both ends of length L are free to rotate

Δ = relative deflection of the ends of length L, perpendicular to the original position.

and all terms are positive clockwise on the member.

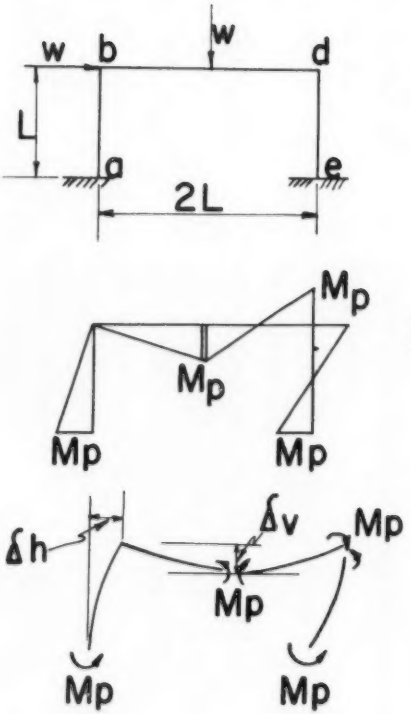

at b $\quad \theta_{ba} = \theta_{bc}$

$$\theta_{ba} = 0 + \frac{\delta h}{L} + \frac{L}{3EI}\left(0 + \frac{Mp}{2}\right)$$

$$\theta_{bc} = 0 + \frac{\delta v}{L} + \frac{L}{3EI}\left(0 + \frac{Mp}{2}\right)$$

$$\delta_v = \delta_h$$

just before hinge forms at a

$$\theta_a = \theta'_a = 0$$

$$0 = 0 + \frac{\delta h}{L} + \frac{L}{3EI}(-Mp + 0)$$

$$\delta_h = \frac{MpL^2}{3EI} = \delta_v$$

FIG. 24

Paper 1399 October, 1957 EM 4

Journal of the
ENGINEERING MECHANICS DIVISION
Proceedings of the American Society of Civil Engineers

ANALYSIS OF CONTINUOUS BEAMS BY FOURIER SERIES

Seng-Lip Lee,[1] A.M. ASCE
(Proc. Paper 1399)

SYNOPSIS

This paper deals with the analysis of continuous beams by means of the expansion of arbitrary load function and the intermediate redundant reactions in infinite trigonometric series.[2] The values of the redundant reactions corresponding to any load distribution are determined by the application of Castigliano's theorem. The same procedure is used to derive expressions for the influence lines for the reactions.

Notations

A_n, A_n', A_n'', A_n^m	Fourier coefficients for loads and reactions.
a_1, a_2, a_m	Span ratio.
B_n	Fourier coefficient for deflection.
C_n	Defined by (10).
C_1, C_2, C_3, C_4	Constants of integration.
c	Distance of concentrated load from left end.
D_{11}, D_{12}, D_{1m} ---	Series defined by (17), (20) and (22).
E	Modulus of elasticity.
F	Defined by (16).
I	Moment of inertia.
l	Span length.

Note: Discussion open until March 1, 1958. Paper 1399 is part of the copyrighted Journal of the Engineering Mechanics Division of the American Society of Civil Engineers, Vol. 83, No. EM 4, October, 1957.

1. Asst. Prof. of Civ. Eng., Northwestern Technological Inst., Northwestern Univ., Evanston, Ill.
2. "Mathematical Methods in Engineering" by T. v. Kármán and M. A. Biot, McGraw-Hill Book Co., Inc., New York, 1940, p. 323.

M_1	Redundant moment on left end.
m	Redundancy.
P	Concentrated load.
p(x)	Arbitrary load function.
q(x)	Given load.
R_1, R_2, R_m	Intermediate, or redundant, reactions.
r	Infinitely small length increment.
U	Strain energy.
W(x)	Deflection.
x	Independent variable, distance from left end.
y(x)	Deflection.
$y_p(x)$	Particular solution for y.
d_1, d_2, d_m	Displacements of intermediate supports.
θ_a	Angular displacement of the tangent to the elastic curve at left end.

INTRODUCTION

The deflection of a beam of constant cross section under arbitrary transverse load p(x) is given by the differential equation

$$EI\frac{d^4y}{dx^4} = p(x) \tag{1}$$

where E is the modulus of elasticity and I the moment of inertia of the beam. The general solution of (1) is

$$y(x) = C_1 + C_2x + C_3x^2 + C_4x^3 + y_p(x) \tag{2}$$

where y_p is a particular solution of (1). For a simply supported beam of span 1, the boundary conditions

$$\left.\begin{aligned} y(0) &= 0 \\ y(l) &= 0 \\ y''(0) &= 0 \\ y''(l) &= 0 \end{aligned}\right\} \tag{3}$$

provide four equations for the determination of the constants of integration C_1, C_2, C_3 and C_4.

Elastic Curve

Let us consider the continuous beam shown in Fig. 1. It may be treated as a simply supported beam of span 1 subjected to the action of a given load q(x) and the reactions of the intermediate supports R_1, R_2 —— and R_m, which can be approximated by Fourier series of the type

$$q(x) = \sum_{n=1}^{\infty} A_n \sin \frac{n\pi x}{l} \tag{4}$$

$$\left.\begin{aligned} R_1 &= \sum_{n=1}^{\infty} A'_n \sin \frac{n\pi x}{l} \\ R_2 &= \sum_{n=1}^{\infty} A''_n \sin \frac{n\pi x}{l} \\ &\cdots\cdots\cdots\cdots\cdots \\ R_m &= \sum_{n=1}^{\infty} A^m_n \sin \frac{n\pi x}{l} \end{aligned}\right\} \tag{5}$$

where

$$A_n = \frac{2}{l} \int_o^l q(x) \sin \frac{n\pi x}{l}\, dx \tag{6}$$

$$\left.\begin{aligned} A'_n &= \frac{2}{l} \lim_{r \to o} \int_{(a_1 l - r)}^{(a_1 l + r)} \frac{R_1}{2r} \sin \frac{n\pi x}{l}\, dx = \frac{2R_1}{l} \sin n\pi a_1 \\ A''_n &= \frac{2}{l} \lim_{r \to o} \int_{(a_2 l - r)}^{(a_2 l + r)} \frac{R_2}{2r} \sin \frac{n\pi x}{l}\, dx = \frac{2R_2}{l} \sin n\pi a_2 \\ &\cdots\cdots\cdots\cdots\cdots\cdots\cdots\cdots\cdots\cdots\cdots\cdots \\ A^m_n &= \frac{2}{l} \lim_{r \to o} \int_{(a_m l - r)}^{(a_m l + r)} \frac{R_m}{2r} \sin \frac{n\pi x}{l}\, dx = \frac{2R_m}{l} \sin n\pi a_m \end{aligned}\right\} \tag{7}$$

Let us approximate $y_p(x)$ by the series

$$y_p(x) = \sum_{n=1}^{\infty} B_n \sin \frac{n\pi x}{l} \tag{8}$$

Substituting (4), (5) and (8) in (1) leads to

$$B_n = \frac{l^4}{EI\, n^4 \pi^4} C_n \tag{9}$$

where

$$C_n = A_n - A_n' - A_n'' - \cdots\cdots\cdots - A_n^m \tag{10}$$

A_n, A_n', A_n'', —— and A_n^m are as given by (6) and (7), in which $q(x)$ is positive if acting downward while R_1, R_2, —— and R_m are positive if acting upward. Substituting (3) and (8) in (2) leads to the equation of the elastic curve

$$y(x) = \frac{l^4}{EI\pi^4} \sum_{n=1}^{\infty} \frac{1}{n^4} C_n \sin \frac{n\pi x}{l} \tag{11}$$

(11) is defined if the values of R_1, R_2, —— R_m in terms of $q(x)$ are known.

Redundant Reactions

Differentiating (11) twice with respect to x leads to

$$y''(x) = -\frac{l^2}{EI\pi^2} \sum_{n=1}^{\infty} \frac{1}{n^2} C_n \sin \frac{n\pi x}{l} \tag{12}$$

The strain energy in the beam is given by the expression

$$U = \frac{EI}{2} \int_0^l [y''(x)]^2 dx = \frac{l^5}{4EI\pi^4} \sum_{n=1}^{\infty} \frac{1}{n^4} (C_n)^2 \tag{13}$$

Application of Castigliano's theorem results in

$$\left.\begin{aligned} \frac{\partial U}{\partial R_1} &= d_1 \\ \frac{\partial U}{\partial R_2} &= d_2 \\ &\cdots\cdots\cdots \\ \frac{\partial U}{\partial R_m} &= d_m \end{aligned}\right\} \tag{14}$$

where d_1, d_2, —— and d_m are respectively the relative vertical displacements of R_1, R_2, —— and R_m with respect to the straight line passing through the points of end supports A and B, being positive if upward. Attention should be given to the difference between the sign convention just stated and that for the differential equation. Substituting (13) in (14), giving regards to (6), (7) and (10), leads to

$$\left.\begin{array}{l} R_1 D_{11} + R_2 D_{12} + \cdots\cdots + R_m D_{1m} = \frac{l}{2} D_1 + F d_1 \\ R_1 D_{12} + R_2 D_{22} + \cdots\cdots + R_m D_{2m} = \frac{l}{2} D_2 + F d_2 \\ \cdots\cdots\cdots\cdots\cdots\cdots\cdots\cdots\cdots\cdots \\ R_1 D_{1m} + R_2 D_{2m} + \cdots\cdots + R_m D_{mm} = \frac{l}{2} D_m + F d_m \end{array}\right\} \qquad (15)$$

where

$$F = \frac{EI\pi^4}{2l^3} \qquad (16)$$

$$\left.\begin{array}{l} D_{11} = \sum_{n=1}^{\infty} \frac{1}{n^4} \sin^2 n\pi a_1 \\ D_{12} = \sum_{n=1}^{\infty} \frac{1}{n^4} \sin n\pi a_1 \sin n\pi a_2 \\ D_{1m} = \sum_{n=1}^{\infty} \frac{1}{n^4} \sin n\pi a_1 \sin n\pi a_m \\ D_{22} = \sum_{n=1}^{\infty} \frac{1}{n^4} \sin^2 n\pi a_2 \\ D_{2m} = \sum_{n=1}^{\infty} \frac{1}{n^4} \sin n\pi a_2 \sin n\pi a_m \\ D_1 = \sum_{n=1}^{\infty} \frac{1}{n^4} A_n \sin n\pi a_1 \\ D_2 = \sum_{n=1}^{\infty} \frac{1}{n^4} A_n \sin n\pi a_2 \end{array}\right\} \qquad (17)$$

$$D_m = \sum_{n=1}^{\infty} \frac{1}{n^4} A_n \sin n\pi a_m$$

$$D_{mm} = \sum_{n=1}^{\infty} \frac{1}{n^4} \sin^2 n\pi a_m$$

Thus, R_1, R_2, —— and R_m can be determined by the solution of (15) for any loading conditions provided the relative displacements of the supports are known. Substituting the values of these reactions in (11) yields the expression for the deflection of the beam. It should be observed that the series in (17) converge very rapidly as shown in the following example.

Example 1

Consider the two-span continuous beam shown in Fig. 2. Assuming that the center support does not yield under the load, $d_1 = 0$ and the first of (15) becomes

$$R_1 = \frac{l}{2} \frac{D_I}{D_{II}} \qquad \text{(a)}$$

Substitution of known quantities in (6) and (17) yields

$$A_n = \frac{2P}{l} \sin \frac{n\pi c}{l} = \frac{2P}{l} \sin \frac{n\pi}{4}$$

$$D_I = \frac{2P}{l} \sum_{n=1}^{\infty} \frac{1}{n^4} \sin \frac{n\pi}{4} \sin \frac{n\pi}{2}$$

$$D_{II} = \sum_{n=1}^{\infty} \frac{1}{n^4} \sin^2 \frac{n\pi}{2}$$

Substituting these values in (a) leads to

$$R_1 = P \frac{\sum_{n=1}^{\infty} \frac{1}{n^4} \sin \frac{n\pi}{4} \sin \frac{n\pi}{2}}{\sum_{n=1}^{\infty} \frac{1}{n^4} \sin^2 \frac{n\pi}{2}} = P \frac{\frac{\sqrt{2}}{2} - \frac{1}{81} \frac{\sqrt{2}}{2} \cdots}{1 + \frac{1}{81} \cdots} = .690P$$

Exact solution yields $R_1 = 11/16P = .6875P$.

Substituting the value of R_1 in (11) leads to

$$y(x) = \frac{2Pl^3}{EI\pi^4} \sum_{n=1}^{\infty} \frac{1}{n^4} \left(\sin \frac{n\pi}{4} - .69 \sin \frac{n\pi}{2} \right) \sin \frac{n\pi x}{l}$$

differentiating which we obtain

$$y'(x) = \frac{2Pl^2}{EI\pi^3} \sum_{n=1}^{\infty} \frac{1}{n^3}\left(\sin\frac{n\pi}{4} - .69\sin\frac{n\pi}{2}\right)\cos\frac{n\pi x}{l}$$

The last two expressions provide a convenient means for determining the deflection and slope of the elastic curve at any point along the continuous beam. It should be mentioned here that while y(x) and y'(x) converge rapidly, the convergence decreases with each differentiation. Knowing the redundant reaction, the bending moment and shear can easily be determined by conventional methods.

Let us next consider the beam shown in Fig. 3, which may be treated as the limiting case of the beam shown in Fig. 1 as $a_1 l$ approaches zero and R_1 approaches infinity while the product $R_1 a_1 l = M_1$ remains constant. For this case, the first of (7) becomes

$$A'_n = \frac{2n\pi M_1}{l^2} \tag{18}$$

and (15) becomes

$$\left.\begin{array}{l} M_1 \frac{\pi}{l} D'_{12} + R_2 D_{22} + \cdots + R_m D_{2m} = \frac{l}{2} D_2 + F d_2 \\ \text{- -} \\ M_1 \frac{\pi}{l} D'_{1m} + R_2 D_{2m} + \cdots + R_m D_{mm} = \frac{l}{2} D_m + F d_m \end{array}\right\} \tag{19}$$

where

$$\left.\begin{array}{l} D'_{12} = \sum_{n=1}^{\infty} \frac{1}{n^3} \sin n\pi a_2 \\ D'_{1m} = \sum_{n=1}^{\infty} \frac{1}{n^3} \sin n\pi a_m \end{array}\right\} \tag{20}$$

The first of (15) drops out in this case since all the coefficients become zero.

Differentiating (13) with respect to M_1, giving regards to (18), leads to

$$\frac{\partial U}{\partial M_1} = \theta_a$$

or

$$M_1 \frac{\pi}{l} D'_{11} + R_2 D'_{12} + \cdots + R_m D'_{1m} = \frac{l}{2} D'_1 + F \frac{l}{\pi} \theta_a \tag{21}$$

where

$$D'_{11} = \sum_{n=1}^{\infty} \frac{1}{n^2} = \frac{\pi^2}{6} = 1.645$$

$$D'_{1} = \sum_{n=1}^{\infty} \frac{1}{n^3} A_n \qquad (22)$$

and θ_a is the angular displacement of the tangent to the elastic curve at A, being positive if in the assumed direction of M_1. Under any loading conditions, M_1, R_2, —— and R_m can be determined by solving (19) and (21) simultaneously.

Example 2

Consider the beam loaded as shown in Fig. 4. For this case $\theta_a = 0$, $d_2 = 0$ and (19) and (21) become

$$M_1 \frac{\pi}{l} D'_{11} + R_2 D'_{12} = \frac{l}{2} D'_1$$

$$M_1 \frac{\pi}{l} D'_{12} + R_2 D_{22} = \frac{l}{2} D_2 \qquad (b)$$

Substitution of known quantities in (6), (17), (20) and (22) yields

$$A_n = \frac{2}{l} \int_0^{\frac{2}{3}l} \omega \sin \frac{n\pi x}{l} dx = \frac{2\omega}{n\pi} \left(1 - \cos \frac{2n\pi}{3}\right)$$

$$D'_{11} = 1.645$$

$$D'_{12} = \sum_{n=1}^{\infty} \frac{1}{n^3} \sin \frac{n\pi}{2} = 1 - \frac{1}{27} \cdots\cdots = .963$$

$$D'_1 = \frac{2\omega}{\pi} \sum_{n=1}^{\infty} \frac{1}{n^4} \left(1 - \cos \frac{2n\pi}{3}\right) = \frac{2\omega}{\pi} \left[\left(1 + \frac{1}{2}\right) + \left(1 + \frac{1}{2}\right) \frac{1}{16} \cdots\cdots\right]$$

$$= 1.015\,\omega$$

$$D_{22} = \sum_{n=1}^{\infty} \frac{1}{n^4} \sin^2 \frac{n\pi}{2} = 1 + \frac{1}{81} \cdots\cdots = 1.012$$

$$D_2 = \frac{2\omega}{\pi} \sum_{n=1}^{\infty} \frac{1}{n^5} \left(1 - \cos \frac{2n\pi}{3}\right) \sin \frac{n\pi}{2} = \frac{2\omega}{\pi} \left[\left(1 + \frac{1}{2}\right) \cdots\cdots\right]$$

$$= 0.955\,\omega$$

Substituting these values in (b) leads to

$$\left.\begin{aligned} 5.17\frac{M_1}{l} + 0.963R_2 &= .5075\,\omega l \\ 3.025\frac{M_1}{l} + 1.012R_2 &= .4775\,\omega l \end{aligned}\right\} \quad (c)$$

Solution of (c) yields $M_1 = .0233\ wl^2$ and $R_2 = .402\ wl$.

Influence Lines for Reactions

The procedure just discussed can be used to derive expressions for the influence lines for the reactions as a unit load passes from one end of the beam to the other. To derive an expression for the influence line for R_1 in the beam shown in Fig. 5(a), let us first consider the force system shown in Fig. 5(b). Displacing the point of support at R_1' a unit distance, keeping $y_2 = 0$ and applying the reciprocal theorem to the two force systems lead to

$$P y - R_1 y_1 = 0$$

or

$$R_1 = P\left(\frac{y}{y_1}\right) = y \quad (23)$$

Thus, the elastic curve shown in Fig. 5(b) is the influence line for R_1. For this case, (15) becomes[3]

$$\left.\begin{aligned} R_1' D_{11} + R_2' D_{12} &= -F \\ R_1' D_{12} + R_2' D_{22} &= 0 \end{aligned}\right\} \quad (24)$$

Solution of (24) yields

$$\left.\begin{aligned} R_1' &= \frac{-F D_{22}}{D_{11} D_{22} - (D_{12})^2} \\ R_2' &= \frac{F D_{12}}{D_{11} D_{22} - (D_{12})^2} \end{aligned}\right\} \quad (25)$$

3. Note that $d_1 = -y_1 = -1$ and $d_2 = y_2 = 0$

Substituting (25) in (11) and (23) leads to

$$R_1 = y = \frac{1}{D_{11}D_{22}-(D_{12})^2}\sum_{n=1}^{\infty}\frac{1}{n^4}\left(D_{22}\sin n\pi a_1 - D_{12}\sin n\pi a_2\right)\sin\frac{n\pi x}{l} \qquad (26)$$

Example 3

In the beam shown in Fig. 5(a), if $a_1 = \frac{1}{3}$ and $a_2 = \frac{2}{3}$, (17) yields

$$\left.\begin{aligned} D_{11} &= \sum_{n=1}^{\infty}\frac{1}{n^4}\sin^2\frac{n\pi}{3} = \frac{3}{4}\left(1+\frac{1}{16}\cdots\cdots\right) = \frac{51}{64} \\ D_{12} &= \sum_{n=1}^{\infty}\frac{1}{n^4}\sin\frac{n\pi}{3}\sin\frac{2n\pi}{3} = \frac{3}{4}\left(1-\frac{1}{16}\cdots\right) = \frac{45}{64} \\ D_{22} &= \sum_{n=1}^{\infty}\frac{1}{n^4}\sin^2\frac{2n\pi}{3} = \frac{3}{4}\left(1+\frac{1}{16}\cdots\cdots\right) = \frac{51}{64} \end{aligned}\right\} \qquad (d)$$

Substituting these values in (26) leads to

$$R_1 = \frac{1}{9}\sum_{n=1}^{\infty}\frac{1}{n^4}\left(51\sin\frac{n\pi}{3} - 45\sin\frac{2n\pi}{3}\right)\sin\frac{n\pi x}{l} \qquad (e)$$

The ordinates of the influence diagram for R_1, as given by (e) are tabulated in Table I for arguments of $\frac{x}{l}$, using only the first two terms of the expansion.

Referring again to the beam shown in Fig. 5(a), an expression for the influence line for R_A shown in Fig. 5(c), may be derived in similar manner with slight modification. Observing that the relative displacements of the points of supports at R_1'' and R_2'', shown in Fig. 5(c), with respect to the straight line passing through AB are respectively $(1-a_1)$ and $(1-a_2)$, it is evident that

$$R_A = y(x) = Z(x) - \omega(x) = \left(1-\frac{x}{l}\right) - \omega(x) \qquad (27)$$

where w(x) is the equation of the elastic curve shown in Fig. 5(d). For the force system shown in Fig. 5(d), employing the same procedure discussed earlier results in the expression

$$\omega(x) = \frac{1}{D_{11}D_{22}-(D_{12})^2}\sum_{n=1}^{\infty}\frac{1}{n^4}\left[\begin{aligned}&\{(1-a_1)D_{22}-(1-a_2)D_{12}\}\sin n\pi a_1 \\ &+\{(1-a_2)D_{11}-(1-a_1)D_{12}\}\sin n\pi a_2\end{aligned}\right]\sin\frac{n\pi x}{l} \qquad (28)$$

Substituting (28) in (27) yields

$$R_A = 1-\frac{x}{l} - \frac{1}{D_{11}D_{22}-(D_{12})^2}\sum_{n=1}^{\infty}\frac{1}{n^4}\left[\begin{aligned}&\{(1-a_1)D_{22}-(1-a_2)D_{12}\}\sin n\pi a_1 \\ &+\{(1-a_2)D_{11}-(1-a_1)D_{12}\}\sin n\pi a_2\end{aligned}\right]\sin\frac{n\pi x}{l} \qquad (29)$$

(29) is actually simpler than it appears to be. The next example illustrates this point.

Example 4

Consider again the beam discussed in Example 3. Substituting (d) in (29) leads to

$$R_A = 1 - \frac{x}{l} - \frac{1}{9}\sum_{n=1}^{\infty}\frac{1}{n^4}\left(19\sin\frac{n\pi}{3} - 13\sin\frac{2n\pi}{3}\right)\sin\frac{n\pi x}{l} \qquad \text{(f)}$$

The ordinates of the influence diagram for R_A, as given by (f), are tabulated in Table I for arguments of x/1, using only the first two terms of the expansion.

CONCLUSIONS

An advantage of this solution lies in the fact that (11), (26) and (29) are continuous over the intermediate supports. Consequently the deflection and slope of the elastic curve as well as the influence lines for the redundant reactions are each given by one expression which takes account of all the spans. The rapid convergence of the series used in the solution reduces the numerical work to a minimum.

TABLE I. Ordinates of Influence Diagrams for R_1 and R_A

$\frac{x}{1}$	0	$\frac{1}{6}$	$\frac{1}{3}$	$\frac{1}{2}$	$\frac{2}{3}$	$\frac{5}{6}$	1
R_1	0	.789	1.000	.577	0	-.211	0
R_A	1.000	.378	0	-.077	0	.0448	0

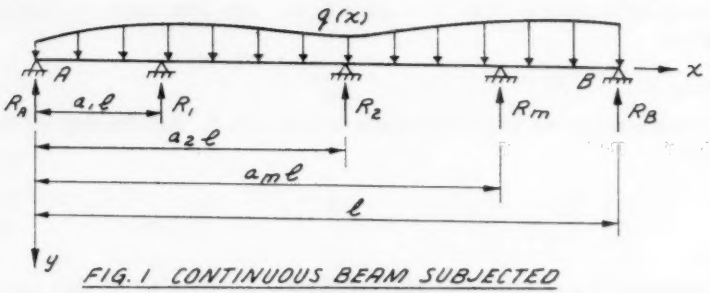

FIG. 1 CONTINUOUS BEAM SUBJECTED TO GIVEN LOAD

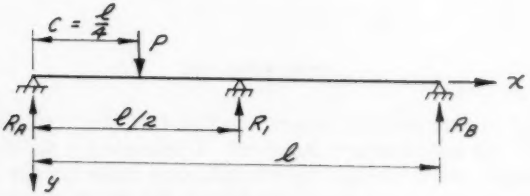

FIG. 2 TWO EQUAL SPANS WITH CONCENTRATED LOAD

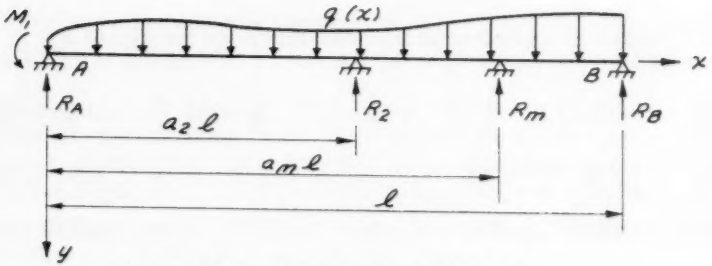

FIG. 3 REDUNDANT MOMENT AT LEFT END

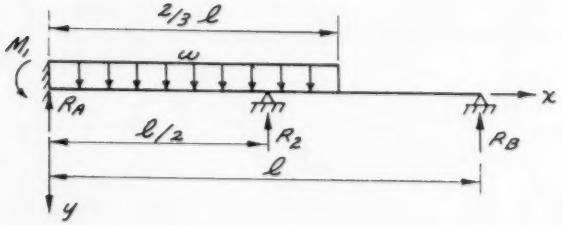

FIG. 4 CONTINUOUS BEAM FIXED AT LEFT END WITH PARTIAL UNIFORM LOAD

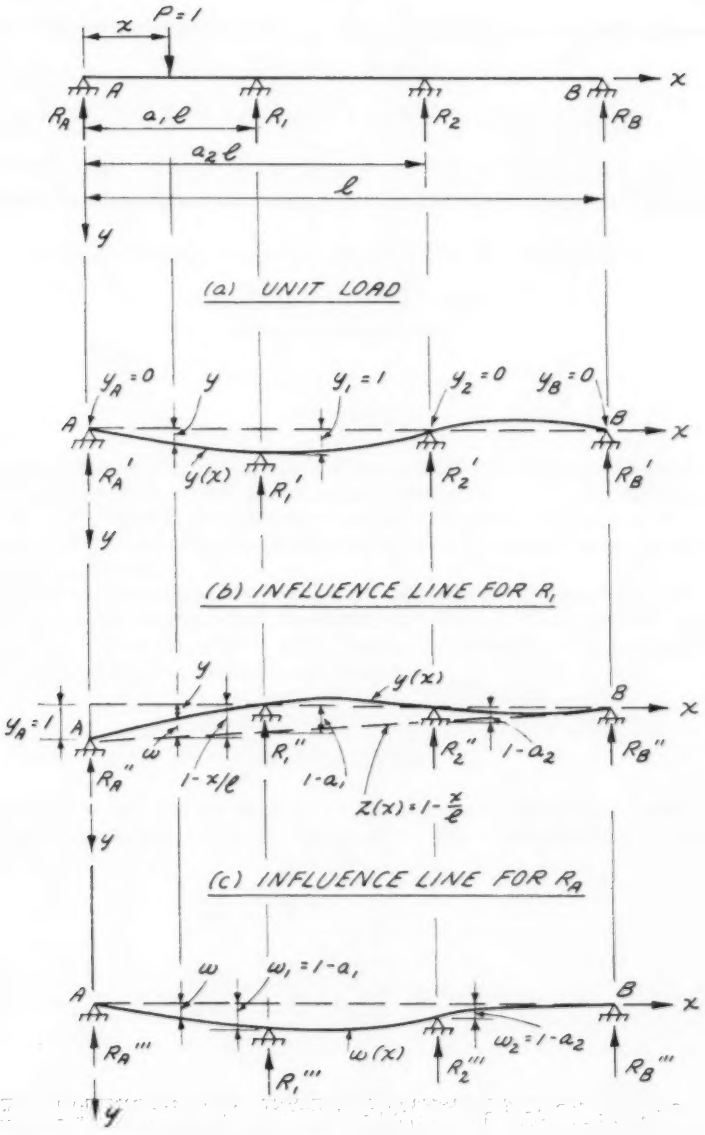

FIG. 5 INFLUENCE LINES FOR REACTIONS

Paper 1412 October, 1957 EM 4

Journal of the
ENGINEERING MECHANICS DIVISION
Proceedings of the American Society of Civil Engineers

GRAPHICAL SOLUTION OF EQUATIONS OF VIBRATIONS

Wen-Hsiung Li,*A.M. ASCE
(Proc. Paper 1412)

SYNOPSIS

A graphical method is presented for the analysis of dynamical systems of oscillations described by two simultaneous first-order ordinary differential equations. This method involves step-by-step graphical integration in a manner similar to Jacobsen's general method of solving second-order ordinary differential equations.

Examples of application are taken from hydraulic vibrations with non-linear damping force and arbitrary forcing function. Systems involving two sets of two simultaneous equations (two surge tanks connected to a conduit; and a differential surge tank) are included as examples.

INTRODUCTION

Many dynamical systems of oscillations are described by two simultaneous first-order ordinary differential equations.(1) The equations to be considered in this paper are

$$\frac{dy}{dt} = f_1(x, y, t) \tag{1a}$$

and

$$\frac{dx}{dt} = f_2(x, y, t) \tag{1b}$$

When analytical solutions are unattainable or difficult to obtain, approximate solutions can be obtained by stepwise integration. In this paper, a graphical method is presented for stepwise integration of Eqs. (1).

Note: Discussion open until March 1, 1958. Paper 1412 is part of the copyrighted Journal of the Engineering Mechanics Division of the American Society of Civil Engineers, Vol 83, No. EM 4, October, 1957.

*Associate Prof. of Civ. Eng., The Johns Hopkins Univ., Baltimore, Md.

When the functions f_1 and f_2 in Eqs. (1) are independent of the variable t, the equations can be reduced to

$$\frac{dx}{dy} = \psi(x, y) \tag{2}$$

which can be integrated by the Method of Isoclines.(1) The method presented in this paper can be used for equations where the functions f_1 and f_2 may involve the variable t. This method is similar to the graphical method of solving second-order ordinary differential equations advanced by Jacobsen.(2)

A Graphical Method of Solving Two First-Order Equations

Before considering two simultaneous first-order ordinary differential equations in a more general form, first take the following linear equations with constant coefficients:

$$\frac{dy}{dt} + mx = \text{constant } M \tag{3a}$$

and

$$\frac{dx}{dt} + ny = \text{constant } N \tag{3b}$$

where m and n are non-zero constants of opposite signs. Eliminate the variable t from these equations:

$$\frac{dy}{mx - M} = \frac{dx}{ny - N} \tag{4}$$

Integrating,

$$(x - x_c)^2 + (u - u_c)^2 = \text{constant} \tag{5a}$$

where

$$u = y\sqrt{\left(-\frac{n}{m}\right)} \tag{5b}$$

$$x_c = \frac{M}{m} \tag{5c}$$

$$u_c = -\frac{N}{m}\sqrt{\left(-\frac{m}{n}\right)} \tag{5d}$$

Here u is directly proportional to y for constant values of m and n. When Eqs. (3) are dimensionally homogeneous, u has the same dimensions as x. The solution of Eqs. (3) in the u-x plane (with u and x in the same scale) is, according to Eqs. (5), a circle with its center at (u_c, x_c), as shown in Fig. 1. The radius of the circle is fixed by a pair of known values of u and x, such as (u_o, x_o) at t_o. Any point on this circle represents the simultaneous values of u and x at a certain value of t. The value of dt required for the simultaneous changes du and dx from one point to another at a distance ds apart

(see Fig. 1) can be shown to be related to the angle $d\theta$: With the angle θ considered positive in the counterclockwise direction in the u-x plane,

$$d\theta = \frac{ds}{\rho} = \frac{dx}{u-u_c} = \frac{(N - ny)\,dt}{y\sqrt{\left(-\frac{n}{m}\right)} + \frac{N}{m}\sqrt{\left(-\frac{m}{n}\right)}} = -n\sqrt{\left(-\frac{m}{n}\right)}\cdot dt \tag{6}$$

Eq. (6) shows that the angle θ increases linearly with t for constant values of m and n.

Next, consider two simultaneous first-order ordinary differential equations in a more general form:

$$\frac{dy}{dt} = f_1(x,y,t) \tag{7a}$$

and

$$\frac{dx}{dt} = f_2(x,y,t) \tag{7b}$$

These equations can be rewritten as

$$\frac{dy}{dt} + mx = f_1(x,y,t) + mx = M(x,y,t) \tag{8a}$$

$$\frac{dx}{dt} + ny = f_2(x,y,t) + ny = N(x,y,t) \tag{8b}$$

The values of the constants m and n are chosen to be non-zero, one being positive and the other negative. For dynamical systems with positive linear restoring forces, this condition is automatically satisfied. Eqs. (8) differ from Eqs. (3) in that, instead of being two constants, M and N are functions of x, y, and t. Since x and y are functions of t alone, the values of M and N depend upon t. Approximate solutions for x and y can be obtained by integrating successively through short intervals Δt, during each of which M and N are taken as constants for approximation. Thus, according to Eqs. (5) and (6), this approximate solution consists of the end-points of a series of circular arcs (see Fig. 2). For each arc, the center is located by Eqs. (5c) and (5d), in which the values of M and N may be computed from the values of x, y, and t at the middle of the interval Δt. These values of x and y can readily be estimated from the graph by extrapolation. The angle $\Delta\theta$ (see Fig. 2) for each arc, according to Eq. (6), is

$$\Delta\theta = -n\sqrt{\left(-\frac{m}{n}\right)}\cdot \Delta t \tag{9}$$

Graphical Method of Solving Second-Order Equations

The method advanced by Jacobsen[2] for solving second-order ordinary differential equations can be deduced from the method presented above. Consider the equation

$$\frac{d^2x}{dt^2} = \phi\left(x, \frac{dx}{dt}, t\right) \tag{10}$$

This equation can be rewritten as

$$\frac{dy}{dx} + p^2 x = \phi(x,y,t) + p^2 x = p^2 \cdot F(x,y,t) \quad (11a)$$

where

$$y = \frac{dx}{dt} \quad (11b)$$

and p is a constant. Comparing Eqs. (11) with Eqs. (8), we have in the u-x plane, according to Eqs. (5) and (9),

$$u = \frac{1}{p} \cdot \frac{dx}{dt} \quad (12a)$$

$$x_c = F(x, \frac{dx}{dt}, t) \quad (12b)$$

$$u_c = 0 \quad (12c)$$

and

$$\Delta\theta = p \cdot \Delta t \quad (12d)$$

The solution of Eq. (10) in the u-x plane, a phase-plane in this case, is given by a series of circular arcs, the centers of which are located on the x-axis. This is Jacobsen's method of solving second-order ordinary differential equations. Examples of application of his method can be found in published papers.(3,4)

Application to Hydraulic Vibrations

While the graphical method presented in this paper is applicable to other dynamical systems described by Eqs. (1), problems from hydraulic vibrations are chosen for demonstrating the application of the method. The characteristics of hydraulic vibrations have been studied by others.(5,6,7,8) This graphical method is used to find quantitative answers with given values of the parameters involved.

Three problems are chosen as examples: (1) The first problem is to find the maximum surge in a simple surge-tank as shown in Fig. 3a. (2) the second problem is to find the surges in two surge-tanks connected to a conduit as shown in Fig. 3b. This problem involves two sets of two simultaneous equations. (3) The third problem is to find the surge in a differential surge-tank as shown in Fig. 3c. In this problem, the motion is described by different sets of simultaneous equations under changing conditions.

The equations used in these examples are those conventionally used by hydraulic engineers.(9) In these equations, water is assumed to be incompressible and the effects of water-hammer are thus excluded from consideration.

Example 1. A Simple Surge-Tank

The problem is to find the maximum surge of the water-surface in the simple surge-tank shown in Fig. 3a when the valve, originally closed, is suddenly opened. The physical constants in ft.-sec. units are:

Length of conduit, L = 27,000 ft.
Cross-sectional area of conduit, A = 80 sq. ft.
Cross-sectional area of tank, A_t = 800 sq. ft.
Reservoir surface above outlet, H = 550 ft.
Head loss in conduit = $c|v|v = 0.5|v|v$

When the valve is opened, the discharge at the outlet is given by

$$Q = 40\sqrt{h}, \quad (\text{for } t > 0) \tag{13}$$

The equations governing the motion are

$$H - h = c|v|v + \frac{L}{g}\frac{dv}{dt} \tag{14}$$

and

$$Av = A_t\frac{dh}{dt} + Q \tag{15}$$

These two equations can be reduced to the following form:

$$\frac{dv}{dt} + \frac{g}{L}h = \frac{g}{L}(H - c|v|v) \tag{16a}$$

and

$$\frac{dh}{dt} - \frac{A}{A_t}v = -\frac{Q}{A_t} \tag{16b}$$

Comparing Eqs. (16) with Eqs. (8), we have, with the variables h and v corresponding to x and y respectively, $m = g/L$, $n = -A/A_t$, $M = (H - c|v|v)g/L$, and $N = -Q/A_t$. Thus from Eqs. (5) and (9), we have, for each Δt in the u-h plane (u and h in the same scale), the solution given by a circular arc subtended by angle $\Delta\theta$, where

$$u = v\sqrt{\frac{AL}{A_t g}} = 9.17\,v \tag{17a}$$

$$h \text{ of center} = H - c|v|v = 550 - 0.5|v|v \tag{17b}$$

$$u \text{ of center} = \frac{Q}{A}\sqrt{\frac{AL}{A_t g}} \tag{17c}$$

that is,

$$v \text{ of center} = \frac{Q}{A} = 0.5\sqrt{h}, \quad (\text{for } t > 0) \tag{17d}$$

and

$$\Delta\theta \text{ in radians} = \sqrt{\frac{A_t g}{A_t L}}\cdot\Delta t \tag{17e}$$

From past experience in stepwise integration for the maximum surge, except in cases where transient disturbances of short durations are involved, eight

or more steps usually prove satisfactory.(10) In this example, a value of 15 seconds for Δt is used. Thus, $\Delta\theta = 9.38$ degrees.

In the u-h plane as shown in Fig. 4, construct the line ($h = 500 - 0.5\,|v|\,v$) which according to Eq. (17b), locates the ordinate of the center of the arc. Also construct the line ($v = 0.5\sqrt{h}$) which, according to Eq. (17d), locates the abscissa of the center of the arc. Thus, with an estimated mean values of v and h during an interval Δt, the center of the arc can easily be located. For example, to locate point 5 in Fig. 4 after point 4 has been obtained, extrapolate from the curve 0-4 to estimate the probable position of the mid-point 4' of the arc 4-5. Point I, the intersection of the ($h = H - c\,|v|\,v$) line and a vertical through point 4', gives the ordinate of the center of the arc 4-5. Point II, the intersection of a horizontal line through point 4' and the line ($v = 0.5\sqrt{h}$), gives the abscissa of the center of the arc 4-5. Thus point III is the center of the arc 4-5. With a radius equal to 4-III and an angle $\Delta\theta$ of 9.38 degrees, point 5 is located.

In constructing Fig. 4, no revision of the estimated position of the center was found necessary except for the first arc 0-1.

Example 2. Two Surge-Tanks Connected to a Conduit

Two simple surge-tanks connected to a conduit are shown in Fig. 3b. The problem is to find the surges in the tanks created by gradual closure of the valve at the outlet. The physical constants, in ft.-sec. units, are:

Conduit lengths: $L_1 = 22{,}400$ feet
$L_2 = 22{,}200$ feet
Cross-sectional area of conduit, $A_1 = A_2 = 80$ sq. ft.
Reservoir surface above outlet, $H = 550$ feet
Initial steady velocity in conduit = 10.0 ft. per sec.
Cross-sectional areas of tanks: $A_{t1} = 892$ sq. ft.
$A_{t2} = 715$ sq. ft.
Head loss in upper conduit = $c_1\,|v_1|\,v_1 = 0.342\,|v_1|\,v_1$
Head loss in lower conduit = $c_2\,|v_2|\,v_2 = 0.435\,|v_2|\,v_2$
Initial surface elevation in upper tank = $550 - 0.342 \times 10^2$
$= 515.8$ ft.
Initial surface elevation in lower tank = $515.8 - 0.435 \times 10^2$
$= 472.3$ ft.

The closure of the valve at the outlet is completed in 90 seconds such that the discharge Q at the outlet is

$$Q = 36.8\left(1 - \frac{t}{90}\right)\sqrt{h_2}, \quad (\text{for } 0 \le t \le 90) \tag{18}$$

The equations governing the motion are

$$\frac{dV_1}{dt} + \frac{g}{L_1}\cdot h_1 = \frac{g}{L_1}\left(H - c_1 |V_1| V_1\right) \tag{19a}$$

$$\frac{dh_1}{dt} - \frac{A_1}{A_{t1}}\cdot V_1 = -\frac{A_2}{A_{t1}}\cdot V_2 \tag{19b}$$

$$\frac{dv_2}{dt} + \frac{g}{L_2} h_2 = \frac{g}{L_2}\left[H - c_2 |v_2| v_2 - (H - h_1) \right] \quad (20a)$$

and

$$\frac{dh_2}{dt} - \frac{A_2}{A_{t2}} \cdot v_2 = - \frac{Q}{A_{t2}} \quad (20b)$$

By comparing Eqs. (19) with Eqs. (8), we have in the u_1-h_1 plane (see Fig. 5), according to Eqs. (5) and (9):

$$u_1 = v_1 \sqrt{\frac{A_1 L_1}{A_{t1} g}} = 7.9\, v_1 \quad (21a)$$

$$h_1 \text{ of center} = H - c_1 |v_1| v_1 \quad (21b)$$

$$u_1 \text{ of center} = \frac{A_2 v_2}{A_1} \sqrt{\frac{A_1 L_1}{A_{t1} g}} \quad (21c)$$

that is,

$$v_1 \text{ of center} = \frac{A_2 v_2}{A_1} \quad (21d)$$

$$\Delta\theta_1 \text{ in radians} = \sqrt{\frac{A_1 g}{A_{t1} L_1}} \cdot \Delta t \quad (21e)$$

With Δt = 15 seconds, $\Delta\theta_1$ = 9.76 degrees.

Similarly, from Eqs. (20), we have in the u_2-h_2 plane,

$$u_2 = v_2 \sqrt{\frac{A_2 L_2}{A_{t2} g}} = 8.8\, v_2 \quad (22a)$$

$$h_2 \text{ of center} = H - c_2 |v_2| v_2 - (H - h_1) \quad (22b)$$

$$v_2 \text{ of center} = \frac{Q}{A_2} \quad (22c)$$

$$\Delta\theta_2 \text{ in radians} = \sqrt{\frac{A_2 g}{A_{t2} L_2}} \cdot \Delta t \quad (22d)$$

With Δt = 15 seconds, $\Delta\theta_2$ = 10.9 degrees.

In Fig. 5, the lines ($h_1 = H - c_1|v_1|v_1$) and ($h_2 = H - c_2|v_2|v_2$) are first constructed. The steps taken to determine points 10 are shown. The mid-point 9' of the arc 9-10 in each plane is first estimated by extrapolation. The center of the arc 9-10 in the u_1-h_1 plane is located with point I on the ($h_1 = H - c_1|v_1|v_1$) curve below (or above) point 9' and the value of v_2 taken from the u_2-h_2 plane. The center of the arc 9-10 in the u_2-h_2 plane is located by point III at a distance ($H - h_1$) from point II which is on the ($h_2 = H - c_2|v_2|v_2$) curve below (or above) point 9'. The abscissa of this center is at $v_2 = Q/A_2$, which is zero for t greater than 90 seconds.

The same problem was solved by the same graphical method with $\Delta t = 30$ seconds instead of 15 seconds. Practically the same results were obtained. However, with the larger value of Δt, it became more difficult to estimate the position of the mid-points by extrapolation. Sometimes a revision of the estimated position was found necessary. No such revision was found necessary with $\Delta t = 15$ seconds.

Example 3. A Differential Surge-Tank

A differential surge-tank is shown in Fig. 3c. The problem is to find the surge in the tank due to a complete rejection of load on the turbines. The physical constants, in ft.-sec. units, are

Headwater surface above tailwater, H = 442 ft.
Length of conduit, L = 43,200 ft.
Cross-sectional area of conduit, A = 251 sq. ft.
Cross-sectional area of riser, A_r = 201 sq. ft.
Net cross-sectional area of tank, A_t = 3,220 sq. ft.
Top of riser above tailwater, H_r = 500 ft.
Port area, a = 40 sq. ft.
Coefficient of discharge of port holes, C = 0.71
Head loss in conduit = $c|v|v = 0.382|v|v$
Initial water-surface elevation in tank and riser = $442 - 0.382 \times 13.15^2$
= 376 ft.

Upon complete load rejection at t = 0, the turbine gates will be closed in 10/3 seconds such that the discharge Q through the turbines is given by

$$Q = 170\left[1 - \left(\frac{3t}{10}\right)^{1.23}\right]\sqrt{h_t}, \quad (\text{for } 0 \le t \le \tfrac{10}{3}) \tag{23}$$

(In practice, Q may also be obtained from the turbine characteristic curves for given value of h_t and gate opening at given value of t).

The equations governing the motion may be divided into two groups:
(1) When the riser is not filled to the top ($h_r < H_r$):

$$\frac{dv}{dt} + \frac{g}{L} \cdot h_r = \frac{g}{L}(H - c|v|v) \tag{24a}$$

$$\frac{dh_r}{dt} - \frac{A}{A_r} \cdot v = -\frac{A_t}{A_r} \cdot \frac{dh_t}{dt} - \frac{Q}{A_r} \tag{24b}$$

$$A_t \frac{dh_t}{dt} = \pm Ca\sqrt{\pm 2g(h_r - h_t)}, \text{ (for } h_t \lesseqgtr h_r) \tag{25}$$

(2) When water is spilling over the top of riser ($h_r = H_r$):

$$\frac{dv}{dt} = \frac{g}{L}(H - H_r - c|v|v) \tag{26a}$$

$$\frac{dh_t}{dt} - \frac{A}{A_t} \cdot v = -\frac{Q}{A_t} \tag{26b}$$

Eqs. (26) should be used only when there is spilling over the top of the riser, i.e.

$$A_t \frac{dh_t}{dt} > Ca\sqrt{2g(H_r - h_t)} \tag{27}$$

Immediately after the rejection of load on the turbines, the water-surface in the riser rises rapidly. Before the surface reaches the top of the riser, Eqs. (24) and (25) are applicable. In order to obtain a graph of proper proportion, it is desirable to rewrite Eq. (24a) as

$$\frac{dv}{dt} + 10\frac{g}{L}h_r = \frac{g}{L}(H - c|v|v + 9h_r) \tag{28}$$

By comparing Eqs. (28) and (24b) with Eqs. (8), we have in the u-h_r plane, according to Eqs. (5) and (9),

$$u = v\sqrt{\frac{AL}{10A_r g}} = 12.95v \tag{29a}$$

$$\begin{aligned} h_r \text{ of center} &= 0.1(H - c|v|v) + 0.9h_r \\ &= 44.2 - 0.0382|v|v + 0.9h_r \end{aligned} \tag{29b}$$

$$u \text{ of center} = \left[\frac{A_t}{A} \cdot \frac{dh_t}{dt} + \frac{Q}{A}\right]\sqrt{\frac{AL}{10A_r g}} \tag{29c}$$

$$\begin{aligned} v \text{ of center} &= \frac{Ca\sqrt{2g(h_r - h_t)}}{A} + \frac{Q}{A} \\ &= 0.908\sqrt{h_r - h_t} + \frac{Q}{A} \end{aligned} \tag{29d}$$

$$\Delta\theta_r \text{ in radians} = \sqrt{\frac{10Ag}{A_r L}} \cdot \Delta t \tag{29e}$$

In order to include the transient effect of closure, a value of 3 seconds for Δt is used during the period when the water-surface in the riser is rising to the top. With $\Delta t = 3$ seconds, $\Delta\theta_r = 16.6$ degrees. The procedure of solution is shown in Figs. 6a and 6b. For example, to determine points 4 in the two planes, the mid-point 3' of the curve 3-4 in each plane is first estimated by extrapolation. The center of the arc 3-4 in the u-h_r plane can be computed from Eqs. (29b) and (29d) with values of v, h_r and h_t of the mid-points 3'. In the u-h_t plane, Δv is obtained from the u-h_r plane, and Δh_t is computed from Eq. (25):

$$\Delta h_t = \pm \frac{Ca}{A_t}\sqrt{\pm 2g(h_r - h_t)}\cdot\Delta t = \pm 0.0707\sqrt{\pm(h_r - h_t)}\cdot\Delta t \tag{30}$$

This procedure is followed until h_r reaches H_r (at t = 21 seconds).

When the water-surface in the riser reaches and remains essentially at the top of the riser, Eqs. (26) should be used. For the convenience of having a u-h_t plane with the same u as defined by Eq. (29a) for the u-h_t plane, Eq. (26a) should be rewritten as

$$\frac{dv}{dt} + 10\frac{A_r g}{A_t L}h_t = \frac{g}{L}\left(H - H_r - c|v|v + 10\frac{A_r}{A_t}\cdot h_t\right) \tag{31}$$

Comparing Eqs. (31) and (26b) with Eqs. (8), we have in the u-h_t plane, according to Eqs. (5) and (9),

$$u = v\sqrt{\frac{AL}{10A_r g}} = 12.95\,v \tag{32a}$$

$$h_t \text{ of center} = h_t - \frac{A_t}{10A_r}(H_r - H + c|v|v) = h_t - 0.61\,|v|v - 92.8 \tag{32b}$$

$$u \text{ of center} = \frac{Q}{A}\sqrt{\frac{AL}{10A_r g}} \quad (=0 \text{ in this case}) \tag{32c}$$

$$\Delta\theta_t \text{ in radians} = \sqrt{\frac{10A_r A g}{LA_t^2}}\cdot\Delta t \tag{32d}$$

With $\Delta t = 20$ seconds, $\Delta\theta_t = 6.9$ degrees. The procedure of solution is shown in Fig. 6b. For example, to determine point 10, the mid-point 9' of the arc 9-10 in the u-h_t plane is estimated by extrapolation. The location of the center of the arc can be determined from Eq. (32b) with the values of v and h_t of point 9'. This procedure is followed as long as Eq. (27) holds, i.e.

$$\Delta h_t > 0.0707\sqrt{500 - h_t}\cdot\Delta t \tag{33}$$

This required condition should be checked at each step.

After point 11 (at t = 101 seconds), Eq. (33) is no longer satisfied. The water-surface in the riser is falling below the top of the riser. Eqs. (24), (25) and (29) should again be used. With Δt = 10 seconds, Eq. (29e) gives $\Delta\theta_r$ = 55.3 degrees. The procedure of solution is the same as for the period immediately after load-rejection.

The same problem has been solved by numerical integration by Rich (p. 152 of Reference 10). His solution gives the same maximum elevation of water-surface in the tank (483.5 ft.) at the same time (262 seconds after load-rejection).

REFERENCES

1. Andronow, A. A. and Chaikin, C. E., "Theory of Oscillations," Princeton Univ. Press, 1949, Chapters V and VI.

2. Jacobsen, L. S., On a General Method of Solving Second-Order, Ordinary Differential Equations by Phase-Plane Displacements, J. Applied Mech., Vol. 19, No. 4, 1952, p. 543.

3. Ayre, R. S., Transient Vibration of Linear Multiple-Degree-of-Freedom Systems by the Phase-Plane Method, Journ. Franklin Inst., Vol. 253, No. 2, 1952, p. 153.

4. Bishop, R. E. D., On the Graphical Solution of Transient Vibration Problems, Proc. Inst. Mech. Eng., Vol. 168, No. 10, 1954.

5. Thoma, D., "Zur Theorie des Wasserschlosses bei selbsttätig geregelten Turbinenanlagen," Oldenbourg, Munich, 1910.

6. Johnson, R. D., The Differential Surge Tank, Trans. ASCE, Vol. 78, 1915, p. 760.

7. Jaeger, C., Present Trends in Surge Tank Design, Proc. Inst. Mech. Eng., Vol. 168, No. 2, 1954.

8. McLachlan, N. W., On a Nonlinear Differential Equation in Hydraulics, Proc. Symposia in Applied Math., Vol. V, Amer. Math. Soc., 1954.

9. Rich, G. R., "Hydraulic Transients," McGraw-Hill Book Co., New York, 1951.

10. Gibson, A. H., "Hydraulics and Its Applications," Constable and Co., London, 1930, p. 549.

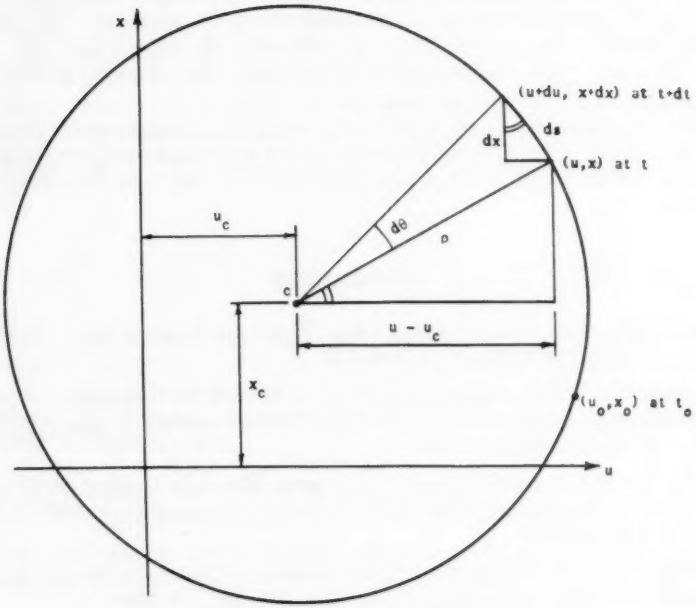

Figure 1. Solution of Equations (3a) and (3b)

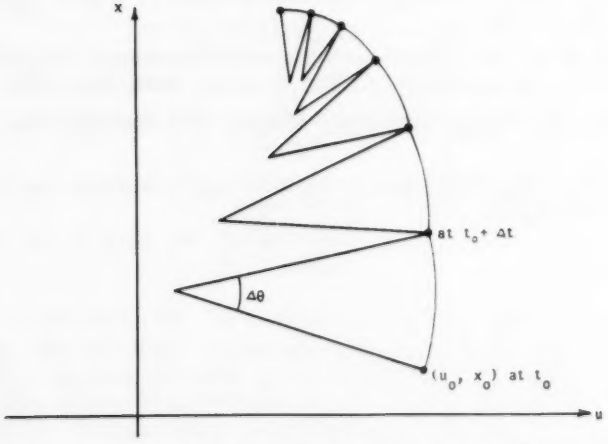

Figure 2. Solution of Equations (8a) and (8b)

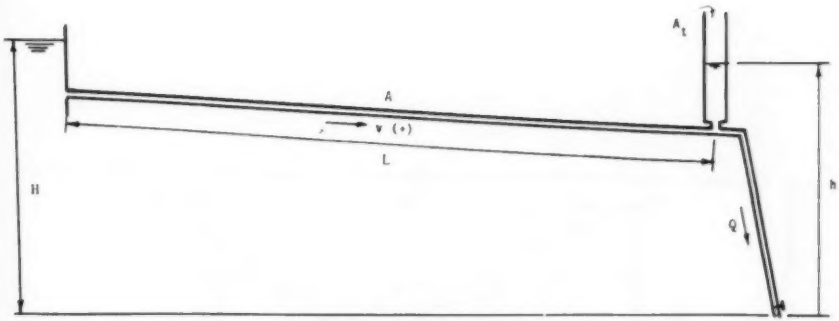

(a) Example 1. A Simple Surge-Tank

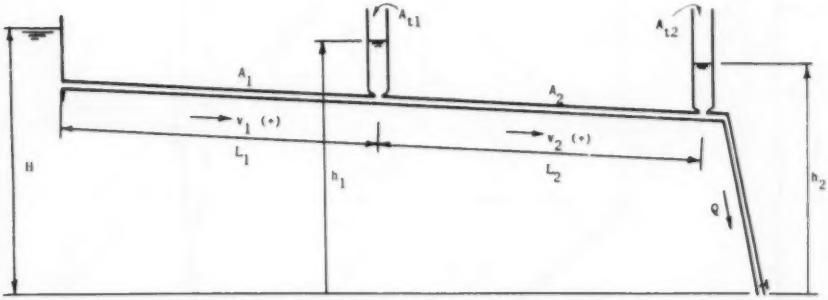

(b) Example 2. Two Surge-Tanks Connected to a Conduit

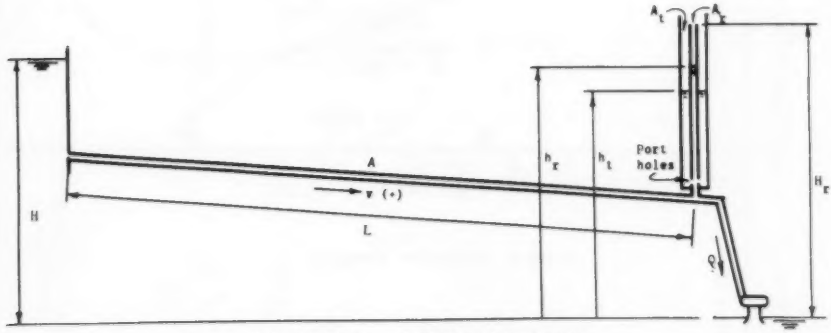

(c) Example 3. A Differential Surge-Tank

Figure 3. Hydraulic Systems in the Examples

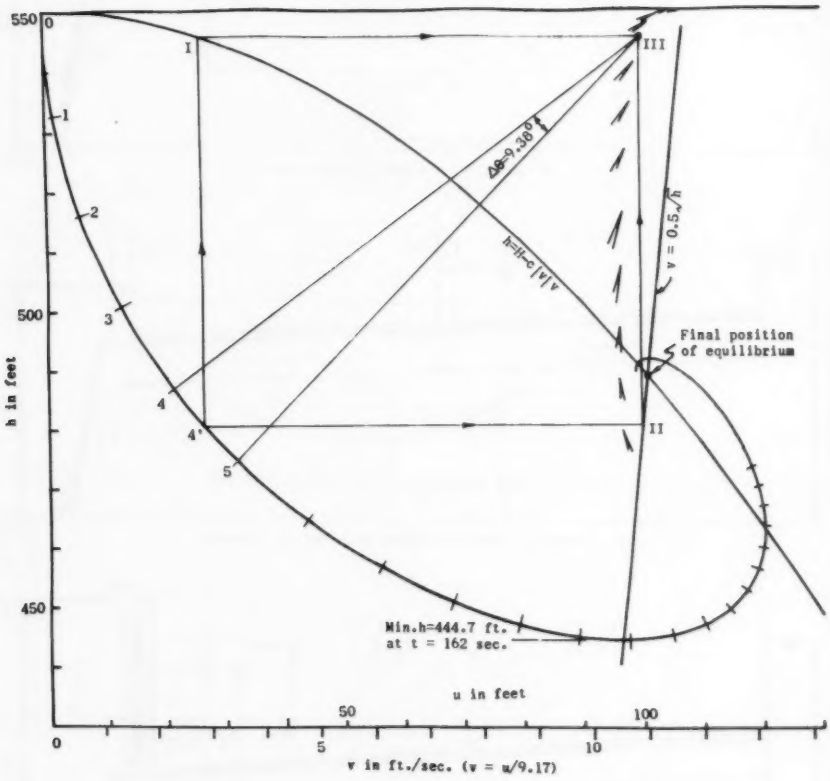

Figure 4. Solution of Example 1.

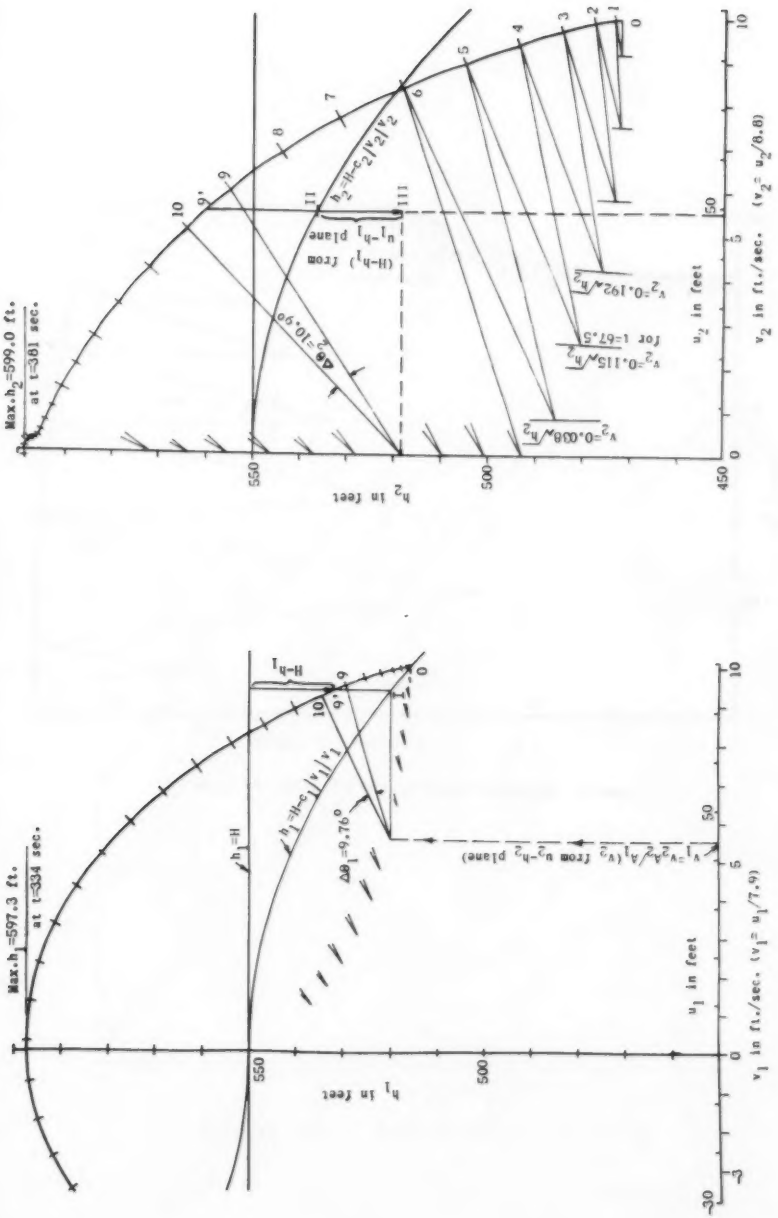

Figure 5. Solution of Example 2.

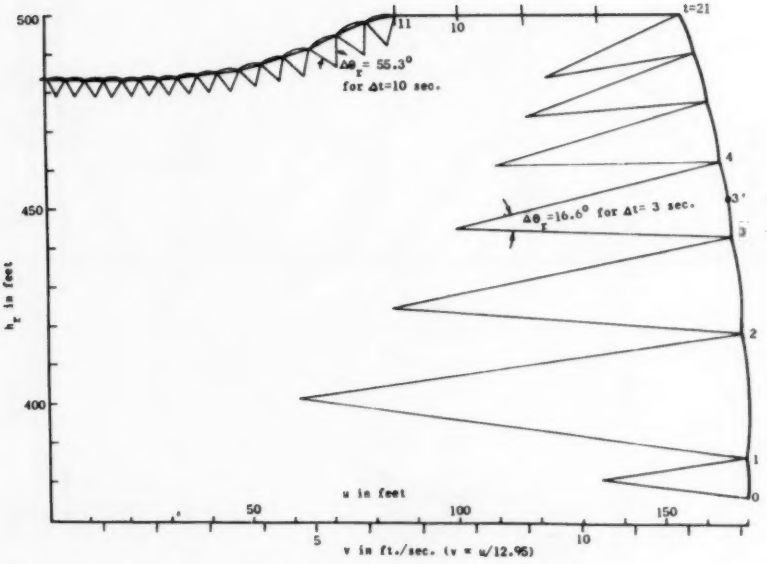

Figure 6a. Solution of Example 3. (For u-h_t plane, see Fig.6b)

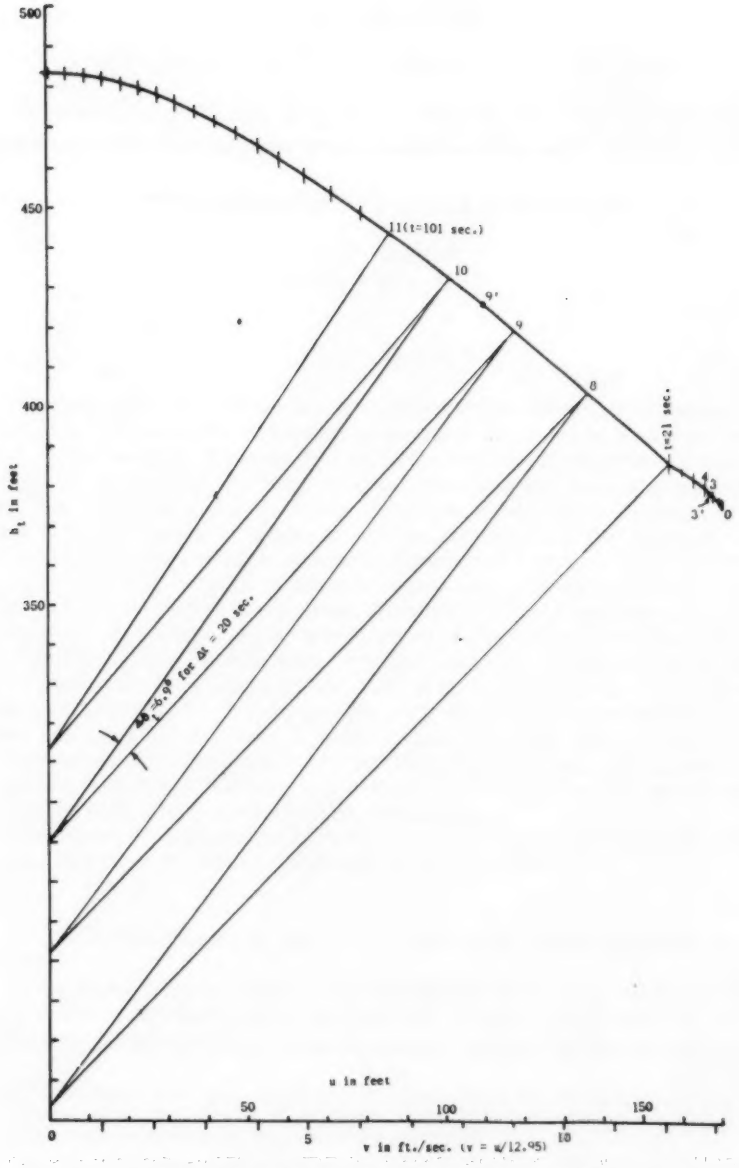

Figure 6b. Solution of Example 3. (For u-h_t plane, see Fig.6a)

Paper 1413 October, 1957 EM 4

Journal of the
ENGINEERING MECHANICS DIVISION
Proceedings of the American Society of Civil Engineers

THE STRENGTH OF VERY SLENDER BEAMS[1]

E. F. Masur[2]
(Proc. Paper 1413)

SUMMARY

The response of a slender beam to lateral loads and twisting couples is affected by the presence of bending moments in the plane of major stiffness much as the bending of beams may be influenced by the presence of axial forces. If, in addition, the major bending moments are statically indeterminate, and if the beam is sufficiently slender to admit relatively large lateral deformations, these may in turn affect the distribution of the principal bending moments. The resulting nonlinear theory is the subject of this paper.

After the establishment of the basic equations, it is shown that the inclusion of nonlinear terms in the strain-displacement relations corresponds generally to a stiffening of the structure as compared with the familiar linear theory. The (redistributed) major bending moments and reactions are shown to satisfy a minimum principle which represents an extension of the classical Castigliano Theorem. It is demonstrated further that, for increasing lateral loads and torsional moments, a limiting major bending moment distribution is approached asymptotically. For certain singular cases, the corresponding equilibrium configuration may not be unique, in which case the possibility of a snap-through (Durchschlag) phenomenon arises.

The theory presented herein is corroborated experimentally with a fair degree of accuracy. Elastic behavior is assumed throughout.

INTRODUCTION AND ESTABLISHMENT OF BASIC EQUATIONS

In the present paper, a beam will be referred to as being "slender" when its moment of inertia I_y about the (vertical) y-axis is much smaller than the moment of inertia I_x; in addition, its torsion constant K will be assumed

Note: Discussion open until March 1, 1958. Paper 1413 is part of the copyrighted Journal of the Engineering Mechanics Division of the American Society of Civil Engineers, Vol. 83, No. EM 4, October, 1957.

1. This investigation was conducted under the sponsorship of the Office of Ordnance Research, U. S. Army.
2. Associate Prof. of Eng. Mechanics, Univ. of Michigan, Ann Arbor, Mich.

small in comparison with I_x. An example of a slender beam is furnished by a rectangular beam, whose thickness t is small compared with its depth h.

The response of such a beam to lateral loads and torsional couples in the presence of bending moments about the x-axis has been the subject of numerous investigations.(1,2)3 It is shown in these papers how the bending moments influence, and often aggravate, the displacements of a slender beam. This is analogous to the behavior of beam-columns, whose response to loads in the presence of axial forces is well known.

In all previous publications on the subject, the assumption is made more or less tacitly that the bending moments are either statically determinate or, in the event of statical indeterminacy in the major plane of stiffness, that they may be computed on the basis of the conventional linear theory. This may actually not be the case. In fact, if the lateral displacements u and the rotations β are sufficiently large, the introduction of nonlinear strain displacement relations may serve to modify the predicted moments. This question is explored in detail in what follows. It is shown that a redistribution of bending moments takes place, which serves to stiffen the structure relative to its predicted stiffness according to conventional theory. For example, if there are no vertical loads acting on the beam, the linear theory predicts, of course, vanishing bending moments everywhere in the absence of initial stresses. However, when certain nonlinear terms are included in the analysis, such moments do arise, and approach limiting values as the magnitude of the lateral loads and torques approaches infinity.

Before proceeding to the analysis, it may be well to point out the limitations of the proposed theory. Actually, the nonlinearity is partial only in that the strain-displacement relations contain terms up to the second order, but ignore those of higher order. Physically this implies that the lateral displacements may be comparable to the thickness of the beam, but are still assumed to be small in relation to its length. Theories of an analogous nature are widely employed in connection with the analysis of structural elements in which at least one dimension is much smaller than the remaining dimensions; the best known example is probably the plate theory of von Kármán.(3) Since, furthermore, the effect of plasticity in this presentation is ignored, it follows that the beam must be very slender to lend physical significance to the proposed theory. In the numerical example treated in a later section, appreciable deviations occur from linear theory at fiber stresses of about 30,000 psi in a beam whose depth-thickness ratio is 16:1.

In what follows, let a beam of the type shown in Fig. 1 be subjected to lateral loads λq and twisting couples λt, in which q and t are given functions of z (measured along the axis of the beam), and λ is a multiplier which is allowed to increase indefinitely. If $\lambda u(z)$ and $\lambda\beta(z)$ are the horizontal displacement and the rotation, respectively, u and β are governed by the equations of equilibrium.

$$(EI_y u'')'' + Pu'' + [(M + Py_o)\beta]'' = q(z) \tag{1}$$

$$(E\Gamma\beta'')'' - [(GK - P\rho^2 - 2kM)\beta']' + (M + Py_o)u'' - pa\beta = t(z) \tag{2}$$

3. Numbers in brackets refer to the Bibliography at the end of the paper. Reference (2) contains a fairly comprehensive list of publications on the subject.

where primes denote differentiation with respect to z. In these equations P represents the axial force (measured positive in compression), M(z) the bending moment about the centroidal x-axis, and p(z) the given vertical load applied at a distance a above the shear center S. E and G are the usual elastic constants, Γ is the warping constant, ρ is the radius of gyration about S, and y_o designates the position of S.[4] Finally, k is a cross-sectional constant and is defined by

$$k = y_o - \frac{1}{2I_x}\int_A y(x^2+y^2)\,dA \tag{3}$$

which vanishes for sections symmetrical about the x-axis.

Equations (1), (2), and (3) are the familiar equations of lateral bending and torsion,[4] although slight discrepancies are present.[5] Through a process which is entirely analogous to the one employed,[5] [5] it can be shown further that the vertical displacement v(z) satisfies the relationship

$$V'' = -(M-M^*)/EI_x + \lambda^2(u''\beta - k\beta'^2) \tag{4}$$

in which the second term on the right side represents the effect of the nonlinearity in the strain-displacement relations. M*(z) designates prestressing moments (if any) and has been incorporated for the sake of completeness.

The inclusion of the nonlinear terms in Eq. (4) and the deletion of analogous terms from Eqs. (1) and (2) imply that the vertical displacements are much smaller than the horizontal and rotational displacements. This in turn requires that the beam be slender, as was outlined above. In the development of Eq. (4) it is assumed further that the force P be much smaller than the critical buckling force about the (strong) x-axis; in view of the slenderness of the beam, however, this represents no added restriction.

The bending moments M(z) and M*(z) satisfy the equations of equilibrium

$$M'' = -p(z) \qquad M^{*\prime\prime} = 0 \tag{5}$$

and a set of appropriate natural boundary conditions. These, together with Eq. (5), determine M and M* uniquely (the latter trivially) if the structure is

4. The assumption that S lies on the principal y axis introduces no significant loss of generality.
5. The writer is indebted to Professor E. Reissner for suggesting, as an alternative, the derivation of these equations from large deflection plate theory. This process can be carried out for the technically most significant case of a thin rectangular beam and, with the exception of the introduction of the term $(1-\mu^2)^{-1}$, leads to relationships which are identical with Eqs. (1) and (2) (properly simplified for this case, of course). However, the form of Eq. (4) is slightly modified by this procedure. This discrepancy, which may affect the results somewhat in the presence of non-uniform bending, is due to a minor variation in the basic assumptions underlying plate theory as compared with the Euler-Bernoulli beam theory on which the present derivation is based.

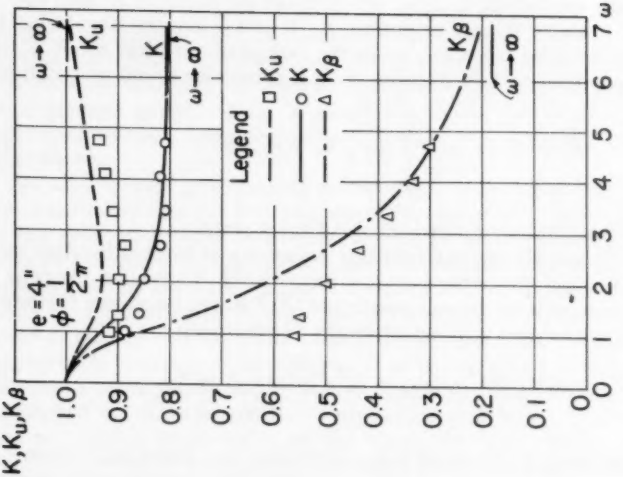

Fig. 2. Reduction factors for small eccentricity.

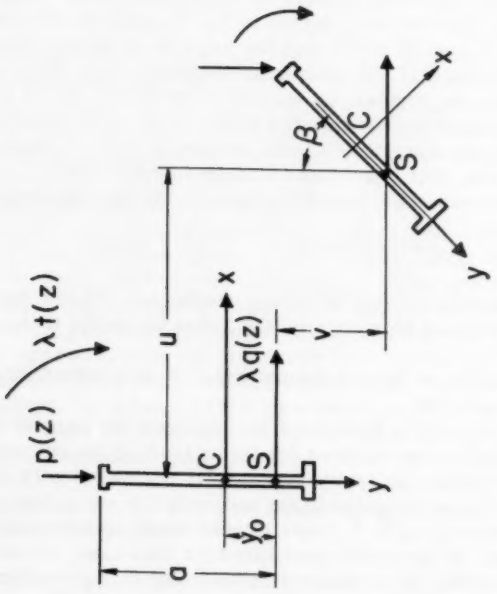

Fig. 1. Typical cross section.

statically determinate relative to its major bending moments. In that event, for given vertical load p(z) and axial force P, the "calibrated" functions u(z) and $\beta(z)$ are also uniquely determined by Eq. (1) and (2) and the associated boundary conditions. Hence the total response λu and $\lambda\beta$ increases in proportion to the total lateral load and torque λq and λt, respectively.

A different picture is presented by a structure whose major bending moments are statically redundant. In that case, the actual moment M(z) is distinguished, among all moments satisfying Eq. (5) and boundary conditions, by being associated with a geometrically compatible vertical deflection v(z). Since the latter is related to M by means of Eq. (4), it becomes apparent that increasing lateral loads and torques, as expressed by increasing values of λ, are accompanied by a redistribution of the principal bending moments. The equations governing this redistribution are developed in the remainder of this section.

In a structure of n^{th} degree of indeterminacy, the most general expression for M and M* is

$$M(z) = m_o(z) + \lambda_\alpha m_\alpha(z) \tag{6a}$$

$$M^*(z) = \lambda^*_\alpha m_\alpha(z) \tag{6b}$$

in which $m_o(z)$ is governed, but not uniquely determined, by

$$m_o'' = -p(z) \tag{7a}$$

and the same boundary conditions which apply to M. The set of self-equilibrated moments $m_r(z)$ (r=1,2. . .n) satisfies

$$m_r'' = 0 \quad (r = 1, 2, \cdots n) \tag{7b}$$

and equivalent homogeneous boundary conditions. The set of numbers λ_r (r =1,2. . .n), as yet unknown, will hereafter be referred to as "redundant parameters," while λ^*_r (r=1,2. . .n) constitutes a set of "prestressing parameters." Repeated Greek subscripts, as in Eq. (6), represent summation over the range 1 to n. It is finally convenient, and always possible, to select the set of functions $m_r(z)$ in such a way that the "orthonormality condition"

$$\int \frac{m_r m_s \, dz}{E I_x} = \begin{cases} 1 & (r = s) \\ 0 & (r \neq s) \end{cases} \quad (r, s = 1, 2, \cdots n) \tag{7c}$$

is satisfied.

The redundant parameters λ_r may now be determined by multiplying Eq. (7b) by $\bar{v}(z)$ and by integrating over the length of the structure; here $\bar{v}(z)$ represents any geometrically admissible vertical deflection function, that is, one which is sufficiently smooth and satisfies the geometric boundary and continuity conditions pertaining to the vertical deflection. In view of these restrictions, two integrations by parts lead to the relationships

$$\int m_r \bar{v}'' dz = 0 \quad (r = 1, 2, \cdots n) \tag{8}$$

In particular, let $\bar{v}(z)$ be the actual deflection function v(z) satisfying Eq. (4). Then, by Eqs. (4), (6), and (7c), Eq. (8) is converted into

$$\lambda_r - \lambda_r^* = \lambda^2 \int m_r (u''\beta - K\beta'^2)\, dz - \int \frac{m_0 m_r\, dz}{EI_x} \qquad (r = 1, 2 \cdots n) \tag{9}$$

There is no generality lost in letting $m_0(z)$ be the actual bending moment, derived on the basis of linear theory, in the beam in the absence of prestressing and of lateral loads and torques. In other words, let the set of redundant parameters λ_r vanish when all prestressing parameters λ_r^* and the load parameter λ also vanish. When this is substituted in Eq. (9), it means that

$$\int \frac{m_0 m_r\, dz}{EI_x} = 0 \qquad (r = 1, 2, \cdots n) \tag{10}$$

In view finally of Eq. (10), which constitutes an expression of the well-known and often used principle of virtual work, the "compatibility" conditions (9) become

$$\lambda_r - \lambda_r^* = \lambda^2 \int m_r (u''\beta - K\beta'^2)\, dz \qquad (r = 1, 2, \cdots n) \tag{11}$$

Discussion of Large-Deflection Theory

It is seen that there are as many Eqs. (11) as there are redundant parameters. Since the bending moment M(z) is expressed in the form (6a), it is apparent that the nonlinear range is governed by the solution of the differential equations (1) and (2), in which M(z) satisfies simultaneously the compatibility equations derived above. The complexity of the resulting system of equations is therefore evident, and hence the necessity of solving it by inverse or trial-and-error methods.

This is relatively easy for singly redundant beams. In that case, a value for λ_1 may be assumed arbitrarily at the start. With the bending moment M(z) so chosen, Eqs. (1) and (2) are solved and the solution (u, β) is inserted in (the single) Eq. (11), which in turn is solved for the load parameter λ. If the value of λ so obtained is real, and if the assumed moment M(z) is statically admissible in the sense defined later on in this section, then, by virtue of the uniqueness of the solution (proved also below), a point has been established in the load-response diagram. The latter may be completed by repeating this process for different values of λ_1.

For higher degrees of redundancy the process may become prohibitively laborious. However, some insight into the nonlinear behavior of the structure may be gained by means of a number of principles which are developed in what follows. In addition, it is possible that these principles may be instrumental in the reduction of the numerical labor involved.

To this end, let a quadratic form U be defined by

$$2U(M; u, \beta) = \int (EI_y u''^2 + E\Gamma\beta''^2 + GK\beta'^2)\, dz - \int [P(u'^2 + \rho^2\beta'^2) - 2(M + Py_0)u''\beta + 2KM\beta'^2 + P\alpha\beta^2]\, dz \tag{12}$$

In Eq. (12) the first integral represents the bending and torsional strain energy, while the second integral can be shown to give the work done by the vertical load p(z) and the axial force P. Also, a bending moment M(z) will hereafter be referred to as being "statically admissible" if it satisfies the equations of equilibrium (5) and the stability condition

$$U(M; \bar{u}, \bar{\beta}) \geqq 0 \tag{13}$$

for all non-trivial functions $(\bar{u}, \bar{\beta})$ which are geometrically admissible, that is, which are sufficiently smooth and satisfy the pertinent geometric boundary conditions.

If further the "potential energy" V is defined by

$$V(M; u, \beta) = U(M; u, \beta) - \int (qu + t\beta)\, dz = U(M; u, \beta) - W(u, \beta) \tag{14}$$

in which the integral expression represents the work done by the lateral loads and the torsional moments, it can readily be shown that

$$V(M; \bar{u}, \bar{\beta}) \geqq V(M; u, \beta) \tag{15}$$

if M is statically admissible and if (u,β) satisfy Eqs. (1) and (2).[6] It may be noteworthy that the equality sign in (15) implies trivial equality between $(\bar{u}, \bar{\beta})$ and (u,β), provided only the inequality (13) is admitted. Conversely, if U=0 for, say, (u_1,β_1), then the equality (15) applies to any $(\bar{u},\bar{\beta}) = (u,\beta) + c(u_1,\beta_1)$, in which c is an arbitrary number. The pair of functions (u_1,β_1) represents the fundamental buckling mode of the beam.

With these definitions, let a bending moment $\bar{M}(z) = m_0 + \bar{\lambda}_\alpha m_\alpha$ be statically admissible, relative to a given load, and let the functions $(\bar{u},\bar{\beta})$ be associated with $\bar{M}$ through the solution of Eqs. (1) and (2). Let further M and (u,β) represent, respectively, the correct bending moment and configuration for the same load; this implies, of course, that Eqs. (6a) and (11) are also satisfied. Since (u,β) are certainly geometrically admissible, it follows that

$$V(\bar{M}; u, \beta) \geqq V(\bar{M}; \bar{u}, \bar{\beta}) \tag{15a}$$

similarly to (15). But

$$V(\bar{M}; u, \beta) = V(M; u, \beta) + (\bar{\lambda}_\alpha - \lambda_\alpha) \int m_\alpha (u''\beta - k\beta^2)\, dz$$

$$= V(M; u, \beta) + \frac{1}{\lambda^2} (\bar{\lambda}_\alpha - \lambda_\alpha)(\lambda_\alpha - \lambda_\alpha^*)$$

in which the second equality is in consequence of Eq. (11).

Moreover, if Eq. (1) is multiplied by u and Eq. (2) by β, and if several integrations by parts are performed, it is readily demonstrated on account of the boundary conditions that

6. Since Eqs. (1) and (2) are the variational Euler equations of V, and since the actual natural boundary conditions are the variational boundary conditions of V, the correct solution (u,β) makes V stationary for all moments satisfying the equations of equilibrium. The additional minimum principle (15) represents an extension to the restricted class of moments which satisfy also the stability condition (13).

$$W(u,\beta) = 2U(M;u,\beta) \tag{16}$$

An identical relationship applies to the system $(\bar{M};\bar{u},\bar{\beta})$. Thus, in view of the definition of V in Eq. (14), the inequality (15a) now becomes

$$U(\bar{M};\bar{u},\bar{\beta}) \geqq U(M;u,\beta) - \frac{1}{\lambda^2}(\bar{\lambda}_\alpha - \lambda_\alpha)(\lambda_\alpha - \lambda_\alpha^*) \tag{17}$$

or:

$$U(\bar{M};\bar{u},\bar{\beta}) + \frac{1}{2\lambda^2}(\bar{\lambda}_\alpha - \lambda_\alpha^*)(\bar{\lambda}_\alpha - \lambda_\alpha^*) \geqq U(M;u,\beta) + \frac{1}{2\lambda^2}(\lambda_\alpha - \lambda_\alpha^*)(\lambda_\alpha - \lambda_\alpha^*) + \frac{1}{2\lambda^2}(\bar{\lambda}_\alpha - \lambda_\alpha)(\bar{\lambda}_\alpha - \lambda_\alpha) \tag{17a}$$

The last term on the right side of (17a) is positive definite. Hence, in the absence of initial bending moments ($\lambda_r^* = 0$), the following inequality is established:

$$U(M;u,\beta) + \frac{1}{\lambda^2}U_b(M) \leqq U(\bar{M};\bar{u},\bar{\beta}) + \frac{1}{\lambda^2}U_b(\bar{M}) \tag{18}$$

with

$$U_b(M) = \frac{1}{2}\int \frac{M^2 dz}{EI_x}$$

U_b represents the familiar expression for the strain energy in bending about the major axis. (18) follows from (17a) through the application of Eqs. (6a), (7c), and (10). An alternate statement of the inequality (18), which takes account of Eq. (16), reads:

$$W(u,\beta) + \frac{2}{\lambda^2}U_b(M) \leqq W(\bar{u},\bar{\beta}) + \frac{2}{\lambda^2}U_b(\bar{M}) \tag{18a}$$

These last two inequalities may be expressed in the following principle:

Of all statically admissible bending moments, the actual one corresponds to the smallest value of $\lambda^2 U + U_b$ (or, alternately, of $\lambda^2 W + 2U_b$) if these values are determined on the basis of a deflected configuration which is related to the bending moments through the solution of Eqs. (1) and (2).

This minimum principle, it may be well to emphasize, relates to the distribution of the redundant moments rather than to the deflection configuration itself; that the latter is itself governed by minimum principles is well-known and was, in fact, utilized in the derivation of the present principle. It represents an extension of the classical Castigliano "Theorem of Least Work" into the nonlinear range. Indeed, the Theorem of Castigliano represents a special case, which can be obtained from either (18) or (18a) by setting λ equal to zero.[7]

To carry the discussion further, let the inequality (15a) be subtracted from (15). This results in the relationship

7. Actually, the customary statement of the Theorem of Castigliano implies not a minimum, but only a stationary property of the strain energy in bending. The present principle can be broadened in a similar fashion. In fact, if M satisfies the equation of equilibrium (5), but not necessarily the stability condition (13), the quantities dealt with in (18) and (18a) can be shown to be stationary. In other words, if (u,β) as solved from Eqs. (1) and (2) are differentiable functions of λ_r, then the satisfaction of Eq. (11) ensures that the derivative of $(\lambda^2 U + U_b)$ or of $(\lambda^2 W + 2U_b)$ with respect to λ_r vanishes.

$$(\lambda_\alpha - \bar{\lambda}_\alpha)\int m_\alpha(\bar{u}''\bar{\beta} - K\bar{\beta}'^2)\,dz \geqq (\lambda_\alpha - \bar{\lambda}_\alpha)\int m_\alpha(u''\beta - K\beta'^2)\,dz$$

If now both $(M{:}u,\beta)$ and $(\bar{M};\bar{u},\bar{\beta})$ are assumed to satisfy the conditions of compatibility (11), it follows that

$$(\lambda_\alpha - \bar{\lambda}_\alpha)(\bar{\lambda}_\alpha - \lambda_\alpha^*) \geqq (\lambda_\alpha - \bar{\lambda}_\alpha)(\lambda_\alpha - \lambda_\alpha^*)$$

or, after some rearrangement of terms,

$$0 \geqq (\lambda_\alpha - \bar{\lambda}_\alpha)(\lambda_\alpha - \bar{\lambda}_\alpha)$$

Obviously, the inequality above is impossible for real values of the redundant parameters. On the other hand, the equality is possible only if M(z) and $\bar{M}(z)$ are trivially identical. This in turn implies the following principle:

If there exists a statically admissible bending moment which satisfies the conditions of compatibility (11) relative to a configuration (u,β) which is a solution of Eqs. (1) and (2), that bending moment is the actual bending moment and is unique.

In general, it follows from the uniqueness of the M(z) that u(z) and $\beta(z)$ are also unique, as discussed before. However, singular cases may occur in which, owing to a condition of "neutral equilibrium," two equilibrium configurations become possible. This was already hinted at following the establishment of the inequality (15). A detailed discussion of this question is contained in the Appendix as well as in later sections in connection with the numerical example and the report on the experiments.

Returning to the minimum principle established above, it is clear then that any statically admissible bending moment furnishes an upper bound to the two functions with which the principle deals. In what follows it will be the object to derive also a lower bound and to discuss a possible application of these bounds toward the simplification of the computational labor.

To this end, let a "kinematically admissible" bending moment $\bar{M}(z)$ be defined as one which satisfies the equation of equilibrium (5) (and which, therefore, can be expressed in terms of Eq. (6a) subject to Eq. (7)), which is compatible in the sense of satisfying Eq. (11) for some geometrically consistent configuration $(\bar{u},\bar{\beta})$, and which finally does not violate the inequality[8]

$$U(\bar{M};\bar{u},\bar{\beta}) - \tfrac{1}{2}W(\bar{u},\bar{\beta}) \leqq 0 \qquad (19)$$

If this inequality is now subtracted from the inequality (15), in which the actual state $(M;u,\beta)$ is compared with the state $(M;\bar{u},\bar{\beta})$, then, in view of Eq. (16),

$$2(\lambda_\alpha - \bar{\lambda}_\alpha)\int m_\alpha(\bar{u}''\bar{\beta} - K\bar{\beta}'^2)\,dz - W(\bar{u},\bar{\beta}) \geqq -W(u,\beta) \qquad (20)$$

where $\bar{\lambda}_r$ represents the set of redundant parameters designating $\bar{M}(z)$. The integrals in (20) may be replaced in line with Eq. (11); after some rearrangement of terms, this leads to

8. The concept of "kinematic" admissibility follows from the fact that if the equality sign in (19) is satisfied the external work equals the "internal work." Note, however, that the equations of equilibrium (1) and (2) need not be satisfied.

$$W(u,\beta)+\frac{1}{\lambda^2}(\lambda_\alpha-\lambda_\alpha^*)(\lambda_\alpha-\lambda_\alpha^*) \geqq W(\bar{u},\bar{\beta})+\frac{1}{\lambda^2}(\bar{\lambda}_\alpha-\lambda_\alpha^*)(\bar{\lambda}_\alpha-\lambda_\alpha^*)+\frac{1}{\lambda^2}(\bar{\lambda}_\alpha-\lambda_\alpha)(\bar{\lambda}_\alpha-\lambda_\alpha)$$

in which the last term, as before, is positive definite. Hence, by the same argument as the one employed previously

$$W(\bar{u},\bar{\beta})+\frac{2}{\lambda^2}U_b(\bar{M}) \leqq W(u,\beta)+\frac{2}{\lambda^2}U_b(M) \tag{21}$$

or, in view of the relations (16) and (19)

$$U(\bar{M};\bar{u},\bar{\beta})+\frac{1}{\lambda^2}U_b(\bar{M}) \leqq U(M;u,\beta)+\frac{1}{\lambda^2}U_b(M) \tag{21a}$$

Since the actual bending moment M(z) is also kinematically admissible, it follows then that:

Of all kinematically admissible bending moments, the actual one corresponds to the smallest possible value of the functions $\lambda^2 W + 2U_b$ or $\lambda^2 U + U_b$.

It appears that this lower-bound principle may be useful in estimating the nonlinear response of the structure. In fact, let an upper and a lower bound be found for a given value of the load parameter λ; an error estimate has then been established. Since the bounds can be narrowed down arbitrarily, a correct solution may presumably be approached in this fashion.

Asymptotic Behavior

As the load parameter λ grows beyond bounds, the bending moment M(z) and with it the deflection mode (u,β) usually approaches a limiting condition. This asymptotic behavior is discussed in this section in regard to both the governing equations and the appropriate energy principles.

For given load p(z), it was shown that the stable domain (that is, the one in which the inequality (13) is satisfied) is generally a closed region in a space in which the coordinates of a point are given by the redundant parameters λ_r associated with M(z) through Eq. (6).[5] As p approaches an ultimate value p_u, this region shrinks to a point; for $p > p_u$, no statically admissible bending moments are available any more. In the present paper, p is assumed to be fixed and less than p_u. Because of the boundedness of the associated stable domain, it follows therefore that all the redundant parameters λ_r remain finite as the load parameter λ goes to infinity.

This determines the form of the governing equations of the limiting state. In fact, if λ approaches infinity in Eq. (11) while the left side remains bounded, the asymptotic deflection mode (u_ℓ, β_ℓ) is seen to satisfy the set of equations

$$\int m_r(u_\ell''\beta_\ell - K\beta_\ell'^2)\,dz = 0 \qquad (r=1,2,\cdots n) \tag{22}$$

together with the equations of equilibrium (1) and (2). It may be of some interest to note that this system of equations does not contain the prestressing parameters λ_r^*. In other words, the "final" state is independent of whatever initial stresses may exist in the structure (due to settlement of support, temperature gradients, etc.), although the "history" of the structure does display such dependence.

By the same token, an asymptotic minimum principle can be derived. For if λ is permitted to approach infinity in the inequality (18), it follows (for $\lambda_r^* = 0$) that

$$U(M_\ell; u_\ell, \beta_\ell) = U(m_o; u_\ell, \beta_\ell) \leqq U(\bar{M}; \bar{u}, \bar{\beta}) \tag{23}$$

or

$$W(u_\ell, \beta_\ell) \leqq W(\bar{u}, \bar{\beta}) \tag{23a}$$

in which $(\bar{M};\bar{u},\bar{\beta})$ represents, as before, any statically admissible bending moment and associated deflection mode. The first equality in (23) follows from Eq. (22). Accordingly:

The limiting bending moment is characterized by making U (or W) smaller than does any other statically admissible bending moment.

In general, this minimum is in the interior of the region of stability. It is approached asymptotically, and the corresponding configuration is unique. The existence of such an interior minimum is proved in the Appendix; also explored are certain singular cases, in which U may assume a minimum on the boundary of the stable domain. Suffice it to state here that in that event the limiting bending moment may be reached for a finite value of the load parameter λ. Also, the deflection mode need not be unique in that case, as would appear reasonable in view of the limitations on the uniqueness principle established in the preceding section.

As before, the upper-bound principle expressed through (23) has a counterpart in the form of a limiting lower-bound principle. This is derived readily by considering (21), with λ going to infinity. If then (u_c,β_c) represents any pair of functions which, in addition to being otherwise acceptable, satisfies the set of equations (22), and if this "collapse mode" furthermore satisfies the condition[9]

$$2U(m_o; u_c, \beta_c) - W(u_c, \beta_c) = 0 \tag{24}$$

then

$$U(m_o; u_c, \beta_c) \leqq U(m_o; u_\ell, \beta_\ell) \tag{25}$$

or

$$W(u_c, \beta_c) \leqq W(u_\ell, \beta_\ell) \tag{25a}$$

In other words:

Of all collapse modes, the actual one corresponds to the largest value of U (or W).

Numerical Example

In this section, the principles and equations of the preceding sections are applied to an illustrative example. For this purpose, consider a beam of

9. Unless one of the terms in Eq. (24) vanishes, this condition can always be satisfied by selecting the amplitude and sign of the assumed collapse mode properly. This follows from the fact that U is quadratic, but W linear in u and β.

length L which is of thin rectangular cross section ($\Gamma = 0$) and of second degree of redundancy relative to bending in its major plane by virtue of being elastically restrained at both ends; however, only one degree of indeterminacy need be considered here owing to the complete symmetry of the problem. Simple supports are provided at both ends, so far as lateral movement is concerned; a single lateral force of magnitude λ is applied halfway between supports and at an eccentricity e above the center line. If, as before, the total response is denoted by $(\lambda u, \lambda\beta)$, and if m is the restraint moment, then, in the absence of the vertical load p(z), Eqs. (1) and (2) and the boundary conditions take the following form:

$$\left.\begin{aligned} EI_y u'' - m\beta'' &= 0 \\ GK\beta'' + m u'' &= 0 \end{aligned}\right\} \quad (0 \le z \le \tfrac{1}{2})$$

$$u(0) = u''(0) = \beta(0) = 0 \qquad (26)$$

$$u'(\tfrac{1}{2}) = EI_y u'''(\tfrac{1}{2}) - m\beta'(\tfrac{1}{2}) + \tfrac{1}{2} = GK\beta'(\tfrac{1}{2}) - \tfrac{e}{2} = 0$$

In Eq. (26) the second set of boundary conditions follows from the symmetry of the problem; hence the solution for (u, β) need only be considered for half the beam, that is, from the left support (z=0) to the center (z=L/2).

For the case under consideration, the compatibility condition (11), in the absence of prestressing, becomes

$$m = -2\lambda^2 (EI_x/L)\, \gamma \int u''\beta\, dz \qquad (27)$$

where

$$\gamma = \frac{C}{C + \frac{2EI_x}{L}}$$

represents the degree of end restraint and varies from zero (no restraint) to unity (full fixity). C denotes the "spring constant" and is measured in in.-lb per radian.

For the range between 0 and L/2, the solution of Eq. (26) is given by

$$u(z) = A(1 - \phi\alpha)\left(\frac{\sin \alpha z/L}{\cos \alpha/2} - \frac{\alpha z}{L}\right)$$

$$e\beta(z) = A\phi\alpha\left[-(1 - \phi\alpha)\frac{\sin \alpha z/L}{\cos \alpha/2} + \frac{\alpha z}{L}\right] \qquad (28)$$

in which

$$A = \frac{L^3}{2EI_y \alpha^3} \qquad \phi = \frac{e}{L}\sqrt{\frac{EI_y}{GK}}$$

and

$$0 \le \alpha^2 = \frac{m^2 L^2}{EI_y GK} < \pi^2 \left(\frac{m}{m_1}\right)^2 < \pi^2$$

where m_1 identifies the moment associated with neutral equilibrium, and ϕ is a dimensionless constant.

If Eq. (28) is substituted in Eq. (27), this can be shown to lead to the relationship

$$\alpha^5 = \frac{I_x}{2I_y} \frac{L^5}{EI_y GK} \gamma \lambda^2 F(\alpha) \qquad (29)$$

with

$$F(\alpha) = (1-\phi\alpha)\left[\left(\tan\frac{\alpha}{2} - \frac{\alpha}{2}\right) + \frac{1}{2}(1-\phi\alpha)\left(\tan\frac{\alpha}{2} - \frac{\alpha}{2} - \frac{\alpha}{2}\tan^2\frac{\alpha}{2}\right)\right]$$

This equation can be made dimensionless. In fact, let the dimensionless ratio ω be defined by

$$\omega = s_y / s_1$$

where

$$s_y = \frac{\lambda L/4}{S_y} \qquad s_1 = \frac{m_1}{S_x} = \frac{\pi}{S_x L}\sqrt{EI_y GK} \tag{30}$$

with S_y and S_x designating, respectively, the section moduli about the y and x axes. It is readily apparent that s_y represents the maximum fiber stress in lateral bending, while s_1 is the maximum fiber stress associated with the buckling moment m_1. With these definitions, and in consideration of the relationship between the moments of inertia and section moduli for rectangular sections, Eq. (29) now takes the simple form:

$$(8\phi\pi^2)\,\omega^2 = \alpha^5 / F(\alpha) \tag{31}$$

As ω (and hence the lateral load λ) approach zero, both numerator and denominator on the right side of Eq. (31) also approach zero. For very small values of ω, Eq. (31) can therefore be replaced, through the usual limit procedure, by

$$(12\phi\pi^2)\,\omega^2 = 3\alpha \qquad (\alpha \ll \pi) \tag{31a}$$

Conversely, as the lateral load becomes increasingly large, it follows from Eq. (31) that

$$\lim_{\omega\to\infty} F(\alpha) = 0 \tag{31b}$$

The best way to establish a functional relationship between α and ω is probably to assume a value for the former and to solve for the latter by means of Eq. (31), although, for small values of α, the inverse procedure may be followed through the use of Eq. (31a). The asymptotic magnitude of α (for very large lateral loads) may be obtained from Eq. (31b); it can readily be verified that the smallest positive root of Eq. (31b) is given by $\alpha = 1/\phi$ for ϕ exceeding π, while for $\phi < \pi$, the smallest root must be computed through a trial-and-error process.

With the ω-α relationship thus established, the maximum lateral deflection, which occurs at the midpoint of the beam, is found to be

$$u_{max} = A(1-\phi\alpha)(\tan\alpha/2 - \alpha/2) = K_u \frac{L^3}{48EI_y} \tag{32}$$

$$K_u = 24/\alpha^3\,(1-\phi\alpha)(\tan\alpha/2 - \alpha/2)$$

In Eq. (32), the quantity A was defined in Eq. (28), while K_u represents the ratio between the computed maximum deflection and the equivalent value determined on the basis of the linear theory, which does not predict the development of restraining moments m (that is, $\alpha = 0$). For very small values of α, Eq. (32) can be approximated by

$$K_u = 1 - \phi\alpha = 1 - (\pi^2/3)\,\gamma\phi^2\omega^2 \qquad (\alpha \ll \pi) \tag{32a}$$

in which the second equality follows from Eq. (31a).

Similary, the maximum rotation occurs also at the middle of the beam and is governed by the equation

$$e\beta_{max} = A\phi\alpha\left[\alpha/2 - (1-\phi\alpha)\tan\alpha/2\right] = K_\beta \frac{e^2 L}{4GK} \tag{33}$$

$$K_\beta = (2/\phi\alpha^2)\left[\alpha/2 - (1-\phi\alpha)\tan\alpha/2\right]$$

in which, similarly to the preceding equation, κ_β is defined as the ratio between the computed maximum rotation and the corresponding rotation computed on the basis of the linear theory. As before, for very small values of α, the second equation of Eq. (33) can be approximated by

$$K_\beta = 1 - (\alpha/12\phi) = 1 - (\pi^2/36)\,\gamma\omega^2 \qquad (\alpha \ll \pi) \tag{33a}$$

Of some interest, finally, is the lateral deflection of the point of application of the force itself. This is found by adding Eqs. (32) and (33), or

$$(u+e\beta)_{max} = A\left[(1-\phi\alpha)^2\tan\alpha/2 - (1-2\phi\alpha)\alpha/2\right] = K\frac{L^3}{48EI_y}(1+12\phi^2)$$

$$K = (24/\alpha^3)(1+12\phi^2)^{-1}\left[(1-\phi\alpha)^2\tan\alpha/2 - (1-2\phi\alpha)\alpha/2\right] \tag{34}$$

Here, κ is defined analogously to κ_u and κ_β. For small values ofα, this goes over into

$$K = 1 - (2\phi\alpha)(1+12\phi^2)^{-1} = 1 - (2/3)\pi^2\phi^2(1+12\phi^2)^{-1}\gamma\omega^2 \qquad (\alpha \ll \pi) \tag{34a}$$

It may be worth noting that, from Eq. (34), $d\kappa/d\alpha$ can be shown to be proportional to $F(\alpha)$. In other words, for very large values of ω, $d\kappa/d\alpha$ vanishes. Since furthermore the second derivative is positive, it is seen that the limiting value of κ is an absolute minimum if only stable values of α (lying in the closed region between $-\pi$ and $+\pi$) are admitted in comparison. This, however, is not surprising. Since κ is a measure of the total work done by the external force (all other terms being independent of α), this property of κ is a natural concomitant of the minimum principle expressed in the inequality (23a).

Some of the results of the preceding discussion become invalid for the singular case of $\phi = 1/\pi$. Physically this means that the force is applied at a point which would not move if the beam were to buckle laterally under the critical end moment m_1 ($\alpha = \pi$). This special case, which was briefly alluded to in the previous section, is treated in a general fashion in the Appendix. In its application to the illustrative example being discussed here, it is analyzed fully in what follows; a comparison with the Appendix shows that the general principles developed there are confirmed for the case under consideration.

It can be verified easily that $F(\alpha)$, which is defined in Eq. (29), has no root in the range $0 < \alpha < \pi$ for the singular case of $\phi = 1/\pi$. $F(\pi)$ is indeterminate, but the customary limit procedure leads to a value of $1/\pi$; hence, by Eq. (31), the boundary of the stable range is reached when ω assumes the finite value governed by

$$\omega_*^2 = \pi^4/8\gamma \tag{35}$$

while, by Eqs. (32), (33), and (34) and similar limit procedures

$$\left.\begin{aligned} K_u(\pi) &= 48/\pi^4 \\ K_\beta(\pi) &= 1 - 4/\pi^2 \\ K(\pi) &= (1 + \pi^2/12) - 1 \end{aligned}\right\} \tag{36}$$

Similarly, the deflection mode approaches the limiting functions

$$\left.\begin{aligned} u_o(z) &= \lim_{\alpha \to \pi} u(z) = \frac{L^3}{\pi^4 E I_y} \sin \pi z/L \\ e\beta_o(z) &= \lim_{\alpha \to \pi} e\beta(z) = \frac{L^3}{\pi^4 E I_y} (\pi^2 z/2L - \sin \pi z/L) \end{aligned}\right\} \quad (0 \leq z \leq \tfrac{L}{2}) \tag{37}$$

For values of $\omega > \omega_0$, the restraint moment m retains its critical value m_1, or $\alpha \equiv \pi$ throughout. However, the solution (37) of Eq. (26) is no longer unique; it can in general be expressed by

$$\left.\begin{aligned} u(z) &= u_o(z) + c \frac{L^{7/2}}{\pi^4 E I_y} u_1(z) \\ e\beta(z) &= e\beta_o(z) + c \frac{L^{7/2}}{\pi^4 E I_y} e\beta_1(z) \end{aligned}\right\} \tag{38}$$

in which c is an as yet arbitrary multiplier; the factor associated with c has been added for convenience, and (u_1, β_1) is the normalized buckling mode given by

$$u_1(z) = (L)^{-1/2} \sin \pi z/L = -e\beta_1(z) \tag{39}$$

The value of c is now determined from the compatibility condition (27) which, in view of Eqs. (37), (38), and (39) and of the definitions of α and ω, becomes

$$c^2 = 1 - (\pi^4/8\pi\omega^2) \tag{40}$$

Let a factor $\tau \leq 1$ be defined by

$$\tau = \omega_0/\omega \tag{41}$$

where ω_0 is given in Eq. (35) and represents (in review) the value of ω as $\alpha = \pi$ is reached initially. Then c is related to τ by the equation of the unit circle

$$c^2 + \tau^2 = 1 \tag{42}$$

It is noted, and indeed expected from the discussion in the Appendix, that for any value of $\tau < 1$ there are two possible values of c; in particular, for $\tau = 0$ (i.e., as the force λ goes to infinity), $c = \pm 1$. In other words, two distinct equilibrium configurations are now possible, which are not adjacent to one another; thus, a "snap-through" (Durchschlag) phenomenon is to be expected.

The reduction factors κ are obtained by considering Eqs. (37), (38), (39), (41), and (42). This leads to the following set of relationships:

$$\left.\begin{aligned} &\kappa_u = (48/\pi^4)(1 \pm \sqrt{1-\tau^2}) && \lim_{\tau \to 0} \kappa_u = (96/\pi^4),\ 0 \\ &\kappa_\beta = 1 - (4/\pi^2)(1 \pm \sqrt{1-\tau^2}) && \lim_{\tau \to 0} \kappa_\beta = 1 - 8/\pi^2,\ 1 \\ &\kappa = (1 + \pi^2/12)^{-1} \end{aligned}\right\} \quad (43)$$

In other words, the limiting configurations represent either predominant bending with little twisting, or else pure twist without any bending. Only one value of κ appears, however, since the transition from one configuration to the others constitutes a rotation about the point of application of the force. Moreover, this value of κ remains constant once the condition $\alpha = \pi$, or $\omega = \omega_0$, is reached. For $\omega > \omega_0$ ($\tau < 1$), the force-displacement relationship is therefore linear, but the apparent stiffness of the structure is almost double that predicted by the linear theory.

In concluding this section, it may be noted that, for sufficiently large values of the applied force, the response of the structure is a discontinuous function of the eccentricity e of the force. In fact, for "small" eccentricities ($\phi < 1/\pi$), the configuration approaches one of mostly bending and little twisting, the ratio being nearly independent of ϕ. More surprisingly, perhaps, the response for "large" eccentricities ($\phi > 1/\pi$) approaches one of pure twist without any bending, the reduction factors κ_u and κ_β being zero and unity irrespective of the value of ϕ. For the singular case ($\phi = 1/\pi$), the two possible configurations discussed above represent limiting cases as the value of ϕ approaches $1/\pi$ from below or from above, respectively.

This type of discontinuity seems to be one of the salient features which distinguishes the present theory from the conventional linear approach. Other examples have been investigated and have been found to lead to similar results. For example, if the same beam is subjected to two forces applied at equal distances from the ends and at equal (nonvanishing) eccentricities, but pulling in opposite directions, then the asymptotic response is found to be a discontinuous function of the ratio of the magnitudes of the forces. In fact, the larger of the two forces dominates the behavior entirely; singularity, that is, snap-through, occurs when they are equal.

Experimental Results

To obtain an experimental check on the results of the preceding section, a test arrangement similar to the one described[5] was employed. The beam specimen used was a strap, one inch high and 1/16 inch thick, which was made of heat-treated steel with a yield point of about 180,000 psi. Spanning a distance of 20 in., it was elastically restrained at both ends in the vertical plane, with the degree of end fixity γ (see Eq. (27)) computed at 0.74. However, by loosening the clamps this end restraint could be removed entirely; in this fashion, the beam was made statically determinate to provide a check for the linear theory. The values for the elastic constants E and μ (Poisson's Ratio) were known to be 30,000,000 psi and 0.3, respectively; this establishes the relationship $\lambda = 1.48\omega$, in which λ is the applied force measured in pounds, and ω is defined in Eq. (30).

A relatively rigid vertical bar was attached to the beam at midspan; this bar was then subjected to a horizontal lateral force of increasing magnitude and varying eccentricity. The results corresponding to eccentricities e of 4 in., 8 in., and 12 in. are discussed in what follows; these eccentricities are associated with values of ϕ equaling, very nearly, $1/2\pi$, $1/\pi$, and $3/2\pi$, respectively, where the second value represents the singular case. The lateral deflections λu and rotations $\lambda\beta$, as well as the total displacement $\lambda(u+e\beta)$ of the applied force, were measured in the usual manner by means of scales and mirrors.

A comparison between the predicted and measured results is given in Figs. 2, 3, and 4, which correspond to the three types of eccentricites (small, singular, and large) mentioned above. In each case, the curves give the computed values of the reduction ratios on the basis of Eqs. (32),(33), and (34) as functions of the dimensionless loading parameter ω (defined in Eq. (30)). For the singular case of e = 8", or $\phi = 1/\pi$, the boundary of the stable domain is reached for $\omega_0 = 4.06$, as given in Eq. (35), with the associated reduction coefficients computed in accordance with Eq. (36). For values of ω in excess of ω_0, these coefficients are governed by Eq. (43).

The experimental points shown in the figures represent average values based on several test sequences. It is seen that reasonable agreement was obtained for small and for large eccentricities. Such quantitative discrepancies as do occur seem to be due to the effects of initial imperfections and of prestressing moments; for large values of ω, other non-linear factors which were ignored in the present analysis cause further discrepancies. In fact, since both the measured deflections and rotations were somewhat in excess of the limitations laid down in the Introduction, a more accurate analysis, which involves, for example, powers of u and β above the second, yields more compatible results. Nevertheless, there is excellent qualitative agreement between the theory and experiment; in particular, the discontinuous character of the asymptotic solution is fully corroborated.

For the singular case (e = 8", $\phi = 1/\pi$) the agreement is confined to values of ω below ω_0. For larger values of ω, two possible solutions (Durchschlag) did indeed occur, but the quantitative agreement between the theory and the experimental values is poor. A possible explanation for this can be found in the effect of initial imperfections. These imperfections, such as initial curvatures, etc., become increasingly important as the boundary of the stable domain is approached, i.e., as the value of α approaches π. In fact, if Eq. (26) is properly modified to include the effect of an initial deviation from perfect shape, it can readily be verified that, in the general case, the solution "blows up" as the support moments approach their critical values. In effect, the orthogonality condition (A7) (see Appendix) is violated, which means that neutral equilibrium is approached only as the load goes toward infinity, instead of the finite value of ω_0 predicted by the idealized theory. This may explain why the double-valued equilibrium configuration was "delayed" beyond its theoretical value.

CONCLUSION

It may be stated that the theory presented herein constitutes a third approximation to the problem of a beam subjected to a combination of bending and torsion. In the first approximation, the strains are assumed to be linear

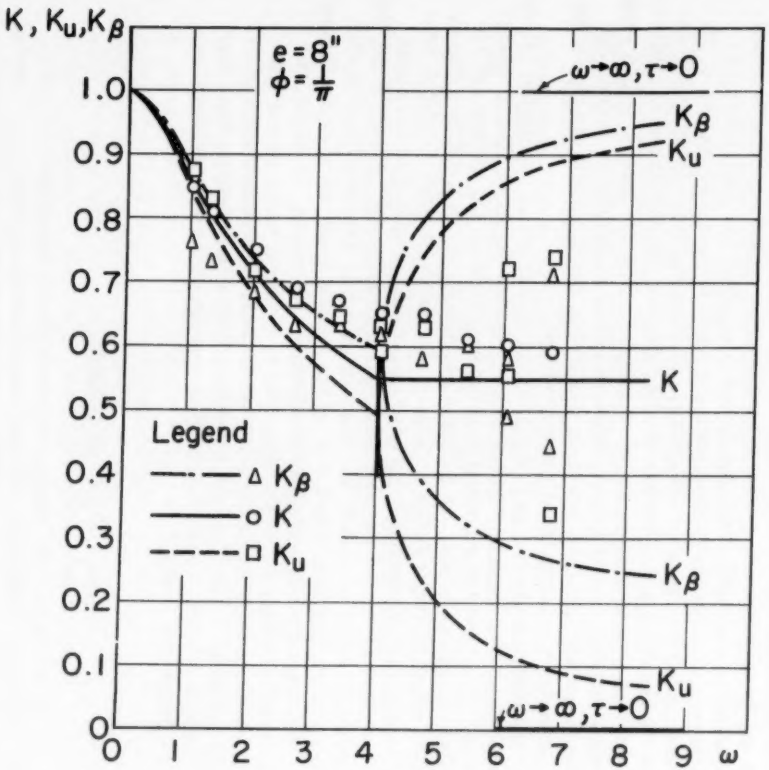

Fig. 3. Reduction factors for singular eccentricity.

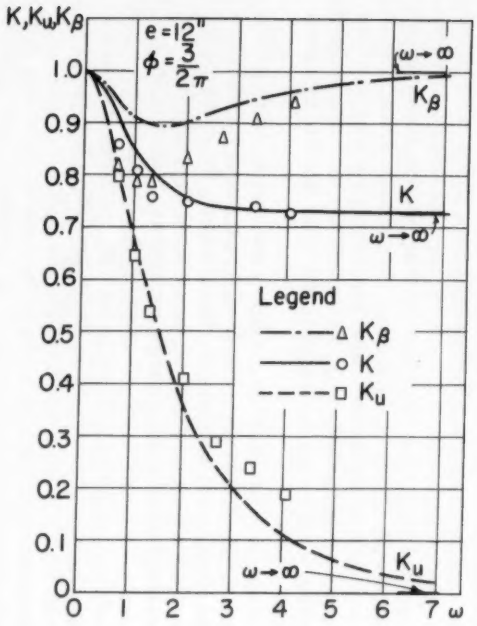

Fig. 4. Reduction factors for large eccentricity.

functions of the displacements, while the equations of equilibrium refer to the undistorted configuration. This leads to an entirely linear theory, to which the principle of superposition applies. Such a theory, which is one commonly used in ordinary design, is valid in case the lateral stiffness of the beam is comparable in magnitude to its major stiffness.

When this condition is violated, the need for a second approximation arises. In fact, the presence of large lateral deflections and rotations makes it imperative that the equations of equilibrium be referred to the distorted geometry. The resulting theory is still linear with respect to the lateral loads and twisting couples; however, the effects of the vertical loads can no longer be added linearly.

The present, or third, approximation further abandons the assumption of linear strain-displacement relations. This is a natural result of the presence of large lateral displacements, in consequence of which the second approximation appears to be illogical. This is not quite the case, however. Actually, at least so far as the lateral displacements and rotations are concerned, the results of the last two approximations are identical for beams which are statically determinate relative to moments in their major plane of stiffness. This may provide an explanation as to why this point has been ignored heretofore. In any event, it appears that, at least in the case of statically redundant structures, the introduction of nonlinear strain-displacement relations leads to substantial modifications in their predicted behavior.

BIBLIOGRAPHY

1. George Winter, "Strength of Slender Beams," Transactions, American Society of Civil Engineers, 109, 1321-1358, (1944).
2. Henrik Nylander, "Torsion, Bending, and Lateral Buckling of I-Beams," Bulletin No. 22, Division of Building Statics and Structural Engineering, Royal Institute of Technology, Stockholm, Sweden (1956).
3. Th. von Kármán, Encyclopaedie der Mathematischen Wissenschaften, 4, 349, (1910).
4. Friedrich Bleich, "Buckling Strength of Metal Structures," McGraw-Hill Book Co., New York, 1952.
5. E. F. Masur and K. P. Milbradt, "Collapse Strength of Redundant Beams after Lateral Buckling," Journal of Applied Mechanics, in Transactions, American Society of Mechanical Engineers, June, 1957.

APPENDIX

In what follows it will be shown that, in general, the function $U(M;u,\beta) \equiv U(\lambda_r)$ (or, equivalently, $W(\lambda_r)$) has an interior minimum, which is approached asymptotically as the load parameter λ goes beyond bounds. In addition, the singular case, in which such an interior minimum may not exist, is explored further.

To this end, consider again the region of stability, which will be assumed to be bounded, as before. In the λ_r-space this region R is enclosed by the boundary B, on which the homogeneous equations (1) and (2) admit a

nontrivial solution (u_1, β_1); on B the equilibrium is therefore "neutral," with (u_1, β_1) representing the buckling mode. Moreover, in the general case, the inhomogeneous equations (1) and (2) admit no solution on B, while U grows beyond bounds as the stress point P (whose coordinates are the redundant parameters λ_r) approaches B. If now U can be shown to be convex, the existence of a unique interior minimum can be postulated.

To show this, it is recalled, in line with footnote 7, that if u and β are differentiable functions of λ_r, then, by the inequality (18) or by an independent calculation,

$$\frac{\partial U}{\partial \lambda_r} = -\frac{1}{\lambda^2}\frac{\partial U_6}{\partial \lambda_r} = -\frac{1}{\lambda^2}(\lambda_r - \lambda_r^*) \tag{A1}$$

Consider now a plane which is tangent to U at some point (λ_r); its equation is given by

$$U_t(\bar{\lambda}_r) = U(\lambda_r) + \frac{\partial U}{\partial \lambda_\alpha}(\bar{\lambda}_\alpha - \lambda_\alpha)$$

or, in view of Eq. (A1), by

$$U_t(\bar{\lambda}_r) = U(\lambda_r) - \frac{1}{\lambda^2}(\bar{\lambda}_\alpha - \lambda_\alpha)(\lambda_\alpha - \lambda_\alpha^*) \tag{A2}$$

It follows therefore as a consequence of the inequality (17) that

$$U(\bar{\lambda}_r) \geqq U_t(\bar{\lambda}_r) \tag{A3}$$

In other words, the surface U does not cross any of its tangent planes; it is therefore convex, and the existence of a unique interior minimum is proved, provided all the other previous assumptions are found to hold also.

The exceptional (singular) case occurs when the inhomogeneous equations (1) and (2) do admit a finite solution. For the sake of simplicity, let Eqs. (1) and (2) be rewritten in the symbolic form

$$L_u(M; u, \beta) = q \qquad L_\beta(M; u, \beta) = t \quad \text{(in R)} \tag{A4}$$

and let, in accordance with the previous discussion,

$$L_u(M_1; u_1, \beta_1) = L_\beta(M_1; u_1, \beta_1) = 0 \quad \text{(on B)} \tag{A5}$$

Then the system of equations

$$L_u(M_1; u, \beta) = q \qquad L_\beta(M_1; u, \beta) = t \quad \text{(on B)} \tag{A6}$$

has a finite solution on that portion B' of B on which the "orthogonality condition"

$$\int (q u_1 + t \beta_1)\, dz = 0 \quad \text{(on B')} \tag{A7}$$

holds. Moreover, since U is finite on B', the existence of an interior minimum can no longer be postulated.

For the purpose of studying singular behavior, let it be assumed that an interior minimum does not exist; this means in turn that U has an exterior

minimum, which lies on B'. In that event, as the load factor λ increases, the stress point P reaches some point on B', from which it proceeds along B' toward the minimum. If B' is represented by a single point, as in the case of the illustrative example, the stress point stays fixed after reaching B' and the structure exhibits the quasi-linear behavior discussed earlier in the paper.

After P has reached the boundary B', the most general solution of Eq. (A6) subject to the condition (A7) can be expressed in the form

$$(u, \beta) = (u_0, \beta_0) + c(u_1, \beta_1) \tag{A8}$$

in which (u_0, β_0) represents some solution of Eqs. (A6) and (u_1, β_1) is governed, subject to an arbitrary multiplicative constant, by Eqs. (A5). It is convenient to identify these functions further by the orthonormality conditions

$$\int (u_0 u_1 + b^2 \beta_0 \beta_1)\, dz = 0$$
$$\int (u_1^2 + b^2 \beta_1^2)\, dz = 1 \tag{A9}$$

in which b is an arbitrary number having the dimension of a length. Except for the sign of (u_1, β_1), conditions (A9) determine all the functions uniquely for given value of b.

Let the point at which the stress path "first" reaches the boundary B' be designated by P', and let P' be associated with a load parameter λ' and a parameter c=c' (see (A8)). Then the value of c' can be determined by a limit process as follows:

While the stress point P is in the interior of the region of stability, the solution of Eq. (A4) can be represented by Eq. (A8), subject to the orthonormality conditions (A9), if (u_1, β_1) satisfies the equations

$$L_u(M; u_1, \beta_1) = \mu u_1 \qquad L_\beta = (M; u_1, \beta_1) = \mu b^2 \beta_1 \tag{A10}$$

in which μ is the eigenvalue of the system (A10). This eigenvalue satisfies the relationship

$$\int [u_1 L_u(M; u_1, \beta_1) + \beta_1 L_\beta(M; u_1, \beta_1)]\, dz = \mu \tag{A11a}$$

which is obtained by multiplying both sides of Eq. (A10) by u_1 and β_1, respectively, by integrating, and by considering the second equation of Eq. (A9). Similarly, the condition

(A11b)

$$\int [u_0 L_u(M; u_0, \beta_1) + \beta_0 L_\beta(M; u_1, \beta_1)]\, dz = \int [u_1 L_u(M; u_0, \beta_0) + \beta_1 L_\beta(M; u_0, \beta_0)]\, dz = 0$$

is obtained, in which the second integral follows from the first through integrations by parts. Finally, from Eqs. (A4), (A8), (A11), and the linearity of the differential operators, the parameter c is seen to be given by the equation

$$c = \left(\frac{1}{\mu}\right) \int (q u_1 + t \beta_1)\, dz \tag{A12}$$

As the point P approaches the boundary B, the eigenvalue μ approaches zero and the factor c increases generally beyond bounds. However, on B'

the numerator in Eq. (A12) also vanishes, as postulated in Eq. (A7); hence the fraction becomes indeterminate, and the following relationship is established by means of the usual limit considerations:

$$c' = \lim_{\mu \to 0} c = \frac{1}{\dot{\mu}} \int (q \dot{u}_1 + t \dot{\beta}_1)\, dz \tag{A13}$$

In Eq. (A13) and in what follows, a dot (such as in $\dot{\mu}$) signifies differentiation along the path, that is, $\frac{\partial}{\partial \lambda_s}$.

The denominator in Eq. (A13) is obtained from Eq. (A11a) through differentiation. This leads to

$$\begin{aligned} \dot{\mu} = &\int \left[\dot{u}_1 L_u(M; u_1, \beta_1) + \dot{\beta}_1 L_\beta(M; u_1, \beta_1) \right] dz \\ &+ \int \left[u_1 L_u(M; \dot{u}_1, \dot{\beta}_1) + \beta_1 L_\beta(M; \dot{u}_1, \dot{\beta}_1) \right] dz \\ &+ \int \left\{ u_1 (m_s \beta_1)'' + \beta_1 \left[m_s u_1'' + 2 (k m_s \beta_1')' \right] \right\} dz \end{aligned} \tag{A14}$$

The last integral on the right side of (A14) follows from the definitions of L_u and L_β and from the fact that $M = m_s$ by Eq. (6a)

The first integral in (A14) vanishes; this can be seen by substituting Eq. (A10) and by differentiating the second equation of Eq. (A9) with respect to λ_s. The second integral vanishes similarly, since it can be converted into the first integral (and hence zero) through four integrations by parts and in view of the boundary conditions. Two more integrations by parts finally convert the third integral into

$$\dot{\mu} = 2 \int m_s (u_1'' \beta_1 - k \beta_1'^2)\, dz \tag{A15}$$

The establishment of the numerator in Eq. (A13) proceeds along analogous lines. In fact, since (u_o, β_o) satisfies Eq. (A4) at P' (for $M = M_1$), it follows that the relationship

$$\begin{aligned} \int (q \dot{u}_1 + t \dot{\beta}_1) dz &= \int \left[\dot{u}_1 L_u(M; u_o, \beta_o) + \dot{\beta}_1 L_\beta(M; u_o, \beta_o) \right] dz \\ &= \int \left[u_o L_u(M; \dot{u}_1, \dot{\beta}_1) + \beta_o L_\beta(M; \dot{u}_1, \dot{\beta}_1) \right] dz \end{aligned}$$

holds. The second equality in the preceding equation is the result of a number of integrations by parts. However, if Eq. (A10) is differentiated with respect to λ_s, and if μ is set equal to zero, it follows that

$$\dot{L}_u(M; u_1, \beta_1) = L_u(M; \dot{u}_1, \dot{\beta}_1) + (m_s \beta_1)'' = \dot{\mu} u_1$$

$$\dot{L}_\beta(M; u_1, \beta_1) = L_\beta(M; \dot{u}_1, \dot{\beta}_1) + m_s u_1'' + 2 (k m_s \beta_1')' = \dot{\mu} b^2 \beta_1$$

on B'. When these relations are substituted in the last integral and the first equation of Eq. (A9) is considered, then, after some more integrations by parts, the relationship

$$\int (q\dot{u}_1 + t\dot{\beta}_1)\,dz = -\int m_s(u_o''\beta_1 + u_1''\beta_o - 2k\beta_o'\beta_1')\,dz \qquad \text{(A16)}$$

is established. Hence, by Eq. (A13), c' is expressed as the quotient of the two integrals appearing on the right side of Eqs. (A15) and (A16).

Offhand, this quotient seems to depend on the direction of the approach path. That this is not the case can be seen from the following considerations:

In the linear space in which the stress point P is defined, the moment component m_s can in general be expressed in the form $m_s = \gamma_\alpha m_\alpha$, in which the set of γ_r represents the direction cosines of the approach path relative to the coordinate axes. Similarly, the integrals on the right side of Eqs. (A15) and (A16) are representable as linear combinations involving these direction cosines.

Now both denominator and numerator components vanish for all directions which are tangent to the boundary surface B'. Indeed, since μ vanishes identically throughout B, $\dot{\mu}=0$ for all directions other than the one normal to B. Similarly, the numerator is different from zero only in the normal direction, which can be verified by considering that the orthogonality condition (A7) is satisfied identically on B'. Hence the direction of the approach path is immaterial, and the limiting coefficient c' can finally be expressed by

$$C' = \frac{\int m_n\,(u_\alpha''\beta_1 + u_1''\beta_o - 2K\beta_o'\beta_1')\,dz}{2\int m_n\,(u_1''\beta_1 - K\beta_1^{12})\,dz} \qquad \text{(A17)}$$

in which m_n represents the moment component normal to B!.

After the bounding surface of instability B' has been reached (for $\lambda = \lambda'$), the stress point P travels on B' as the load parameter λ is increased further. The response $\lambda(u,\beta)$ continues to satisfy Eq. (A8); when this is substituted in the compatibility conditions (11), the following system of equations is obtained:

$$\lambda_n - \lambda_n^* = \lambda^2\int m_n(u_o''\beta_o - k\beta_o'^2)\,dz + C\lambda^2\int m_n(u_o''\beta_1 + u_1''\beta_o - 2k\beta_o'\beta_1')\,dz$$
$$+ C^2\lambda^2\int m_n(u_1''\beta_1 - k\beta_1'^2)\,dz \qquad \text{(A18n)}$$

$$\lambda_t - \lambda_t^* = \lambda^2\int m_t(u_o''\beta_o - k\beta_o'^2)\,dz \qquad \text{(A18t)}$$

The subscript n denotes the direction of the outer normal to B', while the subscript t designates the totality of all directions which are tangent to B' and for which the condition (A7) is identically satisfied. In the set of equations (A18t) only one integral appears on the right side; two more integrals, similar in form to the second and third integrals in (A18n), can be shown to vanish.

In general, P moves on B' in such a way as to minimize further the value of $U+U_b/\lambda^2$. With λ going to infinity, a limiting point P_ℓ is approached, which corresponds to the smallest value of U on B'. This point is found by setting the integrals appearing on the right side of the system of equations (A18t) equal to zero; a limiting value of c is then obtained by substituting the functions (u_o,β_o) so determined in Eq. (A18n). (Note that there are two solutions.)

In special cases the stress point P may remain at P'. This happens when either P' is the only point on B' (such as in the illustrative example), or else when P' happens to be the point associated with the lowest value of U on B'; this latter case occurs when the vector $\overline{P^*P'}$ is normal to the instability surface. In either case, the final state of stress designated by P' is generally reached when the load parameter is finite ($\lambda = \lambda'$). For $\lambda > \lambda'$, the response functions $\lambda(u_o, \beta_o)$ increase linearly with λ similarly to a statically determinate structure. However, as before, two solutions for c are possible according to Eq. (A18n).[10] In other words, two distinct equilibrium configurations are possible such that one may be reached from the other only through a snap-through (Durchschlag) process. As before, a limiting value of c is approached as the parameter λ grows beyond bounds.

10. In the $(\lambda, c\lambda)$ plane, Eq. (A18n) defines a hyperbola. This becomes apparent from the fact that, if multiplied by two, the right side can be converted into the form $-\lambda^2 W + c\lambda^2 B + c^2\lambda^2\dot{\mu}$, in which the dot represents differentiation in the n-direction. It is clear that $\dot{\mu}$ is negative, since μ is positive inside the region of stability and negative outside of it. Similarly, $\dot{W}$ is seen to be negative; indeed if it were positive then W would exhibit an interior minimum, in which case P would not reach (or stay) on the boundary. And finally, if $\dot{W}$ were zero, P' would be reached only in the limit. The quadratic form has therefore a negative discriminant; hence it designates a hyperbola.

Paper 1415 October, 1957 EM 4

Journal of the
ENGINEERING MECHANICS DIVISION
Proceedings of the American Society of Civil Engineers

CONTENTS

DISCUSSION
(Proc. Paper 1415)

Discussion of
"MINIMUM-WEIGHT DESIGN OF A PORTAL FRAME"

by W. Prager
(Proc. Paper 1073)

Author's Closure

W. PRAGER,[1] M. ASCE.—The purpose of the paper was to investigate the influence of the usual linearization of the expression for the structural weight. For this purpose, it seemed sufficient to consider a single condition of loading. Minimum-weight design for multiple conditions of loading has been treated by Foulkes.*

1. Prof. of Applied Mechanics, Brown University, Providence, R. I.
* J. Foulkes, "Linear Programming and Structural Design," Proceedings, 2nd Symposium on Linear Programming, National Bureau of Standards, vol. I, pp. 177-184 (1955).

Discussion of
"WIND INDUCED VIBRATION OF CYLINDRICAL STRUCTURES"

by Joseph Penzien
(Proc. Paper 1141)

ANATOL ROSHKO.[1]—The phenomenon of wind-induced vibrations of elastic structures is a very interesting problem in mechanics and one of great concern to the engineer. A basic understanding of the problem is still lacking. The main contribution of the present paper is to point out that strong vibrations of a cylinder may occur at the natural frequency even when this does not coincide with the vortex-shedding frequency. The author describes these as "self-induced" vibrations, as distinguished from those induced by vortex shedding.

From the data given in the paper one can compute the Reynolds number for each velocity. It is seen then that the "self-induced" vibrations occurred at Reynolds numbers somewhat higher than 10^5 but lower than 10^6; that is, in the range of critical Reynolds number. In this critical range one ordinarily observes intermittent changes in the flow, between a configuration in which separation is upstream and one in which it is downstream of the 90^o points of the cylinder. Since these movements of separation point are not necessarily symmetric with respect to flow center line, it may be expected that intermittent changes of lift will occur under these conditions. These randomly occurring changes of lift could produce the "bursts" of vibration at natural frequency, which the author describes as self-induced. Of course, the terminology may be quite appropriate, but it is important to know whether this phenomenon is related to the flow intermittency or whether it occurs also in other ranges of Reynolds number.

The author's presentation of the data would have been considerably more useful if the data had been reduced to coefficient form. As it is, one cannot see how the observed amplitude depends on the Reynolds number, the flow dynamic pressure and the dynamic characteristics of the elastic system. The reader may compute for himself the values of Reynolds' number, from the data presented, but there is no way of calculating the actual aerodynamic forces or force coefficients, for the dynamic characteristics of the elastic system are not given, and were not taken into account in the data presented.

The main criticism of the paper is that it is hardly more than a presentation of the raw data, so that one can only speculate about the observed effects, and about their appearance under other conditions.

1. Guggenheim Aeronautical Laboratory, California Institute of Technology, Pasadena 4, Calif.

Discussion of
"BENDING OF A RECTANGULAR PLATE WITH ONE FREE EDGE"

by W. Nachbar
(Proc. Paper 1196)

I. K. SILVERMAN,[1] A.M. ASCE.—With the drudgery of calculation removed by the use of a high-speed digital computer, the author has been able to present in numerical and graphical form the results of the analysis of a plate problem, the solution of which follows the classical methods of plate theory. The presence of a completely free boundary always makes the solution of a plate problem quite difficult, and it is for this reason that few attempts have been made to solve approximately the type of problem described in this paper. To construct approximate functions for w which satisfy the free boundary condition, as well as the supported boundaries, presents as difficult a problem as solving the equations and boundary conditions exactly. The difficulty lies in the moment and shear condition at the free edge which involves the value of w, w', w'', and w''' at the free edge. This boundary condition can, of course, be simplified by assuming that the moment condition is $\overline{w}_n'' = 0$ and the shear condition is $\overline{w}_n''' = 0$, equivalent to assuming that $\mu = 2$ and $\mu = 0$ simultaneously.

The Kirchhoff treatment of the plate problem furnishes conditions at the free edge which may be used in lieu of equations 20 (a,b). It can be shown for the problem treated by the author that the following relationships must hold:

(N is used instead of the author's D)

$$\iint \left(\nabla^4 w - \frac{q}{N} \right) \delta w \, dx \, dy = 0 \qquad \text{(A)}$$

$$y = b : \int_{-\frac{a}{2}}^{+\frac{a}{2}} N \left[\frac{\partial^2 w}{\partial y^2} + \mu \frac{\partial^2 w}{\partial x^2} \right]_{y=b} \delta \left(\frac{\partial w}{\partial y} \right)_{y=b} dx = 0 \qquad \text{(B)}$$

$$\int_{-\frac{a}{2}}^{+\frac{a}{2}} N \left[\frac{\partial^3 w}{\partial y^3} + (2 - \mu) \frac{\partial^3 w}{\partial x^2 \partial y} \right]_{y=b} (\delta w)_{y=b} \, dx = 0 \qquad \text{(C)}$$

$$x = \pm \frac{a}{2} : \quad \frac{\partial^2 w}{\partial x^2} + \mu \frac{\partial^2 w}{\partial y^2} = 0 \qquad \text{(D)}$$

1. Engr., Bureau of Reclamation, U. S. Dept. of the Interior, Denver, Colo.

$$w = 0 \tag{E}$$

$$y = 0 : \quad \frac{\partial^2 w}{\partial y^2} + \mu \frac{\partial^2 w}{\partial x^2} = 0 \tag{F}$$

$$w = 0 \tag{G}$$

If w is taken as a product of two functions $X_o Y$ where X_o is chosen so that conditions (D) and (E) hold, then (A) will be satisfied if Y is a solution of the following differential equation

$$a_3 Y^{iv} + 2a_2 Y'' + a_1 Y - \frac{a_4}{N} q = 0 \tag{H}$$

The solution of (H) is given by

$$Y = A \psi_1(y) + B \psi_2(y) + C \psi_3(y) + D \psi_4(y) + f(y) \tag{I}$$

and the conditions (B), (C), (F), and (G) will be satisfied by appropriate choice of the constants A, B, C, and D of (I).

The exaction solution of the problem satisfies equations (2) and 20(a,b) in lieu of equations (A), (B), (C) above.

The above sketched-out method has been used by the writer to solve plate problems with free edges. Only slide rule accuracy is needed in most cases. For the plate shown in Figure 1, where the notation differs as shown from the author, under uniform load q_o ($\overline{K} = 0$)

$$X_o = \left(\frac{x^4}{a^4} - 6 \frac{x^2}{a^2} + 5 \right) \tag{J}$$

$$f(y) = \frac{a^4 q_o}{24N} = K \; ; \quad \psi_1(y) = \text{sh}\alpha y \sin \beta y \; ; \quad \psi_2(y) = \text{ch}\alpha y \sin \beta y \; ;$$

$$\psi_3(y) = \text{sh}\alpha y \cos \beta y \; ; \quad \psi_4(y) = \text{ch}\alpha y \cos \beta y \; ; \; \alpha = \frac{1.57115}{a} \; ; \; \beta = \frac{0.026,666}{a}$$

The constants A, B, C, D of equation (I) are determined from the following simultaneous equations:

$$a_3 Y''(o) + \nu a_2 Y(o) = 0 \tag{K}$$

$$a_3 Y'''(o) + (2 - \nu) a_2 Y'(o) = 0 \tag{L}$$

$$Y(h) = 0 \tag{M}$$

$$Y''(h) = 0 \tag{N}$$

The constants a_3 and a_2 are defined by

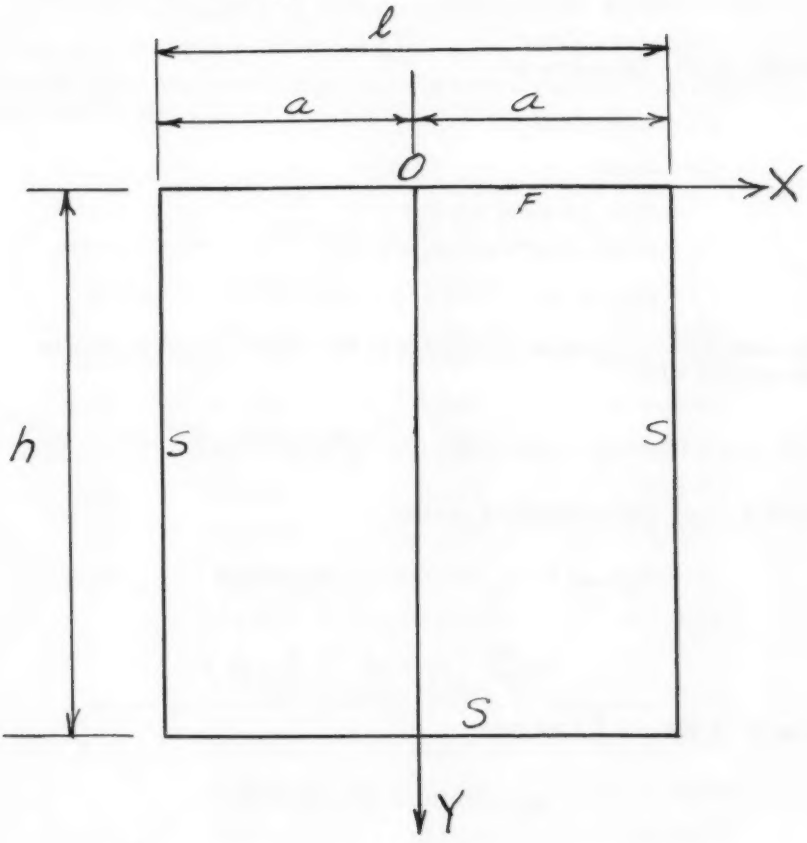

Fig. 1.

$$a_2 = \int_{-a}^{a} X_o X_o'' \, dx = -\frac{2176}{35a}$$

$$a_3 = \int_{-a}^{a} X_o^2 \, dx = \frac{7936a}{315}$$

For a hydrostatic load $\overline{K} = 1$, the same equations must be satisifed, but $f(y) = \frac{\gamma a^4}{24N} y$ where γ is the fluid unit weight so that $\gamma h = q_o$.

Application to Author's Case of $\frac{b}{a} = 1$; $\overline{K} = 0$ (Uniform Load); $\nu = 0.3$

$$\psi_1(h) = 0.6161 \; ; \quad \psi_2(h) = 0.6184 \; ; \quad \psi_3(h) = 11.5406; \quad \psi_4(h) = 11.5837$$

Equations (K) - (N) reduce to

$$D = 0.4286K - 0.04852A$$

$$C = 0.03151B$$

$$0.0541A + 0.9825B + 5.964K = 0$$

$$68.7A + 210B + 757.65K = 0$$

$$A = +\,9.09K \; ; \quad B = -\,6.56K \; ; \quad C = -\,0.207K \; ; \quad D = -\,0.0134K$$

The deflection w(o,o) which corresponds to the author's w(o,b) is given by w(o,o) = 5(K + D)

$$w(o,o) = 5\,(0.9866)K = 4.933\left(\frac{q_o a^4}{24N}\right) = \frac{4.933 \times 10.92}{24 \times 16} \times \frac{q_o \ell^4}{E_t^3} = 0.140\,\frac{q_o \ell^4}{E_t^3}$$

where ℓ = span and t = thickness of slab.

$$M_x(o,o) = -\,N\left[\,X''(o)Y(o) + \nu X(o)Y''(o)\,\right]$$

$$= -\,\frac{5N}{7a^2}\left(51K - A\sqrt{3}\right)\left(\frac{9\nu}{62} - \frac{8}{17}\right)$$

using A = 9.09K; a = $\frac{\ell}{2}$; ν = 0.3

$$M_x(o,o) = 10.82\,\frac{NK}{a^2} = 43.28\,\frac{NK}{\ell^2}$$

$$\frac{NK}{\ell^2} = \frac{q_o \ell^2}{16.24} = \frac{q_o \ell^2}{384}$$

$$m_x(o,o) = \frac{43.28}{384}\,q_o \ell^2 = 0.113\,q_o \ell^2$$

$$R(a,o) = -\,2M_x y(a,o) = -\,2N(1-\nu)\,X_o'(a)\,Y_o'(o)$$

$$= -\,2N(0.7)\left(-\frac{8}{a}\right)(B\beta + C\alpha)$$

$$= +\,0.854\,\frac{NB}{a^2} = -\,0.854(6.56)4\,\frac{NK}{\ell^2}$$

$$= -\,0.854(6.56)(4)\,\frac{q_o \ell^2}{384} = -\,0.0583\,q_o \ell^2$$

It is seen that the proposed approximate method gives results which are coincident with those of the author to at least two significant figures and which may be obtained by use of the slide rule. To indicate that such results are not limited to the square plate, the table below compares coefficients for w(o,o), M_x(o,o), R(a/2,o) for various $\left(\frac{b}{a}\right)$ ratios, both for hydrostatic and uniform loads. The figures in parentheses are values taken from author's tables and curves.

TABLE

$\frac{b}{a}$	Coeff w(o,o)	Coeff M_x(o,o)	Coeff R(a/2,o)
Uniform Load ($\bar{K}$ = 0)			
0.5	0.080	0.064	- 0.064
	(0.077)	(0.060)	(0.064)
1.0	0.140	0.113	- 0.058
	(0.140)	(0.112)	(0.060)
2.0	0.164	0.131	- 0.049
	(0.165)	(0.132)	(0.049)
Hydrostatic Load $\bar{K}$ = 1			
0.5	0.0248	0.0198	- 0.0177
	(0.0251)	(0.0197)	(- 0.0174)
1.0	0.0397	0.0317	- 0.0087
	(0.0402)	(0.0325)	(- 0.0086)
2.0	0.0328	0.0261	+ 0.0009
	(0.032)	(0.0256)	(0)

An iteration process is obviously possible since with the value of Y given by (I), a new value of X_o may be obtained.

Maximum departures from the exact solution occur when derivatives higher than the second are required, such as in the values for shear and edge reaction forces. For example, under uniform load the coefficients for Vx($\frac{a}{2}$,b) (author's coordinates) are (0.16, 0.29, 0.33) to be compared with the

author's values of (0.16, 0.25, 0.29) for ratios 0.5, 1.0, and 2.0.

While comparable approximate results for uniformly loaded plates may be obtained by using a finite number of terms in the Fourier expansion, the proposed approximate method has been found useful in obtaining results for partial loadings, especially for free boundaries combined with conditions of fixity.

Paper 1418 October, 1957 EM 4

Journal of the
ENGINEERING MECHANICS DIVISION
Proceedings of the American Society of Civil Engineers

INELASTIC ANALYSIS OF ECCENTRICALLY-LOADED COLUMNS

Marlyn E. Clark* A.M. ASCE, Omar M. Sidebottom* and
Robert W. Shreeves** J.M. ASCE
(Proc. Paper 1418)

ABSTRACT

This paper presents a theory by which the collapse load of an eccentrically-loaded column can be rationally determined. Experimental verification of the theory was obtained from tests made on aluminum alloy rectangular- and T-section columns. A study of the effect of time on the magnitude of the collapse load was also made using SAE 1020 steel columns.

I. INTRODUCTION

1. Preliminary Statement

In the design of slender members subjected to compression loads, it is important to realize that the determination of the load corresponding to failure is usually a problem in unstable equilibrium. The failure is manifested in the form of a sudden buckling or collapse whenever the balance between internal resisting moment and the externally applied moment is destroyed. It should be noted that the determination of the failure load is not dependent on the critical stress level at which failure is initiated in the most-stressed fibers except for columns having small values of the slenderness ratio. Here the type of failure changes from one of instability to one of yielding or crushing.

Stress values, in themselves, are of no concern whatsoever in the design of Euler columns—the size and shape of the cross-section of the members

Note: Discussion open until March 1, 1958. Paper 1418 is part of the copyrighted Journal of the Engineering Mechanics Division of the American Society of Civil Engineers, Vol. 83, No. EM 4, October, 1957.

* Associate Profs. of Theoretical and Applied Mechanics, University of Illinois, Urbana, Ill.

** Instructor in Theoretical and Applied Mechanics, University of Illinois, Urbana, Ill.

and the stiffness of the material are the only significant variables. For intermediate values of the slenderness ratio, the collapse load is reached only after inelastic deformation has been initiated and its magnitude depends not only on the stiffness of the material but upon the shape of the stress-strain diagram for small inelastic strains.

It can be said therefore, that an instability type of analysis must be used to calculate the failure load for all columns with slenderness ratios large enough to fail by buckling type of action. In such columns, the analysis must be capacle of relating the interval resisting moment with the externally applied moment making use of the properties of the cross-sectional area and the stress-strain diagram of the material used.

Several methods are available for designing centrally-loaded columns. When the material making up the column has a yield point, empirical equations of many types have been used. For materials which strain-harden, the rational tangent or the double (reduced) modulus theories are available. When the column is eccentrically loaded, the maximum elastic load can be predicted by the secant formula, but the column will not collapse until inelastic action occurs. In some cases the collapse load may be twenty to thirty percent greater than the maximum elastic load, and this increase can be obtained by allowing only a small amount of inelastic deformation.

The exact solution for determining the collapse load of an eccentrically-loaded column has not as yet been developed. By numerical procedures, the exact solution may be closely approximated, but from the standpoint of design, these solutions are extremely unwieldy. Various usable approximations to determine this load have been presented by Ketter,(1) Jordan,(2) Shanley,(3) and others.

2. Purpose and Scope

The primary purpose of this paper is to present a theory of inelastic column behavior which offers a relatively simple semi-graphical method for the determination of the collapse load. In the development of this purpose, analytical expressions for interaction curves* and moment-load curves** have been derived. The method utilized has been applied to rectangular- and T-section members; however, it can be applied to cross-sections of many other shapes.

The theoretical value of the collapse load for an eccentrically-loaded column, as herein presented, is obtained as follows: first, moment-load interaction curves for various depths of yielding are constructed using the equations herein derived; second, the intersection of the theoretical moment-load curve with each of these interaction curves is located; finally, a smooth curve is faired in through these intersections and the maximum or collapse load selected graphically.

The interaction curve for a given depth of yielding can be obtained by locating several points on the curve and then drawing a smooth curve through

---

* In this paper, an interaction curve is a curve which represents all possible combinations of moment and load which, when applied to a column, result in a given depth of yielding or inelastic deformation.

** A moment-load curve is a curve which, for a given loading system, relates changes in load with the corresponding changes in moment.

these points. To locate any one point, a strain distribution must be assumed, the stress distribution constructed using appropriate values from the stress-strain diagram, and the load P and the moment M calculated using the stress distribution and the equilibrium conditions. Five depths of yielding (0, 1/8, 1/4, 1/2, and 3/4) have been considered so as to provide several points on the theoretical moment-load curve for a given column.

The intersection of the theoretical moment-load curve for a column and the interaction curve for a given depth of yielding has been obtained by equating the radius of curvature of the column at the critical section to the radius of curvature needed to produce a given depth of yielding. In order to obtain an expression for the radius of curvature of the column, it is necessary to assume a configuration of the deflected axis of the column. Two assumptions have been made—first, an assumption of an arc of a circle, and second, the usual assumption of a cosine curve.

An experimental program was undertaken to determine the ability of the proposed theory to predict collapse loads. Test data corroborating the theory were obtained from rectangular columns made of annealed SAE 1020 steel and rectangular- and T-section columns made of 24ST aluminum alloy.

A secondary purpose of this paper is to study the effect of time on the magnitude of the collapse load. Since previous investigations on mild steel beams by Clark, Corten, and Sidebottom[4] indicated that the yield strength of mild steel can be lowered if sufficient time is allowed for inelastic deformation to be completed at a given load, the steel columns were tested under similar conditions in a constant-load testing machine.[5] Several columns were loaded in steps and each successive load was maintained for 6 minutes or longer. The results of tests under these conditions indicate that the yield strength was from 5 to 10 percent below that usually obtained in an ordinary tension test. This is of the same order of magnitude as the value found in the beam investigation.[4] Other mild steel columns were tested so as to complete the loading to failure in less than two minutes. These data indicate that the yield strength of the material in the column had been raised in the presence of rapid loading.

II. Theory

3. Derivation of Moment and Load Interaction Equations

The derivation of interaction equations for a given depth of yielding is based on the assumption that plane sections in the column remain plane and that the stress-strain diagram of the material may be represented by two straight lines as indicated by Fig. 1. Depth of yielding has been chosen as the invariant (instead of some other quantity such as maximum strain or maximum stress) because of the ease with which the derivations are made when this quantity is chosen.

The interaction curve for any given depth of yielding is usually made up of one or two linear segments and one curved segment. The interaction curve is linear so long as yielding has not occurred on both sides of the member.[6] Therefore, the most convenient method of constructing an interaction curve for a given depth of yielding is to (1) locate the terminal points of the linear segments, (2) determine the coordinates of several points on the curved portion, and (3) "fair in" a smooth curve.

To illustrate the method of computing a point on an interaction curve,

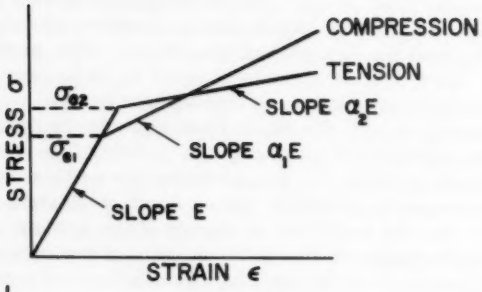

FIGURE 1

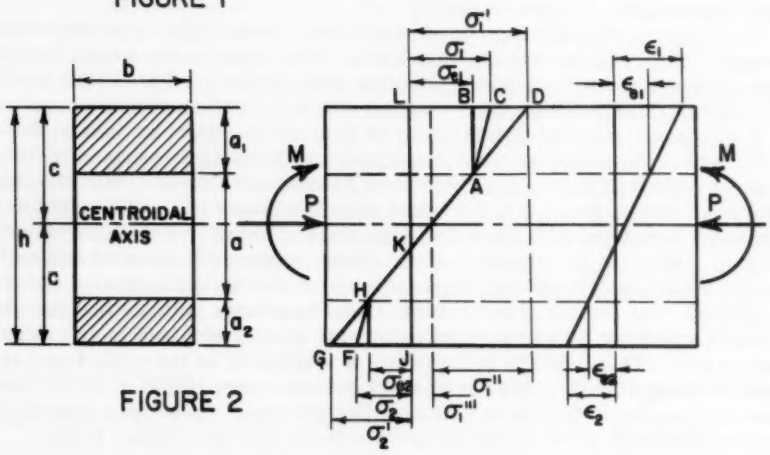

FIGURE 2

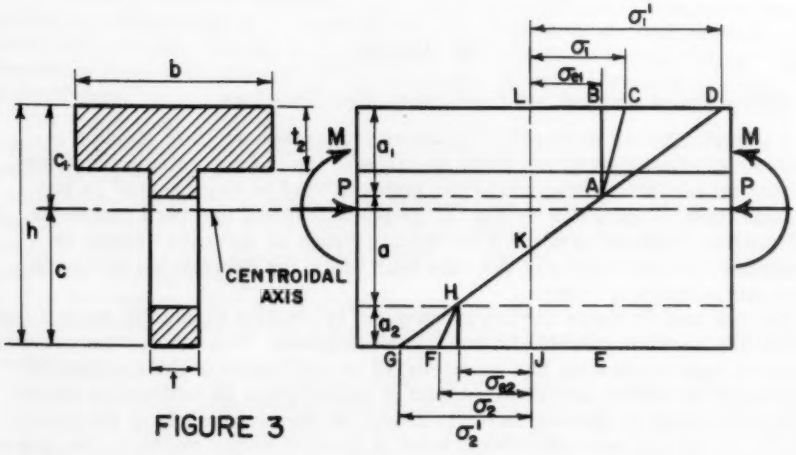

FIGURE 3

consider the column of rectangular cross-section shown in Fig. 2. The column has a width b and a depth h. For the strain distribution, the depth of yielding on the compressive side of the column is a_1 and the depth of yielding on the tension side of the column is a_2.

The stress distribution shown in Fig. 2 was constructed from the strain distribution and the stress-strain diagram for the material as shown in Fig. 1. It will be noted that the stress-strain diagrams for tension and compression are represented by two straight lines. In the elastic portion, the slope of the straight line is equal to the modulus of elasticity, E. In the inelastic portion, the slope is $\alpha_1 E$ for compression and $\alpha_2 E$ for tension where α_1 and α_2 may be considered the strain-hardening factors for the material.

The load P and the moment M on the column may now be determined by making use of the stress distribution K-L-C-A-H-F-J. The work involved in using the equations for P and M will be reduced if they are derived so that P and M are functions only of a_1, the depth of yielding on the compression side, a_2, the depth of yielding on the tension side, and a, the elastic depth or core.

In calculating the load P, it should be noted that for elastic conditions (such as stress distribution K-L-D-G-J), the load P would be equal to the product of the cross-sectional area A and the stress at the centroid σ_1''' The desired load P is equal to this load for elastic conditions minus the load corresponding to the stress distribution A-C-D plus the load corresponding to the stress distribution H-F-G. From similar triangles, it can be seen that

$$\frac{2\sigma_e}{a} = \frac{\sigma_1' - \sigma_{e_1}}{a_1} = \frac{\sigma_1''}{c}$$

where the yield stress σ_e is the average of σ_{e1} and σ_{e2}. The stress at the centroid then becomes

$$\sigma_1''' = \sigma_1' - \sigma_1'' = \sigma_{e_1} - \frac{2\sigma_e}{a}(c - a_1) \tag{1}$$

To obtain the loads corresponding to the stress distributions A-C-D and H-F-G, it is necessary to obtain the stresses represented by C-D and F-G. Stress C-D becomes

$$(1 - \alpha_1)(\sigma_1' - \sigma_{e_1}) = (1 - \alpha_1)\frac{2\sigma_{e_1} a}{a} \tag{2}$$

and an identical expression (with suitable subscripts) gives stress F-G. Using the relations given in Eq. 1 and 2, an expression for the load P may be written as

$$P = 2\sigma_{e_1} bc - \frac{4\sigma_e bc}{a}(c - a_1) - (1 - \alpha_1)\frac{\sigma_e b a_1^2}{a} + (1 - \alpha_2)\frac{\sigma_e b a_2^2}{a} \tag{3}$$

In calculating the bending moment M corresponding to stress distribution K-L-C-A-H-F-J, it is convenient to subtract from a fictitious elastic moment M_I (equal to $\sigma_1'' I/c$ from the stress distribution K-L-D-G-J) the moments of

the loads resulting from stress distributions A-C-D and H-G-F. Using similar triangles, the elastic moment can be written as $2\sigma_e I/a$. The bending moment M can now be written as shown below.

$$M = \frac{2\sigma_e I}{a} - (1 - \alpha_1)\frac{\sigma_e b a_1^2}{a}\left(c - \frac{a_1}{3}\right) - (1 - \alpha_2)\frac{\sigma_e b a_2^2}{a}\left(c - \frac{a_2}{3}\right) \qquad (4)$$

It should be noted that Eq. 3 and 4 are valid if either a_1 or a_2 is zero.

Attention will now be turned to the derivation of the load and moment relations for a T-section member. The cross-sectional dimensions of this member are shown in Fig. 3. The calculations are more complex than those for the rectangular section because of the change in width of the section. The expressions for the load P and the moment M will be different depending upon whether the depth of yielding on the compression side, a_1, is less than or greater than the thickness of the flange, t_2. If a_1 is less than or equal to t_2 the expressions for the load and moment are similar to Eq. 3 and 4. Taking into consideration the difference in width of the section for the stress distribution A-C-D and H-F-G, the load and moment are given as follows:

$$P = \sigma_{e_1} A - \frac{2\sigma_e A}{a}(c_1 - a_1) - (1 - \alpha_1)\frac{\sigma_e b a_1^2}{a} + (1 - \alpha_2)\frac{\sigma_e t a_2^2}{a} \qquad (5)$$

$$M = \frac{2\sigma_e I}{a} - (I - \alpha_1)\frac{\sigma_e b a_1^2}{a}\left(c_1 - \frac{a_1}{3}\right) - (1 - \alpha_2)\frac{\sigma_e t a_2^2}{a}\left(c_2 - \frac{a_2}{3}\right) \qquad (6)$$

If the depth of yielding on the compression side of the T-section member extends through the flange, i.e., if a_1 is greater than t_2, the calculations of the load and moment for the stress distribution A-C-D is complicated by the abrupt change in width of the section. The computation of the load can be simplified by calculating the load corresponding to the area $a_1 b$ and then subtracting from this the load corresponding to area $(a_1 - t_2)(b - t)$. From geometry, the magnitude of the stress at the inside of the flange minus the yield stress σ_{e1} is given by the relation $2\sigma_e (a_1 - t_2)/a$. Using this relation along with Eq. 1 and 2, the load expression becomes

$$P = \sigma_{e_1} A - \frac{2\sigma_e A}{a}(c_1 - a_1) - (1 - \alpha_1)\left[\frac{\sigma_e b a_1^2}{a} - \sigma_e \frac{(b-t)(a_1 - t_2)^2}{a}\right] + (1 - \alpha_2)\frac{\sigma_e t a_2^2}{a} \qquad (7)$$

The determination of the moment corresponding to stress distribution A-C-D is simplified if it is realized that the moment of the stress distribution A-C-D is equal to the product of $(1 - \alpha_1)$ and stress distribution A-B-D. But this calculation is complicated by the change in width of section over the depth a_1. This difficulty can be circumvented by noting that the magnitude of the fictitious elastic moment M_I depends only on the stress gradient since a uniform stress distribution superimposed on a bending stress distribution does not affect the magnitude of the resisting moment. Therefore, the moment resulting from the stress distribution A-B-D is equal to M_I minus the moment of the stress distribution A-E-G which does not have a change in width. Thus,

$$M = M_I - (1 - \alpha_1)\left[M_I - \frac{\sigma_e (a + a_1)^2 t}{a}\left(c_2 - \frac{a + a_1}{3}\right)\right] - (1 - \alpha_2)\frac{\sigma_e t a^2}{a}\left(c_2 - \frac{a}{3}\right) \quad (8)$$

Again it is noteworthy that a_1 and a_2 can assume the value of zero without affecting the validity of Eq. 5, 6, 7 and 8.

4. Interaction Curves

Interaction curves for a column of rectangular cross-section have been constructed by the use of Eq. 3 and 4 and are shown as the solid curves in Fig. 4. These curves are for a mild steel having equal yield stresses in compression and tension, i.e., $\sigma_{e1} = \sigma_{e2} = \sigma_e$, and for a strain-hardening factor α equal to zero. It will be noted that for a depth of yielding not equal to zero, the interaction curve is made up of a curved portion and a straight line. For instance, consider the curve A-B-C for three-quarter depth yielding. From A to B, yielding occurs on both faces of the member. From B to C, yielding occurs over the same total area of cross-section, but the stress on the compression side remains constant at σ_e, while the stress on the tension side of the member varies from σ_e tension to σ_e compression. The proof of the linearity of line B-C may be found in a paper by Brush and Sidebottom.(6)

For the T-section columns, the interaction curves can be obtained by making use of Eq. 5 through 8. Typical curves for the aluminum alloy columns are shown in Fig. 10 to 12. It can be noted that all interaction curves have been plotted in dimensionless form. The load and moment equations have been divided by the maximum elastic load, P_e, and the maximum elastic bending moment, M_e, respectively. In these expressions the compressive yield stress σ_{e1} should be used to determine P_e, and either σ_{e1} or σ_{e2} should be used to determine M_e depending upon which yield stress is reached first when the member is subjected to pure bending. Accordingly, c_1 or c_2 should be selected to correspond with the appropriate stress.

5. Development of Moment-Load Curves

A moment-load curve for a column is a plot of corresponding values of the load P and the moment M. The moment M can be seen to be directly dependent on the eccentric load and equal to $P\Delta$, where Δ is the initial eccentricity e plus the deflection δ of the column. It is the stated purpose, therefore, of this section to set forth a procedure whereby the moment-load curve can be determined analytically. Once the moment-load curve for a given column is known, it is a simple matter to determine the collapse load from it. The load corresponding to a point on the moment-load curve at which an increase in load is impossible can be defined as the collapse load, P_c. This point can be found graphically by drawing a vertical line tangent to the moment-load curve. The abscissa of this point of tangency is the ratio of the collapse load to the maximum elastic load, P_e. The method herein presented makes use of the interaction curves for determining the moment-load curve.

Instability and collapse of an eccentrically-loaded column will take place when the externally applied moment exceeds the internal resisting moment offered by the type of material and the shape of the cross-section of the column. Stability can then be assured if there is a balance between these two

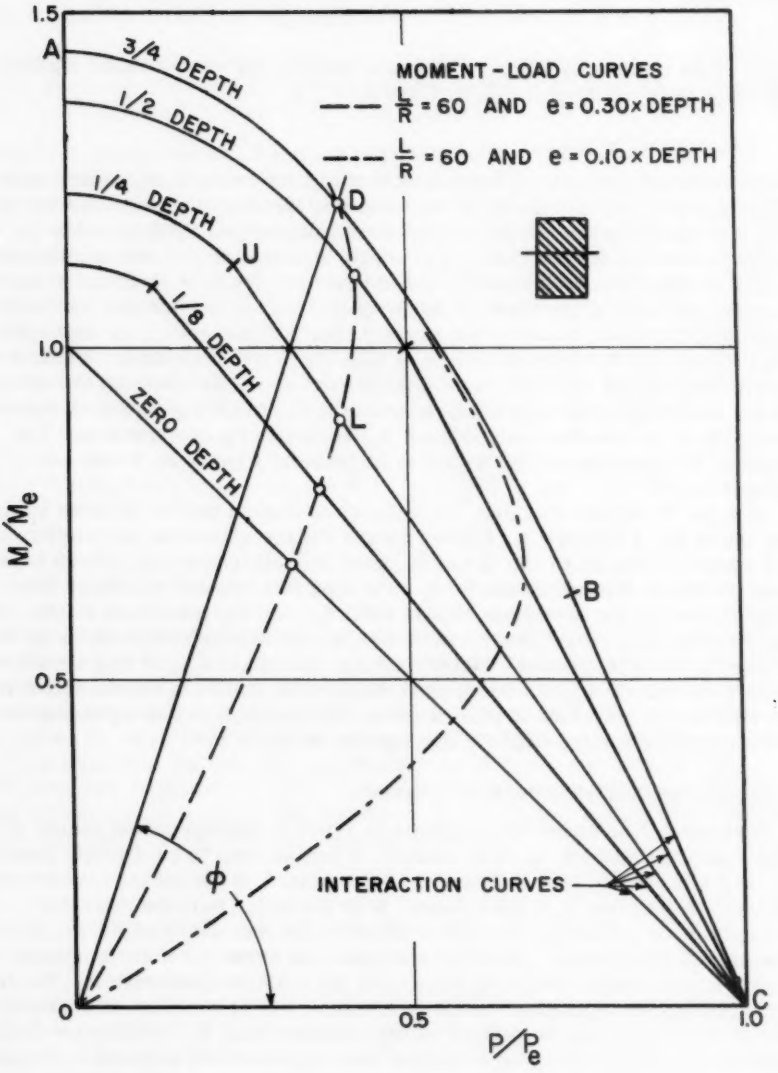

FIG. 4 THEORETICAL INTERACTION AND MOMENT-LOAD CURVES FOR ECCENTRICALLY LOADED MILD STEEL COLUMNS HAVING RECTANGULAR CROSS-SECTIONS.

moments. A moment-load curve for stable conditions can be derived on this basis as follows: The interaction curves shown in Fig. 11 through 15 give combinations of axial load and moment which may be applied to the member to produce a given depth of yielding. For a column with a given eccentricity and deflection pattern, only one point on each curve represents the internal resisting conditions which prevail in this loading. This one point, therefore, is a unique point on the moment-load curve for this depth of yielding; when a method is found to determine the intersection of the moment-load curve with each interaction curve, it will be possible to locate enough points so that a representative curve can be drawn.

It should be noted that each interaction curve is a curve for a constant depth of yielding. For the non-linear portion of a given curve, yielding occurs on both sides of the member and the radius of curvature of the member remains constant. When the expression for the radius of curvature of the column, as determined from its assumed deflected axis, is equated to the radius of curvature expression, as determined from the interaction curve, it is equivalent to equating the applied moment to the resisting moment (since moment and curvature are proportional if the deflection is small compared with the length of the column). In order to determine the radius of curvature for a column, the configuration of the column must be known. Since the exact configuration is impractical if not impossible to obtain, one must be assumed. In this paper, two assumptions will be presented. The first assumption will be that of a segment of a circle—this will yield a conservative estimate of the collapse load since each section of the column is assumed to be stressed the same as the central section. To provide a means of comparison with work done in this field by other investigators, the second assumption will be that of a cosine curve configuration.

By assuming that the column deforms into a segment of a circle, the radius of curvature can be obtained from the expression (see Fig. 5)

$$R^2 = \left(\frac{L}{2}\right)^2 + (R - \delta)^2$$

For the cosine curve assumption, an expression involving the radius of curvature at the center of the member can be obtained if the following equation is differentiated twice with respect to x.

$$y = \delta \cos \frac{\pi x}{L}$$

Assuming small deflections, the following simple relations between radii of curvature and deflection are obtained.

$$\frac{1}{R} = \frac{8\delta}{L^2} \text{ (circle)} \qquad \frac{1}{R} = \frac{\pi^2\delta}{L^2} \text{ (cosine)} \tag{9}$$

The radius of curvature can also be found from the strain distribution in the column. For the strain distribution shown in Fig. 2, the strains at both edges of the elastic material are known and are equal to ϵ_{e1} and ϵ_{e2}, the yield strain in compression and tension, respectively. Since plane sections are assumed to remain plane throughout the straining, a consideration of this

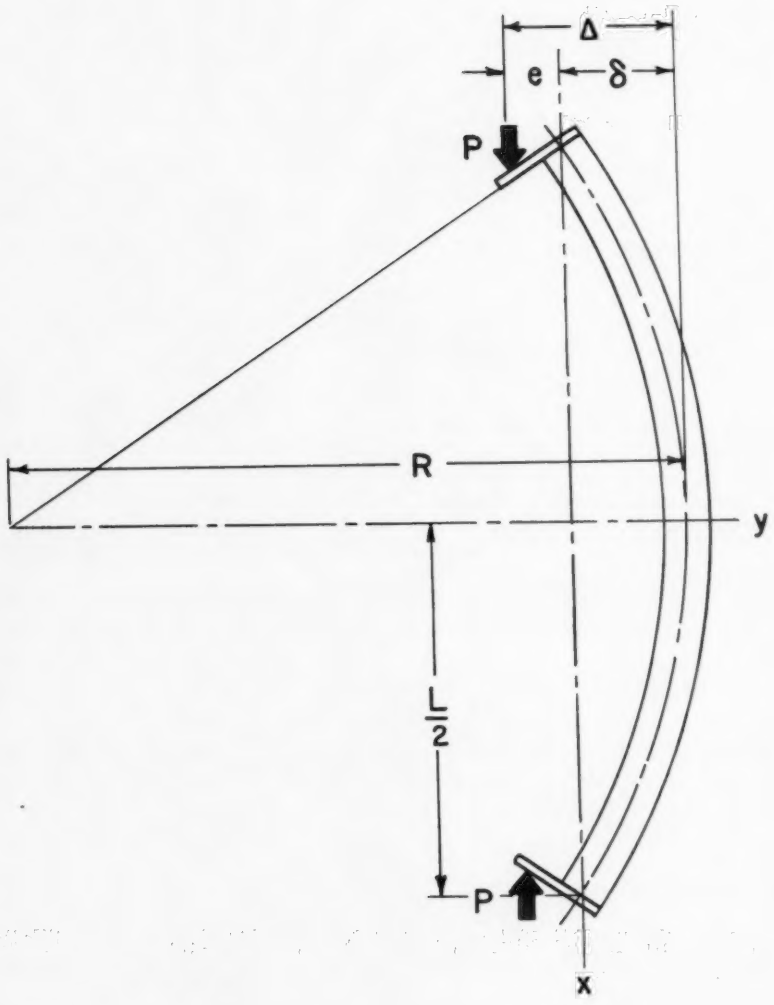

FIGURE 5

geometry of deformation will show that the reciprocal of the radius of curvature can be written in terms of these strains and the distance, a, between them. When the elastic core distance, a, is set equal to kh (where k is a proportionally constant denoting the elastic core depth), the expression can be written

$$\frac{1}{R} = \frac{\epsilon_{e1} + \epsilon_{e2}}{kh} = \frac{2\epsilon_e}{kh} \tag{10}$$

where ϵ_e is the average of the yield strains ϵ_{e1} and ϵ_{e2}. It should be noted that k remains constant for any given depth of yielding. By equating Eq. 9 and 10, the deflection of the column can be obtained in terms of the geometry of deformation, the dimensions of the cross-section, and the properties of the material as follows:

$$\delta = \frac{L^2 \epsilon_e}{4kh} \quad \text{(circle)} \qquad \delta = \frac{2L^2 \epsilon_e}{\pi^2 kh} \quad \text{(cosine)} \tag{11}$$

Eq. 11 is valid as long as yielding occurs on both faces of the member.

By making use of Eq. 11, it is now possible to construct the moment-load curve for the column for each assumption. The moment M can be written in terms of the load P, the eccentricity e, and the deflection δ. Using the circular segment representation,

$$M = P(e + \delta) = P\left[e + \frac{L^2 \epsilon_e}{4kh} \right]$$

In order to make use of the dimensionless interaction curves, the above expression must be divided through by the maximum elastic moment M_e (equal to $\frac{\sigma_{e1} I}{c_1}$ or $\frac{\sigma_{e2} I}{c_2}$, whichever is valid) while the right side of the expression must be multiplied and divided by the maximum compressive load P_e (equal to $\sigma_{e1} A$). The expression which results, if M_e equals $\frac{\sigma_{e1} I}{c_1}$, is

$$\frac{M}{M_e} = \frac{P}{P_e} \frac{Ac_1}{I} \left[e + \frac{L^2 \epsilon_e}{4kh} \right]$$

By dividing by $\frac{P}{P_e}$, the above relation can be put in a form useful for entering the interaction curves. This result is

$$\tan \Phi = \frac{M/M_e}{P/P_e} = \frac{c_1 e}{\rho^2} + \frac{c_1 L^2 \epsilon_e}{\rho^2 \, 4kh} \tag{12}$$

where $\rho^2 = I/A$. In Fig. 4, the line OD of slope Φ was obtained for

three-quarter depth yielding by substituting k = 1/4 in Eq. 12. The intersection of this line and the curve for three-quarters depth of yielding is point D, a point on the moment-load curve O-L-D. By assuming other values for k, other intersection points between the interaction curves and the moment-load curve are obtained.

Since Eq. 12 is only valid when yielding occurs on both sides of the member, it is not valid for the straight line portion of the interaction curve. This difficulty is easily overcome since the deflection of the column at any point on the straight line portion of the interaction curve is proportional to the bending moment. The proof of this statement is given in Appendix A. Thus, the deflection corresponding to point L in Fig. 4 is

$$\delta_L = \delta_U \frac{M_L}{M_U} \tag{13}$$

where δ_U is the deflection of the column corresponding to point U the end of the straight-line segment in Fig. 4 and is obtained from Eq. 11. M_U is the value of the moment at this point. M_L is the value of the moment at some lower point where the moment-load curve intersects the interaction curve.

Since M_L/M_U appears in the equation for tan ϕ in the case when there is yielding on one side only, Eq. 12 must be solved by trial and error. For every value of M_L that is selected, there is a corresponding value for tan ϕ. When the value chosen for tan ϕ is equal to the right hand side of Eq. 12, the desired point on the moment-load curve is determined. The following equations summarize the foregoing:

$$\delta = \frac{L^2 \epsilon_e}{4kh} \frac{M_L}{M_U} \tag{14}$$

$$\tan \phi = \frac{c_1 e}{\rho^2} + \frac{c_1 L^2 \epsilon_e}{\rho^2 4kh} \frac{M_L}{M_U} \quad \text{for } M_e = \frac{\sigma_{e1} I}{c_1} \tag{15}$$

$$\tan \phi = \frac{c_2 e}{\rho^2} \frac{\sigma_{e1}}{\sigma_{e2}} + \frac{c_2 L^2 \epsilon_e}{\rho^2 4kh} \frac{\sigma_{e1}}{\sigma_{e2}} \frac{M_L}{M_U} \quad \text{for } M_e = \frac{\sigma_{e2} I}{c_2} \tag{16}$$

If the cosine curve configuration was to be utilized instead of the circle, Eq. 14 through 16 would be identical with those given above except that the number 4 would be replaced by $\frac{\pi^2}{2}$.

III. Experiment

6. Description of Materials and Members

In the experimental program to determine the correlation between theory and experiment, a total of 4 columns made of 24ST aluminum alloy and 9

columns made of SAE 1020 steel were tested. The aluminum alloy was chosen to represent those materials which strain-harden at the onset of inelastic deformation and which are nominally time-insensitive. The steel was known to possess time-dependent characteristics, and, therefore, it was chosen to study the effects of time (rate of loading and time at a given load) on the inelastic behavior of eccentrically-loaded columns.

Two different types of cross-sections (rectangular- and T-section) were used for the aluminum alloy columns whereas only rectangular columns were made from the steel. In the as-received condition, both materials possessed a variation in properties across the diameter of the bar-stock that was used. A survey of this variation (made using plate tension specimens 1/4 x 1/2 in. in cross-section and 10 in. long) showed that the yield stress for both materials was approximately 10 percent greater at the periphery of the bar than at the center.

Fig. 6 shows the three different types of column specimens used, their dimensions, and their locations in the original bar-stock. In Fig. 7 are shown three different sets of stress-strain data for the aluminum alloy material. Because of the variation in properties mentioned above, in each set of curves in Fig. 7 the properties reported were obtained from specimens cut from the bar stock near the place where the significant stress occurred in the column. For example, in the T-section column the critical tension fibers were located near the periphery of the bar, hence, the tension specimens were cut from this location. For the steel columns, the variation in properties was accounted for by a greater number of compression tests, many specimens being cut directly from the undeformed ends of the columns. An overall average of 30,000 psi, obtained from some 24 yield point values from both tension and compression tests, was used.

In order to be utilized in the theoretical relations developed in Section II, it is necessary for the stress-strain diagram to be represented by two straight lines. No difficulty is presented for the SAE 1020 steel since the yield range is well represented by just a horizontal line. However, the diagrams for the aluminum alloy shown in Fig. 7 present more of a problem. The question arises as to whether the straight line in the inelastic region should represent the stress-strain diagram accurately for large inelastic strains or for small inelastic strains. In general, the type of columns tested in this investigation reached their collapse load before excessive deformation took place and the small strain representation should be more apropos. Both representations were investigated and are discussed in Section IV.

The accepted published value of the modulus of elasticity were used for both materials; 10,600,000 psi for the 24ST aluminum alloy and 30,000,000 psi for the SAE 1020 steel.

7. Method of Testing

Fig. 8 shows a sketch of the double knife-edge column fixtures and Fig. 9 shows a typical set-up in the constant-load testing machine. Note that the two knife-edges are placed perpendicular to each other and point loading is achieved. The eccentricity was pre-set by moving the column seat to one side or the other of the center line of the knife-edge. All rectangular-section members were supported in the manner shown in Fig. 8; however, the T-section members were supported by only one knife-edge at each end (thus, line loading was achieved) in order to insure that the column would buckle about the desired axis. Since the effective length of a column must be

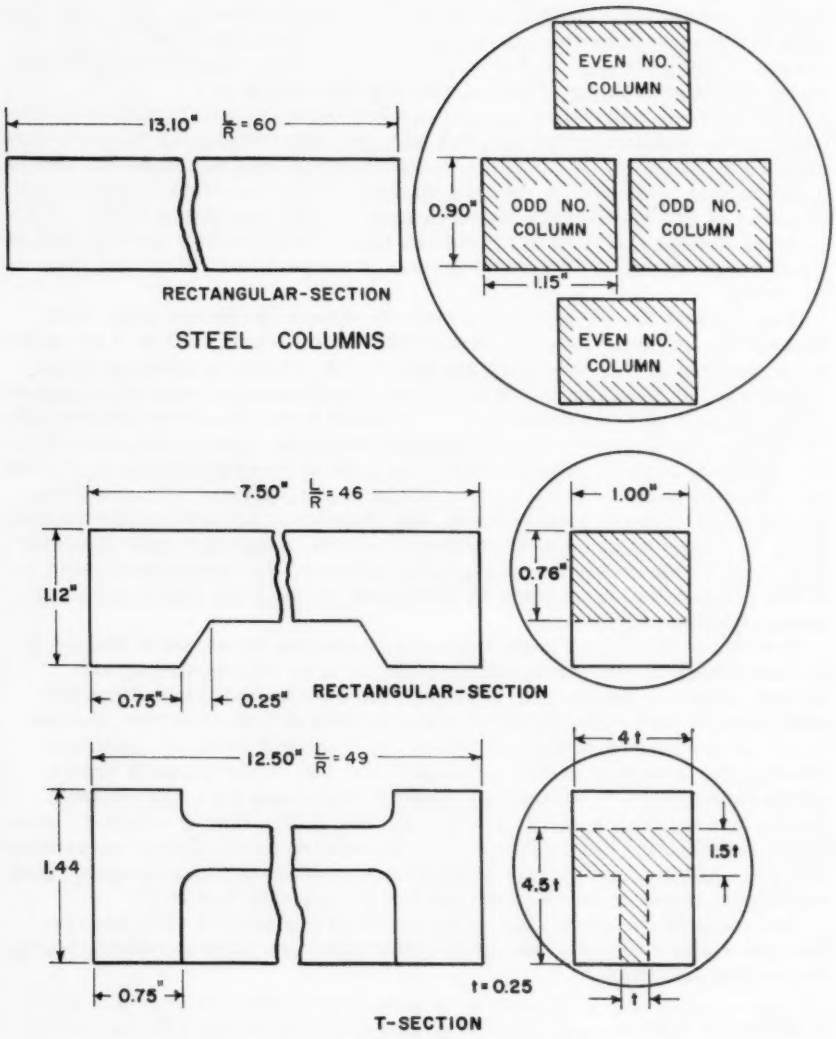

FIG. 6 SKETCHES OF COLUMNS SHOWING DIMENSIONS AND RELATIVE POSITIONS IN BAR-STOCK.

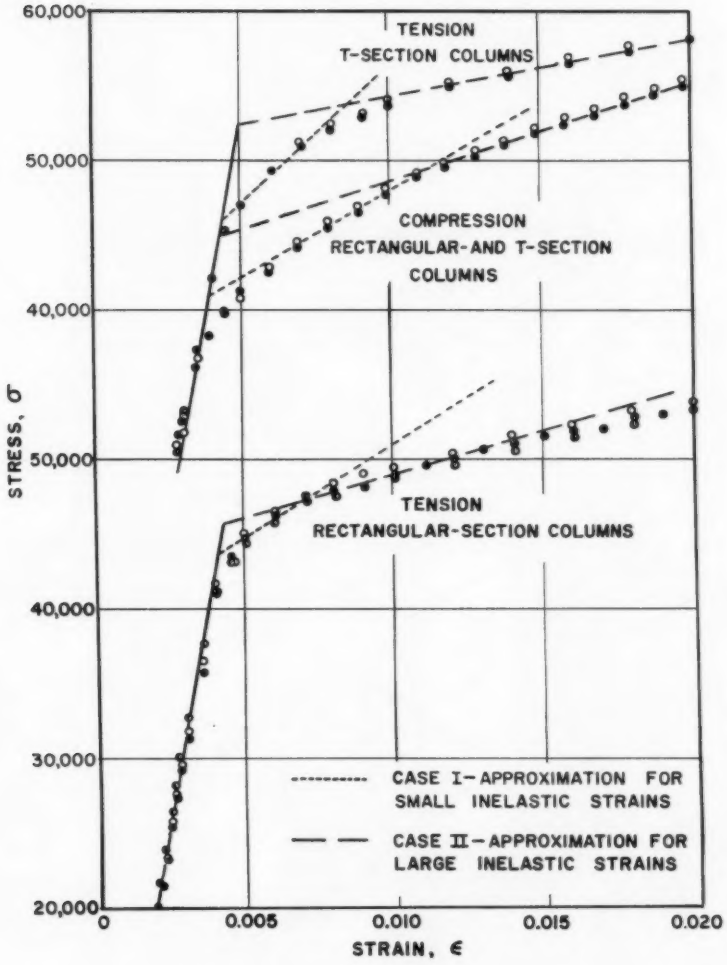

FIG. 7 STRESS-STRAIN DIAGRAMS FOR THE 24S-T ALUMINUM ALLOY.

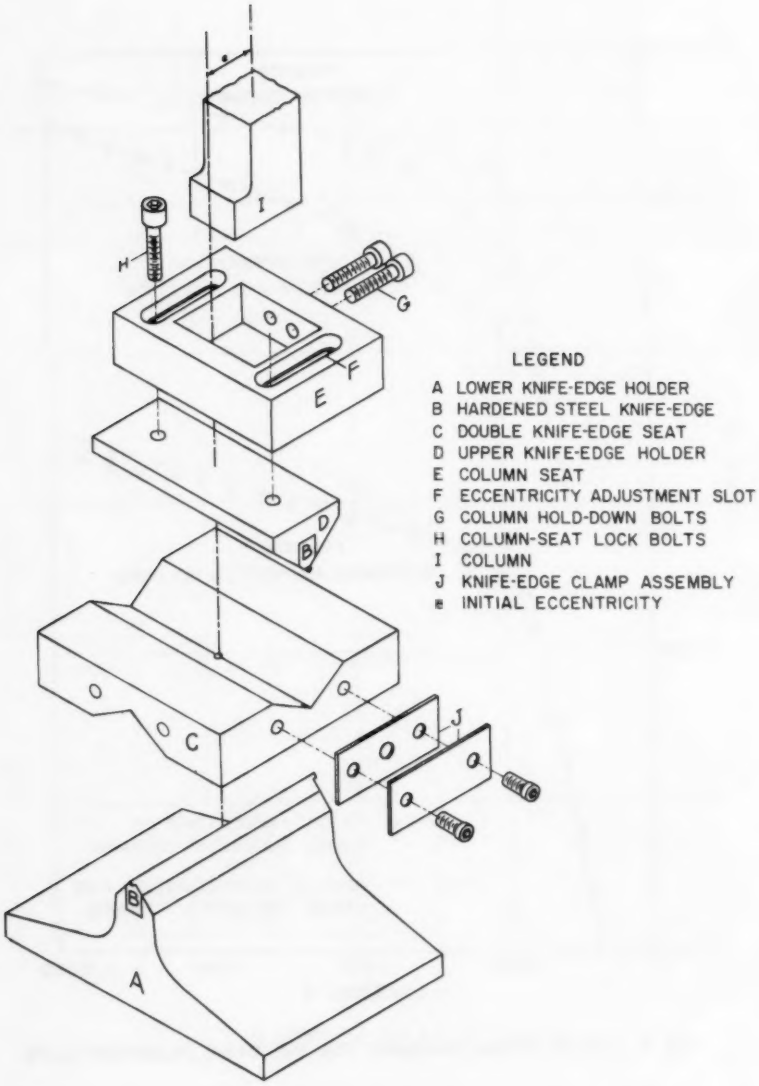

FIG. 8 DOUBLE KNIFE-EDGE COLUMN FIXTURE

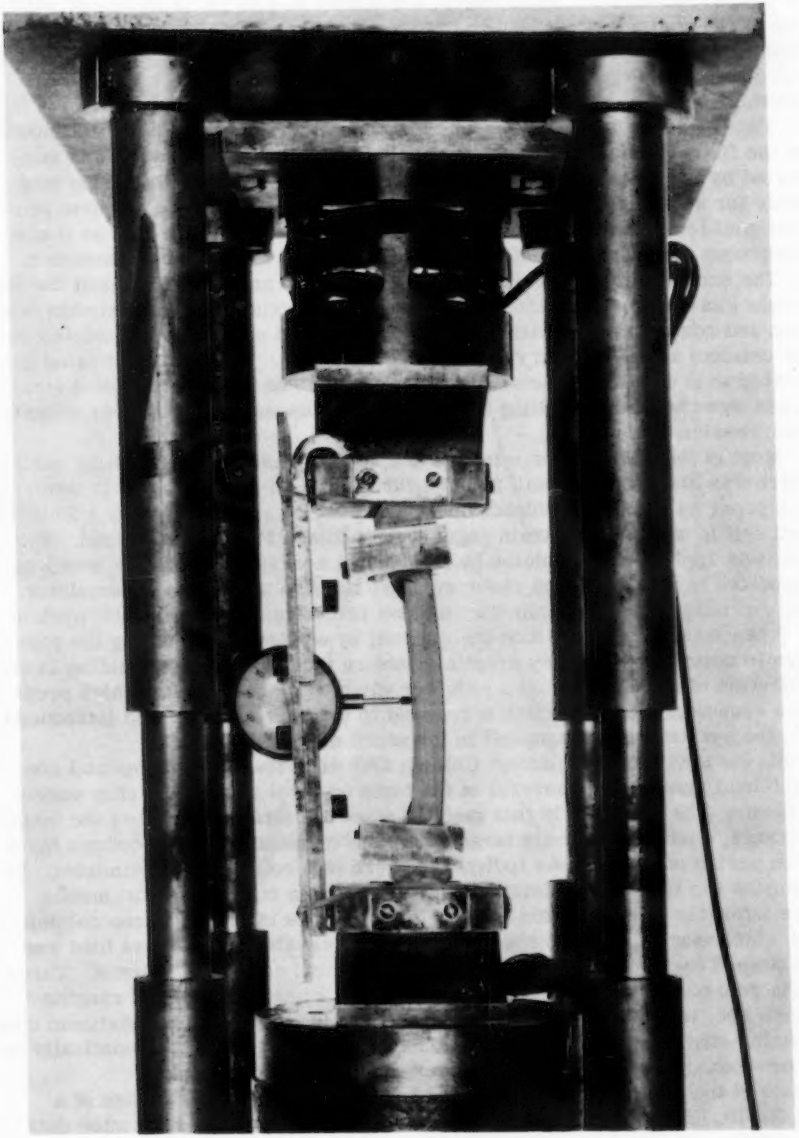

FIG. 9 TYPICAL SETUP OF COLUMN IN CONSTANT LOAD TESTING MACHINE

measured between the knife-edges, a distance of 2.50 in. (1.25 in. for each end of the column) was added to the length of each machined column to account for the length of the knife-edge fixtures. The aluminum alloy columns were provided with increased dimensions of the ends so as to avoid local crushing of the material.

The deflection at the center of each column was obtained by a dial mounted on the fixture shown in Fig. 9. It should be noted that the fixture was supported by the blocks which contained the knife-edge seats. Provision was made for a deflectometer, capable of generating an electrical impulse proportional to the deflection, to be connected in series with the dial so that a continuous record of the deflection could be made on a Sanborn Recorder.

The eccentricity for each column was adjusted on the fixtures and the magnitude was checked analytically using measured values of the maximum tension and compression strains (obtained from SR-4 strain gages mounted on the column) and measured values of the deflection. The computed value correlated well with the value set on the fixtures. The accuracy of SR-4 strain gages was checked in bending before the columns were tested under eccentric compression loads.

Most of the columns were tested in a special constant-load testing machine which was designed and built for this investigation. The machine is described in a paper by Clark and Sidebottom.(5) The load was measured by a 20,000 lb. load cell in which SR-4 strain gages were utilized for indicating load. The load was applied to the column by means of a hydraulic jack. The jack was connected to a ballast-type reducing valve through an oil-gas accumulator. The reducing valve maintained a constant pressure on the hydraulic system (and hence, a constant load on the column) by continually adjusting the pressure to compensate for any drop in pressure (and load) due to yielding in and deflection of the column. The reducing valve was connected to a high pressure source of nitrogen which it reduced to the correct value and introduced into the system when a drop-off in pressure was indicated.

All the steel columns except Column SR7 were tested in the special constant-load machine. In several of the tests on steel columns, a step method of loading was adopted. In this method, when the stresses reached the inelastic range, each successively larger load was maintained on the column for a given period of time unless indications were that collapse was imminent. In this case the load was maintained until the column collapsed. Six-minute time intervals were selected for use in this series of tests. In one column test which started out with six-minute load intervals, the collapse load was maintained for approximately an hour before final collapse occurred. Three of the columns were in the inelastic range for a total time period ranging from 6 sec. to 82 sec. For these columns the load, deflection, maximum compression strain, and maximum tension strain were recorded automatically on a four-channel Sanborn Recorder.

One of the steel columns (SR7) was tested on the 20,000 lb. range of a 200,000 lb. Riehle screw-power testing machine in order to determine data beyond the collapse load. The screw-power testing machine was equipped with a load-holder, making it possible to maintain the load on the column as with the constant-load testing machine.

The aluminum alloy columns AT1 and AT2 were tested in the Riehle testing machine, and columns AR1 and AR2 were tested in the constant-load testing machine. The schedule of loading was similar to that for the steel columns.

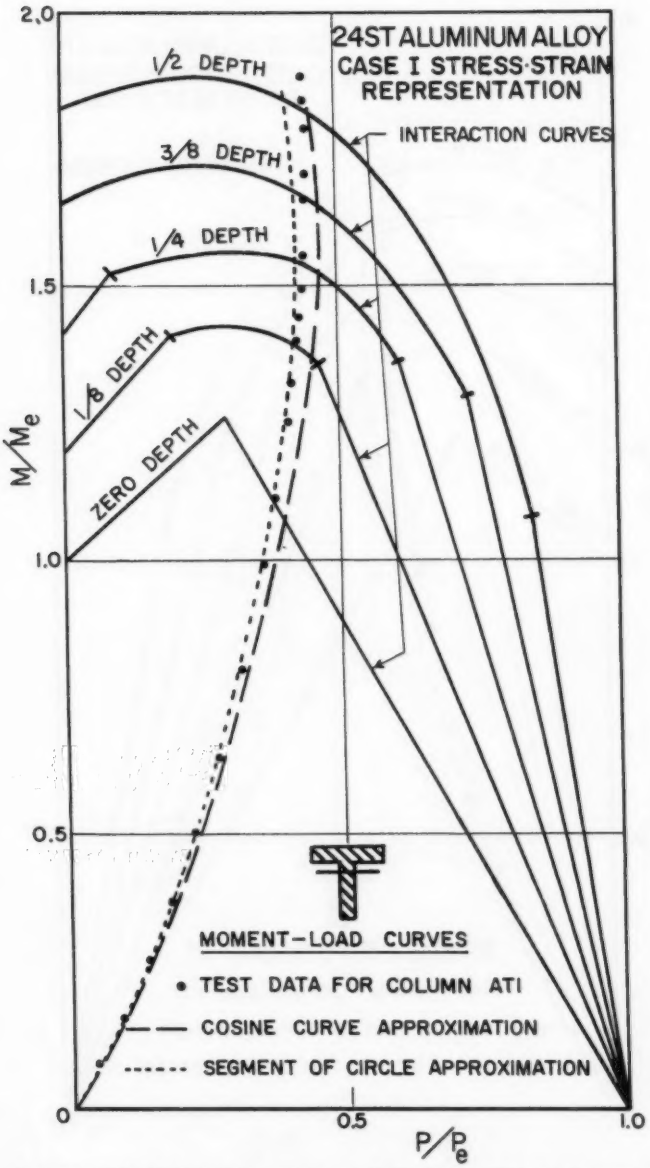

FIG. 10 EXPERIMENTAL AND THEORETICAL MOMENT-LOAD CURVES FOR 24S-T ALUMINUM ALLOY T-SECTION COLUMN ATI. $\sigma_{e1} = 41{,}000$psi, $\sigma_{e2} = 46{,}000$psi, $\alpha_1 = 0.111$, AND $\alpha_2 = 0.237$.

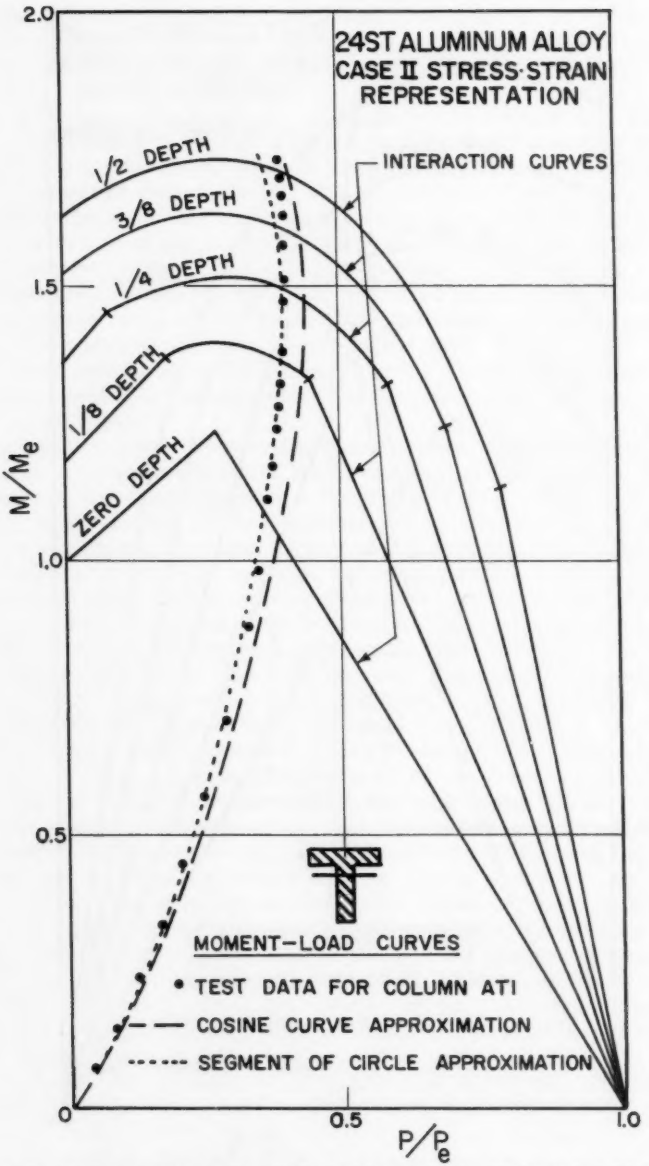

FIG. 11 EXPERIMENTAL AND THEORETICAL MOMENT-LOAD CURVES FOR 24S-T ALUMINUM ALLOY T-SECTION COLUMN ATI. $\sigma_{e1} = 45{,}000$ psi, $\sigma_{e2} = 52{,}400$ psi, $\alpha_1 = 0.061$, AND $\alpha_2 = 0.037$.

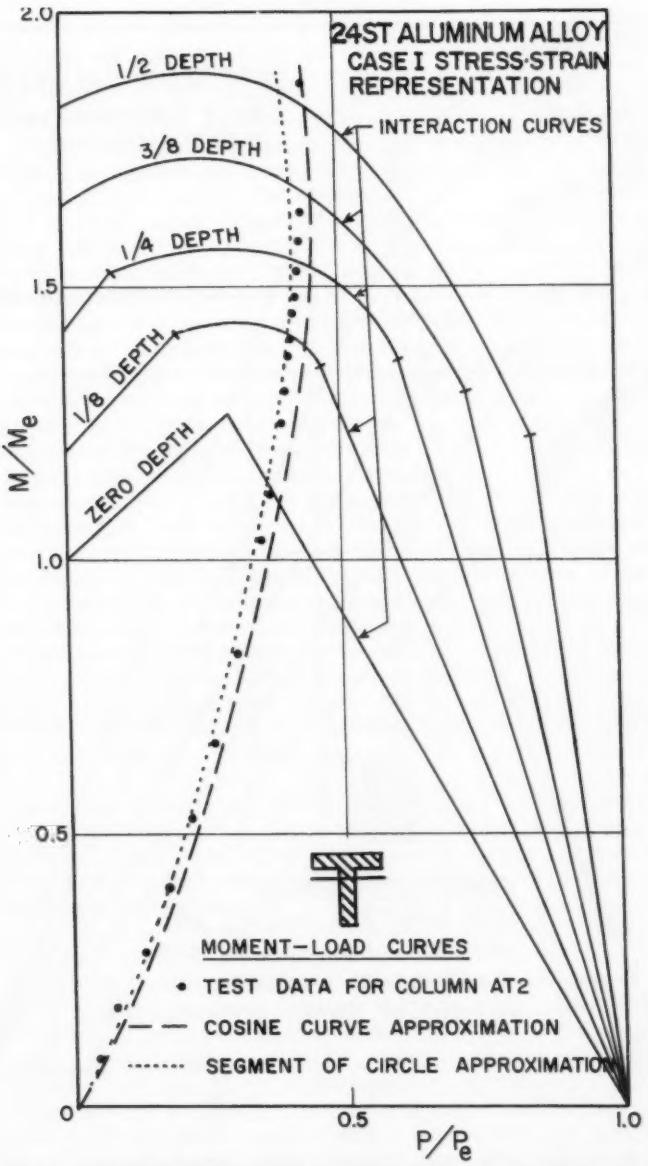

FIG. 12 EXPERIMENTAL AND THEORETICAL MOMENT-LOAD CURVES FOR 24S-T ALUMINUM ALLOY T-SECTION COLUMN AT2. σ_{e1}=41,000 psi, σ_{e2}=46,000 psi, α_1=0.111, AND α_2=0.237.

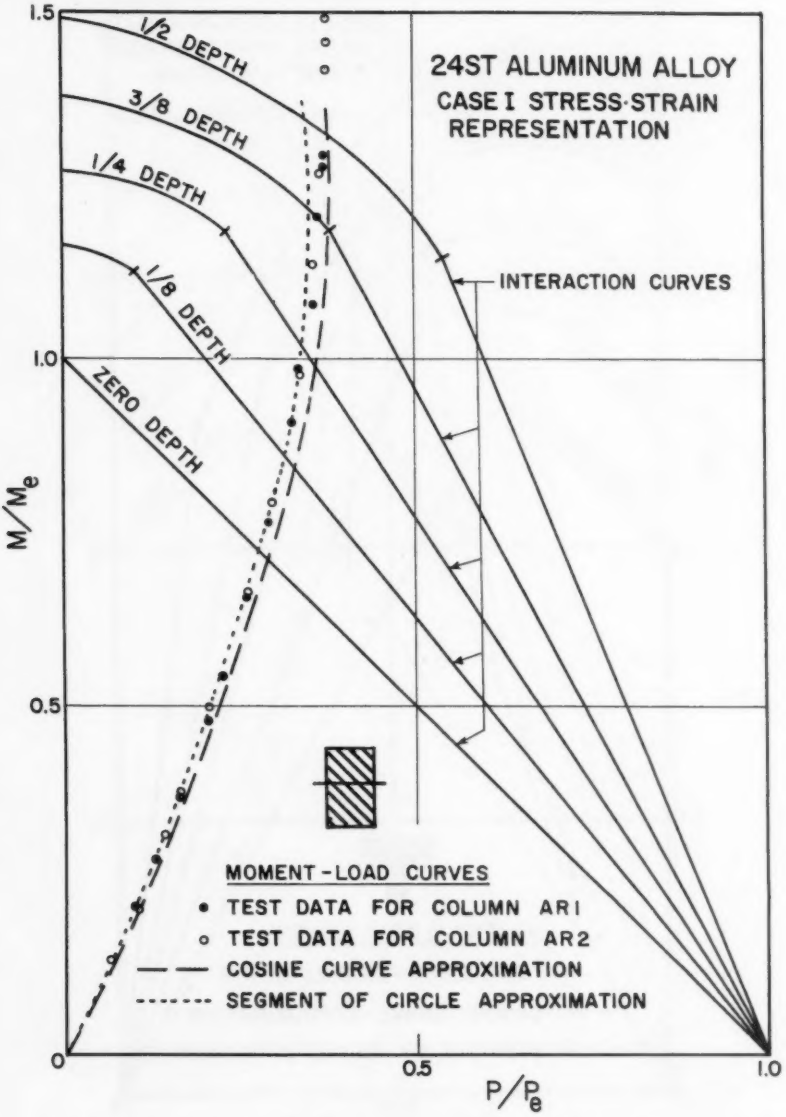

FIG. 13 EXPERIMENTAL AND THEORETICAL MOMENT-LOAD CURVES FOR 24S-T ALUMINUM ALLOY RECTANGULAR-SECTION COLUMNS. σ_{e1} = 41,000psi, σ_{e2} = 43,700psi, α_1 = 0.111, AND α_2 = 0.118.

IV. Analysis of Results

8. 24S-T Aluminum Alloy Columns

The test results for the T-section columns are presented in Fig. 10, 11, and 12, and the curves for the rectangular-section columns are shown in Fig. 13. Pertinent information for all columns is presented in Table 1.

The T-section columns had cross-sectional dimensions approximately equal to those given in Fig. 6. The thickness t in Columns AT1 and AT2 was 0.24 inches and 0.25 inches, respectively, and the eccentricity of load for each column was 0.230 inches and 0.259 inches, respectively. The experimental moment-load curve for Column AT1 is shown in Fig. 10. The applied moment was computed at various stages of loading using the value of the deflection as measured at the center of the column and the pre-set eccentricity. The theoretical circular segment and cosine curve approximations to the moment-load curve were obtained by making use of Eq. 7 and 8 (to determine the interaction curves) and the procedure outlined in Article 5. These curves are shown in Fig. 10 by the dotted and dashed lines, respectively.

In constructing the theoretical curves shown in Fig. 10, it was necessary that each of the tension and compression stress-strain diagrams of the material be represented by two straight lines. Since the stress-strain diagram for 24S-T aluminum alloy is curved at the region of transition from elastic to inelastic behavior, it was impossible to find two straight lines which would represent the stress-strain diagram for all inelastic strains. Therefore, two idealized stress-strain diagrams were considered—one for the case in which small inelastic strains were closely approximated (this hereafter will be referred to as Case I), and the other for the case in which large inelastic strains were closely approximated (hereafter Case II). Actually, Column AT1 collapsed at measured strains of about 0.0065 in both compression and tension; therefore, the best agreement should be seen for Case I (see Fig. 7). In order to gain some idea of how critical the representation of the stress-strain diagram might be, the data for Column AT1 were analyzed using both Case I and II. Accordingly, the interaction and moment-load curves in Fig. 10 have been computed making use of the stress-strain diagram as represented by the dotted lines in Fig. 7, while for Fig. 11, the dashed lines in Fig. 7 were used. It can be seen that the shapes of the curves are greatly altered by the two different representations. Regardless of this great difference, however, the test data for Column AT1 lie between the two approximations of the moment-load curves in both Fig. 10 and 11.

As indicated in Table 1, the test value of the collapse load for Column AT1 was found to be 9,840 lb. The magnitude of the collapse load based on the circular segment approximation is 9,520 lb. and 9,740 lb. for Case I and II, respectively. Corresponding values for the cosine curve approximation are 10,750 lb. and 10,450 lb. The circular segment approximation is based on the assumption that each section of the column is subjected to the same moment as the critical central section; since this is not the case, the theoretical deflection will be larger than the actual deflection and the theoretical collapse load will be smaller than the actual collapse load if the stress-strain diagram has been accurately represented. Fortunately, the representation of the stress-strain diagram is not too critical for determining collapse loads. The theoretical collapse load for Column AT1 (9,740 lb. by the circular segment approximation) is less than the actual value even if use is made of the

stress-strain diagram for Case II (i.e. for strains of about 2 per cent). This is a rather poor representation since the strains at collapse were less than 1 per cent; however, this did cause a shift of the theoretical load toward the actual value. Similar conclusions could be drawn from the results of other trial representations of the data for the aluminum alloy columns although those data are not presented.

The test data for the T-section Column AT2 are presented in Fig. 12. The theoretical curves were obtained using Case I. The results are similar to those found for Column AT1 in Fig. 11. It can be noted that for Columns AT1 and AT2, the experimental moment-load curves show data beyond the collapse load. This was made possible by using the screw-powered testing machine. For all other columns except SR7, the data cease at the collapse load since at this point (under conditions of a constant load) catastrophic deflection took place.

The rectangular-section columns were tested in the special constant-load testing machine. The dimensions of the two columns were identical (see Fig. 6) and the eccentricity for each column was 0.32h (0.259 in.). The data for both columns are plotted in Fig. 13. The theoretical curves were plotted using Case I for the stress-strain representation. The test data indicate that the two columns were almost identical in behavior. Again, the experimental collapse load was found to lie between the two theoretical approximations (see Table 1).

9. Mild Steel Columns

The mild steel columns were tested primarily to study the effect of time on the heterogeneous type of inelastic deformation found in mild steel material. Results of previous investigations[4] indicated that inelastic deformation continued for long periods of time at constant load and that the moment corresponding to a plastic hinge was approximately 10 percent less than the calculated hinge moment (based on conventional stress-strain properties of the material) when the tests were carried out in a dead-load testing machine. In this same investigation, the yield point, as determined from tension members subjected to the same schedule of loading as were the beams, was found to be the same as that computed from the hinge moments in the beams. Thus, in the column investigation, it would be reasonable to assume the best comparison of theory and experiment would be obtained if the stress-strain specimens were subjected to the same schedule of loading as the columns. This would be impractical for design purposes, however, because the stress-strain data as commonly reported are obtained from conventional testing procedures. In view of this, the tension and compression specimens were tested at a rate of loading such that the strain at the end of flat portion of the stress-strain diagram was reached in from three to five minutes.

a) Sustained Loading Tests. All of the mild steel columns, except one, were tested in the specially designed constant-load testing machine. Since time at a given load and rate of loading were both believed to have a considerable influence on the collapse load, six columns were loaded in a stair-step manner with each load being maintained for a period of time. The increase in each increment of load was from two to three percent of the yield point load and the load was maintained for six minutes unless the inelastic deformation continued to increase as it did at the collapse load. In Table 1 are listed the times required for each column to fail at the collapse load. In one case

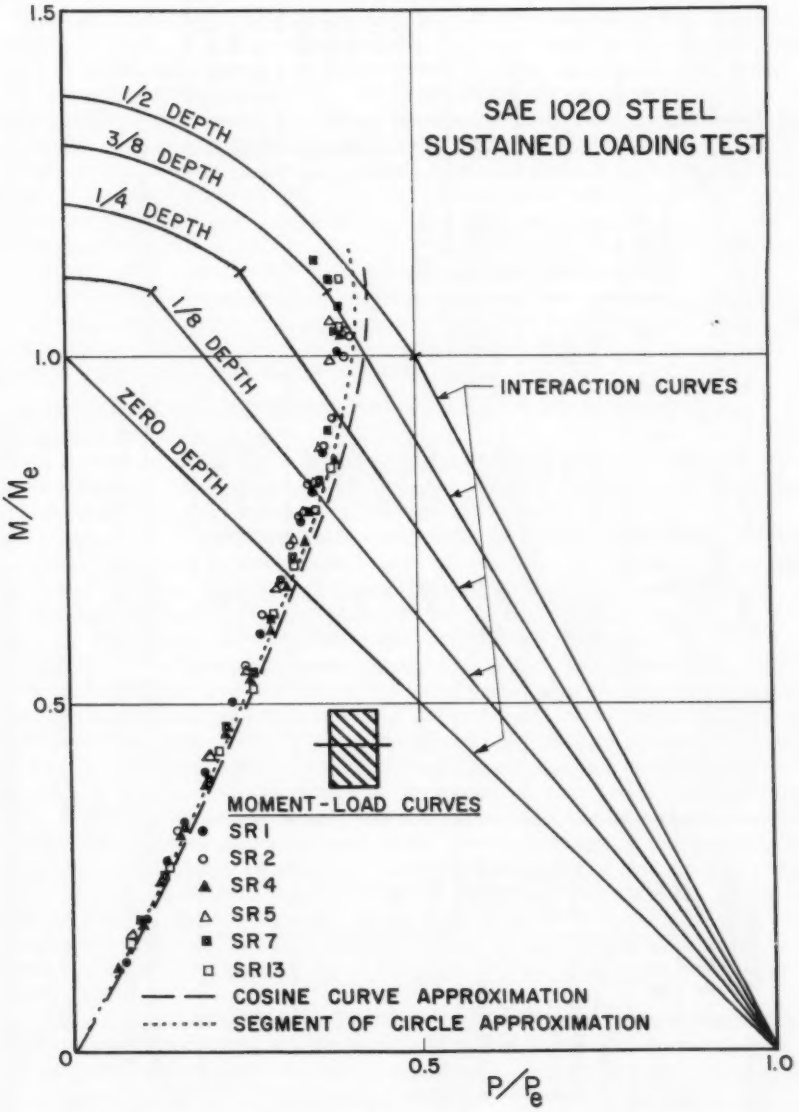

FIG.14 EXPERIMENTAL AND THEORETICAL MOMENT-LOAD CURVES FOR SAE 1020 STEEL RECTANGULAR-SECTION COLUMNS SUBJECTED TO SUSTAINED LOADING.

TABLE 1. Pertinent Information for Columns Used in the Experimental Program

COL. NO.	YIELD STRESS, psi		STRAIN-HARDENING FACTOR		ECCENT., PERCENT OF DEPTH	MAX. ELASTIC LOAD, P_y, lb.	COLLAPSE LOAD, P_c, lb.	THEORETICAL COLLAPSE LOAD, lb.		$\frac{P_c}{P_y}$	TIME AT COLLAPSE LOAD
	Comp.	Ten.	α_1	α_2				Circle	Cosine		
AT1[a]	45,000	52,400	0.061	0.037	0.21	8,860	9,840	9,740	10,750	1.11	
"	41,000	46,000	0.111	0.237	0.21	8,490	9,840	9,520	10,450	1.16	
AT2	41,000	46,000	0.111	0.237	0.23	8,550	10,080	9,580	10,420	1.18	
AR1	41,000	43,700	0.111	0.118	0.32	8,740	11,800	11,100	12,120	1.35	
AR2	41,000	43,700	0.111	0.118	0.32	8,650	12,000	11,160	12,190	1.39	
SR1	30,000	30,000	0	0	0.30	9,640	12,000	12,730	13,450	1.25	[b] 8 min
SR2	"	"	"	"	"	9,470	12,700	"	"	1.34	11 min
SR4	"	"	"	"	"	10,250	12,400	"	"	1.21	6 min
SR5	"	"	"	"	"	9,440	11,800	"	"	1.25	5 min
SR7	"	"	"	"	"	10,060	12,300	"	"	1.22	4 min
SR13	"	"	"	"	"	9,760	12,300	"	"	1.26	53 min
SR9	"	"	"	"	"	9,720	13,200	"	"	1.36	[c] 20 sec
SR11	"	"	"	"	"	9,900	14,300	"	"	1.44	6 sec
SR15	"	"	"	"	"	9,650	13,300	"	"	1.38	82 sec

[a] The first letter designates material (either A for 24S-T aluminum alloy or S for SAE 1020 steel) and the second letter designates cross-section (either T for T-section or R for rectangular-section).

[b] All inelastic loads previous to collapse load were maintained for 6 min.

[c] Number designates time from initiation of inelastic deformation to final collapse.

inelastic deformation continued for almost an hour before final collapse.

The results of the sustained load column tests are shown in Fig. 14 and listed in Table 1. It will be noted that the collapse loads for the columns subjected to sustained load all fall below the theoretical value predicted by the circular segment representation. The theoretical curves were based on a lower yield point stress of 30,000 psi as obtained from tension and compression tests. Theoretically, the circular segment representation should be conservative; however, the average collapse load was about 6 per cent below this value. This would indicate that the actual lower yield point stress for the material was at least 6 percent below the value obtained from the conventional tension and compression test. Thus, the time-dependent heterogeneous type of yielding which is characteristic of mild steel was influential in bringing about the same decrease in load-carrying capacity for columns subjected to sustained loads as for beams subjected to sustained loads. Furthermore, the collapse load data show considerably more variation than those for strain-hardening materials such as the aluminum alloy.

b) Short-Time Loading Tests. Three columns were loaded to failure through the inelastic range in time intervals of 6, 20, and 82 sec. The results shown in Fig. 15 and Table 1 indicate that the collapse load has been appreciably increased. Since the greatest increase resulted for the column with the fastest rate of loading, these tests indicate the dependence of the collapse load on time. It is interesting to note that the variation in the yield point with the rate of strain is in itself sufficient to account for the variation in the magnitudes of collapse load. These three columns collapsed at a strain of approximately 0.40 percent. The strain at the beginning of yielding was 0.10 percent. Therefore, the rates of strain for Columns SR9, SR11, and SR15 through the inelastic region were approximately 15×10^{-5}, 50×15^{-5}, and 3.7×10^{-5} per sec., respectively. The strain rate used in the testing of tension specimens was approximately 5×10^{-5} per sec. Thus, Columns SR9 and SR15 were tested at about the same strain rate as the tension specimens and the experimental collapse loads for these two columns fall between the two theoretical values, i.e., the theory is corroborated by the test data. Column SR11, which was loaded in 6 sec., had a strain rate that was about one order of magnitude greater than that used in the tension testing. It has been found in rate of loading tests on mild steel tension specimens[7] that, in this range of strain rate, an increase of one order of magnitude will cause an increase in yield point of about 7 percent. If the yield point for Column SR11 had been increased 7 percent, the collapse load for this column would have fallen between the theoretical values. More data are needed to strengthen this conclusion, however.

It should be noted in Fig. 15 that there is an increase in the moment at which the column collapses with increased speed of testing. For Columns SR9 and SR15, the collapse loads as well as the depth of yielding at collapse were found to confirm the theoretical analysis. However, the load on the column was found to remain constant for a considerable increase in moment while the theoretical curves show a decrease in moment as soon as the collapse load is reached. This difference can be attributed to the time-sensitive behavior of the mild steel. The heterogeneous yielding in the form of Lueder's bands requires a certain length of time to be initiated and to be completed. Hence, any increase in the rate of straining will cause an increase in the collapse load and will also cause this collapse load to remain constant for greater deflections while the yielding is taking place.

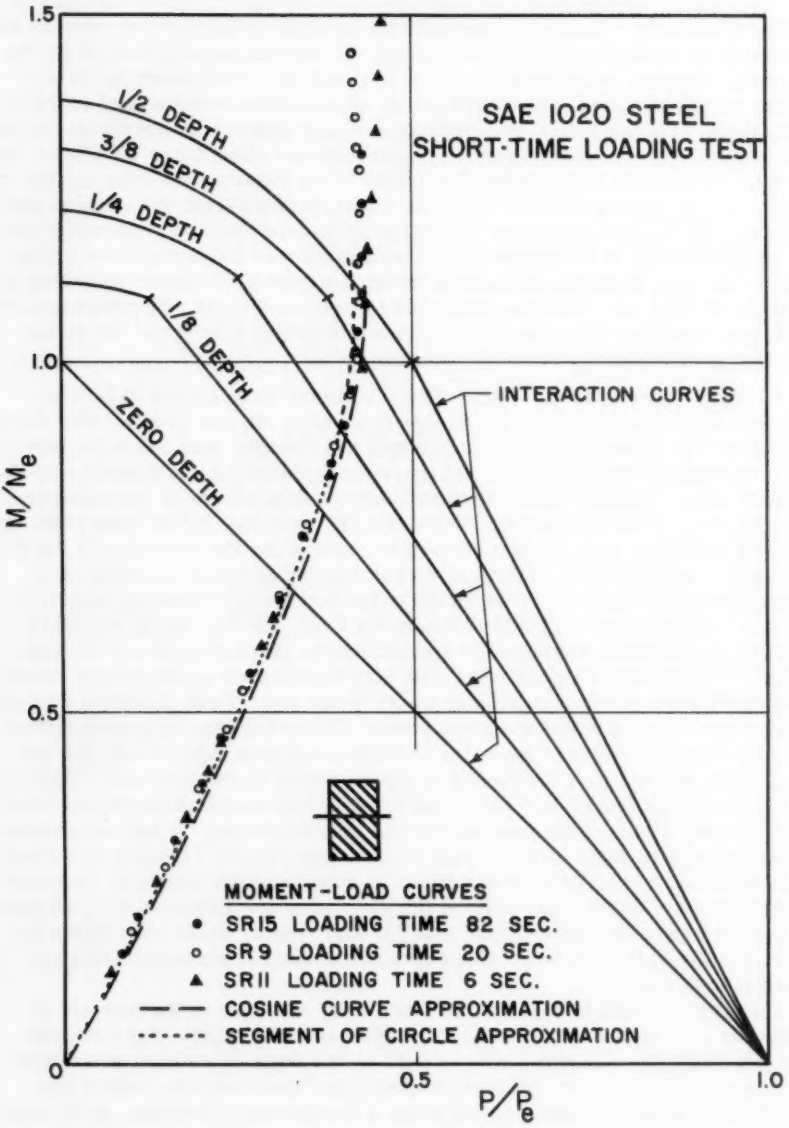

FIG. 15 EXPERIMENTAL AND THEORETICAL MOMENT-LOAD CURVES FOR SAE 1020 STEEL RECTANGULAR-SECTION COLUMNS SUBJECTED TO SHORT TIME LOADING.

V. SUMMARY AND CONCLUSIONS

10. Summary

This investigation was conducted to obtain a more simplified procedure for determining the collapse load of an eccentrically-loaded column. The application of this procedure to columns made from time-sensitive and time-insensitive materials was also studied. The simplified procedure involved the use of constant depth of yielding interaction curves. Also involved was the construction of moment-load and load-deflection curves. These curves necessitate an approximation of the deflected axis of the column. Two approximations were made—(1) the column was assumed to deflect into a segment of a circle, and (2) it was assumed to deflect into the shape of a cosine curve.

Rectangular- and T-section 24S-T aluminum alloy columns were tested to determine the validity of the approximations used in the theory since this material is known to be relatively time-insensitive. Nine rectangular-section SAE 1020 steel columns were used to investigate the effect of the time-sensitive behavior of this material on the collapse load. Six of these columns were tested in a constant-load testing machine where each inelastic load was maintained for six minutes unless inelastic deformation continued to increase as it did at the collapse load. The time required for collapse at these sustained loads was as much as one hour. Three steel columns were also loaded through the inelastic range in time intervals varying from 6 sec. to 82 sec.

11. Conclusions

1. Once the interaction curves for columns of a given material and cross-section are known, the theoretical moment-load and load-deflection curves for the column can be quickly constructed. The collapse load then can be obtained from either curve.

2. The theoretical equations developed require that the stress-strain diagram be represented by two straight lines. For aluminum alloy material, the transition from the elastic to the inelastic region of the stress-strain diagram is somewhat uncertain. Therefore, the experimental collapse load data were analyzed using two different representations of the stress-strain diagram (see Fig. 7). Both of these representations were considered in the construction of the interaction curves and the theoretical moment-load curves. It was found that the representation of the stress-strain diagram greatly influenced the shapes of the theoretical curves but that the effect on the collapse load of the column was relatively small.

3. For all aluminum alloy columns, the actual collapse load was found to be greater than the collapse load as predicted by the theory using the segment of a circle approximation but less than that using the cosine curve approximation. Therefore, the circular segment is recommended for use in the design of columns made from this and similar materials.

4. For the six rectangular SAE 1020 steel columns subjected to sustained loads, the theoretical collapse loads were computed using the yield point stress as obtained from conventional compression and tension tests. In all cases the experimental collapse loads fell below the theoretical collapse load based on the segment of a circle approximation. Since this approximation gives a conservative estimate of the collapse load, it can be concluded

that the yield point stress in members subjected to sustained loads is reduced from 5 to 10 percent below the value obtained by standard testing procedures.

5. Three rectangular steel columns were loaded through the inelastic range in time intervals totaling 6, 20, and 82 sec. For the latter two times, the rate of straining was comparable to that used in conventional tension and compression tests and the collapse loads were found to lie between the values computed using the two theoretical approximations. For the test completed in 6 sec., a higher collapse load was obtained and it can be concluded that the yield point stress was raised from 5 to 10 percent above the value obtained from standard testing procedures.

VI. ACKNOWLEDGMENTS

This investigation was conducted as a part of the work of the Engineering Experiment Station of the University of Illinois, of which Dean W. L. Everitt is the director, in the Department of Theoretical and Applied Mechanics of which Professor T. J. Dolan is the head.

The project was sponsored by the National Science Foundation (G. H. Hickox, Program Director for Engineering Sciences) through Research Grant NSF G1200. Part of the work described herein was performed by Mr. Shreeves while satisfying the thesis requirements for the degree of Master of Science in Theoretical and Applied Mechanics at the University of Illinois. Acknowledgment is made to Mr. P. Van Lierde for the valuable suggestions he gave in the development of the theoretical analysis.

VII. BIBLIOGRAPHY

1. R. L. Ketter, "Stability of Beam Columns Above the Elastic Limit," Proceedings A.S.C.E., Vol. 81, No. 692, Oct. 1955.

2. W. D. Jordan, "The Inelastic Behavior of Eccentrically-Loaded Columns," unpublished Ph.D. Thesis, University of Illinois, 1952.

3. F. R. Shanley, "Strength Analysis of Eccentrically-Loaded Columns," Department of Engineering, University of California, Report 54-57, May 1954.

4. M. E. Clark, H. T. Corten, and O. M. Sidebottom, "Inelastic Behavior of Ductile Members Under Dead Loading," University of Illinois Engineering Experiment Station, Bulletin Series No. 426, Oct. 1954.

5. M. E. Clark and O. M. Sidebottom, "An Inexpensive Constant-Load Testing Machine," A.S.T.M. Bulletin No. 203, Jan. 1955.

6. D. O. Brush and O. M. Sidebottom, "Axial Tension and Bending Interaction Curves for Members Loaded Inelastically," Transactions A.S.M.E., Vol. 75, No. 1, Jan. 1953.

7. M. J. Manjoine, "Influence of Rate of Strain and Temperature on Yield Stresses of Mild Steel," Journal of Applied Mechanics, Vol. 11, No. 4, Dec. 1944.

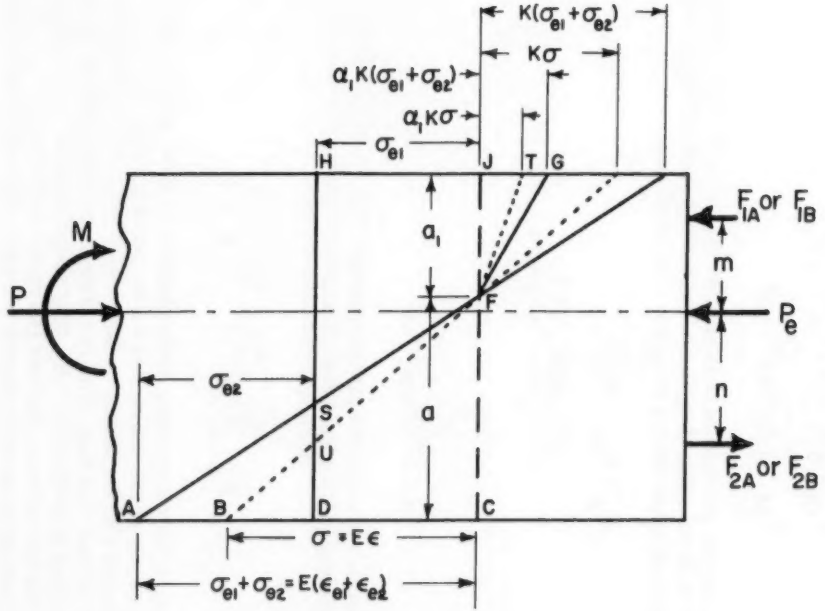

(a) FREE BODY DIAGRAM

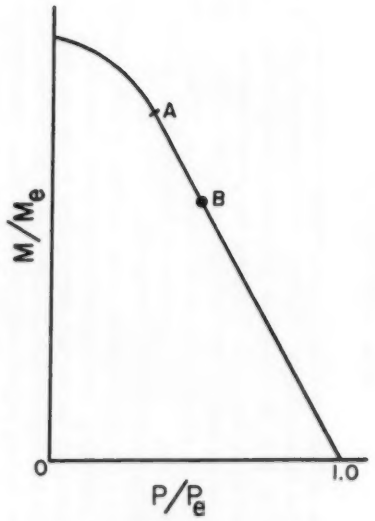

(b) INTERACTION CURVE

FIG. 16 FREE BODY DIAGRAM SHOWING STRESS-DISTRIBUTIONS AT VARIOUS POSITIONS ON THE STRAIGHT LINE PORTION OF THE INTERACTION CURVE.

VIII. APPENDIX A

Proof that the Deflection of an Eccentrically-Loaded Column Varies Linearly Along the Straight-Line Portion of a Constant Depth of Yielding Interaction Curve—In Fig. 16a is shown a member subjected to a compression load P and a bending moment M. Yielding has penetrated to a depth equal to a_1 on the compression side of the member while the strain on the tension side of the member is equal to the yield strain ϵ_{e2}. Thus the depth a of the cross-section is elastic. This condition of deformation corresponds to point A on the interaction curve shown in Fig. 16b.

The stress distribution resulting from the load P and moment M is S-D-A-F-G-H. Instead of working with this stress distribution it is more convenient to represent the stress distribution by the rectangular distribution D-C-J-H plus the triangular distribution F-G-J minus the triangular distribution F-C-A. The forces represented by these three distributions are

$$P_e = \sigma_{e1} A$$

$$F_{1A} = \frac{1}{2} A_i \alpha_1 K (\sigma_{e1} + \sigma_{e2})$$

$$F_{2A} = \frac{1}{2} A_e (\sigma_{e1} + \sigma_{e2})$$

where A_i and A_e are the portions of the area that are inelastic and elastic, respectively, and K is the ratio of a_1 to a. The bending moment M_A is equal to the moment of these three forces about the centroidal axis.

$$M_A = F_{1A} + F_{2A}$$

$$= \left(\frac{m A_i \alpha_1 K}{2} + \frac{n A_e}{2}\right)(\sigma_{e1} + \sigma_{e2})$$

or

$$M_A = CE (\epsilon_{e1} + \epsilon_{e2})$$

where C is a constant for a given depth of yielding. The curvature of the member corresponding to the stress distributions S-D-A-F-G-H is given by Eq. 10 as

$$\frac{1}{R_A} = \frac{\epsilon_{e1} + \epsilon_{e2}}{kh} = \frac{\epsilon_{e1} + \epsilon_{e2}}{a}$$

This is the curvature for the member corresponding to point A at the end of the straight line portion of the interaction curve (see Fig. 16b). For any point B on the straight line the stress on the tension side of the member is given by D-B and is less than σ_{e2}. The resulting stress distribution for the same depth of yielding is U-D-B-F-T-H. This distribution is represented by the same rectangular distribution and two triangular distributions F-T-J and F-B-C. The moment arms m and n remain constant and, hence, the following expressions can be written:

$$F_{1B} = \frac{1}{2} A_i \alpha_1 K \sigma$$

$$F_{2B} = \frac{1}{2} A_e \sigma$$

$$M_B = F_{1B} m + F_{2B} n = \left(\frac{m A_i \alpha_1 K}{2} + \frac{n A_e}{2}\right) \sigma = CE\epsilon$$

The curvature corresponding to point B is given by the geometry of deformation as (see Eq. 10)

$$\frac{1}{R_B} = \frac{\epsilon}{kh} = \bar{a}$$

Comparison of the radii of curvature corresponding to points A and B shows that

$$\frac{\frac{1}{R_B}}{\frac{1}{R_A}} = \frac{\epsilon}{\epsilon_{e1} + \epsilon_{e2}}$$

But it has been shown that

$$\epsilon = \frac{M_B}{C}$$

and

$$\epsilon_{e1} + \epsilon_{e2} = M_A/C$$

Therefore,

$$\frac{1}{R_B} = \frac{1}{R_A}\left(\frac{M_B}{M_A}\right)$$

Since the radius of curvature and the deflection are proportional, the deflection corresponding to any point B on the straight line portion of the interaction curve is given by the following relation:

$$\delta_B = \delta_A \frac{M_B}{M_A}$$

Paper 1424 October, 1957 EM 4

Journal of the
ENGINEERING MECHANICS DIVISION
Proceedings of the American Society of Civil Engineers

THE PRESSURE LINE AND THE INELASTIC BUCKLING OF COLUMNS[a]

Frank Baron* M. ASCE and Harold S. Davis** A.M. ASCE
(Proc. Paper 1424)

SYNOPSIS

The pressure line concept developed for elastic arches and rigid frames,(1,2) and for the inelastic deformations of structural elements ds in length,(3) is applicable to studies of the inelastic behavior of columns and of rigid frames. The concept is extended herein for the inelastic behavior of such structures and for eccentrically and laterally loaded columns. In the same way as for structural elements, ds in length, the inelastic behavior of such columns can be stated in terms of the elastic behavior modified to take into account the effects of plasticity.

INTRODUCTION

The concept of a pressure line for a group of loads on an elastic structure is not new. For readers not familiar with the concept, a pressure line is for the present defined to be a string polygon that shows the successive resultants of the reactions and loads acting on a structure. The concept apparently has its origin in studies of masonry construction(4) and in the development of graphical methods of analysis. It has been used in studies of walls, buttresses, and chimneys. It has also been used in studies of structures that lie in a plane and consist of single closed circuits. Examples of such structures are arches and rigid frames. For these structures, the concept has ordinarily been used for elastic behavior and for loads that lie in the planes of the structures.

The concept was recently extended(5) to structures that lie in a plane, are loaded normal to their plane, and are continuous between two supports. It was also extended(6) to structures that are curved in space, are loaded in any

Note: Discussion open until March 1, 1958. Paper 1424 is part of the copyrighted Journal of the Engineering Mechanics Division of the American Society of Civil Engineers, Vol. 83, No. EM 4, October, 1957.

a. Presented at a meeting of the American Society of Civil Engineers in Pittsburgh, Pa., October, 1956.

* Prof. of Civ. Eng., Univ. of Calif., Berkeley, Calif.
** Senior Structural Engr., Hanford Atomic Products Operation, General Electric Co., Richland, Wash.

direction, and are continuous between two supports. In each case, however, elastic behavior only was considered.

More recently, a procedure based on the pressure line concept was developed(7) for quickly estimating the effects of inelasticity on the behavior of structural elements, ds in length, subjected to axial and flexural loads. The procedure consists of obtaining an initial estimate by means of an elementary theory of mechanics and adjusting the estimate to fit the conditions of a theory of plasticity. In this way, the moment-angle change relationship can readily be obtained for any value of axial thrust and moment. The procedure was demonstrated pictorially. It can also be used in conducting algebraic studies. The latter is demonstrated herein for several kinds of stress-strain curves.

The concept of the pressure line can also be used in studies of the inelastic behavior of arches and rigid frames and the inelastic buckling of eccentrically and laterally loaded columns. This is demonstrated herein in two ways; namely, pictorially for arches and frames and algebraically for columns.

The Pressure Line for Arches and Frames

This discussion is restricted to arches and frames that lie in a plane and are loaded in their plane. It is assumed that the loads are increased from zero to their final values. In addition, it is assumed that the effects of shear and residual strains can be neglected and that the dimensions of the undeflected structure can be considered in determining the pressure line. It is further assumed that localized buckling, lateral-torsional buckling, or any other kind of buckling does not occur. Failure, if developed, is assumed to be caused by a sufficient number of hinges being formed to produce a mechanism in the plane of the arch.

In 1879, Winkler of Berlin stated(8) in the "Zeitschrift des Architekten und Ingerieur Vereins zu Hannover," page 199, a theorem concerning the position of the pressure line, or line of resistance, for single-span elastic arches. He stated, "For an arch ring of constant cross section that line of resistance is approximately the true one which lies nearest to the axis of the arch ring, as determined by the method of least squares." This theorem was drawn from conclusions based on studies of the voussoir masonry arch and is only approximately correct for the elastic theory of solid arches.

The above theorem was extended by Hardy Cross, Hon. Mem. ASCE, in lectures at the University of Illinois and at Yale University for loads lying in the plane of single-span elastic arches and closed rings.(9) He restated the theorem in three forms as follows:

1. "The pressure line for a group of loads lying in the plane of an arch is that string polygon for the loads which most nearly fits or hugs the axis of the arch." ("Fit" in this statement is to be judged by eye.)

2. "The pressure line for a group of loads is that string polygon which makes the moment areas balance or vanish." (For vertical loads, the moments in the arch are proportional to the vertical intercepts between the string polygon and the axis of the arch. For horizontal loads, the moments are proportional to horizontal intercepts. In general the moment at any point in a loaded arch is equal to the force represented by the corresponding string of the pressure line times the perpendicular distance from the point to the

string. "Balance" in this statement means that the total positive area of the moment diagram equals the total negative area and that the centroid of the total positive area coincides with the centroid of the total negative area. This statement is for fixed-end arches of constant cross-section and can easily be modified for arches with hinges.)

3. "The pressure line for a group of loads is that string polygon which makes the M/EI diagram balance or vanish." (This statement is the same as the preceding statement except that provisions now are made for variations in I along the axis of the arch.)

For obtaining quick estimates of the effects of loads on an arch, Statement 1 is the most useful of the above statements. Statements 2 and 3 successively modify the definition of "fit" and lead to a greater precision in computed effects. Statement 3 fulfills the same requirements of statics and of geometry as are observed in the column analogy, the hydrostatic analogy, the neutral point method, and other formalized statements of the theory of the elastic arch. Statics is satisfied by specifying that the pressure line for a group of loads is a string polygon for the loads. All statical relationships in the arch - such as shears, thrusts, and moments - can be read directly from the string polygon. A force polygon for the loads is not needed in constructing the string polygon nor in obtaining the scale of moments in the arch. For example, the diagram of moments in an arch for a group of vertical loads on the arch is drawn to the same scale as that of the moments in a cantilevered beam or of the moments in a simple beam supporting the same loads and having the same span length as the arch. Also the intercept (parallel to a load and at a unit perpendicular distance away from the load) measured between the two rays of a string polygon intersecting at the load is proportional to the load and to the moment of the load about an axis at the intercept. The latter statement is particularly useful in obtaining all shears and thrusts in a loaded arch.

The requirements of geometry for fixed-end arches loaded in the elastic range are fulfilled in Statement 3 by specifying that the M/EI diagram must balance. The requirements, stated in a more formal way, are as follows:

$$\int_0^L \frac{M}{EI}\, ds = 0 \qquad (1a)$$

$$\int_0^L x \frac{M}{EI}\, ds = 0 \qquad (1b)$$

$$\int_0^L y \frac{M}{EI}\, ds = 0 \qquad (1c)$$

For the inelastic behavior of arches and rigid frames, Statement 3 needs to be slightly modified to take into account the effects of non-linear stress-strain characteristics of materials. The modification is as follows:

4. The pressure line for a group of loads on an arch is that string polygon for the loads which makes the $M/E_b I$ diagram balance or vanish. In this statement, E_b is a modified modulus of elasticity and for an element one unit

in length is a measure of stiffness to relative rotation of the adjacent cross-sections. The value of E_b at a section depends on the shape of the cross-section, the stress-strain relationship, the history of loading, and on the magnitudes of the thrust and moment. For ultimate loads provisions can be made for the development of "plastic hinges."

For a specific case, the values or E_b can be obtained by means of the pressure line concept developed for the inelastic bending of structural elements.(10) This is illustrated in Fig. 1 for a rectangular cross-section subjected to given values of P and M. As in the usual theory of plasticity,(11) the distribution of strains across the section is assumed to be planar. In this paper, a history of loading is assumed that is statical. The strain in each fiber is assumed to be increased from zero to its final tensile or compressive value. Other histories of deformations are possible and are discussed elsewhere.(12) The pressure line concept for other histories of deformations is illustrated in Ref. 3. In this paper, the stress-strain relationships for the fibers of a member subjected to a simultaneous axial and flexural load are assumed to be the same as those obtained from simple tension and compression tests. In Fig. 1, the stress-strain relationship of the material is represented by curve AOB and is assumed to be the same for each longitudinal fiber. As previously stated, the effects of a shear, Poisson's ratio, residual strains, and local instability of projecting elements of the cross-section are herein neglected. In addition, the effects of lateral-torsional instability are not considered.

In Fig. 1 the stress as given by the usual theory of plasticity is interpreted to be equal to the stress computed by the elementary theory of mechanics ($s_o = s_a + s_b$; where $s_a = P/A$ and $s_b = My_c/I$) plus a correction stress to account for the non-linear stress-strain characteristics of the material. That is,

$$s = s_o + s_c \tag{2}$$

The ordinates bounded by the stress-strain curve AOB are in accordance with the theory of plasticity whereas those bounded by the straight line CD are in accordance with the elementary theory. The shaded diagram of Fig. 1 represents the correction stresses as defined in Eq. 2. The correction stresses indicated in the figure must balance or vanish. "Balance" in this case means (1) the sum of the positive correction forces must equal the sum of the negative correction forces, and (2) the centroid of the positive correction forces must coincide with the centroid of the negative correction forces. A correction force is equal to a correction stress times its corresponding differential area. A pictorial procedure for effecting such balance has been presented elsewhere(13) and will not be described herein. The procedure is similar to that used in sketching the pressure line for fixed-end beams.

Two modified moduli of elasticity are represented in Fig. 1. These are as follows:

$$E_a = s_a/\epsilon_a \tag{3a}$$

$$E_b = \Delta s_b/\Delta\epsilon \tag{3b}$$

where $s_a = P/A$, $\Delta s_b = Mh/I$, ϵ_a is the strain of the fibers along the centroidal axis, and $\Delta\epsilon$ is the difference in the strains of the extreme fibers.

The value of E_b in this case is the slope of the line CD shown in the figure.

The revised statement of the pressure line (Statement 4) used jointly with the above procedure for obtaining values of E_b is useful for quickly estimating the inelastic behavior of structures such as arches and rigid frames. The suggested procedure for making these estimates consists of the following steps:

1) Draw a string polygon for a given set of loads which you think is the best "fit" to the axis of the given arch. Obtain scale on the magnitudes of the moments as interpreted through the string polygon.

2) Check "fit" by inspecting whether the moment diagram balances. Revise, if necessary, the string polygon to obtain a more satisfactory balance.

3) Draw the M/EI diagram and check the balance of this diagram. Revise the string polygon until a satisfactory balance of the M/EI diagram is obtained. (The revision is aided by noting that a section with a small value of I tends to draw the pressure line toward itself whereas a section with a large value of I tends to push the pressure line away. In other words, a section with a small value of I tends to attract less moment whereas a section with a large value of I tends to attract more moment). Now by means of the string polygon, obtain all shears, thrusts, and moments in the arch. (Note that the results at this stage are in accordance with the elastic theory based on the original dimensions of the structure.)

4) For the distribution of moments and corresponding thrusts obtained above, estimate the values of E_b. (If convenient, draw diagrams relating moments with angle-changes for different values of thrust. See Fig. 5a)

5) Draw the M/E_bI diagram and check the possible unbalance. If necessary, revise the string polygon and the values of E_b until the M/E_bI diagram is considered sufficiently balanced. (The revision here is aided by noting that a section with a reduced modulus of elasticity tends to draw the pressure line toward itself.) Now interpret all shears, thrusts, and moments by means of the string polygon.

Step 3 is not necessary in studies restricted to inelastic behavior. However, it is useful in developing judgment as to the final position of the pressure line. It also is useful in comparing the results of the elastic theory with those of the inelastic theory. This in itself suggests that interaction diagrams, as for columns with axial and flexural loads, can be developed for the elastic and inelastic behavior of arches and rigid frames.

In the above procedure, the distributions of angle-changes per unit of length are assumed to be known for both theories. Consequently, estimates can be made of the corresponding deflections. If desired, the above procedure can be extended to the theory of the flexible arch. The pressure line in that case must fit the axis of the deflected arch. For these studies, larger scales usually are required for the sketches of the arch and more accuracy in the computations of fit. The latter computations however become sensitive to changes in the modified moduli of elasticity resulting from changes in moments and deflections of the arch. This is particularly true when total yielding is approached. For these cases, the sketching procedure becomes inadequate and a numerical procedure of successive approximations, similar to that of Vianello,[14,15] is usually required.

Numerical Example

A numerical example of a rigid frame with fixed ends and a concentrated load, W, at mid-span is shown in Fig. 2. The dimensions and properties of the frame are given in the Fig. A pressure line also is drawn in the Fig. for each of three ranges of loading. In Range 1, the load is 105 kips and produces a maximum stress of 33 ksi in an extreme fiber of the section at mid-span. The distributions of moments and angle-changes are shown and the requirements of geometry are checked. In Range 2, the load is 171 kips and produces a plastic "hinge" at the mid-span of the frame. The maximum moment, M_u, that the given cross section can resist is 594 K ft. A plastic zone extends over a portion of the horizontal member as shown in the Fig. The distribution of angle-changes along this portion was obtained from a diagram relating moments and angle-changes as shown in Fig. 5a. For the rise to span ratio considered, the influence of the thrust on the moment-angle change relationship is negligible and consequently is neglected. The requirements of geometry for Range 2 are checked as for Range 1 except that provisions now are made for the effects of plasticity. Compare the pressure line for Range 2 with that for Range 1 and observe that the plastic zone attracts the pressure line toward itself whereas the sections at the abutments and the knees push the pressure line away.

In Range 3, the load is 216 kips and produces yielding at a sufficient number of sections to cause collapse. This load was obtained by means of the pressure line as well as by means of the "mechanism" criterion discussed elsewhere.(16) For the pressure line drawn in the Fig., observe the extent to which it hugs the axis of the frame. As for Range 2, the influence of the thrust on the maximum moment that a section can take is negligible and consequently was discounted.

For small rise to span ratios, the influence of the thrust on the moment-angle change relationship can be appreciable and merits consideration. In addition, the influence of deflections on moments is usually important for such ratios and needs to be taken into account.

In the above example, no consideration was given to lateral-torsional instability. It is assumed that the frame is sufficiently braced for such instability not to occur. Obviously, if such instability can occur, the limiting load should be less than that obtained as the moment capacities of the "plastic hinges" could not be developed.

Inelastic Buckling of Columns

The inelastic behavior of a column can be studied in the same way as above except that the pressure line for a group of loads must now be in agreement with the final deflections of the column. In addition, the curvatures of the column, proportional to $\Delta\phi = M/E_bI$, must be in agreement with the values of E_b and with the deflections of the column. As indicated in Fig. 1, the value of E_b at a section depends on the shape of the cross-section, the stress-strain relationship, and on the magnitudes of the thrust and moment. The value of E_b also depends on the history of loading. The history of loading and the mode of failure are of such importance in column theory that certain assumptions made in the preceding discussion are herein repeated. The strain in each fiber is assumed to gradually increase from zero to its final tensile or compressive value. Other histories of deformations are possible,

including residual strains, and are discussed elsewhere.(17) Local instability and lateral-torsional instability are not considered. The latter type of instability can be important and is frequently obtained in laboratory tests.(18) In such tests, no resistance is frequently offered to a twist at the ends or to a yaw and a twist at the mid-portion of a column. In actual practice, such resistance is frequently offered by end connections and by walls or bracing along the length of the column. The succeeding discussion is based on the assumption that the failure of a column is due to excessive bending about the axes of moments. The discussion illustrates the use of the pressure line concept for such columns. The development is analytical rather than pictorial or numerical.

Fig. 3 shows some typical pressure lines (curves of moments) for various conditions of loading on columns. It is assumed for the present that the loads are less than the critical loads at which instability occurs. In each diagram, curve e represents the deflected position of the column as if the behavior of the column was completely elastic. A generalized statement concerning the behavior of such columns was given by the late H. M. Westergaard.(19) The statement was given in the form of a Fourier series and considerable liberty is taken by the writers in restating it as follows: The elastic behavior (lateral deflections and moments) of a structural member subjected to axial and lateral loads is equal to its behavior as a laterally loaded member multiplied by a magnification factor. The magnification factor depends on the ratio of the axial load to the Euler load for an idealized straight column.

In Fig. 3, a comparison also is shown between the elastic and the inelastic behavior of each column. Curve i in each diagram represents the deflections of the column in accordance with a theory of inelasticity. The inelastic behavior of the column can be stated in the same way as the elastic behavior modified to take into account the effects of plasticity.(20) This is illustrated for the case of a column as shown in Fig. 3c. The column is assumed to have a symmetrical distribution of lateral loads along its length and to have a load P of equal eccentricity at each end. The initial eccentricity is designated by y_o. It is assumed that the column has a symmetrical curve of deflections, that bending occurs about axes normal to the plane of the bent column, and that the cross-section of the column has an axis of symmetry lying in this plane. The final deflections at the center of the column for conditions of elastic and inelastic behavior respectively are designated y_e and y_i. The effects of residual strains, lateral and torsional instability, and local buckling are not considered. In addition, uncertainties in the properties of materials are not a part of this discussion.

In the succeeding discussion, the elastic and inelastic behavior of the column will be paralleled and will respectively be associated with the subscripts e and i. The final deflections at the center of the column are defined by

A. Elastic	B. Inelastic	
$y_e = y_o + y_{ae}$	$y_i = y_o + y_{ai}$	(4)

where y_{ae} and y_{ai} are the additional deflections caused by the loads. The pressure line for the group of loads must coincide with the resultant of the stress distribution across the section. By definition, the moments at the center of the column are given by

A. Elastic B. Inelastic

$$M_e = M_L + P(y_o + y_{ae}) \qquad M_i = M_L + P(y_o + y_{ai}) \tag{5}$$

where M_L is the moment due to the lateral loads. Eqs. 5 can be rewritten as

A. Elastic B. Inelastic

$$M_e = M_{om} + M_{ae} \qquad M_i = M_{om} + M_{ai} \tag{6a}$$

where

$$M_{ae} = P y_{ae} \qquad M_{ai} = P y_{ai} \tag{6b}$$

$$M_{om} = \left[1 + M_L/M_o\right] M_o \qquad M_{om} = \left[1 + M_L/M_o\right] M_o \tag{6c}$$

and where $M_o = Py_o$ for elastic and inelastic behavior. It is observed that M_{om} is the moment at the center of the column with respect to the original dimensions of the column and is a constant for a given case of loading.

The additional deflections caused by the loads can be written as follows:

A. Elastic B. Inelastic

$$y_{ae} = \frac{1}{k_e} \Delta\phi_e L^2 \qquad y_{ai} = \frac{1}{k_i} \Delta\phi_i L^2 \tag{7}$$

where k_e and k_i are coefficients depending on the distributions of the angle-changes (or curvatures) along the length of the column and $\Delta\phi_e$ and $\Delta\phi_i$ are the angle changes per unit of length at the center of the column. The angle-changes per unit of length are related to the moments as defined by

A. Elastic B. Inelastic

$$\Delta\phi_e = \frac{M_e}{EI} \qquad \Delta\phi_i = \frac{M_i}{E_b I} \tag{8}$$

where E is the tangent modulus at the origin of the stress-strain curve and E_b is a reduced modulus of elasticity.

By means of the above relationships and definition of the Euler load, $P_E = \pi^2 EI/L^2$, the deflections at the center of the column are as follows:

A. Elastic B. Inelastic

$$y_{ae} = \left[\frac{1}{C_e \frac{P_E}{P} - 1}\right] y_{om} \qquad y_{ai} = \left[\frac{1}{C_i \frac{P_E}{P} - 1}\right] y_{om} \tag{9a}$$

$$y_e = y_o + \left[\frac{1}{c_e \frac{P_E}{P} - 1}\right] y_{om} \qquad y_i = y_o + \left[\frac{1}{c_i \frac{P_E}{P} - 1}\right] y_{om} \tag{9b}$$

where

$$c_e = \frac{k_e}{\pi^2}\frac{E}{E} \qquad c_i = \frac{k_i}{\pi^2}\frac{E_b}{E} \tag{9c}$$

and where $y_{om} = (1 + M_L/M_o)\, y_o$ for each behavior. Consequently, $M_{om} = Py_{om}$. In the same way as for deflections, the moments at the center of the column are given by

A. Elastic B. Inelastic

$$M_{ae} = \left[\frac{1}{c_e \frac{P_E}{P} - 1}\right] M_{om} \qquad M_{ai} = \left[\frac{1}{c_i \frac{P_E}{P} - 1}\right] M_{om} \tag{10a}$$

$$M_e = \left[\frac{c_e \frac{P_E}{P}}{c_e \frac{P_E}{P} - 1}\right] M_{om} \qquad M_i = \left[\frac{c_i \frac{P_E}{P}}{c_i \frac{P_E}{P} - 1}\right] M_{om} \tag{10b}$$

In Eqs. 9a to 10b, the terms in the brackets can respectively be interpreted as modification factors of y_{om} & M_{om}. A comparison of the moments defined by Eqs. 10a and 10b yields

A. Elastic B. Inelastic

$$\frac{M_e}{M_{ae}} = c_e \frac{P_E}{P} \qquad \frac{M_i}{M_{ai}} = c_i \frac{P_E}{P} \tag{11}$$

It is of interest to note that the form of Eqs. 4 to 11 are the same for elastic and inelastic behavior except for the values of c_e and c_i. A further comparison of the moments defined by Eqs. 10a and 10b yields the following relationship:

$$\frac{M_i}{M_{ai}} \Big/ \frac{M_e}{M_{ae}} = \left[\frac{c_i}{c_e}\right] = \left[\frac{k_i}{k_e}\frac{E_b}{E}\right] \tag{12}$$

Thus, in a general way the inelastic behavior is the elastic behavior modified by the terms in the brackets of Eq. 12.

Values of c_e for elastic columns have been reported by H. M. Westegaard(21) for various conditions of axial and lateral loads. For a

symmetrical condition of load, the value of c_e is not sensitive to the type of loading and is approximately equal to 1.0; that is, $k_e \cong \pi^2$. The values of c_i in the above Eqs. depend on the deflected shape of the column and on the P-M- $\Delta\phi$ relationships for a given cross-section and stress-strain characteristics of the column.

The values of E_b/E in the expression for c_i can be obtained by means of the pressure line concept developed for the inelastic deformations of structural elements. For example, consider an element with a rectangular cross-section and an idealized stress-strain curve as shown in Fig. 4. The stress-strain curve consists of three straight lines defining material properties which are the same for tension as for compression. The slope of the line through the origin is designated by E and that of the other lines by E_t, (where $n = 1 - E_t/E$). For reference, the coordinates of the intersections of these lines are defined by s_y, ϵ_y and $-s_y$, $-\epsilon_y$. Other shapes of cross-sections and stress-strain relationships can be considered. These are dealt with elsewhere.(22)

In Fig. 4, several ranges of loading (1 to 4) are defined. In Range 1, the behavior of a column is elastic, whereas in the other Ranges the behavior is inelastic. In Range 2, only the compressive stresses on the concave side of a column exceed s_y. In Range 3, the compressive stresses on the concave side exceed s_y and the tensile stresses on the convex side exceed $-s_y$. In Range 4, all stresses are compressive and exceed s_y. The shaded diagrams in the Figure represent the correction stresses to the elementary theory of mechanics as defined by Eq. 3. The slope of line CD for each range of loading represents the corresponding value of the modified modulus of elasticity, E_b. The expressions for E_b can be obtained by observing that the shaded diagrams must balance.(23) They can also be obtained by observing that the correction stresses at the extreme fibers of the cross-section are numerically the same as the fixed-end moments of a fictitious beam having a span-length of t and having concentrated loads equal to $E-E_t$ at the corresponding positions of the abrupt changes in the stress-strain curve. This is illustrated in Fig. 4.

In the succeeding discussion, particular consideration is given to a material having a well defined yield point; that is, $n = 1 - E_t/E = 1$. Significant equations associated with the generalized stress-strain curve are summarized in Fig. 4. When n = 1, the equations for E_b/E and $\Delta\phi/\Delta\phi_y$ are as follows:

Range 2: (n = 1) Range 3: (n = 1)

$$\frac{E_b}{E} = \frac{1-P/P_y}{\Delta\phi/\Delta\phi_y}\left\{3-2\sqrt{\frac{1-P/P_y}{\Delta\phi/\Delta\phi_y}}\right\}; \quad \frac{E_b}{E} = \frac{1}{2\Delta\phi/\Delta\phi_y}\left[3\left\{1-(P/P_y)^2\right\} - \frac{1}{(\Delta\phi/\Delta\phi_y)^2}\right] \tag{13a}$$

$$\frac{E_b}{E} = \frac{M}{M_y}\frac{\left[3(1-P/P_y)-M/M_y\right]^2}{4(1-P/P_y)^3}; \quad \frac{E_b}{E} = \frac{M}{M_y}\left[3\left\{1-(P/P_y)^2\right\} - 2\,M/M_y\right]^{1/2} \tag{13b}$$

$$\frac{\Delta\phi}{\Delta\phi_y} = \frac{4(1-P/P_y)^3}{\left[3(1-P/P_y)-M/M_y\right]^2}; \quad \frac{\Delta\phi}{\Delta\phi_y} = \left[3\left\{1-(P/P_y)^2\right\} - 2\,M/M_y\right]^{-1/2} \tag{13c}$$

where the subscripts i previously associated with $\Delta\phi_i$ and M_i have been dropped for convenience in writing. Families of curves,[24] based upon the relationships defined by these Eqs. are shown in Fig. 5.

In Fig. 5, curves also are given which relate the maximum values of M/M_y for WF sections when the values of P/P_y are kept constant. More complete curves and corresponding expressions for P - M - $\Delta\phi$ relationships of WF and other rolled sections are given in Reference 20 and elsewhere.[25,26] In Figure 6, curves are given[27] which relate P/P_y, M/M_y, and $\Delta\phi/\Delta\phi_y$ for rectangular cross-sections when $E_t E = 0.1$. The influence of the stress-strain characteristics of a material on the resulting P - M - $\Delta\phi$ relationships can be seen by comparing Fig. 5a with Fig. 6b.

Critical Loads

Ros[28] defined a critical load to be obtained when the external moment at any section of a column increases at a rate equal to the rate of increase of the internal resisting moment offered at the same section. This criterion stated in the form of an equation is as follows:

$$\left[\frac{d(M)}{d(\Delta\phi)}\right]_{ext.} = \left[\frac{d(M)}{d(\Delta\phi)}\right]_{int.} \tag{14}$$

It is used herein[29,30] to develop significant expressions associated with critical loads. Since the external moment (See Fig. 3) at a section can be written as

$$M_{ext.} = M_L + P(y_o + y_{ai}) \tag{15}$$

its rate of increase becomes

$$\left[\frac{d(M)}{d(\Delta\phi)}\right]_{ext.} = \frac{d(P y_{ai})}{d(\Delta\phi)} = \frac{d(P y_{ai})}{d\left(\frac{k_i}{L^2} y_{ai}\right)} = P\frac{L^2}{k_i} \tag{16}$$

This assumes that k_i is a constant during the increase. The critical load then becomes

$$P_{cr} = \frac{k_i}{L^2}\left[\frac{d(M)}{d(\Delta\phi)}\right]_{int.(cr)} = P_E \frac{k_i}{\pi^2 EI}\left[\frac{d(M)}{d(\Delta\phi)}\right]_{int.(cr)} \tag{17}$$

This permits a more direct means for determining critical values of slope along P - M - $\Delta\phi$ curves than semi-graphical methods used in the past.

Proceeding as previously, we obtain by means of Eqs. 13, the following Eqs. for $\left[d(M)/d(\Delta\phi)\right]_{int}$, namely;

Range 2: (n = 1) Range 3: (n = 1)

$$\left[\frac{d(M)}{d(\Delta\phi)}\right]_{int.} = EI\left[\frac{1-P/P_y}{\Delta\phi/\Delta\phi_y}\right]^{3/2} ; \left[\frac{d(M)}{d(\Delta\phi)}\right]_{int.} = EI\left[\frac{1}{\Delta\phi/\Delta\phi_y}\right]^{3} \quad (18a)^*$$

$$\left[\frac{d(M)}{d(\Delta\phi)}\right]_{int.} = EI\left[\frac{3(1-P/P_y)-M/M_y}{2(1-P/P_y)}\right]^{3} ; \left[\frac{d(M)}{d(\Delta\phi)}\right]_{int.} = EI\left[3\left\{1-(P/P_y)^2\right\}-2M/M_y\right]^{3/2} \quad (18b)$$

Substituting these Eqs. into Eq. 17 and noting that $\frac{\Delta\phi}{\Delta\phi_y} = \frac{E}{E_b} \times \frac{M}{M_y}$, the following relationships associated with critical loads are obtained:

Range 2: (n = 1) Range 3: (n = 1)

$$\frac{\Delta\phi_{cr}}{\Delta\phi_y} = \left(1-\frac{P_{cr}}{P_y}\right)\left(\frac{P_E}{P_{cr}}\frac{k_i}{\pi^2}\right)^{2/3} ; \frac{\Delta\phi_{cr}}{\Delta\phi_y} = \left(\frac{P_E}{P_{cr}}\frac{k_i}{\pi^2}\right)^{1/3} \quad (19a)$$

$$\frac{M_{cr}}{M_y} = \left(1-\frac{P_{cr}}{P_y}\right)\left[3-2\left(\frac{P_{cr}}{P_E}\frac{\pi^2}{k_i}\right)^{1/3}\right] ; \frac{M_{cr}}{M_y} = \frac{3}{2}\left\{1-\left(\frac{P_{cr}}{P_y}\right)^2\right\}-\frac{1}{2}\left(\frac{P_{cr}}{P_E}\frac{\pi^2}{k_i}\right)^{2/3} \quad (19b)$$

(19c)

$$\left(\frac{E_b}{E}\right)_{cr} = \frac{P_{cr}}{P_E}\frac{\pi^2}{k_i}\left[3\left(\frac{P_E}{P_{cr}}\frac{k_i}{\pi^2}\right)^{1/3}-2\right] ; \left(\frac{E_b}{E}\right)_{cr} = \left(\frac{P_{cr}}{P_E}\frac{\pi^2}{k_i}\right)^{1/3}\left[\frac{3}{2}\left\{1-\left(\frac{P_{cr}}{P_y}\right)^2\right\}-\frac{1}{2}\left(\frac{P_{cr}}{P_E}\frac{\pi^2}{k_i}\right)^{2/3}\right]$$

The relationships defined by these Eqs. are represented graphically in Fig. 7. The relationships shown in Fig. 7a are of particular interest as they consist of straight lines for P_{cr}/P_E equal to a constant.

Interaction diagrams, as suggested by Shanley,(31) can now be determined by means of the preceding equations and

$$\left[\frac{M_{om}}{M_y}\right]_{cr} = \frac{P_{cr}}{M_y}\left[y_{om}\right]_{cr} = \frac{P_{cr}}{M_y}\left[y_{ai}\left\{c_i\frac{P_E}{P}-1\right\}\right]_{cr} = \frac{M_{cr}}{M_y}-\frac{\pi^2}{k_i}\frac{P_{cr}}{P_E}\frac{\Delta\phi_{cr}}{\Delta\phi_y} \quad (20)$$

Substitution into this Eq. of the relationships defined by Eqs. 7, 19a, and 19c yields the following results:

Range 2: (n = 1) Range 3: (n = 1)

$$\left[\frac{M_{om}}{M_y}\right]_{cr} = 3\left(1-\frac{P_{cr}}{P_y}\right)\left[1-\left(\frac{\pi^2}{k_i}\frac{P_{cr}}{P_E}\right)^{1/3}\right] ; \left[\frac{M_{om}}{M_y}\right]_{cr} = \frac{3}{2}\left[1-\left(\frac{P_{cr}}{P_y}\right)^2-\left(\frac{\pi^2}{k_i}\frac{P_{cr}}{P_E}\right)^{2/3}\right] \quad (21)$$

These Eqs. can be rewritten in terms of L/r, since

*See Fig. 4 for the corresponding equations when n is not equal to 1.0.

$$\frac{\pi^2}{k_i}\frac{P_{cr}}{P_E} = \frac{s_y}{k_i E}\frac{P_{cr}}{P_y}\left(\frac{L}{r}\right)^2 \qquad (22)$$

for each range of loading. The resulting expressions define interaction diagrams as drawn in Fig. 8. Values of $k_i = \pi^2$ and $s_y/E = 33/30{,}000$ were assumed in plotting this Figure.

The eccentricity ratio, $y_{om}/h2r^2$, associated with the value of a critical axial load on a laterally loaded column can readily be determined in Fig. 8 by observing that

$$\frac{y_{om}h}{2r^2} = \frac{M_{om}}{M_y}\Big/\frac{P}{P_y} \qquad (23)$$

Thus, the inverse value of the slope of a line drawn from the origin of the Fig. is equal to the eccentricity ratio associated with the corresponding values of P_{cr}/P_y and M_{om}/M_y. The intersection of such a line in Fig. 8 with a curve for L/r equal to a constant defines the corresponding values of P_{cr}/P_y and M_{om}/M_y of the loaded column. This same concept has been used in constructing interaction diagrams for the flexural stresses and deflections of flexible arch ribs[32] and of the stiffening girders of suspensions bridges.[33] Similar constructions can be made in several of the other Figs., as for example in Fig. 5a where

$$\frac{E_b}{E} = \frac{M}{M_y}\Big/\frac{\Delta\phi}{\Delta\phi_y} \qquad (24)$$

The values of k_i in the preceding equations are not sensitive to reasonable assumptions concerning the distributions of angle changes along a column.[34] This is particularly true for straight columns loaded eccentrically at their ends and for columns resisting axial and lateral loads. The values of k_i for triangular, parabolic, sinesoidal, and rectangular distributions of angle-changes along a pin-ended column respectively are 12, 9.6, 9.87, and 8. For a straight column loaded eccentrically at its ends, the value of k_i is usually between 8 and π^2. However, for rectangular columns which are initially bent, studies reported elsewhere[35] show that the values of k_i may vary from around π^2 to 16. For these cases, values of k_i equal to π^2, 12 and 16 correspond to columns having slenderness ratios of about 100, 40 and 15, respectively.

For k_i equal to π^2, Eqs. 21 yield the same results as those interpreted by means of the Eqs. developed by Jezek.[36] The Eqs. herein, however, are more general and permit allowances to be made for variations in k_i. It also is observed that the methods and concepts presented herein are general and can be used to determine P - M - $\Delta\phi$ relationships and interaction diagrams for columns having other shapes of cross-sections and stress-strain curves than those presented in this paper.

Again, no consideration has been given in the preceding discussion to the possibility of lateral-torsional instability. Consequently the expressions and diagrams that are given are only valid when failure occurs due to excessive

bending about the axes of moments. It is recognized that if lateral-torsional instability can occur the critical loads for eccentrically and laterally loaded columns can be less than those given herein. For example see Fig. 8.

CONCLUSIONS

The concept of the pressure line is useful for estimating the inelastic behavior of structural frameworks. It is equally useful for making analytical studies of the inelastic behavior of columns.

In addition, the inelastic behavior of columns for the cases studied can be stated in terms of the elastic behavior modified to take into account the effects of plasticity.

REFERENCES

1. "Continuous Frames of Reinforced Concrete," by Hardy Cross and N. D. Morgan, John Wiley and Sons, Inc., New York, N. Y., 1932.
2. "Laterally Loaded Plane Structures and Structures Curved in Space," by Frank Baron and James P. Michalos, Transactions, ASCE, Vol. 117, 1952, p. 279.
3. "A Pressure Line Concept for inelastic Bending," by Frank Baron, Proceedings of the ASCE, Separate 1157, Jan. 1957.
4. "Treatise on Masonry Construction" by Ira O. Baker, John Wiley and Sons, New York, N. Y., 1902, see especially p. 463.
5. Op. cit., Ref. 2.
6. Op. cit., Ref. 2.
7. Op. cit., Ref. 3.
8. Op. cit., Ref. 4.
9. Op. cit., Ref. 1.
10. Op. cit., Ref. 3.
11. Op. cit., Ref. 3. See also, "Plasticity" by A. Nadai, McGraw-Hill Book Co., Inc., New York, N. Y., 1931.
12. Op cit., Ref. 3. See also, "Theory of Elasticity" by S. Timoshenko, McGraw-Hill Book Company, Inc., New York, N. Y., 1936, p. 156.
13. Op. cit., Ref. 3.
14. See "Theory of Elastic Stability" by S. Timoshenko, McGraw-Hill Book Company, New York, New York, 1936, p. 84.
15. "Numerical Procedure for Computing Deflections, Moments, and Buckling Loads," by N. M. Newmark, Transactions, ASCE, Vol. 108, 1943, p. 1161.
16. "Simple Plastic Theory," by B. Thurlimann, AISC National Engineering Conference Proceedings, 1956, Lehigh University, Bethlehem, Penna., p. 13.

17. Op. cit., Ref. 12.

18. "Steel Columns of Rolled Wide Flange Section," by B. G. Johnston and L. Cheney, Progress Report No. 2, AISC, Nov. 1942.

19. "Buckling of Elastic Structures" by H. M. Westergaard, Transactions, ASCE, Vol. 85, 1922, p. 576.

20. "The Elastic and Inelastic Behavior of Columns" by Harold S. Davis, September, 1949. A doctoral dissertation prepared by the junior author at Northwestern University under the direction of the senior author.

21. Op. cit., Ref. 19.

22. Op. cit., Ref. 20.

23. Op. cit., Ref. 3.

24. Op. cit., Ref. 20.

25. "Plastic Deformation of Wide-Flange Beam-Columns" by Robert L. Ketter, Edmund L. Kaminsky, and Lynn S. Beedle, Proceedings of the ASCE, Separate 330, Oct., 1953.

26. "Stability of Beam Columns Above the Elastic Limit," by Robert L. Ketter, Proceedings of the ASCE, Separate 692, May, 1955.

27. Op. cit., Ref. 20.

28. "Die Knicksichevheit von an beiden Enden gelenkig gelagerten Staben aus Konstruktionsstahle, by M. Ros, Proceedings of the 2nd International Congress of Applied Mechanics, Zurick, 1926, p. 368.

29. Op. cit., Ref. 20.

30. Op. cit., Ref. 26.

31. "Applied Column Theory," by F. R. Shanley, Transactions ASCE, Vol. 115, 1950, p. 698.

32. "Design of Flexible Steel Arches by Interaction Diagrams," by O. J. Sotillo, June, 1956, Doctoral dissertation prepared at Rensselaer Polytechnic Institute under the direction of Professor Haaren A. Miklofsky.

33. "Bending Interaction in Suspension Bridges," by Haaren A. Miklofsky, Proceedings of the ASCE, Separate 652, March, 1955.

34. Op. cit., Refs. 20 and 26.

35. Op. cit., Ref. 20.

36. "Die Festigkeit von Druckstaben aus Stahl," by K. Jezek, Julius Springer, Wien, 1937.

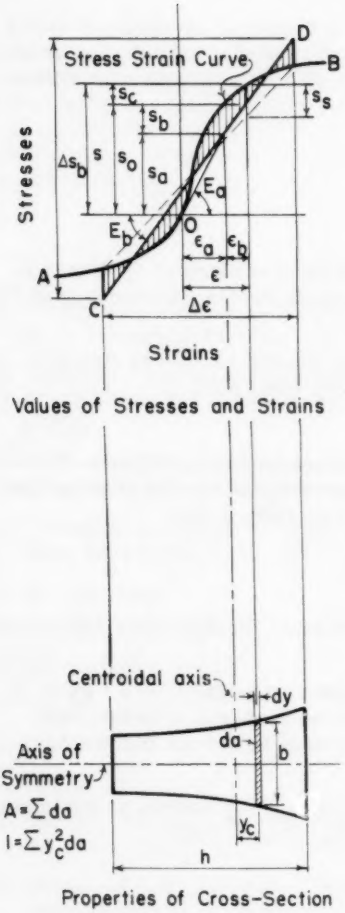

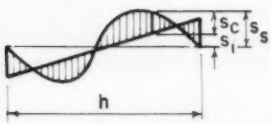

Correction Stresses to the Elementary Theory

Stresses

$$s = s_o + s_c \qquad \sum s_c\,da = 0$$

$$s_o = s_a + s_b \qquad \sum s_c y_c\,da = 0$$

$$s_a = \frac{P}{A};\quad s_b = \frac{My_c}{I}$$

$$\Delta s_b = \frac{Mh}{I}$$

Strains

$$\epsilon = \epsilon_a + \epsilon_b$$

Modified Modulii of Elasticity

$$E_a = \frac{s_a}{\epsilon_a} \qquad E_b = \frac{\Delta s_b}{\Delta \epsilon}$$

Angle-Changes

$$\Delta\phi = \frac{\Delta\epsilon}{h} = \frac{\Delta s_b}{E_b h} = \frac{M}{E_b I}$$

FIG. 1- THE ELEMENTARY THEORY OF MECHANICS COMPARED TO A THEORY OF PLASTICITY

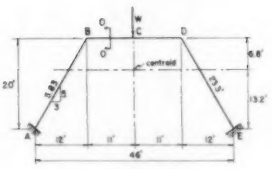

E = CONSTANT
E = 30,000 KSI
σ_y = 33 KSI
M_y = 296 K'
P_y = 237 K
M_u = 1.5 M_y = 594 K'

A = 0.5 ft^2
I = 0.0417 ft^4
r = 0.288 ft

PROPERTIES AND DIMENSIONS

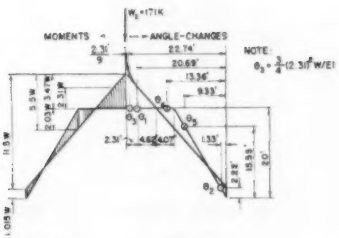

STATICS		GEOMETRY	
LOAD		θ_1 = 12.0 W/EI	
W_2 = 171 K		θ_2 = 3.94 W/EI	
THRUSTS: P		θ_3 = 4.0 W/EI	
P_{AB} = 113 K		θ_4 = -4.14 W/EI	
P_{BD} = 77.3 K = H_2		θ_5 = -15.8 W/EI	
MOMENTS: M		$2\sum\theta$ = 0	
M_A = 173.6 K'			
M_B = 347.1 K'		20 θ_1 = 240. W/EI	
M_C = 593.4 K' = M_u		2.22 θ_2 = 8.7 W/EI	
M_B = M_C = 940.5 K'		20 θ_3 = 80. W/EI	
$M_{S.BM}$ = 1967 K'		20 θ_4 = -82.8 W/EI	
		15.55 θ_5 = -245.7 W/EI	
		$2\sum_{1\theta}$ = 0, & $\sum x\theta$ = 0	
		DEFLECTION	
		Δ_{C2} = 1.62"	

RANGE 2

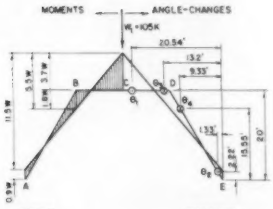

STATICS		GEOMETRY	
LOAD		θ_1 = 13.7 W/EI	
W_1 = 105 K		θ_2 = 3.5 W/EI	
THRUSTS: P		θ_3 = -3.24 W/EI	
P_{AB} = 68.46 K		θ_4 = -13.96 W/EI	
P_{BD} = 45.68 K = H_1		$2\sum\theta$ = 0	
MOMENTS: M			
M_A = 94.5 K'		20 θ_1 = 274 W/EI	
M_B = 189.0 K'		2.22 θ_2 = 7.8 W/EI	
M_C = 388.5 K'		20 θ_3 = -64.8 W/EI	
M_B = M_C = 577.5 K'		15.55 θ_4 = -217. W/EI	
$M_{S.BM}$ = 1208 K'		$2\sum_{1\theta}$ = 0, & $\sum x\theta$ = 0	
MAX. STRESS (AT C)		DEFLECTION	
S_{max} = 33 KSI		Δ_{C1} = 0.791"	

RANGE 1

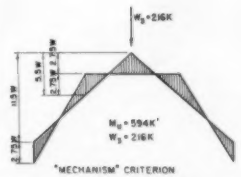

"MECHANISM" CRITERION
N = 5 POSSIBLE HINGES
X = 3 REDUNDANTS
2 INDEPENDENT MECHANISMS

W_3 5.5θ = 2$M_u\theta$/2 + $M_u\theta$
W_3 = M_u/2.75
M_u = 594 K'
$\therefore W_3$ = 216 K

W_3 11θ = $M_u(\theta+\theta+2\theta)$
W_3 = M_u/2.75
M_u = 594 K'
$\therefore W_3$ = 216 K

RANGE 3

COMPARISON:
W_3/W_1 = 2.06; W_3/W_2 = 1.26, W_2/W_1 = 1.63, Δ_{C2}/Δ_{C1} = 2.05

FIG 2 - NUMERICAL EXAMPLE OF A LOADED RIGID FRAME FIXED AT ITS ENDS

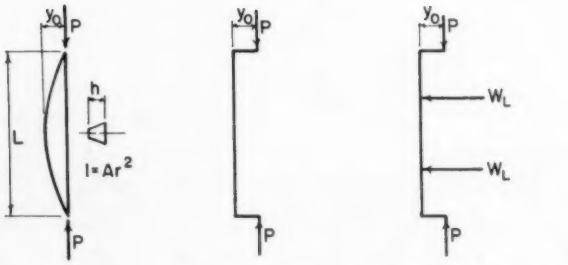

(a) Initially Crooked (b) Eccentric Loads (c) Eccentric & Lateral Loads

LOADS AND INITIAL DIMENSIONS

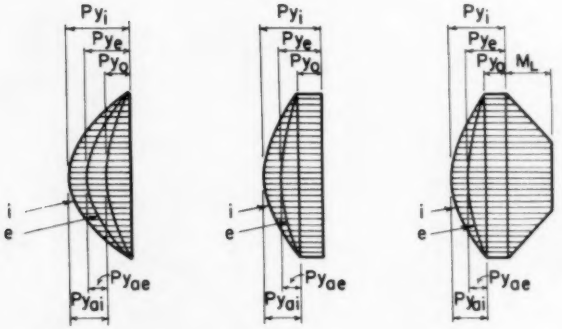

ELASTIC INELASTIC

Deflections	Moments	Deflections	Moments
$y_e = y_o + y_{ae}$	$M_e = M_L + P(y_o + y_{ae})$	$y_i = y_o + y_{ai}$	$M_i = M_L + P(y_o + y_{ai})$
	$M_e = M_{om} + M_{ae}$		$M_i = M_{om} + M_{ai}$
$y_{ae} = \frac{1}{c_e \frac{P_E}{P} - 1} y_{om}$	$M_{ae} = Py_{ae}$; $M_o = Py_o$	$y_{ai} = \frac{1}{c_i \frac{P_E}{P} - 1} y_{om}$	$M_{ai} = Py_{ai}$; $M_o = Py_o$
$y_{om} = \left[1 + \frac{M_L}{M_o}\right] y_o$	$M_{om} = \left[1 + \frac{M_L}{M_o}\right] M_o$	$y_{om} = \left[1 + \frac{M_L}{M_o}\right] y_o$	$M_{om} = \left[1 + \frac{M_L}{M_o}\right] M_o$

FINAL DEFLECTIONS AND MOMENTS

FIG. 3_ ECCENTRICALLY AND LATERALLY LOADED COLUMNS

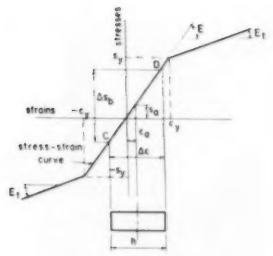

$\frac{E_b}{E} = 1.0$

$\left[\frac{d(M)}{d(\Delta\phi)}\right]_{int} = EI$

RANGE 1

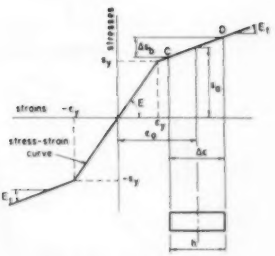

$\frac{E_b}{E_t} = 1.0$

$\left[\frac{d(M)}{d(\Delta\phi)}\right]_{int} = E_t I$

RANGE 4

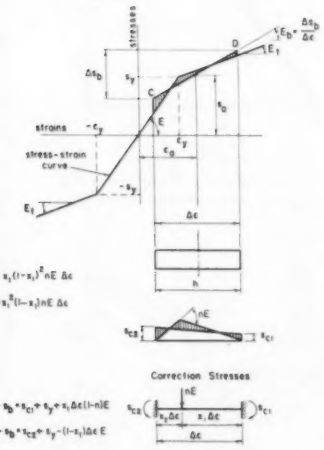

$s_{c1} = x_1(1-x_1)^2 nE\,\Delta\epsilon$

$s_{c2} = x_1^2(1-x_1)nE\,\Delta\epsilon$

$s_o + s_b = s_{c1} + s_y + x_1\Delta\epsilon(1-n)E$

$s_o - s_b = s_{c2} + s_y - (1-x_1)\Delta\epsilon\, E$

$\frac{E_b}{E} = \frac{2}{n}\cdot\left[\frac{2}{n}\left[4(\frac{1}{n}-1)+3a\right]-\frac{2}{n}\left[4(\frac{1}{n}-1)+a\right]\left[1-n(1-a)\right]^{1/2}\right]$

$\left[\frac{d(M)}{d(\Delta\phi)}\right]_{int} = EI\left[4(\frac{2}{n}-1)(\frac{1}{n}-1)+\frac{\left[4(\frac{1}{n}-1)+a\right]a}{\left[1-n(1-a)\right]^{1/2}}-\frac{8}{n}(\frac{1}{n}-1)\left[1-n(1-a)\right]^{1/2}\right]$

RANGE 2

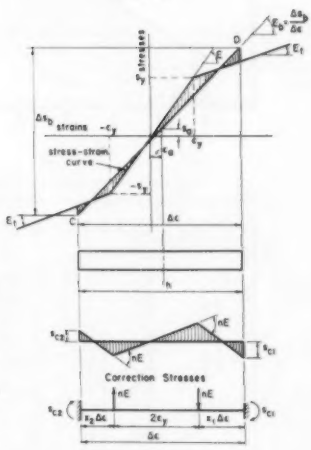

$s_{c1} = x_1(x_2+\frac{1}{\Delta\phi/\Delta\phi_y})^2 nE\,\Delta\epsilon - x_2^2(x_1+\frac{1}{\Delta\phi/\Delta\phi_y})nE\,\Delta\epsilon$

$s_{c2} = x_1^2(x_2+\frac{1}{\Delta\phi/\Delta\phi_y})nE\,\Delta\epsilon - x_2(x_1+\frac{1}{\Delta\phi/\Delta\phi_y})^2 nE\,\Delta\epsilon$

$s_o + s_b = s_{c1} + s_y + x_1\Delta\epsilon(1-n)E$

$s_o - s_b = s_{c2} - s_y - x_2\Delta\epsilon(1-n)E$

$\frac{E_b}{E} = \frac{\Delta\phi_y}{\Delta\phi}\left[(1+\frac{n}{2})+(1-n)(\frac{\Delta\phi}{\Delta\phi_y}-1)-\frac{n}{2(\Delta\phi/\Delta\phi_y)^2}-\frac{3}{2}n\left[\frac{P/P_y}{\frac{\Delta\phi}{\Delta\phi_y}(1-n)+n}\right]^2\right]$

$\left[\frac{d(M)}{d(\Delta\phi)}\right]_{int} = EI\left[(1-n)\left\{1+\frac{3n(P/P_y)^2}{\left[\frac{\Delta\phi}{\Delta\phi_y}(1-n)+n\right]^3}\right\}+\frac{n}{(\Delta\phi/\Delta\phi_y)^3}\right]$

RANGE 3

FOR EACH RANGE:

$n = 1-E_t/E,\quad a = \frac{1-P/P_y}{\Delta\Phi/\Delta\Phi_y},\quad s_o = P/A,\quad \Delta s_b = Mh/I,\quad P_y = As_y,\quad E_b = \Delta s_b/\Delta\epsilon,\quad M_y = 2s_y I/h,\quad \Delta\phi = M/E_b I,\quad \Delta\phi_y = M_y/EI$

FIG. 4 RELATIONSHIPS FOR GENERALIZED STRESS-STRAIN CURVE

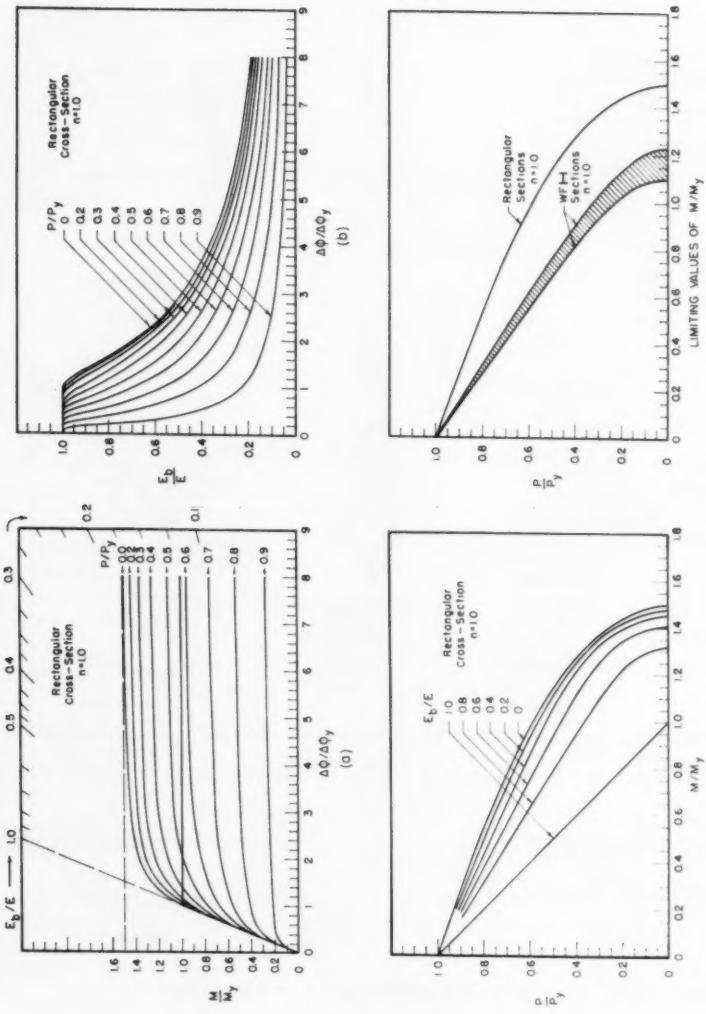

FIG 5 - RELATIONSHIPS BETWEEN P, M, Δφ, AND E_b WHEN n=1.0

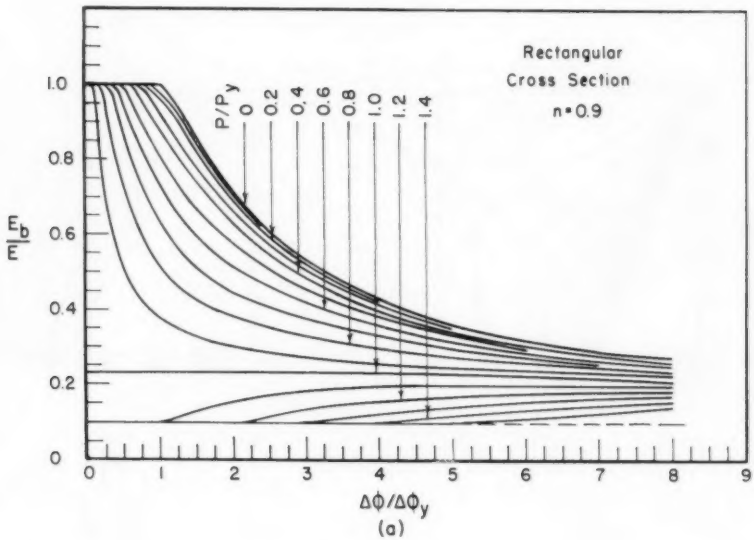

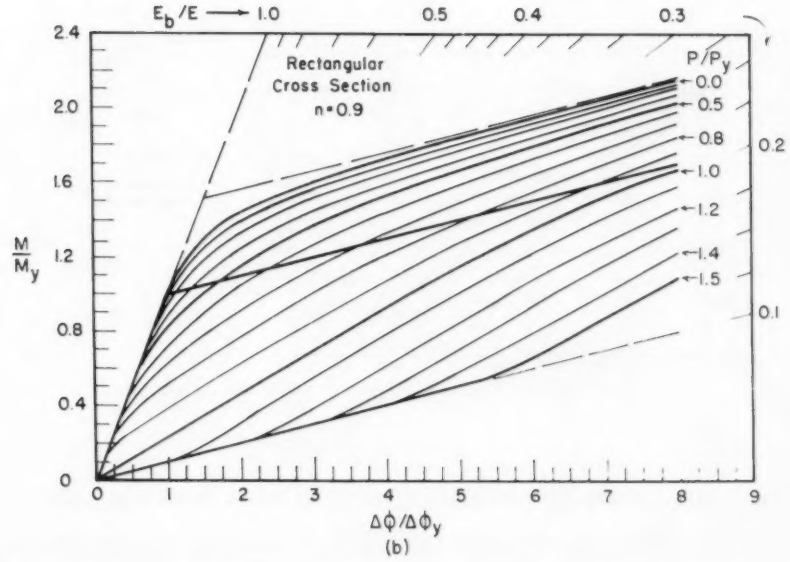

FIG.6_RELATIONSHIPS BETWEEN P, M, Δφ AND E_h WHEN n = 0.9

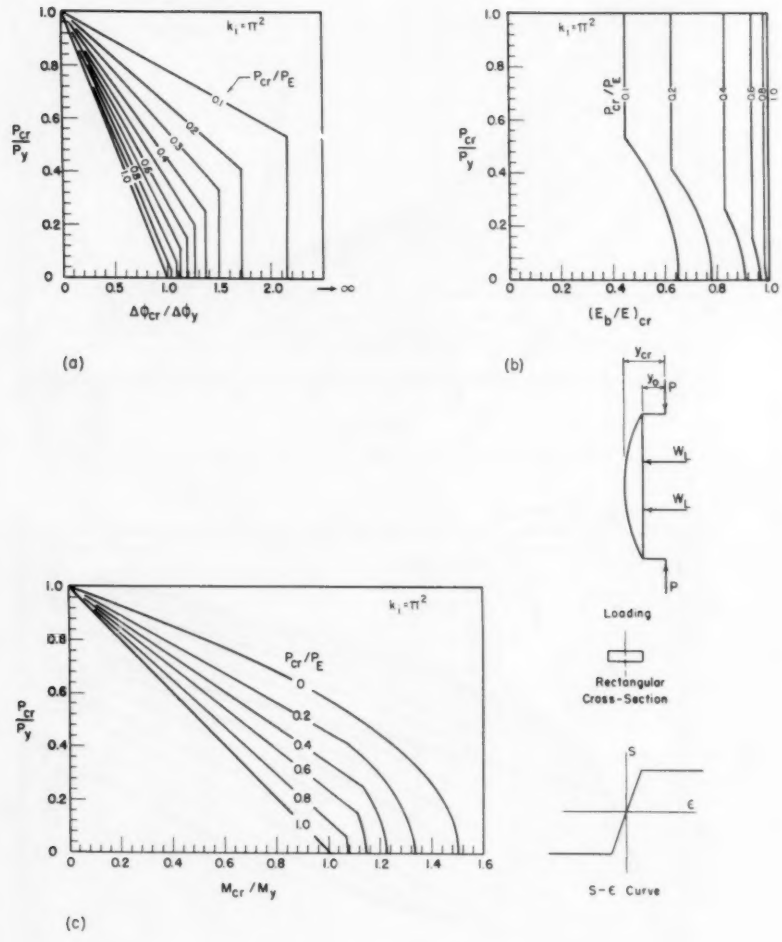

FIG. 7 - RELATIONSHIPS BETWEEN $P, M, \Delta\phi, E_b$ AND P_E AT VALUES OF CRITICAL LOADS

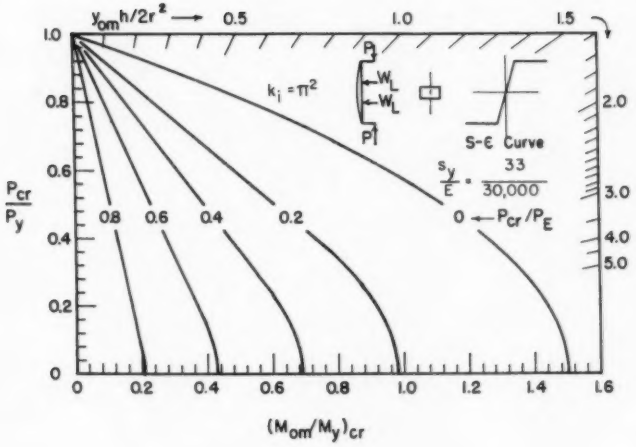

(a)

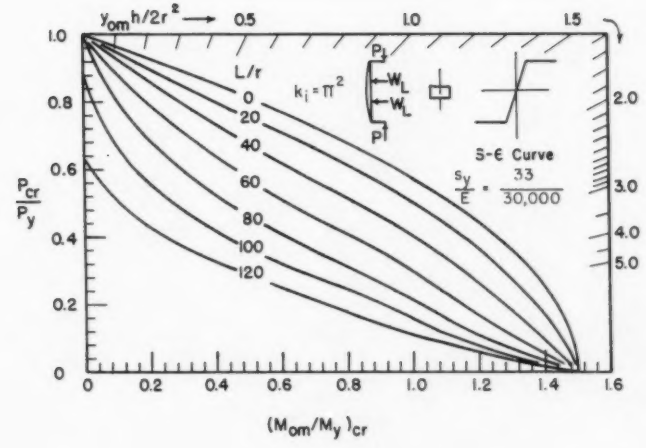

(b)

FIG. 8 – INTERACTION DIAGRAMS FOR ECCENTRICALLY AND LATERALLY LOADED COLUMNS

PROCEEDINGS PAPERS

The technical papers published in the past year are identified by number below. Technical-division sponsorship is indicated by an abbreviation in the case of each Paper Number, the symbols referring to: Air Transport (AT), City Planning (CP), Construction (CO), Engineering Mechanics (EM), Highway (HW), Hydraulics (HY), Irrigation and Drainage (IR), Pipeline (PL), Power (PO), Sanitary Engineering (SA), Soil Mechanics and Foundations (SM), Structural (ST), Surveying and Mapping (SU), and Waterways and Harbors (WW) divisions. Papers sponsored by the Board of Direction are identified by the symbols (BD). For titles and order numbers, refer to the appropriate issue of "Civil Engineering." Beginning with Volume 82 (January 1956) papers were published in Journals of the various Technical Divisions. To locate papers in the Journals, the symbols after the paper numbers are followed by a numeral designating the issue of a particular Journal in which the paper appeared. For example, Paper 1113 is identified as 1113 (HY6) which indicates that the paper is contained in the 6th issue of the Journal of the Hydraulics Division for 1956.

VOLUME 82 (1956)

OCTOBER: 1070(AM1)[2], 1071(CP1), 1072(AM1), 1073(CP1), 1074(HW3), 1075(HW1), 1076(HW1), 1077(HY5), 1078(SA2), 1079(SA1), 1080(AM1), 1081(SA1), 1082(HY5), 1083(SA2), 1084(SA2), 1085(SA2), 1086(PO5), 1087(SA2), 1088(SA5), 1089(SM1), 1090(HW1), 1091(AM1)[3], 1092(HY5), 1093(HY5)[3], 1094(PO5)[3], 1095(SA4)[3].

NOVEMBER: 1096(ST6), [illegible], 1098(ST6), [illegible], 1100(ST6), 1101(IR1), 1102(HW1), 1103(IR1), 1104(SU2), 1105(SU2), 1106(ST6), 1107(ST6), 1108(ST6), 1109(AT5), 1110(AT5)[3], 1111(HY6)[3], 1112(HY6).

DECEMBER: 1113(HY6), 1114(HY6), 1115(SA5), 1116(SU5), 1117(SU5), 1118(SU5), 1119(WW5), 1120(WW5), 1121(CP5), 1122(WW5), 1123(WW5), 1124(SA5), 1125(PO5)[3], 1126(SA5), 1127(SA5), 1128(WW5), 1129(SA5)[3], 1130(SA5)[3], 1131(HY5)[3], 1132(PO5), 1133(PO5), 1134(PO5), 1135(PO5).

VOLUME 83 (1957)

JANUARY: 1136(ST1), 1137(ST1), 1138(SM1), 1139(SM1), 1140(SM1), 1141(SM1), 1142(SM1), 1143(SM1), 1144(SM1), 1145(SM1), 1146(ST1), 1147(ST1), 1148(ST1), 1149(ST1), 1150(ST1), 1151(ST1), 1152(CO1)[3], 1153(HW1)[3], 1154(SM1)[3], 1155(ST1)[3], 1156(ST1)[3], 1157(EM1), 1158(EM1), 1159(SM1), 1160(SM1), 1161(SA1).

FEBRUARY: 1162(HY1), 1163(HY1), 1164(HY1), 1165(HY1), 1166(HY1), 1167(HY1), 1168(SA1), 1169(SA1), 1170(SA1), 1171(SA1), 1172(SA1), 1173(SA1), 1174(SA1), 1175(SA1), 1176(SA1), 1177(HY2), 1178(SA1), 1179(SA1), 1180(PO1), 1181(SA1), 1182(PO1), 1183(PO1), 1184(PO1), 1185(PO1).

MARCH: 1186(ST2), 1187(ST2), 1188(ST2), 1189(ST2), 1190(ST2), 1191(ST2), 1192(ST2)[3], 1193(EM1), 1194(PL1)[3], 1195(EM1).

APRIL: 1196(HW2), 1197(HY2), 1198(HY2), 1199(HY2), 1200(HY2), 1201(HY2), 1202(ST2), 1203(ST2), 1204(ST2), 1205(SM2), 1206(SM2), 1207(SM2), 1208(SM1), 1209(SM1), 1210(WW1), 1211(WW1), 1212(WW1), 1213(WW1), 1214(SU1), 1215(SU1), 1216(SU1), 1217(PO2), 1218(PO2), 1219(SA2), 1220(SA2), 1221(SA2), 1222(SA2), 1223(SA2), 1224(SA2), 1225(SA2), 1226(SA2), 1227(WW2)[3], 1228(WW2)[3], 1229(WW2)[3].

MAY: 1230(ST3), 1231(ST3), 1232(ST3), 1233(ST3), 1234(SM1), 1235(HW2), 1236(WW2), 1237(WW2), 1238(WW2), 1239(WW2), 1240(WW2), 1241(WW2), 1242(WW2), 1243(WW2), 1244(WW2), 1245(WW2), 1246(WW2), 1247(WW2), 1248(WW2), 1249(WW2), 1250(HW2), 1251(WW2), 1252(WW2), 1253(WW2), 1254(ST3), 1255(ST3), 1256(WW2)[3], 1257(HY3)[3], 1258(ST3)[3].

JUNE: 1259(HY3), 1260(HY3), 1261(HY3), 1262(HY3), 1263(HY3), 1264(HY3), 1265(HY3), 1266(ST3), 1267(PO3), 1268(PO3), 1269(SA3), 1270(SA3), 1271(SA3), 1272(SA3), 1273(SA3), 1274(SA3), 1275(SA3), 1276(SA3), 1277(ST3), 1278(ST3), 1279(WW2), 1280(HW2), 1281(PL1), 1282(SA3), 1283(SA3), 1284(PO3), 1285(SA3), 1286(PO3), 1287(PO3)[3], 1288(SA3)[3].

JULY: 1289(SM2), 1290(SM2), 1291(ST4), 1292(SM2), 1293(SM2), 1294(HW2), 1295(HW2), 1296(HW2), 1297(HW2), 1298(HW2), 1299(HW2), 1300(SM2), 1301(CP1), 1302(ST4), 1303(ST4), 1304(ST4), 1305(ST4), 1306(ST4), 1307(ST4), 1308(ST4), 1309(ST4), 1310(ST4), 1311(EM2)[3], 1312(EM2)[3], 1313(EM2)[3], 1314(ST4)[3], 1315(ST4)[3], 1316(ST4)[3], 1317(ST4)[3], 1318(ST4)[3], 1319(SM2)[3], 1320(SM2)[3], 1321(SM2)[3], 1322(SM2)[3], 1323(AT1), 1324(AT1), 1325(AT1), 1326(AT1), 1327(AT1), 1328(AT1)[3], 1329(AT1)[3].

AUGUST: 1330(HY4), 1331(HY4), 1332(HY4), 1333(SA4), 1334(SA4), 1335(SA4), 1336(SA4), 1337(SA4), 1338(SA4), 1339(PO4), 1340(CO1), 1341(CO1), 1342(CO1), 1343(PO4), 1344(HW3), 1345(CO1)[3], 1346(CO1)[3], 1347(CO1), 1348(CO1), 1349(SA4), 1350(PO4), 1351(HW3), 1352(HW3), 1353(HW3), 1354(HW3), 1355(HW3), 1356(HW3), 1357(HW3), 1358(HW3), 1359(HW3), 1360(HW3), 1361(ST5), 1362(ST5), 1363(HW3), 1364(HW3), 1365(HW3), 1366(WW3), 1367(WW3), 1368(WW3), 1369(WW3), 1370(WW3), 1371(HW3), 1372(HW3), 1373(HW3), 1374(HW3), 1375(HW3), 1376(HW3), 1377(HW3), 1378(HW3), 1379(HW3), 1380(HW3), 1381(HW3), 1382(HW3), 1383(HW3), 1384(HW3), 1385(HW3), 1386(HW3), 1387(HW3), 1388(HW3), 1389(HW3), 1390(HW3), 1391(HW3), 1392(HW3), 1393(HW3), 1394(HW3), 1395(HW3), 1396(HW3), 1397(HW3), 1398(HW3), 1399(HW3), 1400(HW3), 1401(HW3), 1402(HW3), 1403(HW3), 1404(HW3), 1405(HY5), 1406(HY5), 1407(HY5), 1408(SA5), 1409(SA5), 1410(SA5), 1411(SA5), 1412(EM3), 1413(EM3), 1414(EM3), 1415(EM3)[3], 1416(EM3)[3], 1417(HY5)[3], 1418(EM3), 1419(PO5), 1420(SA5), 1421(SA5), 1422(SA5), 1423(SA5), 1424(CP2).

---

[2] Discussion of several papers grouped in a single closure.